UNIVERSITÀ DEGLI STUDI DI UDINE

Dipartimento di Ingegneria Elettrica, Gestionale e Meccanica

Dottorato in Ingegneria Industriale e dell'Informazione

- XXVI Ciclo -

Tesi di Dottorato

MANUFACTURING OF HIGH PRECISION MECHANICAL COMPONENTS

Relatore:

Dr. Ing. Marco Sortino

Correlatore:

Dr. Ing. Giovanni Totis

Dottorando:

Francesca Prosperi

Coordinatore:

Prof. Paolo Gardonio

Anno Accademico 2013 - 2014

UNIVERSITY OF UDINE

Department of Electrical, Management and Mechanical Engineering

Doctorate School in Industrial and Information Engineering

- XXVI Cycle -

Doctorate Thesis

MANUFACTURING OF HIGH PRECISION MECHANICAL COMPONENTS

Supervisor:

Dr. Ing. Marco Sortino

Co-examiner:

Dr. Ing. Giovanni Totis

Candidate:

Francesca Prosperi

Coordinator:

Prof. Paolo Gardonio

Academic Year 2013 - 2014

Contents

iv

List of figures

vi

List of tables

Chapter 1.

INTRODUCTION

AND THESIS STRUCTURE

The purpose of a product or a mechanical component is to fulfill its function during its life cycle. Therefore, the main goal of the industrial production is to transform a raw workpiece into a product with definite shape and features, which should satisfy the multiple specifications determined by the product designer.

Nowadays there is a strong trend towards miniaturization of high-tech engineered components, especially for automotive, aerospace, microelectronics or biomedical applications. Miniaturization does usually imply more restrictive dimensional and form tolerances, as well as higher surface quality.

Moreover, such components are frequently made of exotic materials or next generation alloys. Unfortunately, these materials are generally affected by considerable machinability problems. Moreover, environmental and safety issues cannot be neglected due to stringent current regulations.

In order to cope with these challenging trends, a sophisticated specialized science called Precision Engineering is being currently developed.

1.1. Precision Engineering

Precision Engineering is based on three disciplines [1]:

- *Design for precision*: it means the total product design (including materials, mechanics, electronics, controls, thermo-mechanics, dynamics and software); it is becoming very important due the rapidly increasing needs for high accuracy machines, instruments and consumer products;
- *Optical and mechanical metrology*: submicron or nanometer accuracy required by precision design shall be reached by suitable and well-designed measuring machines (i.e. measurement software, error modeling, error compensation system etc.);
- *Precision manufacturing*: it refers to the realization of products with high shape accuracy and surface quality, minimizing, if possible, total production costs; accuracy may be at nanometer levels, so both machine design phase and process behavior, or interaction between machine tool and workpiece shall be well understood.

In the light of these definitions, Precision Engineering does not focus only in consumer components, but also in design and manufacturing of the whole system where the component will be integrated.

As reported by Taniguchi through his famous chart (Fig. 1.1), there exist an increasing needs for high precision machines and products. The graph shows and predicts tendencies in machining accuracy, identifying trends for normal machining, precision machining, high precision and ultrahigh precision manufacturing. The author supposed that machining system will reach the highest accuracy in 2020: for example conventional machining on CNC machine tools (such as CNC lathes or CNC milling machines) is expected to achieve 0,1 µm accuracy; precision machining (including ordinary grinding or lapping) is expected to achieve 0,001 µm of accuracy, whereas ultra-precision machines (like high precision

grinders, lappers or polishers) should reach an accuracy 0,0003 µm. These future results will be driven by the specifications required by emerging fields such as biomedical engineering, IC technologies, MEMS and other future technologies developed at micro and nano scale.
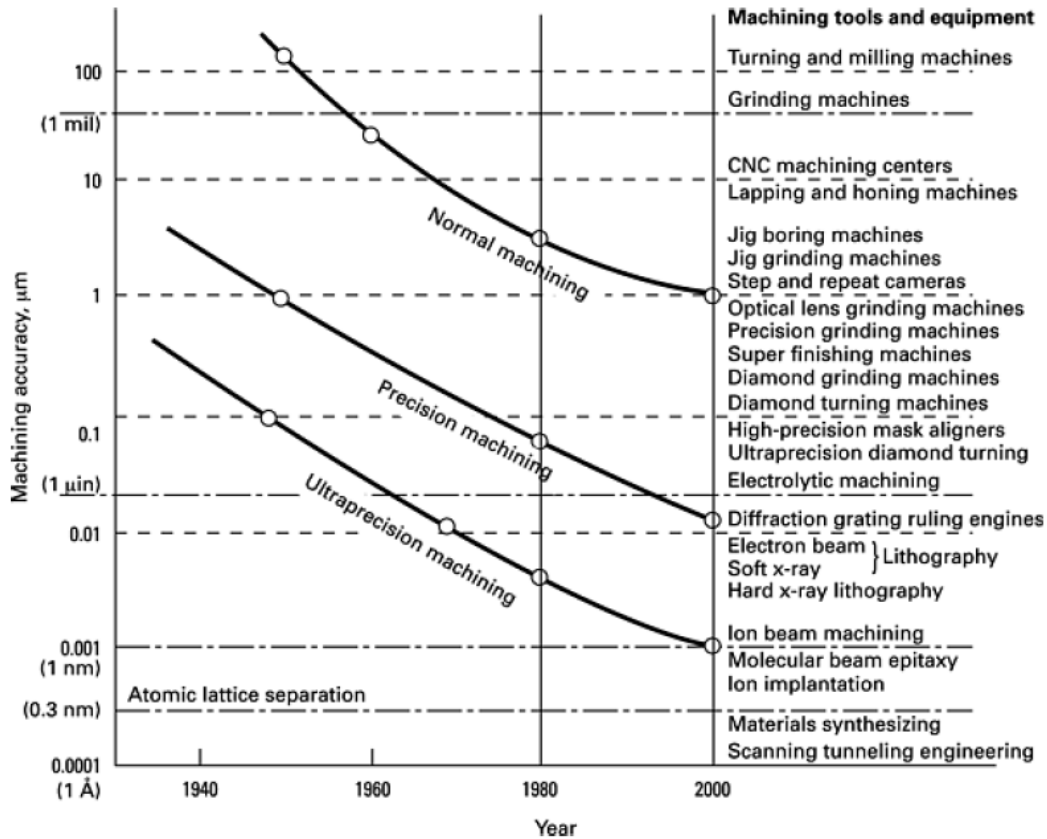
Fig. 1.1 Taniguchi's chart [2]

1.2. Precision design and precision manufacturing

The main goal of design department is twofold: it has to design the component and to define its characteristics. Subsequently, the production department has to assure that the machined component complies with the defined requirements.

Main functionalities of the workpiece are determined in the design stage. They can be divided in several groups [3]:

1. *mechanical functions*, for example the capability of sustaining mechanical loads;
2. *thermal functions*, such as heat resistance and temperature conductivity;
3. *tribological functions,* i.e. the resistance to wear mechanisms acting on the component, at the interfaces with other parts or media; specifically, resistance to chemical reactions such as corrosion, oxidation or diffusion, …
4. *optical functions*, for example light reflection behaviour;
5. *flow functions,* i.e. the influence of workpiece characteristics on the behaviour of a flow of fluids.

In precision manufacturing, components should be designed by taking into account their special functionalities, which may require unconventional tolerances and surface quality. Manufacturing process has to be chosen and set up accordingly.

Dividing the workpiece into geometrical features, each feature can be analyzed at different levels, from a macro scale representing the shape of the part, scaling down to the nano-scale which involves the chemical interaction at the atomic scale. Intermediate levels are the micro-scale that considers the surface topography and the meso-scale which considers materials structure and physical and mechanical properties. The manufacturing process may influence the workpiece properties at all levels and thus it may strongly affect the part functionalities.

Consequently, in the field of high-precision manufacturing, considering only shape and form accuracy is no more sufficient, as it was in conventional machining. On the contrary, it may be crucial to consider the surface integrity of machined surface (presence of micro-cracks, residual stresses or metallurgical changes) and the preservation of the initial properties of the cutting material during machining (Fig. 1.2).
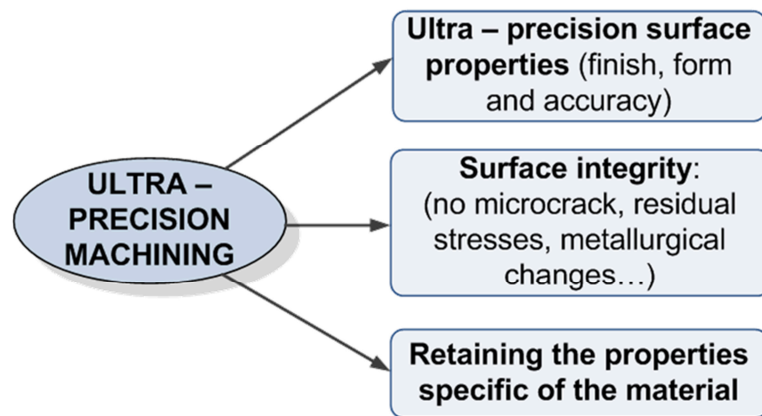
Fig. 1.2 Ultra-precision manufacturing needs

For example, a specific material should be selected during the design phase to fulfill some functionalities which could depend on surface hardness, fatigue strength, and ductile elongation before breakage. Moreover, the characterization of machined surfaces is very important in high precision manufacturing in order to fulfill the final performances of the component [4] [5]. A given manufacturing process can modify the surface layer's microstructure due to the mechanical and thermal load in the contact area between tool and workpiece. This change is not visible at macro-scale, but at micro-sale it may cause undesired variations of mechanical and physical characteristics such those afore mentioned. A further example is represented by surface topography: the final surface quality does not correspond to the nominal properties implicitly assumed during the design phase. The effective surface texture due to the machining process may cause undesired microscopic notches which may lead to stress concentration. On the other side, reaching the desired surface integrity is crucial, since it dictates the functionality of the component: it can affect the resistance to wear and corrosion of the part, it can assist or destroy effective lubrication, increase or decrease friction and/or abrasion phenomena in mating parts.

1.3. The production cycle in high-precision manufacturing

In precision manufacturing, a typical production cycle can be imagined as a sequence of operation, as represented in Fig. 1.3.

CHIP REMOVAL ACTIONS

Certificated and controlled rough material → Rough and Semi-Finish Machining | Heat Treatment | Finishing operations | Super-finishing operations → Product

Cleaning — Inspection | Cleaning — Inspection | Cleaning — Inspection | Cleaning — Inspection — Packaging

ALTERNATIVE ACTIONS
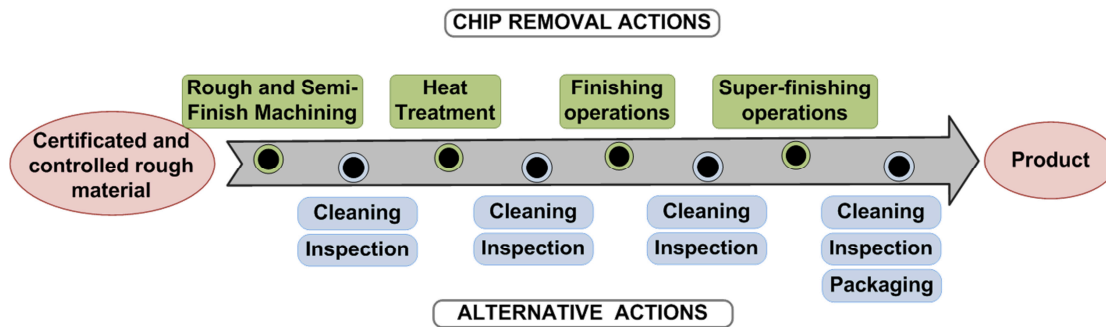
Fig. 1.3 Schematization of a general production cycle

The input of the process flow is the raw material, whose properties are defined in the design stage: its selection depends on the characteristics and functionalities of the final product. For this reason, to reach high accuracy of the component and optimize the cutting process, raw material has to respond to several specifications (proper chemical composition, physical and mechanical properties…). The quality of semi-finished raw material is also critical and it should be adequately checked. For example, among the technical requirements of the raw material, one of the most important specifications is the absence of superficial or sub-superficial defects on the semi-finished part. For this reason, acceptance certificate of raw material has to document the chemical composition, together with its mechanical and physical properties, and it shall include the results of the inspection controls performed on the semi-finished parts, such as circograph or defectomat techniques.

In order to obtain the final product, the raw material will be transformed by several actions. Transformation carries out thanks to machining operations and other intermediate actions.

Chip removal processes are rough and semi-finishing machining, finishing and super-finishing operations. Rough and semi-finishing machining generally aim at approaching the final shape of the part at a macro level, without achieving the effective geometry and the required surface quality.

Other cutting process, like finishing and super-finishing operations are necessary. They focus on the micro and nano-scale, to obtain final features of the product. To distinguish these operations, we can address to definitions found in literature [6] [7], i.e. finishing concerns in operations that imply a shape variation of the workpiece (i.e. rough grinding, rough lapping, deburring actions) whereas superfinishing are operations that involve an improvement of part accuracy and surface quality, without any variation on geometry (i.e. polishing). However, these definitions are not always adopted in the real industrial field.

In adding, if necessary, heat treatments shall be carried out to improve the mechanical properties of the material.

Intermediate actions, such as cleanliness process, inspection of the component and packaging do usually play important roles in Precision Manufacturing. Cleanliness operations could be essential for avoiding the effects of contaminants on the subsequent manufacturing process or to facilitate dimensional controls. Inspection stage, that could be visual or performed by precision metrology instruments is crucial to guarantee the accuracy, and so the functionalities, of parts.

1.4. Optimization of high-precision manufacturing: critical issues

In high-precision manufacturing, there are several interacting factors which influence the overall process performance. Optimizing the production cycle of high-precision mechanical components is the main goal of the manufacturing company. The key concept is "Maximum accuracy of component, minimum production costs and no time-consuming approaches".

Extremely narrow dimensional and geometrical tolerances and high surface quality, together with cleanliness requirements, demand a specific manufacturing process executed on

advanced machine tools and special tooling systems, by applying innovative machining strategies.

Therefore, main targets of Precision Manufacturing are:

1. satisfying very strict workpiece requirements in terms of dimensional and form accuracy, as well as surface quality and integrity;

2. enhancing cutting tool performance (in terms of machinability/chip formation mechanisms, tool life and tool wear);

3. satisfying advanced part requirements arising from Precision Design such as very stringent cleanliness levels, absence of burrs, dents and other geometrical defects.

Several factors can strongly affect accuracy of the workpiece and optimization in general.

Dimensional and geometrical workpiece accuracy does mainly depend on programmed tool trajectory accuracy, machine tool positioning accuracy and kinematics, undesired deflection of tool tip or workpiece. Such deflection is typically due to mechanical compliance of the machining system, differential thermal expansions, tool wear and other causes. Besides, unacceptable surface quality is mainly due to anomalous tool tip/workpiece vibrations or cutting mechanics, worn cutting edge.

Therefore, static and dynamic behaviour of the cutting process plays a key role on the accuracy of the machined part. Moreover, undesired vibrational phenomena can reduce tool wear resistance, can cause tool breakage and in the worst case can damage the tooling system and/or the machine tool, affecting the optimization of the process. Methodologies for chatter avoidance, detection or suppression are fundamental during machining of high precision components. In order to develop effective methodologies for chatter avoidance, it is fundamental to carry out the following activities: identification of machining system dynamics, cutting force modeling and the tool-workpiece dynamic interaction modeling.

Furthermore, the optimization of a machining process is strictly related to the physical interaction of the cutting tool and the workpiece material: it can affect the tool performance, reducing tool life, and can influence the accuracy of the workpiece, in terms of dimensional and geometrical tolerances and surface integrity. The cutting process is a complex dynamical system, whose stochastic outputs depends on several inputs. The combination of cutting material, cutting tool properties and cutting conditions dictates the performance of the cutting process that can be evaluated by dedicated experimental investigation. Several aspects are involved in analysing machinability of a difficult-to-cut material, such as the accuracy of the workpiece, the mechanics and the stability of the cutting process, the chip morphology, the tool wear and tool life. These process outputs are generally strictly related to each other.

Finally, it has to be pointed out that the highly requirements of a mechanical components are not generally achievable by conventional cutting processes. Defects on the edges of parts, such as burrs or dents, and contaminants have to be removed in order to fulfill the functionalities of the final product. Consequently, additional and specific working actions have to be carried out, such as finishing or superfinishing processes and cleaning action. In spite of an improvement of the part accuracy, these technique are generally time-consuming and very expensive.

1.5. Objective and structure of the thesis

This thesis studies some key aspects of Precision Manufacturing. Innovative experimental methodologies, as well as advanced modeling techniques are presented, aiming at optimizing some critical manufacturing processes for the production of high-precision mechanical

components. The proposed techniques will be applied to case studies of great industrial interest, which have been successfully optimized.

The thesis is structured as follow:

In *Chapter 2* the dynamic behaviour of the tooling system in internal turning operation is studied. It represent the first important step in developing a chatter avoidance method. A literary review about modelling approaches of dynamics of slender tooling system is reported and an innovative hybrid dynamic model of tooling system in internal turning is presented and experimentally validated.

In *Chapter 3* cutting forces modelling techniques are investigated from the analysis of the state of art. A semi-empirical approach for cutting force modelling in turning operation is developed and the cutting forces coefficients are experimentally estimated.

In *Chapter 4* the stability of the cutting process is investigated paying attention to the anomalous vibrations phenomena; accordingly, new approaches for avoidance and prediction of such undesired phenomena in internal turning are presented; they are developed by combining the analysis of machining dynamics, of the cutting forces and of the cutter-workpiece dynamic interaction.

In *Chapter 5* the state of art of methodologies for optimization of machining processes of advanced difficult to cut materials are illustrated; in addition, an innovative experimental strategy for optimization of cutting process of exotic materials is presented and experimentally tested in dry turning of sintered Molybdenum.

In *Chapter 6* conventional mass finishing strategies are compared; an innovative mass finishing technology is presented and experimentally tested in order to verify its effectiveness in reaching workpiece accuracy.

In *Chapter 7* the cleanliness requirements of high precision mechanical components are analysed. An overview of the conventional wet cleaning techniques is given together with guidelines for the selection of a proper washing configuration; moreover, strategies for the optimization of cleanliness process are presented. Then, an innovative washing machine is introduced and experimentally tested in order to evaluate its performance in cleaning a specific case study.

Finally, the main conclusions are drawn.

Chapter 2.

MODELLING AND IDENTIFICATION OF MACHINING SYSTEM DYNAMICS

2.1. Introduction

In precision manufacturing of mechanical components, the dynamic and static behaviour of the machining system plays an important role since it can affect the required accuracy of the machined part. Flexibility of the cutting system, especially at tool – workpiece contact point causes poor surface quality and dimensional errors.

Dynamics of the machining system during the cutting process is dependent on the dynamic behaviour of its elements and on their dynamical interactions. Cutting system is generally composed of the machine structure, machine tool drive, tooling system, spindle, workpiece and workpiece fixture.

The most flexible element of the kinematic chain dominates the dynamic relative compliance between tool and workpiece at the instantaneous point of contact. For example, in end milling or internal turning the weakest element is usually the slender tooling system, whereas in external turning it could be the workpiece. Therefore it is necessary to evaluate the flexibility effects on precision manufacturing. For this purpose it is fundamental:

1. to identify the most flexible element of the kinematic chain;
2. to estimate the dynamic characteristics of such element by experimental modal analysis and/or by numerical techniques;
3. to generate simple parametric mathematical models capable of representing the relative vibrations between cutting tool and workpiece.

The experimental techniques and modelling approaches presented in this chapter are mostly dedicated to the identification and modelling of the dynamics of tooling systems for internal turning applications. Main results of this research were recently published in *Mechanical Systems and Signal Processing* [8].

However, the basic ideas behind these techniques can be easily extended and adapted to other manufacturing processes of relevance for Precision Manufacturing.

2.2. Theoretical background

Internal turning is a special turning operation. It is performed by a tool, named boring bar, on which is fixed a cutting insert. The boring bar, clamped on the toolholder-spindle system is characterized by its material and geometry, i.e. the external diameter D and the length L (see Fig. 2.1). It has to be pointed out that the length L of the tooling system corresponds to the applied tool overhang: it derives from the desired workpiece geometry, thus it should be considered as a fixed constraint.
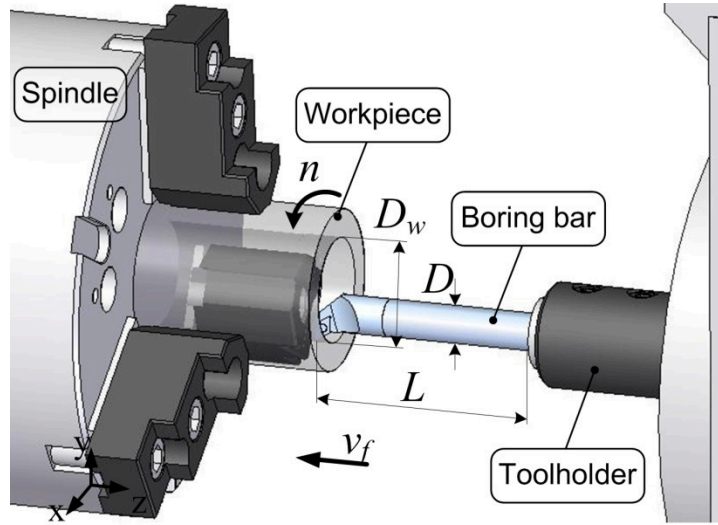
Fig. 2.1 Schematization of internal turning cutting process

If relatively high (*L/D*) ratio is required, the machining system can be affected by anomalous vibrations during machining called chatter. Onset of chatter vibrations crucially depends on tool tip dynamic compliance. For this reason, it is crucial analyse and understand the dynamic behaviour of the tooling system.

Boring bar is usually modelled as two equivalent mass-spring-damper systems at the tool tip point (see Fig. 2.2). A good approximation is to consider axial stiffness infinitely large [9]. The workpiece can be endowed with additional degrees of freedom, when its flexibility is not negligible.
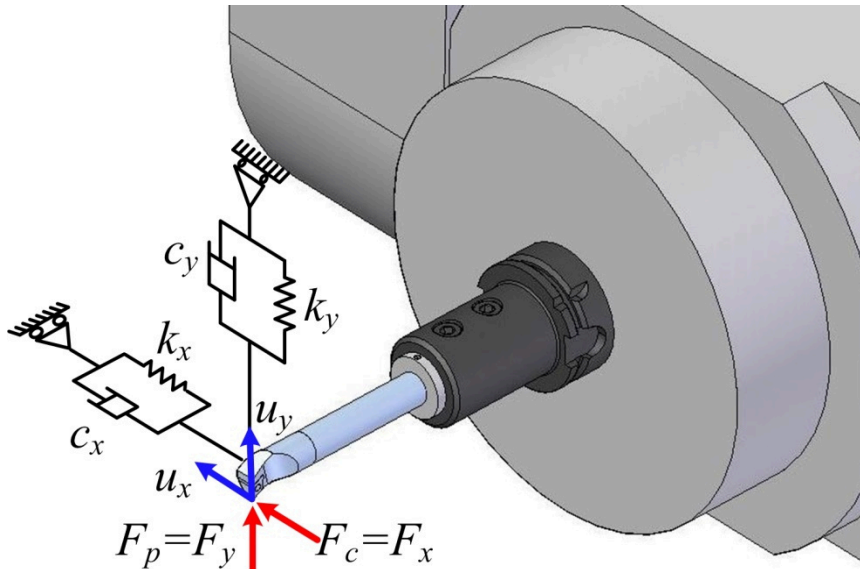
Fig. 2.2 Boring bar dynamics: Schematization

Based on this assumption, system of Fig. 2.2 is represented by:

$$\begin{cases} m_x \ddot{u}_x + c_x \dot{u}_x + k_x u_x = F_x = F_c \\ m_y \ddot{u}_y + c_y \dot{u}_y + k_y u_y = F_y = F_p \end{cases}$$ (2. 1)

where m_x and m_y are equivalent modal masses, c_x and c_y are equivalent damping coefficients and k_x and k_y are the values of equivalent stiffness; the terms u_x e u_y are the displacements at the tool tip along the radial and tangential directions, respectively. Usually, axial and torsional vibrations are neglected thanks to the high axial and torsional rigidity of the system.

In matrix form, the system in Eq. 2.1 can be formulated as:

$$M\ddot{u} + C\dot{u} + Ku = F \tag{2.2}$$

where M is the global mass matrix, C is the global damping matrix and K is the global stiffness matrix. u is the displacement vector, F is the external excitation acting on the system. Matrices result from a combination of the finite element matrices representing the spindle shaft, the tooling system and the workpiece, as illustrated by Genta [10].

The transfer function is expressed as:

$$W_{qq}(j\omega) = \frac{u_q(j\omega)}{F_q(j\omega)} = \frac{G_q}{\left(j\omega/\omega_{n,q}\right)^2 + 2\xi_q\left(j\omega/\omega_{n,q}\right) + 1}$$
$$with\ q = x, y, xy, yx \tag{2.3}$$

When more than a mode for each direction exists, transfer function $W_{qq}(j\omega)$ may include the other relevant, as a combination of the modal contribution of the single mode as follow:

$$W_{qq}(j\omega) = \frac{u_q(j\omega)}{F_q(j\omega)} = \sum_{k=1}^{M_q} \frac{G_{q,k}}{\left(j\omega/\omega_{n,q,k}\right)^2 + 2\xi_{q,k}\left(j\omega/\omega_{n,q,k}\right) + 1}$$
$$with\ q = x, y, xy, yx \tag{2.4}$$

Eq. 2.1, Eq. 2.2 and Eq. 2.4, can be expressed in the state-space form, yielding:

$$\begin{cases} \dot{x} = Ax + BF \\ u = Cx \end{cases} \tag{2.5}$$

which is a system of first-order linear differential equations with time invariant coefficients; x is the state space vector representing the internal state of the system; F represents cutting forces between cutting tool and workpiece and u is the output vector which contains the values of the vibrations of the tool in radial and tangential directions. The matrix A is the dynamic matrix, B is the input gain matrix whereas C is the output gain matrix [10].

Generally, modal parameters are unknown and they have to be estimated by performing experimental modal tests and analytical calculations. Experimental modal testing is usually performed in order to provide force and vibration signals (F(t) and u(t)) that are analysed for the system dynamics identification.

For a successful identification of the dynamic behaviour of the system, some aspects may affect accuracy and reliability of the measurements procedure, such as:
- Sensors set-up and location:

- o real excitation point does not correspond to the nominal and ideal point of excitation;
  - o the point of inspection of the sensor does not correspond to the nominal and ideal point of inspection;
  - o the direction of excitation is not perfectly aligned to the ideal direction of excitation;
  - o the sensing direction of the displacement sensor is not aligned with the ideal direction of inspection;
- Static and dynamic behavior of sensors: the effective force applied to the mechanical system is measured by a dedicated sensor (for example by impact hammer), while vibration signals are measured by displacement sensors (for example by eddy current probes); thus, static and dynamic behavior of the force and displacement sensors affect input forces and displacement signals, respectively (linearity, noise, hysteresis, sensibility…);
- The load effect due to the interaction between force sensors, or displacement sensors, and the mechanical system.

Therefore, modelling dynamic behaviour of a tooling system, i.e. the identification of modal parameters of the system, plays a key role in providing an effective predictive model or a special device in order to avoid vibrational phenomena while machining, such as chatter onset.

2.3. Literary review

Aiming at analysing the dynamic behaviour of a cutting process, three different approaches for modelling slender tooling system are found in literature:

- *Analytical approach* (Tab. 2.1): a mathematical model or a FE model of the system is derived basing on physical and structural equations which govern dynamic behaviour;
- *Hybrid approach* (Tab. 2.2): experimental transfer functions of a subsystem (for example spindle-toolholder) are coupled with FE model of the second subsystem (for example the slender bar);
- *Empirical approach* (Tab. 2.2): modal parameters of the system are derived from experimental tests.

In general, dynamic response of a structure cannot be adequately described by a single degree of freedom model. Therefore, multiple degree of freedom model or a set of discrete points of structure should be adopted.

In internal turning, a possible simple analytical model is given by a fixed-free end Euler-Bernoulli cantilever, as applied by Andren et al. [11]. Authors estimated the first resonance frequency along the cutting speed direction and the cutting depth of cut direction; however the estimated values were greater than the experimental pulsations due to the applied exemplifications of clamping condition which was modelled as an ideal constraint. To solve this inaccuracy, Akesson et al. [12] applied the simple theory of Euler-Bernoulli beam considering different clamping conditions. By performing modal analysis, they found that boring bar was characterized by a non-linear dynamic behaviour; moreover, the dynamics of a clamped tool was better modelled by multi-span Euler-Bernoulli beam models with elastic or pinned boundary conditions rather than a fixed-free beam. The Euler-Bernoulli theory was also used to simulate cutting process by Moetakef-Imani et al. [13]: they integrated the tooling system model with a representation of the chip shape. Aiming at reducing the low accuracy of the bar model due to boundary conditions, authors performed modal analysis to

estimate a theoretical length of the bar able to match the real frequency resonance value; their procedure was based on the approach proposed by Andren et al. [14].

In adding, Euler-Bernoulli theory was implemented in scientific research works aiming at vibration control or chatter suppression, for modelling the tooling system by a simple analytical expression [15] [16] [17].

Even if Euler-Bernoulli theory is extensively adopted, it has intrinsic limitations in modelling dynamics of a boring bar: it assumes that the deflection of the centreline is small and only transverse; moreover it considers the presence of a transverse shear force but it neglects any shear deformation due to rotational inertia that are very important for non-slender component at high frequencies [18]. Therefore, it can be suitable for modelling very slender boring bar ($L/D > 10$); however high L/D ratios are not always applicable in cutting operation. For this reason, Timoshenko theory is sometimes applied in order to increase model accuracy on prediction of modal parameters.

Analytical approach basing on Timoshenko beam theory was adopted by Budak et al. [18] to understand dynamics of spindle-holder-tool assembly in milling process. The proposed method was implemented by same authors [19] in a later work to conduct a proper selection of design and operational parameters regarding the spindle-holder-tool assembly.

Tab. 2.1   Modelling dynamic behaviour of tooling system by analytical approach: Literary review

Ref.	Main purpose	Cutting process	Beam model	Domain Analysis	Tooling system	Sensors for dynamic identifications
[11]	Modelling boring bar dynamics	Internal turning	Euler-Bernoulli	Time	D=40mm L/D=5	Accelerometers
[12]	Modelling clamped boring bar	Internal turning	Euler-Bernoulli	Time	D=40mm L/D>6	Shaker Accelerometers
[13]	Simulation of cutting process dynamics	Internal turning	Euler-Bernoulli	Time	D=20mm L/D=7	Impact test equipment
[15]	Increase boring bar stiffness	Internal turning	Euler-Bernoulli	Time	D=15.9mm L/D=12	Impact hammer Accelerometers
[17]	Chatter suppression	Internal turning	Euler-Bernoulli	Time	D=20mm L/D=15	Not specified
[18]	Modelling spindle-holder-tool	Milling	Thimoshenko	Frequency	D≈15mm L/D=3.5	Impact test equipment
[19]	Chatter prediction	Milling	Thimoshenko	Frequency	D=12mm L/D=5-8	Impact hammer Accelerometer

Alternatively to the pure analytical approach, a further method, named hybrid approach, is often implemented for modelling tooling system: it is obtained by coupling an experimental ETFE of a substructure of the cutting system – composed by tool-holder, spindle, and machine tool – with an analytical, or numerical, discrete modal model of the tool, which represents the second substructure, based on free-free beam shape analytical eigenfunctions (see Fig. 2.3).

This approach derives from the necessity to improve accuracy of analytical model of the dynamics behaviour of the cutting system: analytical or numerical prediction of FRFs for the entire kinematic chain of spindle and machine tool are generally less accurate, due to the

unknown stiffness and damping coefficients at each joint. Moreover, applying pure analytical approach, tool changing or modification of the system characteristics are not ease to consider because modal parameters are analytically evaluated by discrete model or experimentally estimated by dedicated and time consuming numerical modelling of the system. On the contrary, a hybrid approach provides a general model of the tooling system, which can be handle easily with tool characteristics changing; however, analysing machine tool dynamics requires extensive experimental tests and signal processing effort.
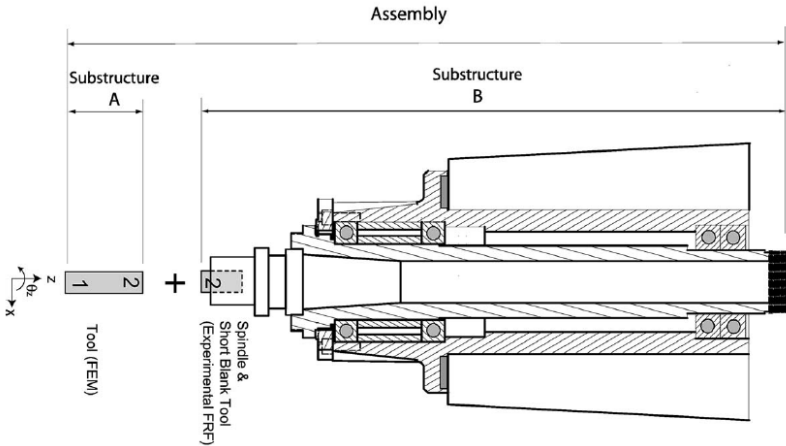
Fig. 2.3 Cutting system decomposition in hybrid approach [20]

The hybrid approach was applied by Park et al. [20] to model the system spindle-holder-tool in milling operation and to evaluate the FRF for end mills with arbitrary dimensions and characteristics. It was useful to identify stable cutting conditions. Similar study was carried out by Catania et al. [21], in milling too, with the aim to predict chatter onset. Similar tooling system models were applied by Wang et al. [22] which included nonlinear friction force in order to create a nonlinear tuned mass damper for chatter suppression in external turning operations.

Tab. 2.2 Modelling dynamic behaviour of tooling system by hybrid and empirical approach: Literary review

Ref.	Main purpose	Cutting process	Modelling approach	Beam model	Tooling system	Sensors for dynamic identifications
[20]	Modelling spindle-holder-tool system	Milling	Hybrid	Timoshenko	D=15-19mm L/D=4-8	Impact hammer Force sensor Accelerometer
[21]	Chatter prediction	Milling	Hybrid	Harmonic oscillator	D=28-40mm L/D=5-10	Impact hammer Accelerometer
[22]	Chatter suppression	External turning	Hybrid	Harmonic oscillator	Not specified	Impact hammer Accelerometer
[23]	Investigation on model parameters	External turning	Empirical	Experimental observations	L=49-59mm	Strain gauges Accelerometers

2.4. Identification of dynamic behaviour of tooling system in internal turning

In the following, a reliable and practical model for describing the tooling system dynamic behavior in internal turning will be proposed. The implemented modelling approach and the scientific evidences are recently published in *Mechanical Systems and Signal Processing* in 2013 [8].

2.4.1 Mathematical modelling of tooling system

Tooling system was composed of several mechanical components, including the toolholder, the boring bar and the cutting insert, see Fig. 2.4. The toolholder was further clamped at the machine tool head.
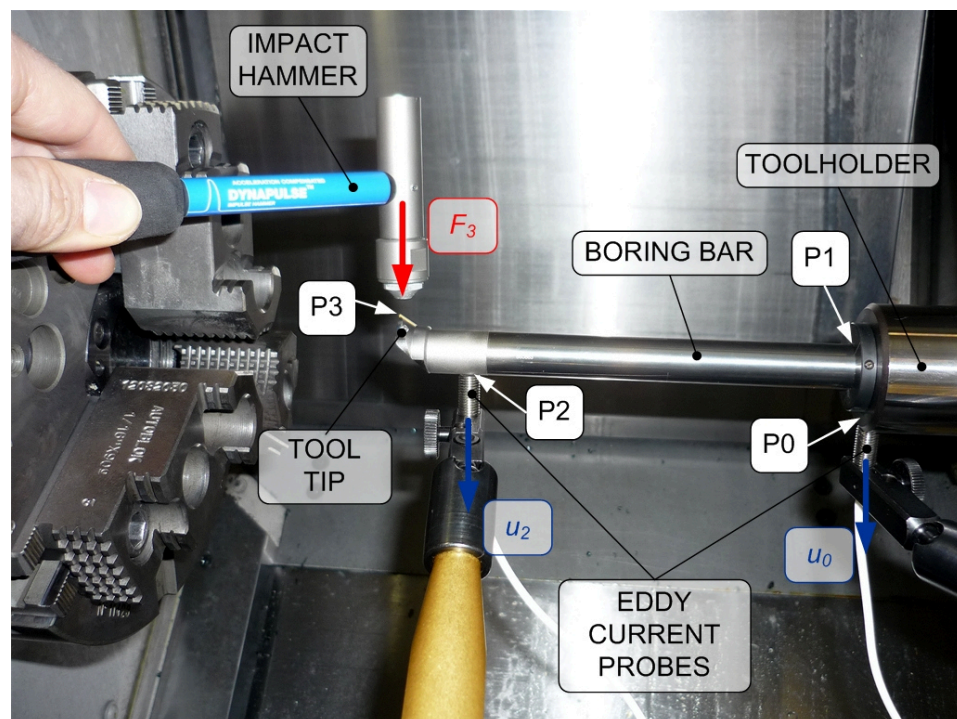
Fig. 2.4 Analyzed tooling system

In the perspective of modelling tooling system dynamic, some nodes were defined along the main axis of the tooling system, as follow (see Fig. 2.4 and Fig. 2.5):

- *Node 3* was the excitation point (*Point 3*) which coincided with the tool tip;
- *Node 2* was the point close to the tool tip along main axis of the boring bar: it coincided with the *Point 2* where displacement u_2 was measured;
- *Node 1* represented the interface between boring bar and tool-holder: its position defined the actual overhang L of the bar;
- *Node 0* coincided with the *Point 0;* it was a further point of inspection for evaluating the displacement u_0 which coincided with the real point of clamping of the boring bar.

Modelling of tooling system was performed following the hybrid approach:

1. Boring bar, representing the first sub-system from *Node 0b* to *Node 3* (see Fig. 2.5 (b)) was analytical modelled by the Timoshenko beam theory;

2. Machine tool head - toolholder receptance at *Node 0t*, which represented the second sub-system, was experimentally determined; the study was found on the key hypothesis that receptance at *Node 0t* did not depend on the boring bar geometry and cutting material.
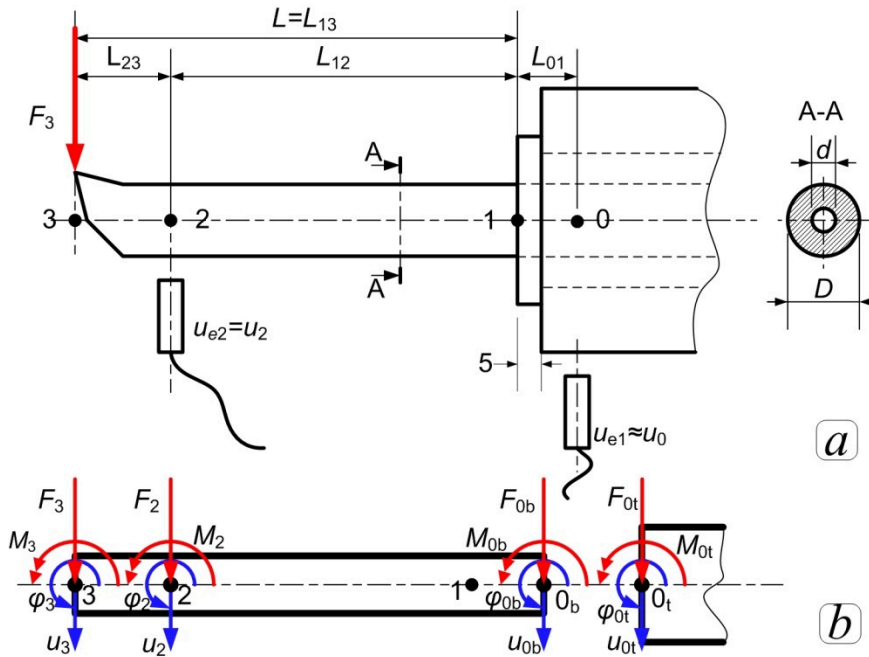
Fig. 2.5 Schematic representation of tooling system (a) and adopted FE model (b) [8]

Following this schematization the total bar overhang was given by the sum of the nominal length L_{13} and the additional overhang L_{01} (see Fig. 2.5-a). The added length L_{01} represents the imperfect constraint at the interface bar-toolholder, which affects analytical models of the system, as highlighted and investigated in literature. Similar approach was followed by Andren et al. [14]: they experimentally obtained an added value to the actual bar length which was able to reduce the gap between analytical and experimental results; unfortunately, the method was strictly related to the geometry of tooling system and so not generally applicable. Also Moetakef-Imani et al. [13] modified actual length of boring bar to compensate the flexibility of the clamping condition in order to correlate natural frequency of the Euler-Bernoulli beam model with experimental results. Authors evaluated the real natural frequency of the structure by modal tests and they estimated the new length of the bar by applying the simple formula:

$$f_n = \frac{\beta_n}{2\pi} \cdot \sqrt{\frac{EI}{\rho A}}$$

(2. 6)

Where $\beta_n = f(L)$ is the eigenvalues of the characteristic equation.

In the research work proposed in this Chapter, a different approach was suggested. The intent was to provide a simple and general solution in order to compensate the flexibility of

clamping condition: the added length L_{01} was supposed independent on boring bar material. The following relation was taken into account:

$$\frac{L_{01}}{D} \cong cost \qquad (2.7)$$

Generally, tooling system dynamics can be expressed in the frequency domain by:

$$\begin{bmatrix} u_{3,x}(j\omega) \\ u_{3,y}(j\omega) \end{bmatrix} = \begin{bmatrix} W_{u3F3,xx}(j\omega) & W_{u3F3,xy}(j\omega) \\ W_{u3F3,yx}(j\omega) & W_{u3F3,yy}(j\omega) \end{bmatrix} \begin{bmatrix} F_{3,x}(j\omega) \\ F_{3,y}(j\omega) \end{bmatrix} \qquad (2.8)$$

where $W_{u3F3,xx}(j\omega)$ and $W_{u3F3,yy}(j\omega)$ are the direct transfer functions, while $W_{u3F3,xy}(j\omega)$ and $W_{u3F3,yx}(j\omega)$ are the cross-transfer functions.

Thanks to the axial symmetry of the holder-boring bar geometry, some simplifications are commonly adopted:

$$W_{u3F3,xy}(j\omega) \approx W_{u3F3,xy}(j\omega) \approx 0 \qquad (2.9)$$
$$W_{u3F3,xx}(j\omega) \approx W_{u3F3,yy}(j\omega) \qquad (2.10)$$

In order to verify this hypothesis, some preliminary impact tests were performed with different tooling system configurations: in general, cross transfer functions were negligible and direct functions were very similar. However, as suggested by Lazoglu et al. [9] radial direction was sufficient to model dynamic behavior of the system because the direction in which cutting forces affect the instantaneous uncut chip thickness. For this reason the model developed in the following will consider only the transfer function on the radial direction $W_{u3F3,xx}$, simply denoted W_{u3F3}.

Tool tip dynamic compliance can be modeled as a sum of vibration mode, such as:

$$W_{u3F3}(j\omega) = \sum_i \frac{G_i}{(j\omega/\omega_{n,i})^2 + 2\xi_i j\omega/\omega_{n,i} + 1} \qquad (2.11)$$

whose modal parameters (mode residues G_i, natural frequencies $\omega_{n,i}$ and damping coefficients ξ_i) depend on boring bar geometry and material and they may slightly change from radial to tangential direction.

For many applications of practical interest, the model can be based on the approximation of the mathematical expression of Eq. 2.11, considering only the dominant mode of vibration:

$$W_{u3F3}(j\omega) = \frac{G_{u3F3}}{(j\omega/\omega_{n,1})^2 + 2\xi_1 j\omega/\omega_{n,1} + 1} \qquad (2.12)$$

where:
- G_{u3F3} represents the total tool tip static compliance;
- $\omega_{n,1}$ is the natural pulsation associated to the main resonance peak;
- $\xi_{n,1}$ is the damping coefficient associated to the main resonance peak.

Therefore, mathematical models for estimating the aforesaid modal parameters was developed and calibrated by using experimental data.

Tool tip static compliance G_{F3u3}

Accordingly to the Timoshenko beam theory, the expression of the four-degree of freedom system, representing the element between *Node 0* and *Node 3*, is:

$$M_{03}\begin{bmatrix}\ddot{u}_0\\\ddot{\varphi}_0\\\ddot{u}_3\\\ddot{\varphi}_3\end{bmatrix} + C_{03}\begin{bmatrix}\dot{u}_0\\\dot{\varphi}_0\\\dot{u}_3\\\dot{\varphi}_3\end{bmatrix} + K_{03}\begin{bmatrix}u_0\\\varphi_0\\u_3\\\varphi_3\end{bmatrix} = \begin{bmatrix}0\\0\\F_3\\0\end{bmatrix} \qquad (2.13)$$

The stiffness matrix K_{03} can be expressed as the combination of the stiffness matrix between *Node 3* and *Node 2* K_{23} and the stiffness matrix K_{02} of the element *2 – 0*. According to the Timoshenko theory, the generic stiffness matrix is expressed by:

$$K_{ij} = \frac{EJ}{L_{ij}}\frac{1}{1+\alpha_{ij}}\begin{bmatrix}\dfrac{12}{L_{ij}^2} & \dfrac{6}{L_{ij}} & -\dfrac{12}{L_{ij}^2} & \dfrac{6}{L_{ij}}\\[2mm]\dfrac{6}{L_{ij}} & 4+\alpha_{ij} & -\dfrac{6}{L_{ij}} & 2-\alpha_{ij}\\[2mm]-\dfrac{12}{L_{ij}^2} & -\dfrac{6}{L_{ij}} & \dfrac{12}{L_{ij}^2} & -\dfrac{6}{L_{ij}}\\[2mm]\dfrac{6}{L_{ij}} & 2-\alpha_{ij} & -\dfrac{6}{L_{ij}} & \dfrac{6}{L_{ij}}\end{bmatrix} \qquad (2.14)$$

being

$$\alpha_{ij} = \frac{12EJ}{L_{ij}^2 A G_\tau K_\tau} \qquad (2.15)$$

where L_{ij} and α_{ij} refer to L_{23} and α_{23} for the first beam element, and to L_{02} and α_{02} for the second beam element to compute the stiffness matrix K_{23} and K_{02}, respectively.
The terms G_τ and K_τ are the shear modulus and Timoshenko shear coefficient for the hollow circular cross section of the boring bar, whose area A and moment of inertia J are given by the well-known relations

$$J = \frac{\pi(D^4 - d^4)}{64}; A = \frac{\pi(D^2 - d^2)}{4} \qquad (2.16)$$

In has to be pointed out that matrix K_{02} will include the machine tool head – toolholder receptance at *Node 0t* expressed by the matrix K_0. It was formulated by approximating two degree of freedom dynamic model:

$$\begin{bmatrix}K_{u0t} & 0\\0 & K_{\varphi0t}\end{bmatrix}\begin{bmatrix}u_{0t}\\\varphi_{0t}\end{bmatrix} = \begin{bmatrix}F_{0t}\\M_{0t}\end{bmatrix} \qquad (2.17)$$

Therefore, the toolholder stiffness 2x2 diagonal matrix K_0 is given by:

$$K_0 = \begin{bmatrix}K_{u0t} & 0\\0 & K_{\varphi0t}\end{bmatrix} = \begin{bmatrix}1/G_{u0t} & 0\\0 & 1/H_{\varphi0t}\end{bmatrix} \qquad (2.18)$$

Unknown coefficients, i.e. toolholder translational compliance G_{u0t} and rotational static compliance $H_{\varphi0t}$, have to be experimentally determined, under the key hypothesis that they are independent of boring bar material and geometry.

As stiffness matrix, also mass matrix M is given as the combination of the mass matrix M_{02} and M_{23}. The 4x4 matrix M_{02} include the 2x2 matrix M_0, which represents the mass matrix of the toolholder. In this study, M_0 was approximated by a diagonal matrix, which elements are constant with sufficiently high values which do not influence the first natural frequency of the cantilever boring bar.

Mass matrix, according to Timoshenko theory is given by:

$$M_{ij} = \begin{bmatrix} m_1 & m_2 & m_3 & -m_4 \\ m_2 & m_5 & m_4 & -m_6 \\ m_3 & m_4 & m_1 & -m_2 \\ -m_4 & -m_6 & -m_2 & m_5 \end{bmatrix} \tag{2.19}$$

where:

$$\begin{cases} m_1 = a\left(312 + 588\alpha_{ij} + 280\alpha_{ij}^2\right) + 36b \\ m_2 = a\left(44 + 77\alpha_{ij} + 35\alpha_{ij}^2\right)L_{ij} + \left(3 - 15\alpha_{ij}\right)L_{ij}b \\ m_5 = a\left(8 + 14\alpha_{ij} + 7\alpha_{ij}^2\right)L_{ij}^2 + \left(4 + 5\alpha_{ij} + 10\alpha_{ij}^2\right)L_{ij}^2 b \\ m_3 = a\left(108 + 252\alpha_{ij} + 140\alpha_{ij}^2\right)L_{ij} - 36b \\ m_4 = a\left(26 + 63\alpha_{ij} + 35\alpha_{ij}^2\right) - \left(3 - 15\alpha_{ij}\right)L_{ij}b \\ m_6 = a\left(6 + 14\alpha_{ij} + 7\alpha_{ij}^2\right)L_{ij}^2 + \left(1 + 5\alpha_{ij} - 5\alpha_{ij}^2\right)L_{ij}^2 b \end{cases} \tag{2.20}$$

with

$$a = \frac{\rho A L_{ij}}{840\left(1 + \alpha_{ij}\right)^2} \tag{2.21}$$

$$b = \frac{\rho J}{30\left(1 + \alpha_{ij}\right)^2 L_{ij}} \tag{2.22}$$

Obviously, for the matrix M_{02} the value L_{ij} is set equal to L_{02}, while for the matrix M_{23}, $L_{ij} = L_{23}$.

Finally, C_{03} is the viscous damping matrix that can be expressed as a diagonal matrix: the elements depend on damping coefficient and on mass and stiffness values:

$$c_{ii} = \xi\left(2\sqrt{m_{ii}k_{ii}}\right) \tag{2.23}$$

Since Timoshenko beam element is chosen for modelling the cantilever boring bar, the only unknown parameter is the effective Young Modulus E, especially for the carbide boring bar. First guess values of the Young Modulus E_{th} for the considered bar materials are listed in Tab. 2.3. In order to determine the effective Young Modulus E, it is necessary compare the static compliance G_{exp} measured at *Node 2* with the theoretical prediction G_{u2F3}. With this purpose in mind, rotation and translation of *Node 0b* was temporarily set at zero. Bar deflection at *Node 2* (u_2) caused by input forces at tool tip F_3 can be derived by the Timoshenko beam element, as follow:

$$\frac{EJ}{L_{02}(1+\alpha_{02})}\begin{bmatrix} \dfrac{12}{L_{02}^2} & -\dfrac{6}{L_{02}} \\ -\dfrac{6}{L_{02}} & (4+\alpha_{02}) \end{bmatrix} \cdot \begin{bmatrix} u_2 \\ \varphi_2 \end{bmatrix} = \begin{bmatrix} F_2 \\ M_2 \end{bmatrix} = \begin{bmatrix} 1 \\ L_{23} \end{bmatrix} F_3 \qquad (2.\,24)$$

From which:

$$u_2 = \left[\frac{L_{02}^2}{3EJ} + \frac{\alpha_{02}L_{02}^3}{12EJ} + \frac{L_{02}^2 L_{23}}{2EJ} \right] F_3 \qquad (2.\,25)$$

Imposing the continuity at *Node 0* and by considering the toolholder flexibility, the expression of the static compliance is obtained as:

$$G_{exp} \cong G_{u2F3} = \frac{1}{E}\left[\frac{L_{02}^3}{J}\left(\frac{1}{3}+\frac{\alpha_{02}}{12}\right) + \frac{L_{02}^2 L_{23}}{2J} \right] + G_{u0t} + H_{\varphi0t}(L_{03}L_{02}) \qquad (2.\,26)$$

The actual Young's modulus value *E* is expected to be close to the theoretical value E_{th}, thus the deviation δ_E can be introduced, as follow:

$$\frac{E_{th}}{E} = 1 + \delta_E, with\ |\delta_E| \ll 1 \qquad (2.\,27)$$

Substituting the expression of Eq. 2.27 in Eq. 2.26 and simplifying notations:

$$\left(1 - \frac{v_1}{G_{exp}E_{th}}\right) \cong \left(\frac{v_1}{G_{exp}E_{th}}\right)\delta_E + \left(\frac{1}{G_{exp}}\right)G_{u0t} + \left(\frac{L_{03}L_{02}}{G_{exp}}\right)H_{\varphi0t} \qquad (2.\,28)$$

$$Q_G \cong V_\delta \delta_E + V_{u_{0t}}G_{u_{0t}} + V_{\varphi_{0t}}H_{\varphi_{0t}} \qquad (2.\,29)$$

where unknown elements (δ_E, G_{u0t}, $H_{\varphi0t}$) can be estimated by linear regression. It has to be pointed out that the renormalization of Eq. 2.26 obtained by dividing both members of the equation by G_{exp} was fundamental for achieving a good distribution of relative errors when applying regression.

After mechanistic estimation of the unknown parameters, tool tip static compliance G_{u3F3} can be computed as:

$$G_{u3F3} = \frac{L_{03}^3}{EJ}\left(\frac{1}{3}+\frac{\alpha}{12}\right) + G_{u0t} + H_{\varphi ut}L_{03}^2 \qquad (2.\,30)$$

It has to be pointed out that static compliance at *Node 2*, G_{u2F3}, was significantly smaller than tool tip static compliance at *Node 3* (G_{u3F3}) because the eigenvectors' shape. Therefore, it was fundamental to take into account the effect of $L_{23} > 0$ in the model, for a correct estimate of the unknown coefficients of Eq. 2.28.

Main natural frequency $f_{n1,th}$

In order to estimate the frequency value associated to the dominant mode of the tooling system $f_{n1,th}$, the transfer function $W_{u3F3}(j\omega)$ between the applied force at *Point 3*, F_3, and the displacement at the same point u_3 was considered. It is derived from matrix expression of the FE model with four degrees of freedom (Eq. 2.13), where toolholder dynamic receptance

18

is combined with the Timoshenko beam element. Viscous damping matrix can be neglected in this phase, since natural frequencies only depend on mass and stiffness matrix.

First guess values of the Young Modulus E_{th} and toolholder compliances G_{u0t} and $H_{\varphi0t}$ are used. However, it has to be noticed that the main natural frequency $f_{n1,th}$ is only slightly influences by G_{u0t} and $H_{\varphi0t}$, therefore such dependences could be neglected. Consequently, the proposed expression, including the only important unknown, is finally obtained:

$$\frac{1}{f_{n1,exp}} \cong \sqrt{1 + \delta_E} \frac{1}{f_{n1,th}} => \left(1 - \frac{f_{n1,exp}}{f_{n1,th}}\right) \cong \left(\frac{f_{n1,exp}}{2f_{n1,th}}\right) \delta_E \tag{2.31}$$

where the last relation is valid provided that δ_E is small. Moreover, the term $f_{n1,exp}$ corresponds to the main resonance peak of each W_{u2F3}.

The previous formulation Eq. 2.31 can be briefly expressed as:

$$Q_f \cong v_f \delta_E \tag{2.32}$$

Main natural frequencies derived from Eq. 2.12 and experimental values can also be compared with the classical Euler-Bernoulli formulation, such as:

$$f_{n1,th} = \frac{v_1}{2\pi} \sqrt{\frac{EJ}{\rho A L_{03}^4}} \tag{2.33}$$

where v_1=3.516 for a cantilever beam.

Accordingly, considering a full circular cross section, main natural frequency can be roughly estimated by

$$f_{n1,th} \approx 0.14 \left(\frac{L}{D}\right)^{-2} D^{-1} \sqrt{\frac{E}{\rho}} \tag{2.34}$$

Damping coefficient ξ_1

Damped mechanical systems exhibit a stochastic dynamic behaviour, so generally it is very difficult to develop predictive physical models of damping phenomena regarding mechanical structure. In order to minimize model complexity and enhance model applicability, semi-empirical models are usually preferred to describe the damping coefficient behaviour.

A well common damping model is that of Rayleigh, representing the damping matrix as a linear combination of mass and stiffness matrix, as follow:

$$\boldsymbol{C_{03}} = \tau \boldsymbol{M_{03}} + \psi \boldsymbol{K_{03}} \tag{2.35}$$

where τ and ψ are unknown elements that must be determined by comparison with experimental data.

By expressing Eq. 2.13 through the eigenvectors base, it is possible demonstrate that:

$$\xi_1 = \frac{1}{2}\left(\tau \frac{1}{f_{n1,th}} + \psi f_{n1,th}\right) \tag{2.36}$$

Which can be used for estimating τ and ψ by linear regression on the experimental values ξ_{1exp}.

2.4.2 Experimental set-up and data analysis

In order to prove the applicability of the proposed models, impact tests were carried out. Input force F_3 was applied on the tool tip by using an impact hammer Dytran type 5500B4 (sensitivity 2.41 mV/N), connected to an amplifier Kistler type 5134B (see Fig. 2.4). Tooling system displacements were measured at *Point 2* and *Point 0* by means of two non-contact eddy current probes Micro-Epsilon type ES1 (measuring range 1mm, sensitivity ≈ 12 mV/µm) connected to eddyNCDT 3010-M controllers. Regarding data acquisition, sensors signal were sampled at 20 kHz by using a National Instruments device (cDAQ-9178) connected to PC via USB. Data were elaborated in MathWorks Matlab environment.

Tooling system constituted of a HSK63A spindle adapter (Sandvik 392.41027-63 25 090B) installed on the machine tool head of an OKUMA MULTUS B300W CN lathe. Four commercial boring bars of different geometries and materials were tested, as listed in Tab. 2.3. Intermediate elements were Sandvik 132L-2516-B (for *D*=16mm) and 132L-2510-B (for *D*=10mm).
Impact tests were performed with different boring bar overhang *L*, i.e. with different aspect ratios *L/D*, as report in Tab. 2.4. Impact tests were executed by hammering the tool tip in the radial direction, since it is the mostly responsible for the generative effect causing chatter. For the sake of comparison, some impact tests were also performed by hammering the tool tip in the tangential direction, confirming the hypothesis outlined in the previous section.

Tab. 2.3   Boring bar characteristics [8]

Number	Commercial code	External diameter D [mm]	Internal diameter d [mm]	Material	Young's modulus E_{th} [GPa]	Density ρ [g/cm^3]
1	Sandvik A10KSDUCR07-ER	10	4	Alloy steel	210	7.87
2	Sandvik A16KSDUCR07-R	16	6	Alloy steel	210	7.87
3	Sandvik E10RSDUCR07-ER	10	4	High damping carbide	580	13.15
4	Sandvik E16RSDUCR07-R	16	6	High damping carbide	580	13.15

Tab. 2.4   Impact testing: Design of the experiments [8]

Parameters	Levels	Values
Boring bar materials	2	Steel, high damping carbide
External diameters D	2	10, 16 mm
Aspect ratio L/D	8	3 ÷ 9
Replications	1 or 2	

Experimental static compliances and natural frequencies

An example of the Empirical Transfer Function Estimate W_{u2F3} and W_{u0F3} are shown in Fig. 2.6, relating to the standard alloy steel boring bar with external diameter D = 10mm. Experimental tool tip static compliance G_{u2F3} was estimated by averaging the amplitude of W_{u2F3} in the low frequency range. An estimate of the toolholder translational compliance at *Node 0* was derived from W_{u0F3}, such as:

$$G_{u0t} = \frac{1}{H_{u0t}} \cong G_{u0F3} \tag{2.37}$$

Unfortunately, the toolholder rotational compliance $H_{\varphi0t}$ could neither derived from W_{u2F3} nor from W_{u0F3}.

Analyzing Fig. 2.6 - a, it emerges that W_{u2F3} is characterized by one dominant peak at the natural frequency of the cantilever bar, and by other minor peaks which are approximately located in the frequency range 500-2000Hz. From the observation of W_{u0F3}, such minor peaks can be attributed to machine tool head – toolholder dynamics.

This is confirmed in Fig. 2.7, where the ETFEs of the other tooling system configurations are illustrated. For each tested bar type, minor resonance peaks are evident in the range 500-2000 Hz, independently of L/D. On the contrary, the relevant resonance peak strongly depends on L/D. Moreover, the importance of the different terms composing the tool tip static compliance was evaluated (see Fig. 2.6 – b). Considering $L/D > 5.5$, the Bernoulli term G_{ber} is dominant (more than 90% of total static compliance). For smaller aspect ratio, other terms become relevant too, such as the translational toolholder flexibility (about 20% of the total static compliance), the rotational toolholder flexibility (5%) and the correction due to the Timoshenko theory (5%). However, the relative importance of the Timoshenko term is considerably higher than 5%, when neglecting toolholder flexibility.

In add, from ETFEs analysis, further observation can be deduced:
- Tooling system static compliance increases when the aspect ratio L/D is increased or when considering smaller bar diameters D;
- For a given bar geometry, high damping boring bars have more than twice the stiffness of those made of conventional alloy steel, due to the higher Young Modulus of sintered carbide;
- Experimental resonance frequencies increase when L/D is decreased, when considering smaller bar diameter D, or when considering high damping carbide boring bars.
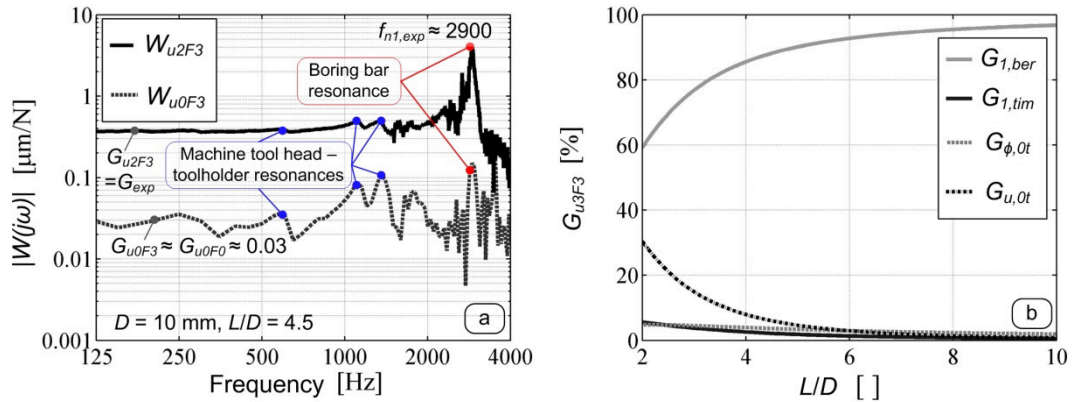
Fig. 2.6 ETFEs measured close to the tool tip and to the tool-holder (a) and importance of different terms for static compliance estimate (b) (Standard alloy steel boring bar, $D = 10$mm) [8]

21
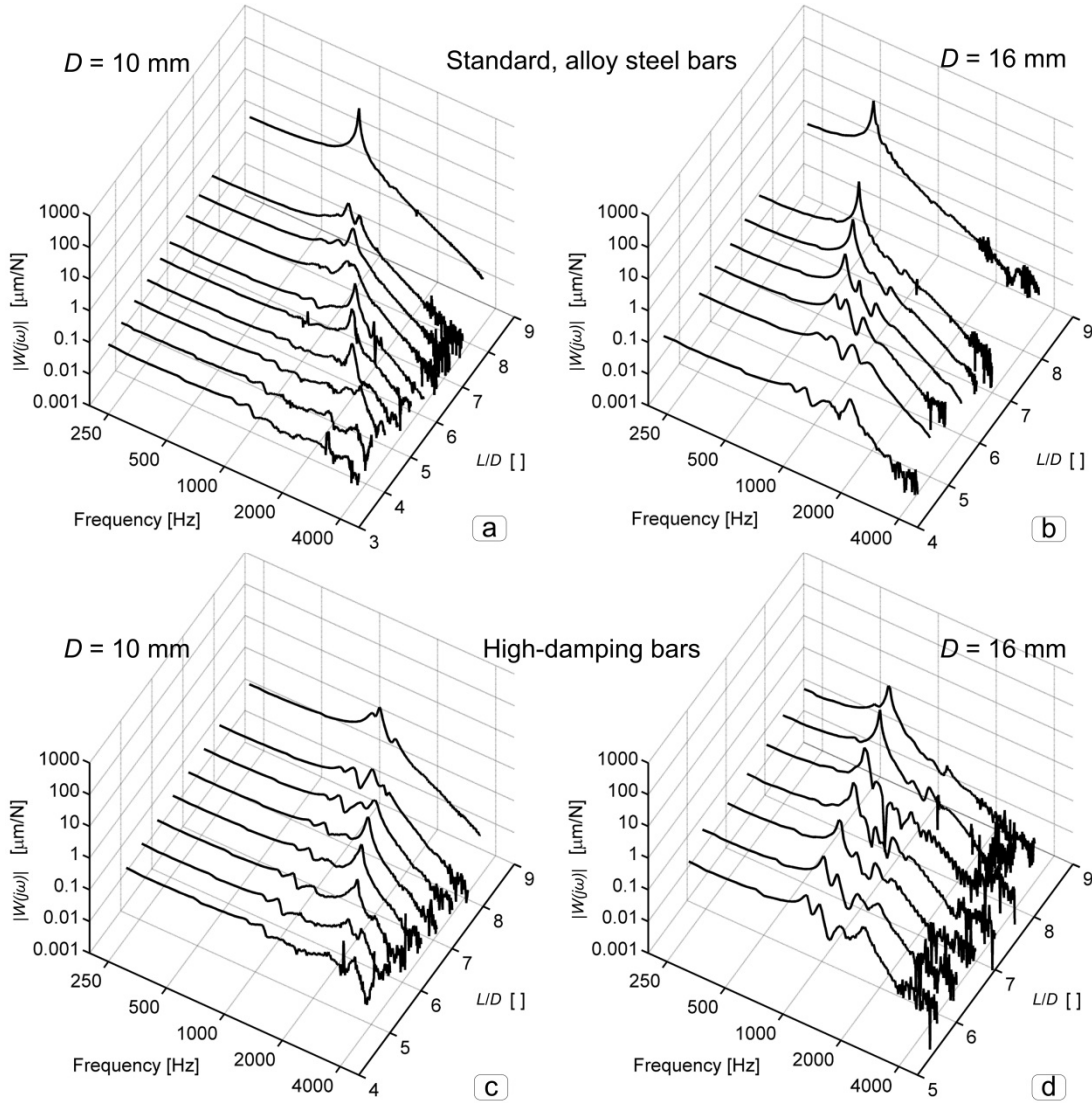
Fig. 2.7 ETFEs for normal steel boring bar (a) and (b) and high damping carbide boring bar (c) and (d), for different *L/D* aspect ratio [8]

As outlined above, natural frequencies correspond to the main resonance peaks of each $W_{u2F3}(j\omega)$: experimental values were used for solving Eq. 2.31. In most of the cases, only one resonance peak was identified, deriving from pure cantilever behaviour, whereas other peaks were negligible. This was particularly true for boring bars with small diameter. On the contrary, in the case of the high damping boring bar with *D*=16mm, multiple resonance peaks were identified, due to its high stiffness.

In order to estimate the unknown Young Moduli and the toolholder static compliances, Eq. 2.29 and Eq. 2.32 were combined in the following system of linear equations comprising both bar materials:

$$
\begin{bmatrix} Q_{G,stl} \\ Q_{G,crb} \\ Q_{f,stl} \\ Q_{f,crb} \end{bmatrix} = \begin{bmatrix} V_{\delta,stl} & 0 & V_{u0t,stl} & V_{\varphi0t,stl} \\ 0 & V_{\delta,crb} & V_{u0t,crb} & V_{\varphi0t,crb} \\ V_{f,stl} & 0 & 0 & 0 \\ 0 & V_{f,crb} & 0 & 0 \end{bmatrix} \begin{bmatrix} \delta_{E,stl} \\ \delta_{E,crb} \\ G_{u0t} \\ H_{\varphi0t} \end{bmatrix}
$$

(2. 38)

where the subscript "*stl*" refers to conventional boring bars made of alloy steel, while "*crb*" refers to high-damping boring bars made of carbide, and the *O*'s are columns of zeros, whose length is equal to the number of experimental points available for each case.

For a fixed L_{01}/D ratio the system in Eq. 2.38 was solved by applying linear regression. Afterwards, relative errors were computed as follow:

$$\varepsilon_{rel,G} = \frac{G_{mod} - G_{exp}}{G_{exp}} \ [\%] \tag{2.39}$$

$$\varepsilon_{rel,fn1} = \frac{f_{n1,mod} - f_{n1,exp}}{f_{n1,exp}} \ [\%] \tag{2.40}$$

where G_{mod} and $f_{n1,mod}$ are the static compliance and the main natural frequency estimated through the obtained model, respectively. The calculation was repeated by varying L_{01}/D and by recalculating the relative errors. By observing the behaviour of the mean μ_{rel} and the standard deviation σ_{rel} of the relative errors against L_{01}/D, an optimal solution was found, as reported in Tab. 2.5 and illustrated in Fig. 2.8 and Fig. 2.9.

The unknown model coefficients calculated by stepwise regression method are listed in Tab. 2.5. According to this modelling and statistical tool, both Young Moduli and toolholder compliance terms gave a significant contribution on the output variance, justifying their presence on the model.

It can be noticed that the estimated value of G_{u0t} reported in Tab. 2.5 is in accordance with experimental range regarding G_{u0F3} that is $0.015 \div 0.045$ µm/N. In add, the estimated Young Moduli are close to the theoretical values listed in Tab. 2.3.

Tab. 2.5 Estimate model coefficients [8]

Model	L_{01}/D	Bar material	E [GPa]	G_{u0t} [µm/N]	$H_{\varphi 0t}$ [µrad/Nm]	$\mu_{\varepsilon rel,G}$ [%]	$\sigma_{\varepsilon rel,G}$ [%]	$\mu_{\varepsilon rel,f}$ [%]	$\sigma_{\varepsilon rel,f}$ [%]
Euler-Bernoulli	0	Steel	144	0.062	2.38	2.9	7.6	22.6	16.7
		Carbide	390			-1.1	4.9	2.9	8.3
Euler-Bernoulli	0.7	Steel	212	0.028	6.08	1.3	7.2	3.7	9.2
		Carbide	558			-2.3	5.2	0.2	8.1
Timoshenko	0.7	Steel	216	0.023	6.45	1.2	7.3	1.6	8.7
		Carbide	563			-2.3	5.3	-0.9	8.2

The comparison between experimental and theoretical results for static compliance and natural frequency against *L/D* ratio is reported in Fig. 2.8, for standard steel boring bar and in Fig. 2.9, for high damping carbide boring bar. Tool tip static compliances G_{u2F3} are predicted with good accuracy by the proposed model. On the other hand, experimental resonance frequencies are nevertheless slightly more scattered around predicted values, especially for boring bars with bigger diameter. The outliers highlighted in Fig. 2.9 are associated to relatively high resonance peaks characterizing the ETFEs, which cannot be accurately predicted by the proposed model due to the adopted model simplifications. For this, such outliers were excluded from the computations.

Moreover, a deeper analysis of relative error distributions revealed a small systematic errors affecting the high-damping boring bars when considered separately. This bias are probably due to the heterogeneous mechanical properties of the high damping material caused by the manufacturing process.

Euler-Bernoulli model (Eq. 2.26 imposing $\alpha_{02}=0$ and Eq. 2.33) was also tested. Optimal values of the unknown parameters were similar to those obtained with the Timoshenko beam theory, but relative errors distributions were slightly worse. Euler-Bernoulli model can be considered sufficiently accurate, provided that aspect ratio *L/D*>3.
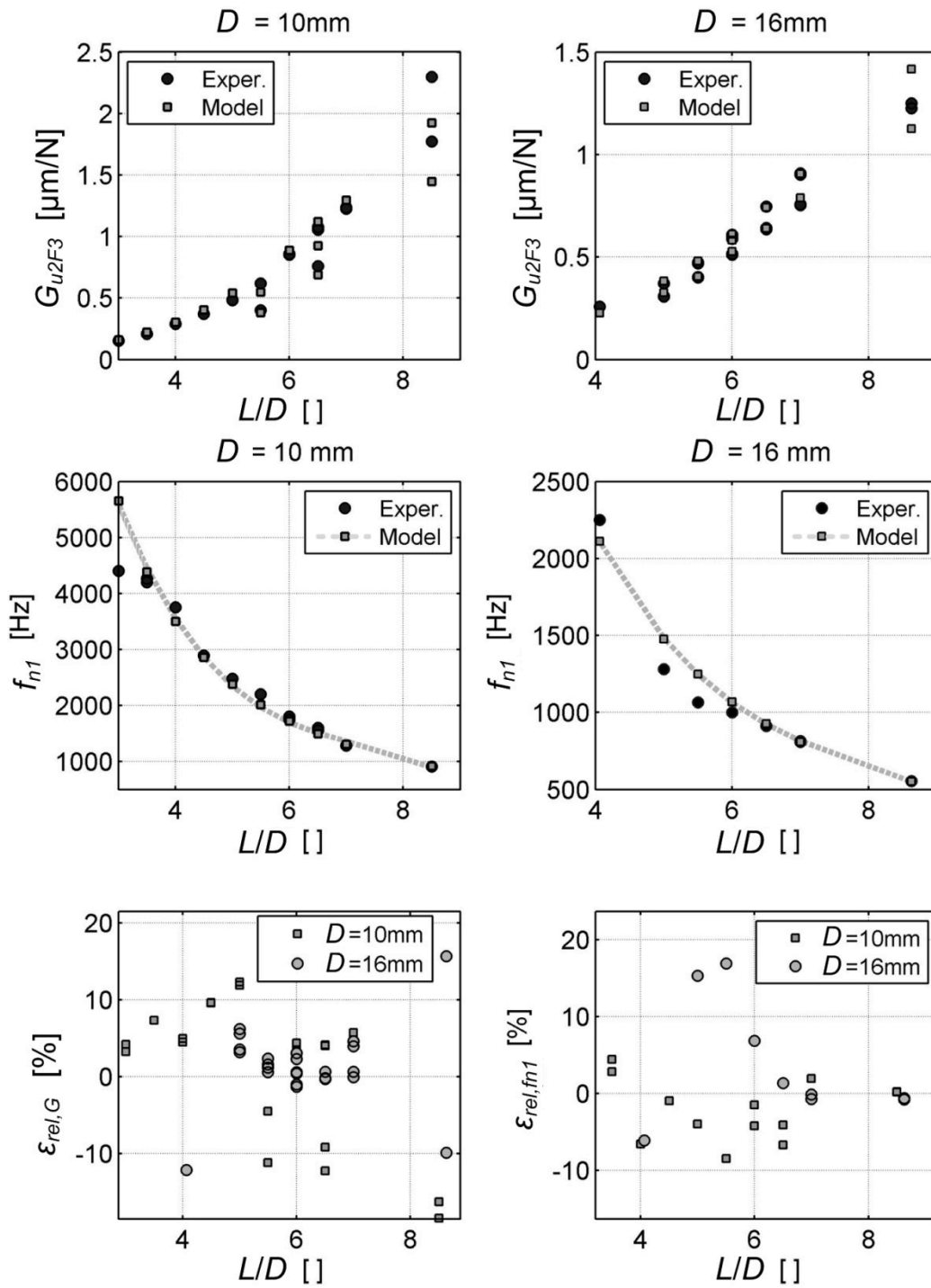
Fig. 2.8 Comparison between experimental and estimated values of static compliance and natural frequency and relative errors against *L/D* ratio, for standard alloy steel boring bars [8]

24
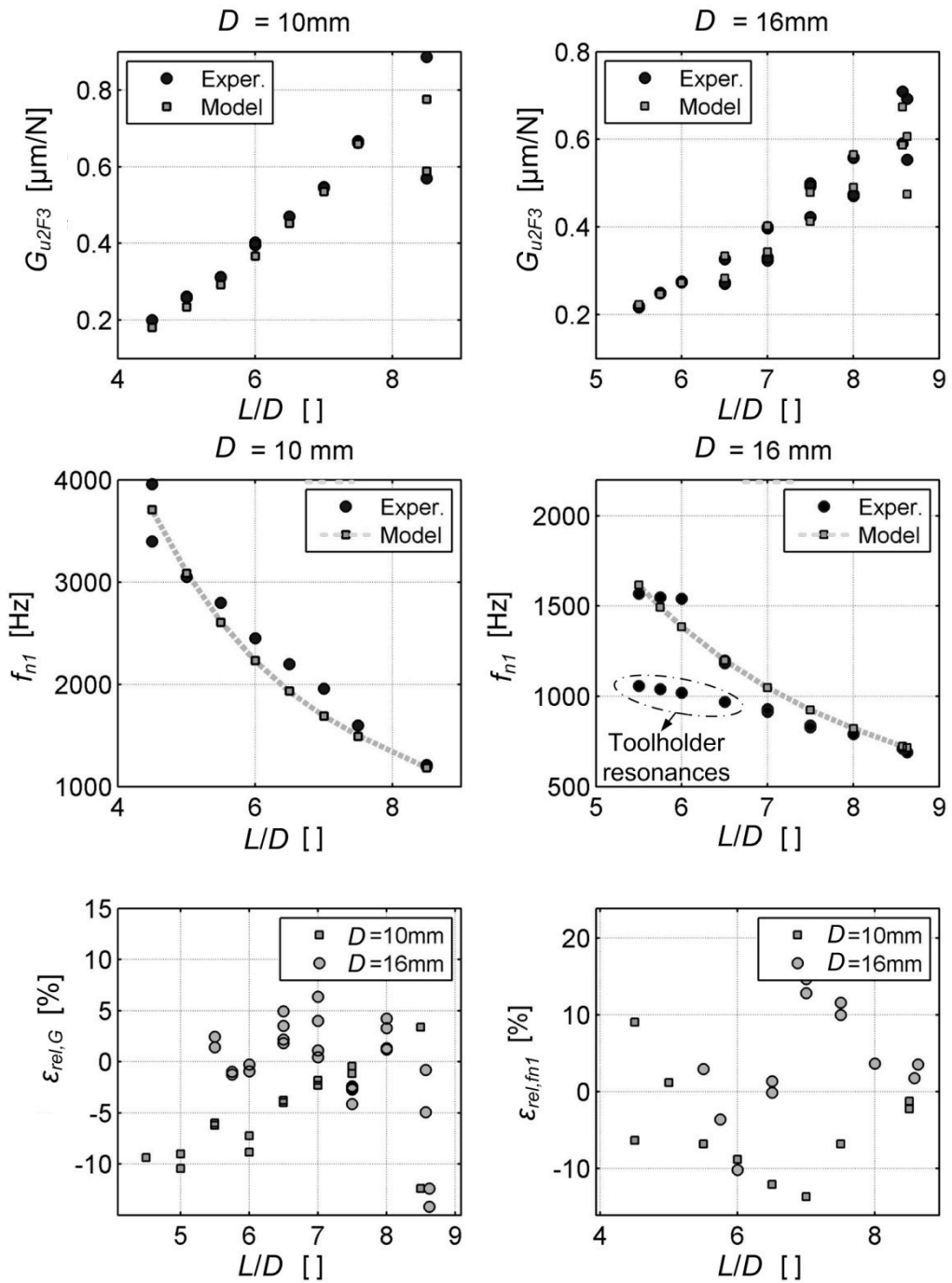
Fig. 2.9 Comparison between experimental and estimated values of static compliance and natural frequency and relative errors against *L/D* ratio, for high damping carbide boring bars [8]

Experimental damping coefficient

From the experimental transfer functions, the damping coefficient $\xi_{1,exp}$ of the dominant mode was estimate as:

$$\xi_{1,exp} = \frac{G_{u2F3}}{2|min[Im(W_{u2F3})]|} \tag{2.41}$$

By analysing $\xi_{1,exp}$ against the considered factors, a significant dependence on *L/D* and on bar material was found out, whereas no significant dependence on bar diameter was evidenced, see Fig. 2.10.
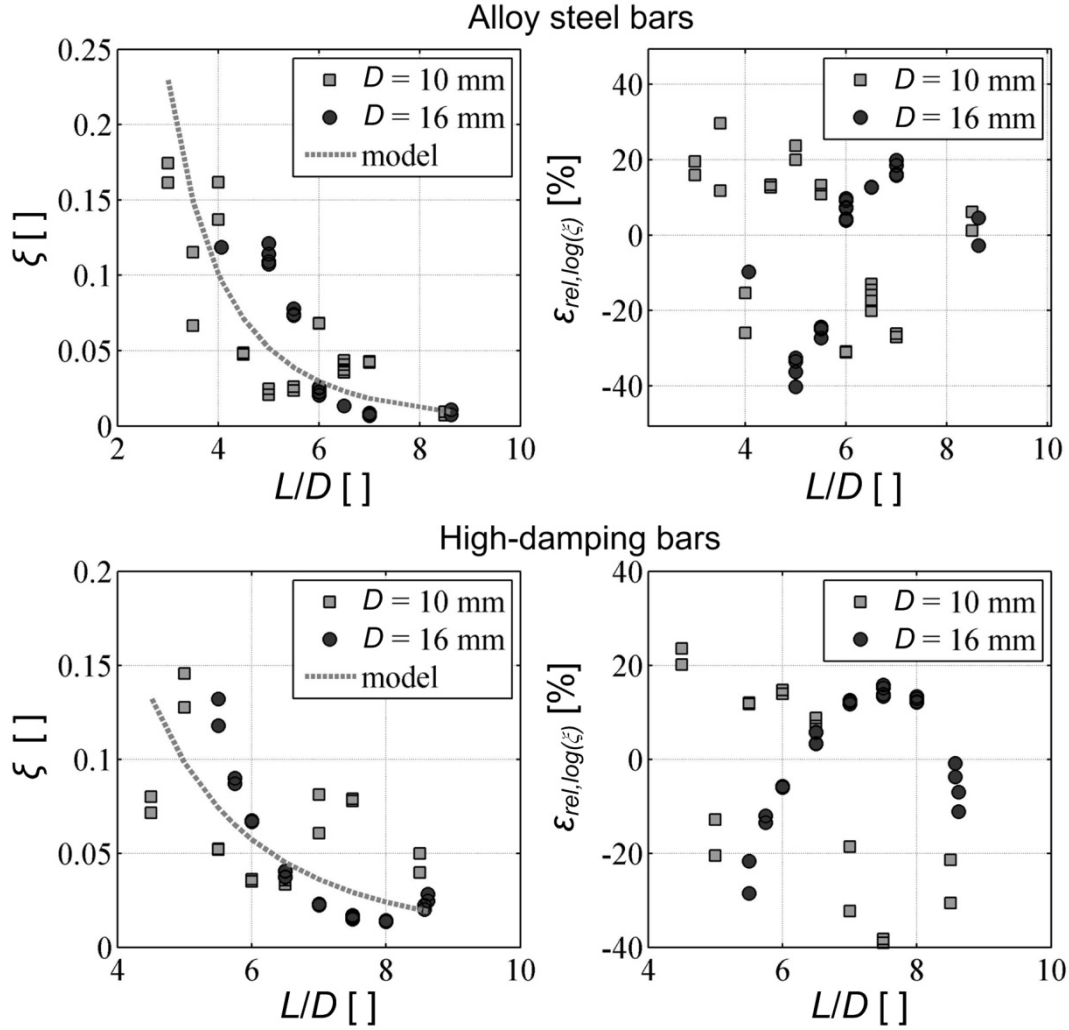
Fig. 2.10 Damping coefficients: experimental results and estimated trends [8]

By linear regression of experimental data, the Rayleigh model coefficients were estimated: unfortunately, evaluating relative errors $\varepsilon_{rel,log\xi}$, the model did not provide the better solution as reported in Tab. 2.6.

$$\varepsilon_{rel,log\xi} = \frac{log(\xi_{1,mod}) - log(\xi_{1,exp})}{log(\xi_{1,exp})} \ [\%] \tag{2.42}$$

Accordingly, a new empirical model was proposed:

$$\xi_{1,exp} \cong \tau(L/D)^{\psi} \tag{2.43}$$

The model is based on two unknown coefficients τ and ψ, the former depending on bar material while the latter being independent of bar material.

On the average, damping coefficients were higher in the case of high-damping boring bars, thanks to the higher intrinsic damping capabilities of sintered carbide materials, as demonstrated by the estimation of τ coefficients for the two analysed boring bar materials (see Tab. 2.6).

The second proposed model demonstrated better interpolation capabilities than the Rayleigh model. Moreover, a smaller number of unknown model coefficients were used (three instead of four).

It has to be pointed out that data dispersion around predicted values is considerable. Nevertheless, it is very difficult to improve the model due to the intrinsically unpredictable behaviour of the most damped mechanical system.

By using the estimated model coefficients it is now possible to obtain the approximate boring bar dynamic model of Eq. 2.12, for any given tooling system configuration. Also, a measure of model accuracy is now available thanks to the analysis of relative errors.

Tab. 2.6 Comparison between Rayleigh and proposed model for damping coefficients estimation [8]

Model	Material	τ	ψ	$\mu_{\varepsilon rel,log\xi}$ [%]	$\sigma_{\varepsilon rel,log\xi}$ [%]
Rayleigh	Standard alloy steel	0.50	5.98e-5	-54.7	97.0
	High carbide material	6.69	6.74e-5	-30.0	63.4
Proposed model	Standard alloy steel	6.52	-3.014	-3.2	20.3
	High carbide material	12.66	-3.014	-2.5	17.0

2.5. Conclusions

In precision manufacturing of mechanical components, the dynamic and static behaviour of the machining system can affect the required accuracy of the machined part. Flexibility of the cutting system, especially at tool – workpiece contact point causes poor surface quality and dimensional errors. Therefore in Precision Manufacturing the knowledge of dynamic and static behaviour of the cutting system is crucial.

The weakest element of the kinematic chain dominates the dynamic relative compliance between tool and workpiece at the instantaneous point of contact. For this purpose, in literature, several dynamic models of tooling systems have been proposed and discussed, especially in internal turning and finishing milling.

In this Chapter, an innovative hybrid dynamic model of the tooling system in internal turning, based on FE beams and empirical models is illustrated. The model was based on physical and geometrical assumptions and it was refined using experimental observations derived from modal testing of boring bars with different geometries and materials.

In light of the experimental results and the consideration presented, the following conclusions may be drawn.

- In most experimental cases, boring bar dynamics measured at the tool tip can be approximated by a single harmonic oscillator: the modal parameters are the static compliance G_{u3F3}, the main natural frequency f_{n1} and the damping coefficient ξ_1 of the dominant mode of vibration.

- In order to model the tooling system dynamic behaviour in internal turning, a hybrid approach was proposed, to combine a Timoshenko FE model of the boring bar with the dynamics of toolholder experimentally evaluated.

- In order to obtain good interpolation results, an additional bar overhang should be considered, modelling the non-ideal constrain at the toolholder-boring bar interface: best results were achieved assuming that both the ratio of the additional bar overhang to bar diameter both the static compliance of the tooling system evaluated at *Node 0* were constant and independent on boring bar material and geometry.

- The developed model was able to estimate static compliance and main natural frequency of the system with good agreement with experimental results considering several aspect ratio *L/D* and different materials of the boring bar.

- Young Modulus estimates of conventional alloy steel and high damping carbide were in accordance with the expected values, confirming the higher stiffness of the latter (between twice and three times).

- The application of Timoshenko beam model did not greatly improve data interpolation in comparison with Euler-Bernoulli beam: the effect of toolholder-boring bar interface was adequately taken into account.

- Estimated static compliances were in good accordance with experimental values, with small relative errors ($|\mu_{\varepsilon rel,G}| < 2.3\%$ and $\sigma_{\varepsilon rel,G} < 7.3\%$ for both bar materials);

- Predicted frequency resonances were in accordance with experimental results, even if values were slightly higher considering high damping carbide boring bar for a fixed bar geometry ($|\mu_{\varepsilon rel,f}| < 1.6\%$ and $\sigma_{\varepsilon rel,f} < 8.7\%$ for both bar materials);

- Frequency resonance estimates regarding boring bar of bigger external diameters were affected by a greater discrepancy due to the dynamic interaction between bar and spindle-tool holder; it caused resonance peaks which could not predicted by the model.

- Experimental damping values mainly depended on the *L/D* ratio and on the bar material; moreover they were about double in the case of high damping carbide boring bar thanks to the higher intrinsic damping properties of sintered carbide material with respect to the alloy steel.

- The combination of higher stiffness and more effective damping can explain the superior dynamic behaviour of high damping boring bars during machining.

- Rayleigh theory for damped mechanical system was not suitable in modelling tooling systems damping behaviour: a new and simpler empirical model based on a smaller number of model coefficients was proposed, achieving a better interpolation capability of experimental data ($|\mu_{\varepsilon rel,log\xi}| < 3.2\%$ and $\sigma_{\varepsilon rel,log\xi} < 20.3\%$ for both bar materials); it is very difficult to further improve the model due to the intrinsically stochastic nature of damped mechanical systems.

Modelling the dynamic behaviour of a cutting system is crucial for optimization of a cutting process. It allows the development of predictive system able to avoid chatter onset, it supports in the selection of a proper tooling system to guarantee a stable cutting process and it can help in tooling system design. Unfortunately, analysing and understanding the dynamics of a cutting system is very complex: it requires specific technical competences and involves extensive and demanding experimental tests.

Chapter 3.

CUTTING FORCES MODELLING IN TURNING PROCESS

Cutting forces models play a key role in tool condition monitoring, thermal analysis, tool life estimation and chatter prediction. Indeed, they are employed with the purpose of analysing and understanding the physical interaction of the workpiece and the cutting tool. Moreover, they are often included in more complex analytical or semi-empirical models aiming at prediction of the static and dynamic behaviour of the cutting process or for detection applications.

In the following, most important cutting force models proposed in literature are exposed. Then a simple semi-empirical approach for cutting forces modelling is proposed and experimentally validated. This approach is recalled in the next chapters of the thesis: it will represent a fundamental module for a chatter prediction model considering an internal turning process (Chapter 4) and it will be applied for investigating the machinability of a difficult to cut material (Chapter 5).

3.1. Cutting forces modelling

In a single point cutting operation, the resultant cutting force F can be decomposed into the main cutting force F_c – parallel to cutting speed v_c –, the feed cutting force F_f – parallel to workpiece axis – and the back cutting force F_p, which is parallel to the radial direction, as illustrated in Fig. 3.1.
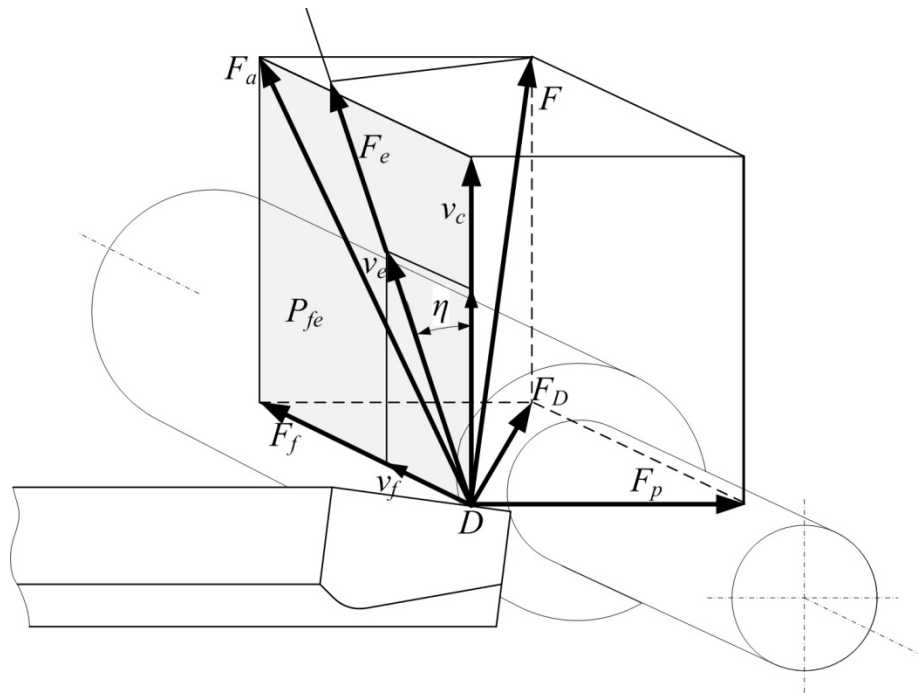
Fig. 3.1 Cutting forces distributions in a single point machining

3.1.1 Main approaches for cutting forces modelling and literary review

While machining, cutting material close to the tool tip shows plastic deformation: it turns in chip after shearing on the rake face of the cutting tool. The plastic deformation mainly occurs at the primary shear zone, which is often modelled by a plane P_{sh} (see Fig. 3.2). The dimension of the deformed zone depends on the cutting conditions: in the case of low cutting speed, the thickness of the shear zone is large, whereas at high cutting speed it becomes very narrow, approaching to a plane.

Several analytical models of cutting mechanics were developed starting from about 1940. The predictive capabilities of such analytical approaches are limited, because of the strong (often unrealistic) simplifications they are based on.
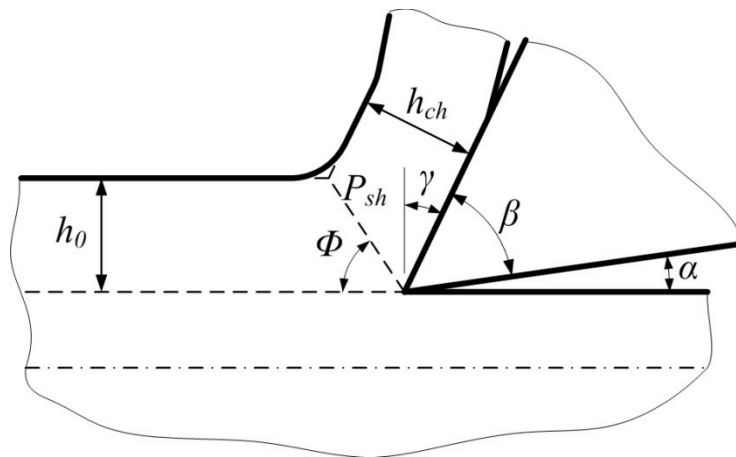
Fig. 3.2 Shear plane P_{sh} and shear angle ϕ in turning process

One of the first analytical model of cutting forces was developed by Ernst and Merchant for the orthogonal cutting process, and subsequently for oblique cutting process [24].The model did not consider the uncut chip area, tool wear and the specific cutting pressure, therefore it was not in accordance with experimental results. Later, Rubenstein [25] proposed an analytical approach for cutting force modelling including the effect of the geometry of cutting edge, especially tool nose radius and the relief angle, but he did not take into account the influence of tool wear and the importance of the geometry of the rake face of the cutting tool. Lee and Shafer [26] considered the influence of cutting temperature and of the inertia on the cutting forces together with tool edge geometry: their model was not effective since only the rigid-perfectly plastic material was analysed.

In order to overcome the modelling shortcomings of previous theories, Oxley [27] proposed an analytical approach to model cutting forces taking into account the influence of the material properties and the effect of strain, strain rate and temperature on the chip formation process. The main contribute of the Oxley's theory was to apply a concept of velocity of modified temperature in order to describe material properties as a function of strain rate and temperature. For this reasons several researchers applied or modified Oxley's approach aiming at modelling cutting forces [28] [29].

Further analytical models for cutting forces were recently proposed by Li et al. [30] and Cheng et al. [31], see Tab. 3.1. The former included the workpiece material properties and the cutting conditions, considering also the cutting temperature effect, the latter considered the influence of the tool wear on cutting forces.

Other theories are based on semi-empirical approaches, due to the inaccuracy of the afore mentioned purely analytical approaches.

Specifically, semi-empirical approaches are based on mechanistic cutting force models inspired by basic physical principles. Such models contain unknown coefficients which are calibrated by means of direct experimental measurements. By so doing, a good compromise between model accuracy and simplicity is achieved.

The cutting pressure k_c can be expressed as the ratio of main cutting force F_c and the uncut chip area A:

$$k_c = \frac{F_c}{A} = \frac{F_c}{b \cdot h} \tag{3.1}$$

In the literature, the specific cutting force is usually denoted by k_s. For the sake of consistent with the formulations in the following Chapter, the notation k_s is used instead on k_c.

In order to describe the behaviour of the specific cutting pressure against cutting parameters, Kienzle-Victor [32] introduced a new formulation of F_c such as:

$$F_c = k_s \cdot A = k_{s1} b h^{(1-m)} \tag{3.2}$$

where b is the cut width whereas k_{s1} (equal to k_s if A is unitary) and m are constant values depending especially from cutting material.

Following author's considerations, the specific cutting force causes the plastic deformation of a small volume of cutting material due to the increasing of cutting specific energy with decreasing of the uncut chip thickness. For this reason, specific cutting force decreases if the uncut chip thickness is increasing. In addition, it also depends on the cutting material properties, cutting speed, cutting tool material and geometry, cutting tool wear and cutting conditions. Therefore, the formulation proposed by Kienzle was:

$$k_s = k_{s11} h^{-z} k_v k_\gamma k_T \tag{3.3}$$

where k_{s11} is the nominal cutting pressure, the term h^{-z} considers the uncut chip thickness, k_v depends on the cutting speed, k_γ is related to the cutting tool geometry and k_T includes the cutting material properties. Saglam et al. [33] based on this theory their cutting forces modelling in turning.

A further semi-empiric approach for modelling cutting pressure is the Shearing and Ploughing model, introduced by Pohl in 1934 [34], which is widely used by several authors [35] [36] [37] [38] (Tab. 3.1).

Accordingly, the cutting pressure can be estimated basing on the formulation:

$$k_s = k_{cs} + \frac{k_{cp}}{h} \tag{3.4}$$

Therefore, the main cutting forces can be expressed by a linear relation:

$$F_c = k_{cs} \cdot A + k_{cp} \cdot B \tag{3.5}$$

where A is the cross-sectional chip area and B is the length of the cutting edge engaged in the workpiece.

Therefore, the cutting force is expressed as the sum of two terms:

1. The shearing term which models the effect of the chip pressure on the tool face, proportional to the uncut chip section area;
2. The ploughing term which models the friction between the flank of the tool and the machined surface, proportional to the engaged cutting edge length.

On the contrary of previous analytical cutting force models, the Shearing and Ploughing model considers the changing of tool edge geometry due to tool wear; tool wear has a strong effect in cutting forces: it induces a growth of the cutting edge thickness, increasing the cutting forces.

In order to be thorough, finally, it has to be pointed out that a further approach is found in literature aiming at modelling cutting forces for a given machining process, i.e. the pure experimental approach, see Tab. 3.1. Its implementation is more recent than the analytical and semi-empirical methods, thanks the deeper knowledge during last years about the statistical design of experiment methodology, computational neural network or genetic algorithm technique [39] [40] [41].

Tab. 3.1 Cutting forces modelling: Literary review

Ref.	Purpose	Approach	Cutting process	Instruments
[28]	Describe effect tool of thermal properties on cutting forces	Analytical (Oxley theory)	Hard turning	None
[29]	Modify Oxley formulation to extend applicability to several cutting materials	Analytical (Oxley theory)	Orthogonal cutting	Thermocouple
[30]	Create predictive model for cutting forces, stress and temperature distributions	Analytical	Orthogonal cutting	None
[31]	Include the effects of tool wear with nose radius in cutting forces prediction	Analytical	Turning	3-axial dynamometer Infrared detector Microscope CMM
[33]	Investigation of effects of tool geometry and cutting speed in cutting forces and temperature	Semi-empirical (Kienzle theory)	Turning	Dynamometer InGaAs radiation sensor
[37]	Provide a cutting force model for internal turning process considering tool geometry and cutting parameters	Semi-empirical (S&P model)	Internal turning	Dynamometer
[39]	Investigate effects of cutting parameters on cutting forces and tool wear	Empirical (Regression technique)	Hard turning	3-axial dynamometer Microscope
[40]	Investigate effects of cutting parameters on cutting forces and surface quality	Empirical (Regression technique)	Hard turning	Dynamometer Surface tester
[41]	Investigate effects of workpiece hardness and cutting parameters on cutting forces and quality surface	Empirical (Response surface method)	Hard turning	Hardness tester Microscope Dynamometer Surface tester

3.2. Cutting forces modelling in turning

For a generic curved cutting edge, distribution of main cutting force and normal cutting force is not uniform along the contact length between cutting edge and workpiece, see the schematization in Fig. 3.3. Cutting force distributions are dependent on the cutting edge geometry (cutting edge angle χ, tool included angle ε, nose radius r_ε) and on the cutting parameters (depth of cut a_p, feed f and cutting speed v_c): these factors determine the shape of the uncut chip area A and the total contact length B.
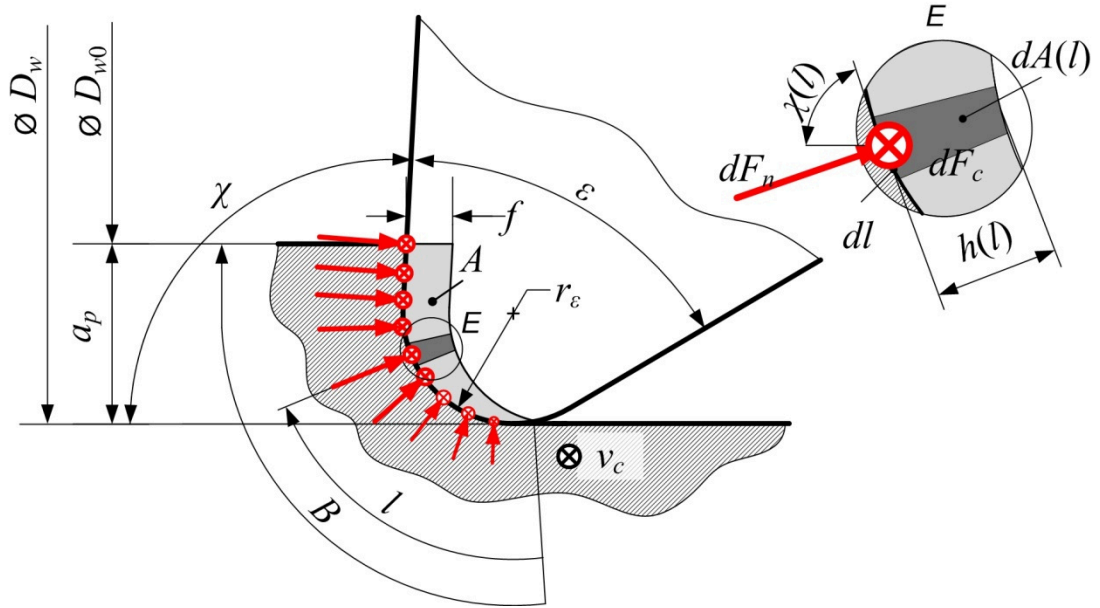
Fig. 3.3 Cutting forces on the tool tip: Schematization for turning process [42]

The Shearing and Ploughing – S&P – model is based on the assumption that the resultant cutting force acting on the tool is a sum of infinitesimal contributions [37] [38]; hence, it will be:

$$\begin{cases} dF_c = k_{cs}dA(l) + k_{cp}dl \\ dF_n = k_{ns}dA(l) + k_{np}dl \end{cases} \tag{3.6}$$

where dF_c and dF_n are the main cutting force and the normal cutting force acting on the infinitesimal cutting edge dl, respectively; dA is the infinitesimal uncut chip area depending on the local uncut chip thickness.

Local uncut chip thickness h is dependent on the curvilinear abscissa l; consequently, local uncut chip area, as well as the infinitesimal main cutting force dF_c and normal force dF_n are dependent on l. The cutting force coefficients $\left(k_{cs}, k_{cp}\right)$ and $\left(k_{ns}, k_{np}\right)$ are used to model the influence of dl and dA on the cutting force components. It has to be pointed out that the influence of cutting speed v_c on S&P cutting force coefficients is neglected.

According to the schematization in Fig. 3.3, integrating along the cutting edge, cutting force components are obtained as follow:

$$\begin{cases} F_c = \int_0^B dF_c = k_{cs}A + k_{cp}B \\ F_p = \int_0^B cos\chi dF_n = k_{ns}\left[\int_0^B cos\chi dA\right] + k_{np}\left[\int_0^B cos\chi dl\right] \\ F_f = \int_0^B sin\chi dF_n = k_{ns}\left[\int_0^B sin\chi dA\right] + k_{np}\left[\int_0^B sin\chi dl\right] \end{cases} \qquad (3.7)$$

It has to be pointed out that the evaluation of the effective shape of the uncut chip section area A, of the total length of contact B and of the elements on the brackets, can be very complicate, especially when feed f is of the same order of magnitude of nose radius r_ε. Therefore, these elements are estimated by regression technique of experimental results, as demonstrated in the following section [42].

3.2.1 Experimental set-up and data analysis

In order to demonstrate the effectiveness of the proposed cutting forces model, S&P cutting force coefficients were estimated experimentally, for a selected combinations of workpiece materials – cutting tool. This investigation was included in a scientific work recently published in the *International Journal of Machine Tools & Manufacture* in 2012 [42].

Cutting tests were performed in a multifunction CNC lathe Okuma Multus B300W in dry condition. A special turning dynamometer [38] was applied for triaxial cutting force measurement in external turning (see Fig. 3.4).
Two workpiece materials, were considered for this research: C45 steel (213HB) and aluminium alloy Al7075 (ERGAL, 151HB).

A Design of Experiment (see Tab. 3.2) was carried out for each selected cutting material.
For each cutting material, rhombic inserts with 11mm side length and included angle ε of 55° was selected. All cutting inserts were fixed on a special toolshank described in [38] in order to allow cutting force measurements. By so doing, the entering angle χ was 93° and the effective cutting edge inclination λ was 0°. The following cutting inserts were applied: Sandvik DCMT11T304PF, DCMT11T308PF, all of grade CT5015 for C45 and Sandvik DCGT11T302UM, DCGT11T304UM, all of grade GC1125 for Ergal.
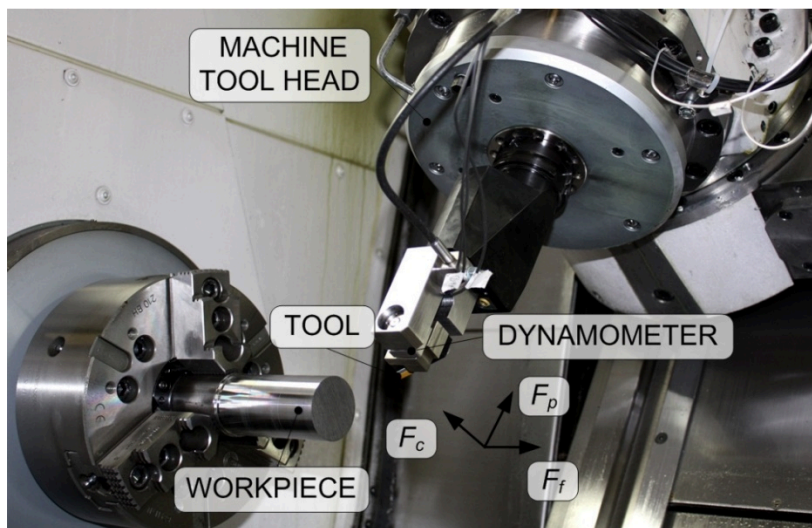
Fig. 3.4 Experimental set-up for cutting forces model coefficients estimation [42]

Tab. 3.2 Cutting forces model coefficients identification: DOE [42]

Factor	Levels	Values
Workpiece material	2	C45, Ergal
Depth of cut a_p [mm]	11	0.1, 0.15, 0.2, 0.25, 0.3, 0.4, 0.5, 0.6, 0.8, 1, 1.2
Cutting speed v_c [m/min]	2 - 3	250, 350, 450 (C45); 600, 800 (ERGAL)
Feed f [mm/rev]	3	0.08, 0.12, 0.16
Tool nose radius r_ε [mm]	3	0.2, 0.4, 0.8

For a fixed workpiece material and tool nose radius, cutting forces were measured, see Fig. 3.5. By analysing the experimental cutting force trends, it was observed that feed force F_f and the main cutting force F_c depended almost linearly on depth of cut a_p and feed f, while their dependence on cutting speed v_c and nose radius r_ε was practically negligible. Specifically, main cutting force F_c was proportional to the uncut chip area A that is given by the product between f and a_p, with good approximation, independently from tool nose radius and cutting parameters, confirming the hypothesis of the Shearing and Ploughing model. On the contrary, back force F_p had a strong nonlinear behaviour against depth of cut a_p, a linear behaviour against feed f, it was very sensitive to nose radius r_ε and it was not considerably affected by cutting speed v_c. These experimental observations were in accordance with the assumptions of the proposed cutting force model, as evidenced by the satisfactory model adequacy parameters listed in Tab. 3.3.
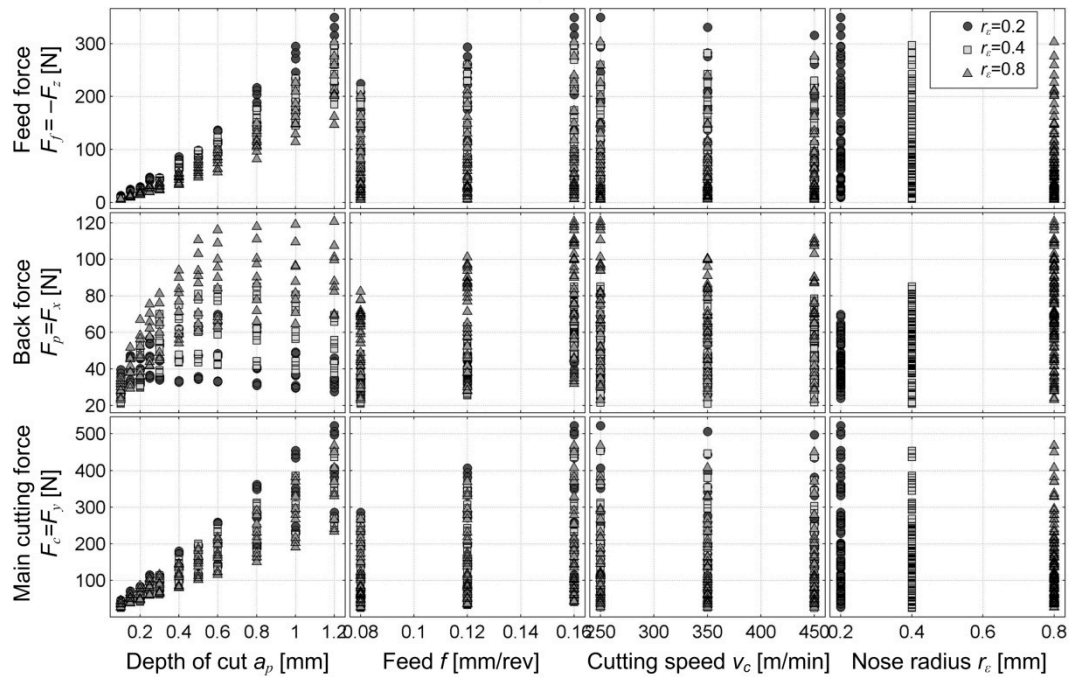
Fig. 3.5 Scatter plot of experimental cutting forces against input factors while machining C45 [42]

Tab. 3.3 Cutting forces model: estimated model coefficients and model adequacy parameters [42]

		Ergal	C45
Average measured cutting pressure	k_s [N/mm^2]	1059	2606
Cutting force model coefficients	k_{cs} [N/mm^2]	796	2428
	k_{cp} [N/mm]	20.4	10.5
	k_{ns} [N/mm^2]	117	1437
	k_{np} [N/mm]	32.8	37.7
Squared correlation coefficients	R^2_{Fc} [ ]	0.997	0.972
	R^2_{Ff} [ ]	0.966	0.964
	R^2_{Fp} [ ]	0.901	0.890
Average of relative errors	$\mu_{\varepsilon Fc}$ [%]	-0.6	-4.2
	$\mu_{\varepsilon Ff}$ [%]	1.7	1.1
	$\mu_{\varepsilon Fp}$ [%]	2.6	-8.9
Standard deviation of relative errors	$\sigma_{\varepsilon Fc}$ [%]	4.2	12.3
	$\sigma_{\varepsilon Ff}$ [%]	14.9	17.0
	$\sigma_{\varepsilon Fp}$ [%]	20.1	22.3

3.3. Conclusions

The physical interaction between the cutting tool edge and the machined surface causes plastic deformations and stress, which in turn result in substantial cutting forces. The knowledge of cutting forces is fundamental in understanding cutting process mechanisms: they affect the tool life, the chip formation mechanism, the stability of the process and the workpiece surface integrity. Therefore, forces modelling is fundamental for optimising of the cutting process: it can be employed for a thermal analysis or for investigating the tool wear mechanisms, but it can be also included in more complex models, for example in chatter prediction technique, in adaptive control applications, or in the formulation of simulation models of the cutting process.

Cutting forces are affected by the tool edge geometry, tool wear rate, cutting temperature and cutting parameters; therefore analytical models can be very complex in order to reach good accuracy in representing the effective cutting mechanics.

For this reason, one of the most applied technique in forces modelling is the semi-empirical approach, especially the Shearing and Ploughing model. According to the definition of the specific cutting pressure k_s, the model includes the effect of the pressure of the chip on the tool face and the influence of the friction between the rake face and machined surface. In adding, it comprises all the most effective cutting factors, such as the tool nose radius, the rake face geometry and cutting parameters (depth of cut and feed).

In this Chapter, a simple semi-empirical model of cutting forces, based on the S&P theory, is presented. By experimental tests, the Shearing and Ploughing coefficients have been estimated by performing the regression technique of the data. From the observation of the experimental trends of the actual forces, the basic hypothesis of the model were confirmed. Accordingly, it was demonstrated the high accuracy of the cutting forces model: the average of relative errors $\mu_{\varepsilon F}$ was less than 3% for Ergal material and less than 9% considering the C45 steel, with maximum standard deviation $\sigma_{\varepsilon F}$ of 20.1% and 22.3%, respectively.

The proposed model has been implemented in two different scientific works which are object of the following Chapters of this thesis.

Chapter 4.

NEW APPROACHES FOR CHATTER AVOIDANCE AND PREDICTION IN INTERNAL TURNING

In this Chapter, the anomalous vibratory phenomena – chatter – which may arise during the cutting process will play a central role. New approaches for avoidance and prediction of such undesired phenomena in internal turning will be presented. These innovative methodologies can be extended to other similar machining operations, therefore they represent an advance in the field of Precision Manufacturing.

Firstly, a theoretical background of the dynamic behaviour in orthogonal metal cutting will be recalled. Afterward, the tool-workpiece dynamic interaction in internal turning will be analysed in order to provide a semi-empirical model for the selection of stable tooling system configuration in internal turning.

Main results presented in this Chapter have been recently published in the *International Journal of Machine Tool & Manufacture* [42].

4.1. Introduction

During a cutting process, vibrations occur between the cutting tool and the workpiece at the instantaneous point of contact. In high precision manufacturing, optimization of the process may be affected by vibrations onset; particularly they can be detrimental for the workpiece accuracy.

Relative displacements between the cutting tool and the workpiece can be split into three main categories:

- *free vibrations*: they always occur due to the action of transient cutting forces (e.g. when the tool enters or exits the workpiece) on the machining system which behaves like a dynamic linear system; they are usually neglected since they do rapidly fade out and have small effects on the process;

- *forced vibrations*: they are the normal consequence of periodic cutting forces which are typical of some machining operations such as milling and turning in interrupted cutting conditions. They may influence the overall machined surface quality. Such vibrations cannot be completely avoided. In most cases of practical interest their effects are small or negligible, unless the harmonics of the input forces excite the resonance frequencies of the mechanical system.

- *Self-excited vibrations, named chatter*: they result from the dynamic instability of the cutting system. Chatter vibrations are unstable and chaotic and negatively affect part precision and surface quality (see Fig. 4.1 as an example). In worst cases chatter can cause abnormal tool wear, tool breakage or damages of the tooling system and/or of the machine tool.

Main physical mechanisms responsible for chatter is the regenerative effect: it derives from the combination of the instantaneous tool-workpiece relative vibrations with the waviness of the machined surface left by the cutting tool at the previous passage [35]. Regenerative chatter is dominant at medium-high spindle speed. At low spindle speed, rubbing of tool major flank against the machined surface tends to attenuate chatter vibrations [43]: this phenomenon is called process damping and it is principally caused by friction between the tool and the chip/workpiece on contact surfaces, stress distribution on the normal rake face, thermoplastic behaviour of the chip material and others.

Avoidance of chatter phenomenon is crucial in high-precision manufacturing. However, prevention or detection of self-exciting vibrations can be very complex due to the several parts composing the tooling system, which define, together with their interactions, its static and dynamic behaviour. In cutting process like internal turning or peripheral milling, the high flexibility of tooling systems determines an higher sensitive to the chatter phenomena rather than other cutting process. For this reason, this Chapter focuses on the investigation of chatter avoidance in internal turning.
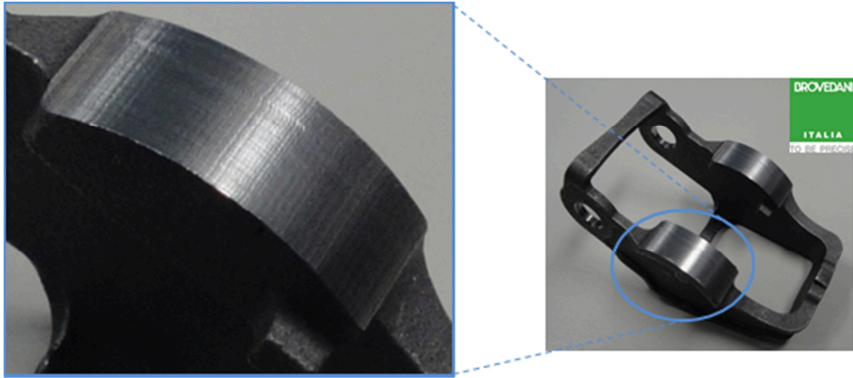
Fig. 4.1 Example of chatter marks in peripheral milling operation (courtesy of Brovedani SpA)

4.2. Theoretical background

Considering a longitudinal single point machining, the transfer function $W(j\omega)$ can be considered as the combination of the workpiece transfer function in the radial direction $W_w(j\omega)$ and the tool transfer function in the feed direction $W_t(j\omega)$, see Fig. 4.2.
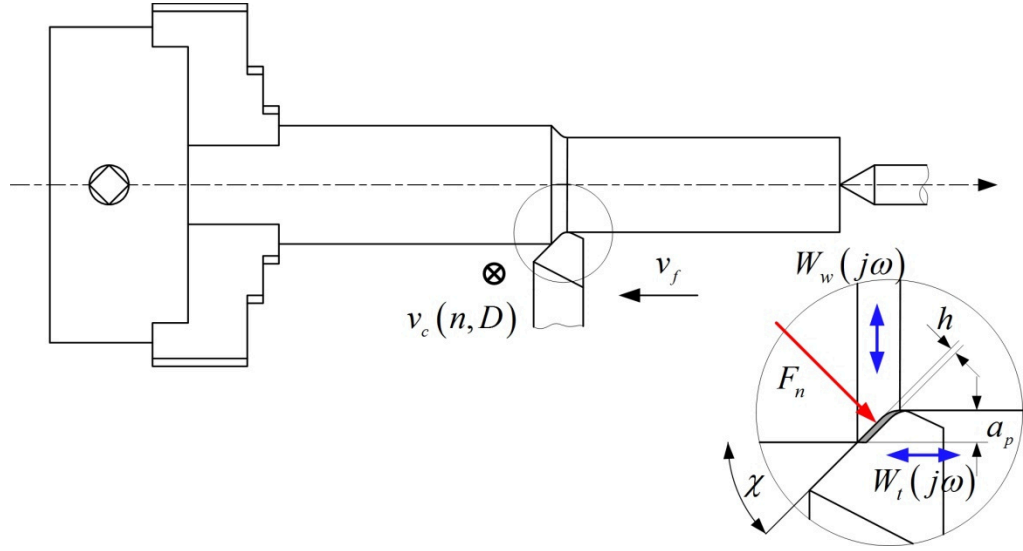
Fig. 4.2 Longitudinal external turning cutting process: schematization

The component F_n due to cutting process mechanics which is orthogonal to the cutting edge and to the cutting velocity can be expressed as a linear function of the instantaneous cross-section chip area $A(t)$:

$$F_n = k_{ns} \cdot A(t) = k_{ns} \cdot a_p \cdot \frac{h(t)}{sen(\chi)} \tag{4.1}$$

where:

- k_{ns} is the normal shearing cutting force coefficient acting in the normal direction;
- $A(t)$ is the instantaneous cross-section chip area;
- a_p is the depth of cut;
- $h(t)$ is the instantaneous uncut chip thickness;
- χ is the working cutting edge angle of the main cutting edge.

By projecting the normal force along axial-feed and radial directions one can obtain the force components acting on the tool and on the workpiece respectively:

$$F_t = F_n \cdot sen(\chi) \tag{4.2}$$

$$F_w = F_n \cdot \cos(\chi) \tag{4.3}$$

Therefore, the corresponding tool and workpiece dynamic vibrations can be expressed as:

$$u_t(j\omega) = W_t(j\omega)F_t(j\omega) = W_t(j\omega)F_n(j\omega)sen(\chi) \tag{4.4}$$

$$u_w(j\omega) = W_w(j\omega)F_w(j\omega) = W_w(j\omega)F_n(j\omega)cos(\chi) \tag{4.5}$$

The total relative vibration, $u(j\omega)$ affecting uncut chip thickness in the direction orthogonal to the main cutting edge is given by:

$$u(j\omega) = u_w(j\omega) \cdot \cos(\chi) + u_t(j\omega) \cdot sen(\chi) \tag{4.6}$$

Thus, by substituting Eq. 4.4 and Eq. 4.5 into Eq. 4.6, one obtains:

$$u(j\omega) = F_w(j\omega)W_w(j\omega) \cdot \cos(\chi) + F_t(j\omega)W_t(j\omega) \cdot sen(\chi) =$$
$$= F_n(j\omega)[W_w(j\omega) \cdot \cos^2(\chi) + W_t(j\omega) \cdot sen^2(\chi)]$$

(4.7)

Accordingly, the oriented transfer function is:

$$W(j\omega) = \frac{u(j\omega)}{F_n(j\omega)} = W_w(j\omega) \cdot \cos^2(\chi) + W_t(j\omega) \cdot sen^2(\chi)$$

(4.8)

At an instant time t, uncut chip thickness $h(t)$ is modelled as the sum of a static component $h_0(t)$ and a dynamic component $h_v(t)$:

$$h(t) = h_0(t) - h_v(t) = h_0(t) - [u(t) - u(t - \tau)]$$

(4.9)

where the delay τ is equal to the spindle period.

Modelling the cutting process as a single degree system with lump mass m, stiffness k and damping c at the cutting point, dynamic model can be written as:

$$m\ddot{u}(t) + c\dot{u}(t) + ku(t) = k_{ns}a_p\{h_0(t) - [u(t) - u(t - \tau)]\}$$

(4.10)

which is a delayed differential equation. The transfer function can be expressed as:

$$\frac{h(s)}{h_0(s)} = \frac{1}{1 + (1 - e^{-s\tau})k_{ns}a_pW(s)}$$

(4.11)

Hence, chatter stability conditions are determined by the characteristic equation:

$$1 + (1 - e^{-s\tau})k_{ns}a_pW(s) = 0$$

(4.12)

If specific cutting pressure k_{ns} is assumed to be constant, chatter stability of the system depends on the depth of cut a_p and spindle rotation period τ. Machining system will be stable, critical stable or unstable depending on the roots of the characteristic equation.
The system is critically stable when the real part of the roots is zero: the vibrations neither grow exponentially nor diminish, but are sustained with equal amplitude, i.e. $u(t) = u(t - \tau)$ at a chatter vibration frequency ω_c [35].
By assuming that the system is vibrating at a chatter pulsation, i.e. $\omega_c \approx \omega_n$, a critical depth of cut is defined, as the value over which the system will be unstable or critical stable:

$$a_{p,cr} = \frac{-1}{2k_{ns}Re(W(j\omega_c))}$$

(4.13)

The formulation is valid if and only if:

$$\omega_c > \omega_n$$ (4.14)

$$Re(W(j\omega_c)) < 0$$ (4.15)

Therefore, chatter does not occur if the applied depth of cut is smaller than the critical value derived from Eq. 4.13.

A common approach is to represent the stable and unstable cutting conditions on the stability lobe diagram (Fig. 4.3): for each spindle speed n, the critical depth of cut a_p can be compute, separating the stable from the unstable areas. The unstable region is represented by a set of lobes: the horizontal position depends on the natural resonance frequency of the machining system.

Stability diagram is very useful in identifying chatter onset for a given specific cutting pressure k_{ns}. Unfortunately, the creation of stability chart for a given cutting system requires the knowledge of the dynamic properties of the system under investigation.
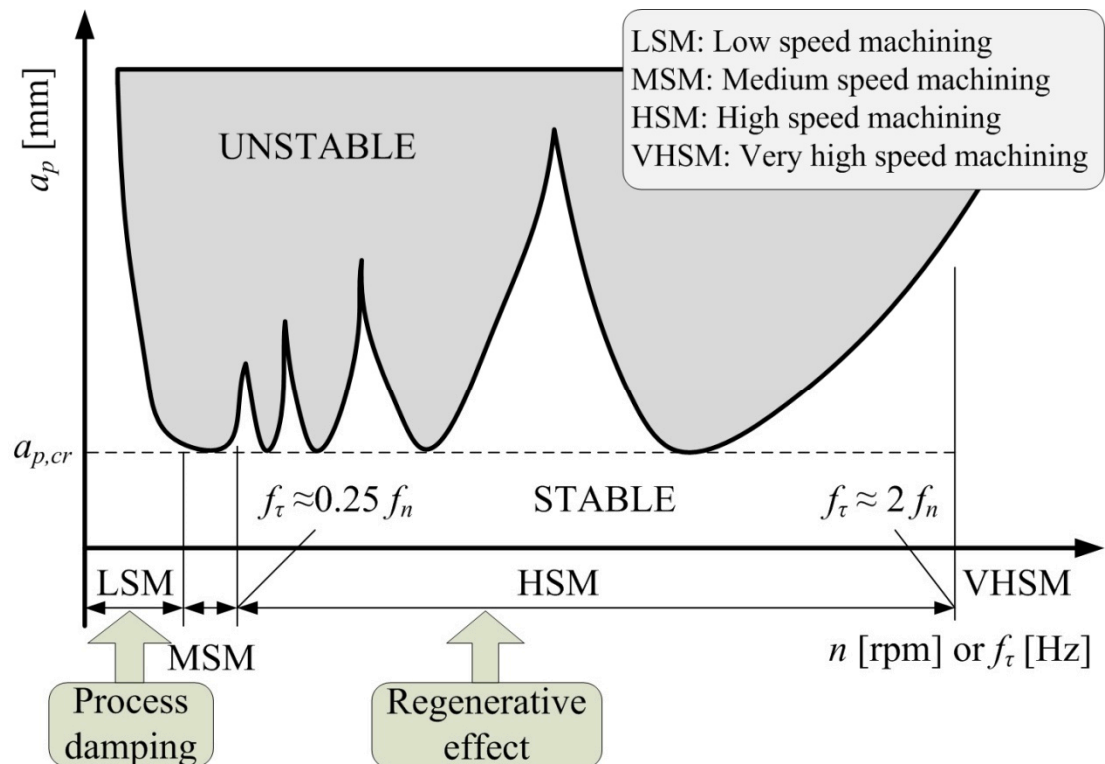
Fig. 4.3 Stability lobe diagram [44]

4.3. Chatter vibrations: literary review

Research works dealing with chatter vibrations can be split into three main categories, depending on their main focus:

1. Chatter detection, see Tab. 4.1;
2. Chatter suppression, see Tab. 4.2;
3. Chatter prediction, see Tab. 4.3.

Chatter detection is based on the application of single or multisensor system installed on the machine tool, in order to monitoring cutting process. Alternatively, special algorithms are generated for in-process chatter identification. For example, Gradisek et al. [36] evaluated

stability of the process basing on the analysis of the coarse grain entropy. Tangjisitcharoen [45] developed a chatter detection system based on the Power Spectrum Density analysis of the dynamic cutting forces. Tansel et al. [46] analysed acceleration signals measured during cutting. A further strategy was applied by Dimla [47]: author took in account tool wear condition as a monitoring phenomenon to detect instability in turning process.

Tab. 4.1   Chatter detection: Literary review

Ref.	Cutting process	Approach / Theory	Sensors	Workpiece
[36]	Dry turning	Coarse grain entropy	Dynamometer	Steel CS45
[45]	Dry turning	Power Spectrum Density	Dynamometer	Steel S45C
[46]	Turning	Laplace transformation	Accelerometer	Steel 1045
[47]	Dry turning	Tool wear	Dynamometer Accelerometer	Steel EN 8 BS 970

Chatter suppression or vibration reduction strategies aim at increasing dynamic stiffness of the machining system; alternatively, special devices are developed in order to change the main natural frequency of the system. For example, Lee et al. [48] proposed a dynamic vibration absorber at the tool tip able to suppress forced vibrations and secondary chatter. Similar system applied in internal turning was developed by Rubio et al. [49]. An Active Mass damper system was developed by Ganguli et al. [50], whereas El-Sinawi et al. [51] provided an active tool holder capable of isolating the cutting tool displacements from the vibration of the machine-tool structure. Mei et al. [16] proposed a magnetorheologic fluid controlled boring bar: using the physical properties of the fluid, it was possible to vary the main natural frequency of the system, achieving suppression of chatter phenomenon. Finally, a tuned holder for increasing boring bar stability was proposed by Houck III et al. [15]: dynamic absorber of the clamped boring bar was constituted by a flexible holder support.

Tab. 4.2   Chatter suppression: Literary review

Ref.	Cutting process	Approach / Theory	Sensors	Workpiece
[48]	Turning	Dynamic absorber	Accelerometers	Steel S45 Aluminium 6061
[49]	Internal turning	Passive dynamic absorber	None	None
[50]	Dry turning	Active mass damper	Laser Oscilloscope	Aluminium
[51]	Dry turning	Feedback active damper by magnetostrictive actuator	Roughness meas.	Aluminium 6061
[16]	Internal turning	Magnetorheological fluid boring bar	Accelerometer	AISI 1020
[15]	Internal turning	Flexible holder support	Impact hammer Accelerometer	None

Chatter prediction is a very common approach for a preventive identification of stable machining system configurations. It is based on the creation of analytical or numerical models, in time or frequency domain, aiming at anticipating chatter onset by selecting proper process parameters. Without a predictive model, the knowledge of the dynamic behaviour of the system may be possible only by applying the trial and error approach, increasing the probability of detrimental effects on the cutting system. Several predictive methods are reported in literature. Altintas et al. [35] reviewed simple prediction models for orthogonal cutting process already proposed in literature. Applying the model at internal turning and boring operations, authors highlighted the difficulties to model nonlinearities in frequency domain. Higher reliability was achieved by multidimensional models proposed by Budak et al. [52]. Authors included the actual process geometry and the tool nose radius in order to demonstrate their influence in process stability. Vela-Martinez et al. [53] proposed a multidimensional stability approach considering cutting forces exerted in an orthogonal cutting process as a function of relative displacement between tool and workpiece. Similar approach was proposed in a previous work by Rao et al. [54]: authors considered cross-coupling between workpiece and cutting tool in order to estimate instant cutting forces value; the proposed force model allowed a stability analysis of 3D turning process in roughing and finishing machining. Moetakef-Imani et al. [13] provided a tool suitable for simulating the dynamics of internal turning process by modelling the cutting tool geometry. Mahdavinejad [55] gave a FE model of a turning process taking into account machine tool structure, tool and workpiece characteristics. Urbikain et al. [56] provided a stability charts for turning deep holes by slender bar considering only one dominant mode in the tangential direction. By a numerical approach based on cutting forces measurements, they included in the model the influence of the tool geometry and of the cutting parameters.

Tab. 4.3   Chatter prediction: Literary review

Ref.	Cutting process	Approach / Theory	Sensors	Workpiece
[35]	Orthogonal cutting, Internal turning, Boring, Milling	Analytical 1DOTF	Literary review	Literary review
[52]	Turning	Analytical Multiple DOTF Frequency domain	Acoustic	Steel AISI 1040
[53]	Orthogonal cutting	Analytical Multiple DOTF Frequency domain	Only simulation	Only simulation (steel)
[54]	Oblique turning	Analytical Frequency domain	Dynamometer Accelerometer	Steel 4140
[13]	Internal turning	Analytical Time domain	Dynamometer	Aluminium
[55]	Turning	Numerical FE model	Impact hammer Accelerometer	Steel
[56]	Turning deep hole	Numerical Frequency domain	Impact hammer Accelerometers Dynamometer	Steel AISI 1045

4.4. Modelling tool tip-workpiece dynamic interaction in internal turning

In this section a developed empirical model for a practical selection of stable tooling system for internal turning cutting process will be presented. The research was recently published in the *International Journal of Machine Tool & Manufacture* in 2012 [42].

Firstly the regenerative effect between cutter and workpiece will be discussed; then a stability analysis will be performed to provide a simple model for the selection of proper tooling system. Finally, the model will be validated by experimental cutting tests.

4.4.1 The regenerative effect

Considering stability of a cutting process, radial cutting force $F_x = F_p$ strongly influences the dynamic behaviour of the system due to the regenerative effect that affects the instantaneous chip thickness [35].

Dynamic compliance measured at the tool tip in the radial direction (*X-axis*) can be approximated as:

$$W_x(j\omega) = \frac{u_x(j\omega)}{F_x(j\omega)} \cong \frac{G}{(j\omega/j\omega_n)^2 + 2\xi(j\omega/j\omega_n) + 1} \qquad (4.16)$$

where G is the static compliance expressed in m/N, ω_n is the main natural pulsation expressed in rad/s and ξ is the adimensional damping coefficients. The influence of tangential vibrations u_y is neglected in this formulation.

Let be τ the spindle rotation period, consider the following expression of the tool displacement in the previous round ($t - \tau$) (see Fig. 4.4):

$$u_{x,\tau} = u_x(t - \tau) \qquad (4.17)$$
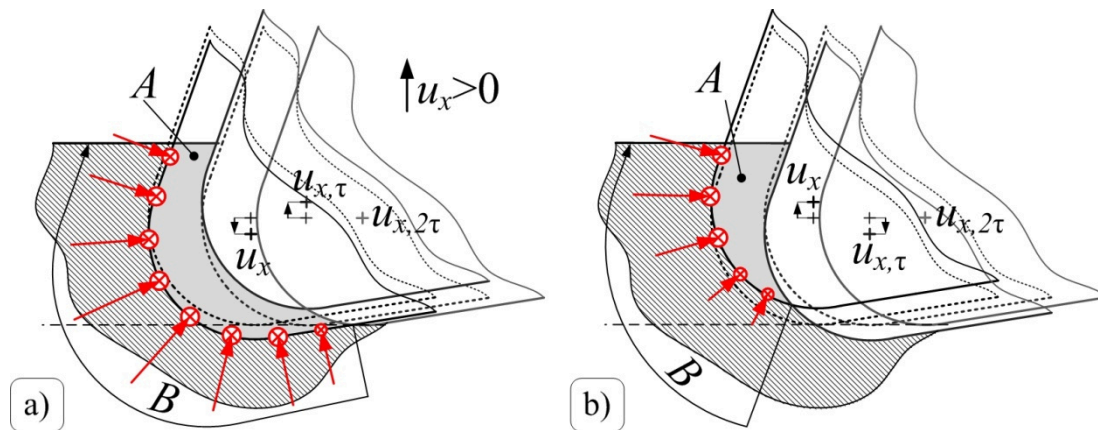
Fig. 4.4 Influence of tool tip current vibration u_x and tool tip vibration at previous round $u_{x,\tau}$ on uncut chip section area *A* and workpiece-cutting edge contact length *B*. Tool tip vibration corresponding to two rounds before $u_{x,2\tau}$ is set to zero for sake of simplicity [42]

The radial back force depends on process parameters, working material and the displacement of the tool tip as follow:

$$F_x = F_x(r_\varepsilon, \chi, a_p, f, k_{ns}, k_{np}, u_x, u_{x,\tau}) \tag{4.18}$$

Nominal back radial force F_{x0} can be formulated considering an ideal tooling system with infinite stiffness (no tool tip displacement, $u_x = u_{x\tau} = 0$) such as:

$$F_{x0} = F_x(r_\varepsilon, \chi, a_p, f, k_{ns}, k_{np}, 0, 0) \tag{4.19}$$

Let us suppose that the tooling system position has been already corrected for compensating the static displacement caused by the nominal radial back force:

$$u_{x0} = u_{x,\tau 0} = GF_{x0} \tag{4.20}$$

Under these hypothesis, the equilibrium configuration is achieved when the effective depth of cut a_p is equal to the nominal value and when no displacement of tool tip occurs, i.e.:

$$u_{x,\tau} = u_x = 0 \tag{4.21}$$

The variation of the radial back force δF_x due to radial displacement on tool tip can be expressed as:

$$\delta F_x = F_x - F_{x0} = \frac{\partial F_x}{\partial u_x} u_x + \frac{\partial F_x}{\partial u_{x,\tau}} u_{x,\tau} \cong -\left(\frac{\partial F_x}{\partial u_{x,\tau}}\right)(u_x - u_{x,\tau}) \tag{4.22}$$

Where the element

$$k_\tau = \left(\frac{\partial F_x}{\partial u_{x,\tau}}\right) \tag{4.23}$$

is defined as the regenerative radial cutting coefficient, that will depend on depth of cut, nose radius of the tool, nominal working cutting edge angle and shearing normal cutting force coefficient. It has a strong influence on the stability of the cutting process.

Theoretical regenerative radial cutting force coefficient $k_{\tau,th}$ is usually computed neglecting the influence of tool nose radius, since the depth of cut a_p is supposed to be considerably greater than nose radius. Also, feed f is generally assumed to be small in comparison with nose radius r_ε. Moreover, the calculation is carried out by considering infinitesimal vibration du_x of the tool tip and by neglecting the variation of the radial back force due to the variation of the cutting edge contact length B. As a result, the estimated regenerative radial cutting coefficient depends on depth of cut a_p, nose radius r_ε, nominal working cutting edge angle χ and shearing normal cutting force coefficient k_{ns}. Nevertheless, in a general cutting conditions, this approach is not sufficiently accurate.

Therefore a numerical approach was conceived, similar to those presented in [9] which is capable of taking into account the effect of non-zero nose radius r_ε, i.e. the effect of $a_p \approx r_\varepsilon$ together with realistic values of feed f, even when r_ε is small, and finite (non-infinitesimal) tool tip vibration δu_x. The entering angle is set to 93°. For a fixed tool nose radius, cutting parameters and cutting force coefficients, the nominal radial back force F_{x0} is first computed. A rectangular grid in the $(u_x, u_{x,\tau})$ plane, centered around the equilibrium condition $(0,0)$ is determined. Grid semi-amplitude was proportional to the static displacement estimated by Eq. 4.20. The radial back force values corresponding to the selected couples $(u_x, u_{x,\tau})$ were computed. Eventually, the regenerative cutting force coefficient k_τ was estimated by linear regression carried out on Eq. 4.22.

The calculation was repeated for different combination of input parameters (see Tab. 4.4): the behaviour of the regenerative radial cutting force coefficient is illustrated in Fig. 4.5.

Tab. 4.4   Numerical DOE for studying the regenerative radial cutting force coefficient [42]

Factor	Levels	Values
Depth of cut a_p [mm]	7	0.1, 0.2, 0.3, 0.4, 0.6, 0.8, 1.2
Feed f [mm/rev]	3	0.08, 0.12, 0.16
Nose radius r_ε [mm]	3	0.2, 0.4, 0.8
Shearing normal cutting force coefficient k_{ns} [N/mm^2]	3	100, 400, 1600
Ploughing normal cutting force coefficient k_{np} [N/mm]	3	10, 40, 160
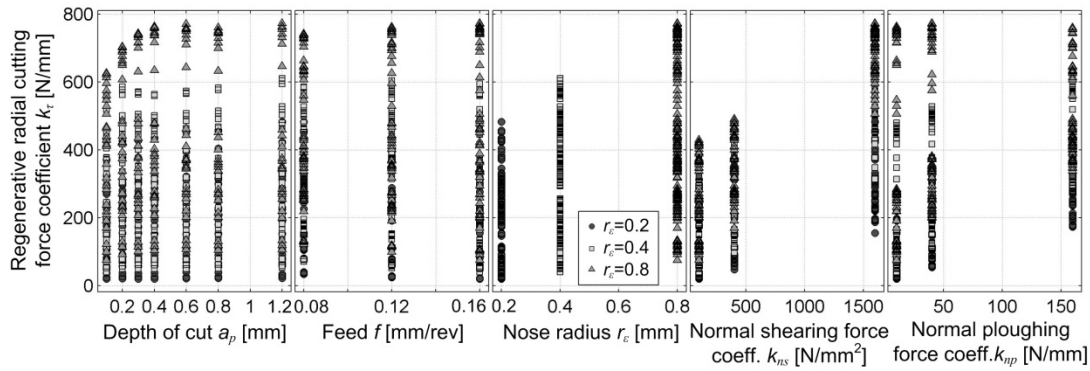
Fig. 4.5 Scatter plot diagram of regenerative radial cutting force coefficient against input factors [42]

Analysis of variance in logarithmic scale was carried out in order to evaluate the influence of input factors on the output variable k_τ. Although all factors had significant effect on the radial regenerative cutting force coefficient, *F-test* values of depth of cut and feed were negligible with respect to the other factors (see Tab. 4.5): the effect of cutting parameters could be neglected at first approximation.

Tab. 4.5   Analysis of variance of radial regenerative cutting force coefficient [42]

Source	Sum Sq.	d. f.	Mean Sq.	F
a_p	71864	6	11977	2.5
f	127216	2	63608	13.4
r_ε	5755899	2	2877949	604.4
k_{ns}	10276654	2	5138327	1079.1
k_{np}	3320306	2	1660153	348.6
Error	2528490	552	4761	
Total	22180430	566		

Accordingly, the following model was obtained to estimate the regenerative radial force coefficient, taking into account the most significant factors:

$$k_\tau \cong 8.89 \, r_\varepsilon^{0.699} \, k_{ns}^{0.438} \, k_{np}^{0.352} \ [N/mm] \tag{4.24}$$

46

where r_ε is expressed in mm, k_{ns} in N/mm^2 and k_{np} in N/mm. The square correlation coefficient R^2 of the model was equal to 0.74.

In the perspective of developing a practical model for the selection of stable tooling configurations, Eq. 4.24 was further simplified by assuming that:

$$k_{ns}^{0.438} \, k_{np}^{0.352} \propto k_s^p \tag{4.25}$$

where k_s is the cutting pressure, i.e. the ratio of the main cutting force F_c to the uncut chip section area A. The relation between cutting pressure and Shearing and Ploughing coefficients can be derived from cutting pressure definition, such as:

$$k_s = \frac{F_c}{A} \cong k_{cs} + \frac{k_{cp}}{h_m} = k_{cs} + \frac{k_{cp}}{A/B} \tag{4.26}$$

where h_m is the average uncut chip thickness.

Shearing and Ploughing coefficients do mostly depend on workpiece material, whereas their dependence on cutting insert geometry and cutting parameters is small. Moreover, the term k_{cs} is dominant: cutting pressure is approximately constant, independently of cutting insert geometry and cutting parameters. In add, cutting pressure k_s can be easily derived from direct measurements or indirectly estimated from other mechanical properties of the workpiece material, such as the tensile strength or Brinnel Hardness [57].

Therefore, Eq. 4.24 becomes:

$$k_\tau \cong \Lambda r_\varepsilon^w k_s^p \; [N/mm] \tag{4.27}$$

where Λ, w, p are constant terms.

4.4.2 Stability analysis

For a given machining system configurations, which can be represented by its modal parameters (G, ω_n and ξ), chatter onset depends, generally, on the spindle speed n and on the regenerative cutting force coefficient k_τ introduced above. Due to the strongly nonlinearities of the function $k_\tau(a_p)$, standard lobes diagram (a_p, n) outlined in the previous section, is changed with a new one based on (k_τ, n) relationship (see Fig. 4.6).
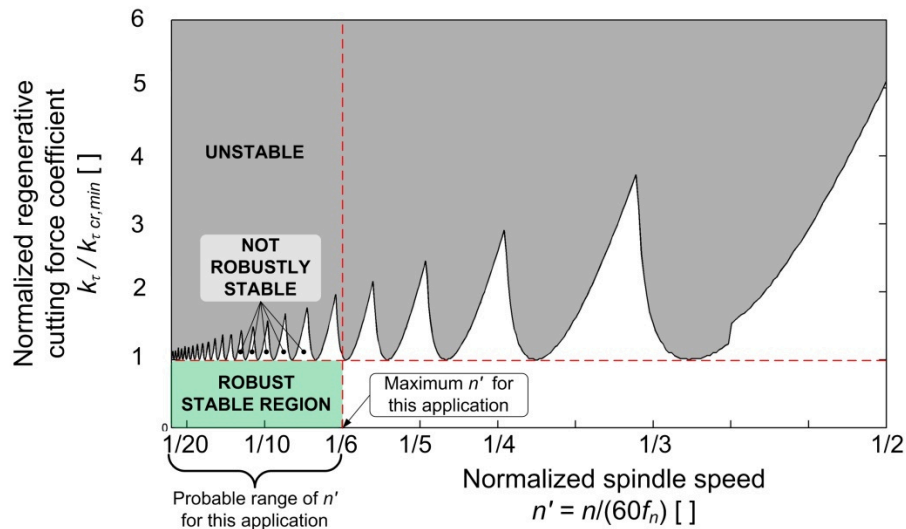
Fig. 4.6 Stability lobes diagram in normalized coordinates [42]

47

Critical regenerative cutting force coefficient can be evaluated by the following expression, where ω_c is the chatter pulsation associated to the spindle speed n.

$$k_{\tau,cr}(n) = -\frac{1}{2Re[W_x(j\omega_c(n))]} \tag{4.28}$$

When the ratio of spindle rotation frequency ($n/60$) to the first natural frequency of the machining system $f_n = \omega_n/(2\pi)$ is relatively high (above 1/5, approximately), some stable cutting parameters can be found between adjacent lobes, which allow to enhance the material removal rate. On the contrary, for lower spindle speed, stability lobes become too dense and the only robustly stable region is that below the stability lobes minima, that can be estimated by searching the maximum value of the denominator of Eq. 4.28 i.e. $\max\{-Re[W_x(j\omega)]\}$ and by substituting the result into Eq. 4.28, yielding

$$k_\tau < k_{\tau,cr,min} = \frac{2\xi(1+\xi)}{G} \tag{4.29}$$

which is independent of the natural pulsation ω_c and of the spindle speed n.
Considering internal turning tooling system, and applying Euler-Bernoulli theory, tool tip static compliance can be estimated by:

$$G \cong \frac{64(L/D)^3}{\pi 3ED} \tag{4.30}$$

where E is the Young modulus of the bar material and the formula refers to a full circular cross section (the small coaxial hole for internal lubricant supply was neglected since it does not considerably affect bar stiffness), whereas L and D are the length and the external diameter of the boring bar, respectively (see Fig. 4.7).
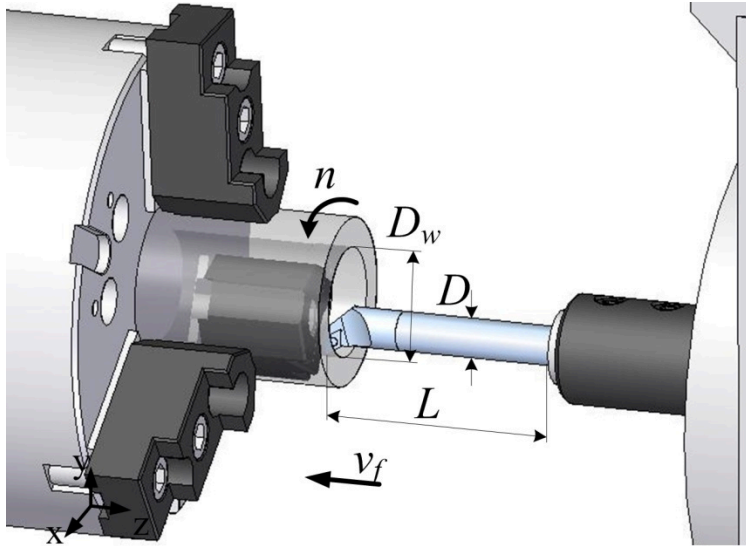
Fig. 4.7 Tooling system schematization for internal turning process [42]

By substituting Eq. 4.27 and Eq. 4.30 in Eq. 4.29, the following expression is obtained:

$$\Lambda r_\varepsilon^w k_s^p < k_{\tau,cr,min} = \frac{2\xi(1+\xi)\pi 3ED}{64(L/D)^3} \tag{4.31}$$

Finally, with the purpose to express stability of the internal turning cutting process in function of the aspect ratio of the boring bar:

$$\frac{L}{D} < \left(\frac{L}{D}\right)_{cr} = \left[\frac{6\pi}{64}\frac{\xi(1+\xi)E}{\Lambda}\right]^{1/3} D^{1/3} k_s^{-p/3} r_\varepsilon^{-w/3} \tag{4.32}$$

where $(L/D)_{cr}$ is defined as the maximum aspect ratio of boring bar assuring stable cutting condition.

It has to be pointed out that inequality of Eq. 4.32 is not dependent of cutting parameters. Accordingly, the effect of feed was not experimentally investigated, since the main aim was to focus on the most important factors affecting stability, which already required extensive and demanding experimental tests. On the contrary, the effect of depth of cut was experimentally investigated since this factor usually plays a fundamental role.
Except Young modulus of the steel, Young modulus of high-damping carbide and damping coefficients of both steel and carbide are generally unknown and difficult to estimate without performing impact tests. In add, constant Λ requires experimental cutting tests to be determined. Therefore, in sake of simplicity, the following model was proposed:

$$\left(\frac{L}{D}\right)_{cr} = QD^a k_s^b r_\varepsilon^c \tag{4.33}$$

where Q, a, b and c are empirical model coefficients that have to be derived by experimental data. The constant Q includes the effects of boring bar material (also Young modulus and damping coefficient), while the term D^a represents the effect of bar geometry. The third term k_s^b considers the effect of the workpiece material, while the last term describes the effect of cutting tool geometry. Finally, exponents a, b and c should be independent of boring bar material.

The chatter predictive semi-empirical model of Eq. 4.33 has to be calibrated by joining the analysis of machining dynamics, characteristics of the cutting forces and the cutter-workpiece dynamic interaction. In the next section, only experimental cutting tests are reported: they were carried out for investigating on the stability of the cutting process for different machining system configurations and cutting parameters combinations. Cutting pressure k_s relating to the selected workpiece materials were estimated by applying the Shearing and Ploughing model in Chapter 3, whereas the dynamic behaviour of the tooling system was experimentally evaluated in Chapter 2.

4.4.3 Experimental set-up

Cutting tests were carried out on a CNC lathe Okuma Multus B300W in dry conditions. The experimental tests were monitored by applying piezoelectric accelerometers Kistler 8704B50 installed on the machine tool head along X and Y directions (Fig. 4.8). Regarding data acquisition, sensors signals were sampled at 20kHz by using a National Instruments device (cDAQ-9178 withNI9215 modules) connected via USB to a PC. Data were elaborated in MathWork MATLAB environment.

Specifically, cutting tests were performed, for finishing internal turning, using boring bar of different diameters, Sandvik A16RSDUCR07-R (with D=16mm) and A10KSDUCR07-ER (D=10mm) made of standard alloy steel and E16RSDUCR07-ER (D=16mm) and

E10MSDUCR0—ER (D=10mm) made of high damping carbide material. Finishing turning operations were performed on two workpiece materials: the steel C45 and the Al-alloy Ergal. Due to the great relevance of the tool geometry, tools with different nose radius were considered. However, local cutting edge geometries and insert grades were selected considering the workpiece material. Specifically, Sandvik DCMT070202PF and DCMT070204PF, grade CT5015, were tested on steel C45; Sandvik DCGT070202UM and DCGT070208UM, grade GC1125, were tested on Ergal. Nose radius r_ε=0.8mm was selected for Ergal to enhance the effect of tool geometry. The effective Design of Experiments is reported in Tab. 4.6.

For each combination of boring bar material, tool insert and workpiece material, different levels of the aspect ratio L/D were tested around the expected critical values $(L/D)_{cr}$, representing the transition from a completely stable to a completely unstable configuration. For a fixed L/D ratio, a dedicated Design of Experiments was carried out for evaluating process stability, involving different levels of depth of cut and spindle speed, as illustrated in Tab. 4.6.
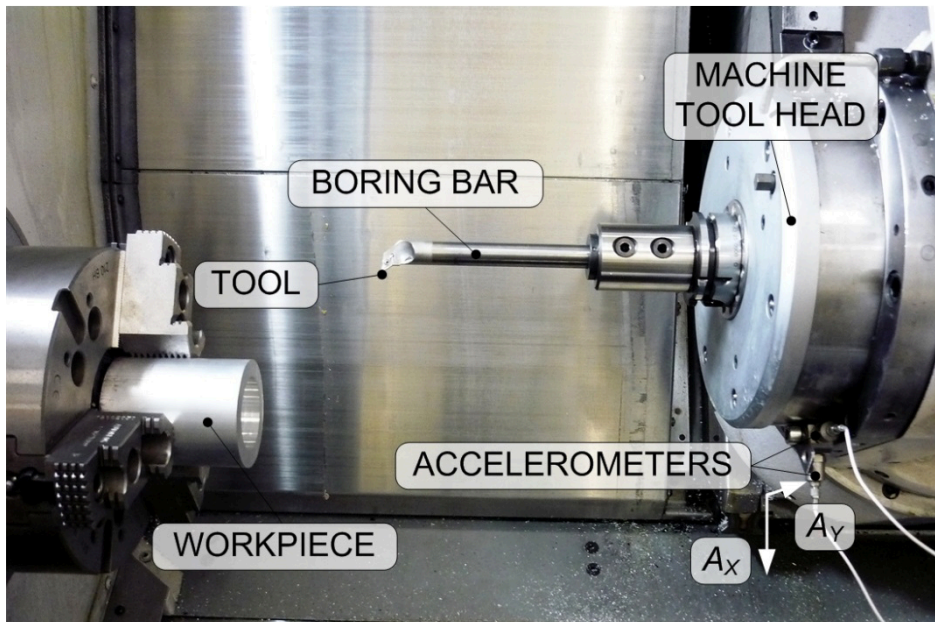
Fig. 4.8 Chatter tests: Experimental set-up [42]

It has to be pointed out that in all case, feed rate was 0.08mm/rev, except the case of Ergal workpiece machined with r_ε=0.8mm which requires f=0.16mm for chip breakage. Workpiece internal diameter was approximately 25mm when machining C45 and about 46mm when machining Ergal, in order to guarantee adequate average cutting speed (v_c of about 350 m/min for C45 and v_c of about 650 m/min for Ergal), as recommended by tool manufacturers. Anyway, chatter vibrations mainly depend on spindle speed, which was indeed considered as an independent factor, rather than on cutting speed. Spindle speed levels were chosen in order to highlight the effect of stability lobes, if any.

The considered L/D ratio was considered stable or unstable according to the stability criteria illustrated in the previous section. On the average, 96 cutting tests were performed for each machining system configuration for a total of about 1600 cutting tests.

Tab. 4.6   Chatter tests: DOE [42]

Factor	Levels	Values
Workpiece material	2	C45, Ergal
Boring bar material	2	Standard alloy steel, High damping carbide
External diameter D [mm]	2	10, 16
Aspect ratio L/D [ ]	~4	3 ÷ 9
Depth of cut a_p [ ]	4	0.1 ÷ 0.6
Spindle speed n [rpm]	9	4100 ÷ 4900
Feed f [mm/rev]	1	0.08 0.16 (for rε 0.8)
Tool nose radius r_ε [mm]	2	0.2, 0.4 (C45) 0.2, 0.8 (Ergal)

4.4.4 Data analysis and model calibration

Cutting tests for each aspect ratio of boring bar were performed to understand chatter stability. Thanks to acceleration signals recorded while machining, it was possible identify stable and unstable configurations. By analysing Fig. 4.9, it is possible identified the transition from stable to unstable process behaviour due to the increase of the aspect ratio of boring bar for a given cutting parameters combination.

Surface quality is usually considered as one fundamental chatter indicator for finishing operations. According to some preliminary cutting tests performed both in stable and unstable conditions, roughness and waviness parameters were in good accordance with theoretical expectations, whereas they were about one order of magnitude greater when chatter occurred, see Fig. 4.10.
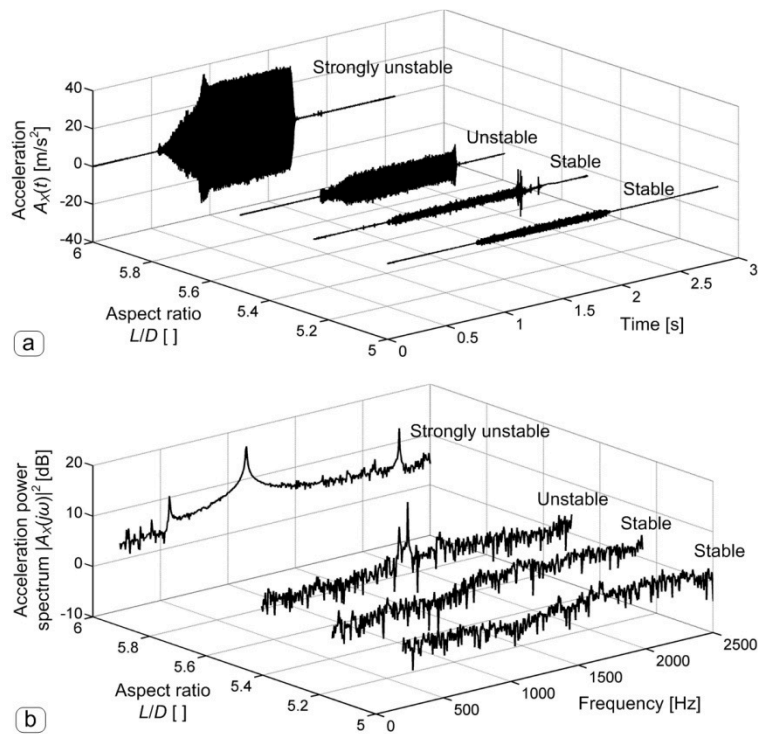
Fig. 4.9 Acceleration A_x behaviour versus aspect ratio L/D: Time (a) and frequency (b) domain (Steel boring bar, D=16mm, r_ε=0.2mm, C45 workpiece, a_p=0.3mm, f=0.08mm/rev, n=4600rpm) [42]
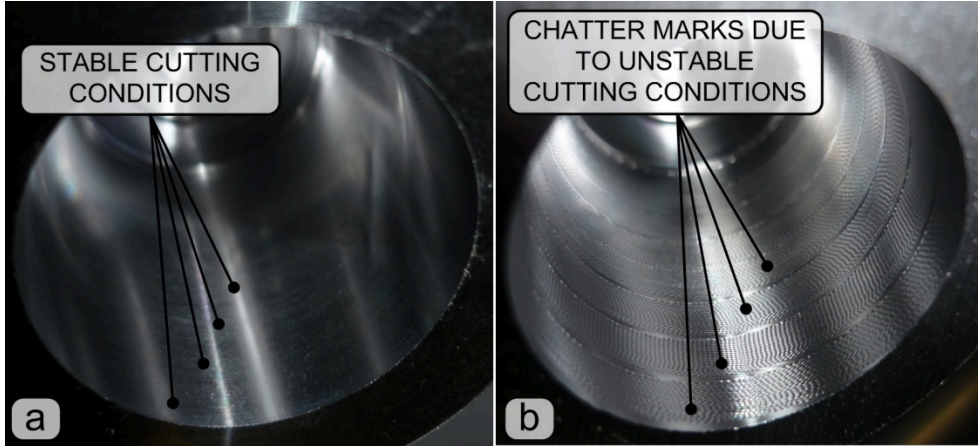
Fig. 4.10   Visual inspection of machined surface to identify chatter marks (Steel boring bar, D=16mm, r_ε=0.2mm, C45 workpiece, a_p=0.3mm, f=0.08mm/rev, n=4100÷4900rpm, L/D=5 (a) and L/D=6 (b)) [42]

Since it was unpractical and in some cases even impossible (due to the very bad surface state) to measure surface profile for characterizing the chatter level, an alternative quantitative parameters extracted from the acceleration signal A_x was used as primary chatter indicator. This approach was inspired by a recent research work [58]. Also, the adopted methodology for chatter detection was successfully validated by direct comparison with surface measurements collected in the preliminary trials.

The following frequency-based chatter indicator was computed as:

$$CI_{ER} = \frac{E_c}{E} = \frac{\int_{\omega_r-\Delta}^{\omega_r+\Delta}|A_x(j\omega)|^2 d\omega}{\int_{\omega_{min}}^{\omega_{max}}|A_x(j\omega)|^2 d\omega} \tag{4.34}$$

where E_c is the spectral energy in a neighborhood of the maximum frequency peak of the spectrum located at ω_c, Δ is the neighbourhood amplitude (10%), E is the total spectral energy within the range of interest. From modal testing reported in the previous Chapter, a proper range of frequency to evaluate total spectrum energy was located between $\omega_{min} = 250\ Hz$ and $\omega_{max} = 4500\ Hz$.

When the system was stable, acceleration signal amplitude was small and its behaviour in the frequency domain was similar to white noise: spectral energy was dispersed over a wide frequency range, and no dominant harmonics were present. In these conditions, CI_{ER} values were relatively small (25%). On the contrary, when the system was unstable, signal amplitude exploded and a few dominant peaks emerged in the power spectral density, which were generally very close to main natural frequencies of the machining system, see Fig. 4.9 - b. In the last conditions, CI_{ER} tended to100%.

To evaluate stability of different process parameters combination, a threshold of CI_{ER} equal to 50% was selected for discriminating stable from unstable cutting conditions, as illustrated in Fig. 4.11. From the analysis of experimental points, it was not possible to distinguish classical stability borders depending on spindle speed n. On the contrary, two opposite situations did typically occur: most cutting parameters combinations were either stable or unstable, depending on the considered L/D ratio, as evidenced in Fig. 4.12. A machining system configuration was considered stable when at least 95% of the testes conditions were stable. Accordingly, critical aspect ratio $(L/D)_{cr}$, was defined as the greatest stable L/D ratio.

Scatter diagram of experimental *(L/D)$_{cr}$* values against input factors are shown in Fig. 4.13. In general, *(L/D)$_{cr}$* is higher when adopting high damping carbide boring bar instead steel boring bar. Moreover *(L/D)$_{cr}$* is higher when the external diameter *D* is higher, when nose radius is smaller or when cutting pressure k_s is smaller.

According to the ANOVA tests, main effects of the investigated factors were proved to be all significant for both boring bar materials. Among 2-level interactions, the effect of the interaction between boring bar material and diameter was the strongest.
In the light of theoretical assumptions of previous section and the above experimental results, multiple linear regression was performed on the output and input factors expressed in logarithmic scale, according to Eq. 4.33, yielding:

$$Q = \begin{cases} 10.097 & \text{for steel boring bar} \\ 10.402 & \text{for high damping boring bar} \end{cases}$$
(4.35)

and, for both boring bar materials

$$D^a k_s^b r_\varepsilon^c = D^{0.3527} k_s^{-0.2379} r_\varepsilon^{-0.1238}$$
(4.36)

where external diameter *D* and tool nose radius r_ε directly derive from the cutting configurations selected to perform cutting process, whereas specific cutting pressure k_s that is related to the cutting material properties, was evaluated by cutting force modelling in Chapter 3.

Scatter diagrams of percent relative residuals against input factors and experimental points are shown in Fig. 4.14. Data dispersion is higher in the case of carbide boring bar in comparison with steel boring bar. No clear trends against input factors and output *(L/D)$_{cr}$* are visible. Standard deviation $\sigma_{\delta LDcr}$ of relative error was only 6%, while maximum relative error was smaller than 12%, confirming the good accuracy of the model.
It should be pointed out that recommendations of boring bar manufacturer in terms of maximum admissible *L/D* ratio (smaller or equal to 4 for conventional alloy steel bars, smaller or equal to 6 for high-damping carbide bars) are generally rather conservative and inadequate in some cases. By applying the proposed model a better estimate of *(L/D)$_{cr}$* can be obtained.

Finally, some practical charts representing the behaviour of *(L/D)$_{cr}$* for different bar diameters and materials, workpiece materials and nose radii are illustrated in Fig. 4.15, showing the applicability of the proposed approach for the selection of stable machining system configurations.
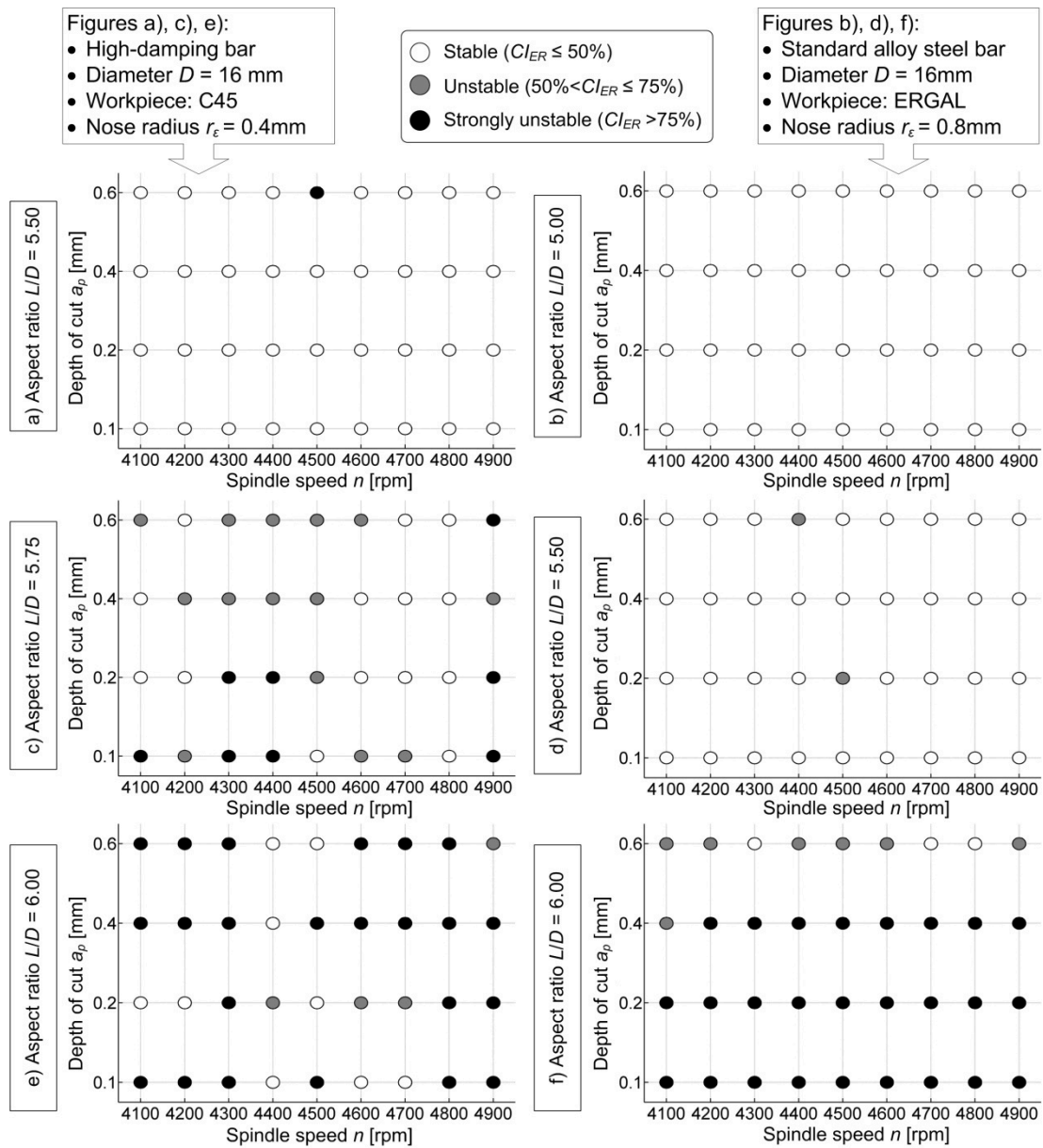
Fig. 4.11 Example of experimental stability charts [42]
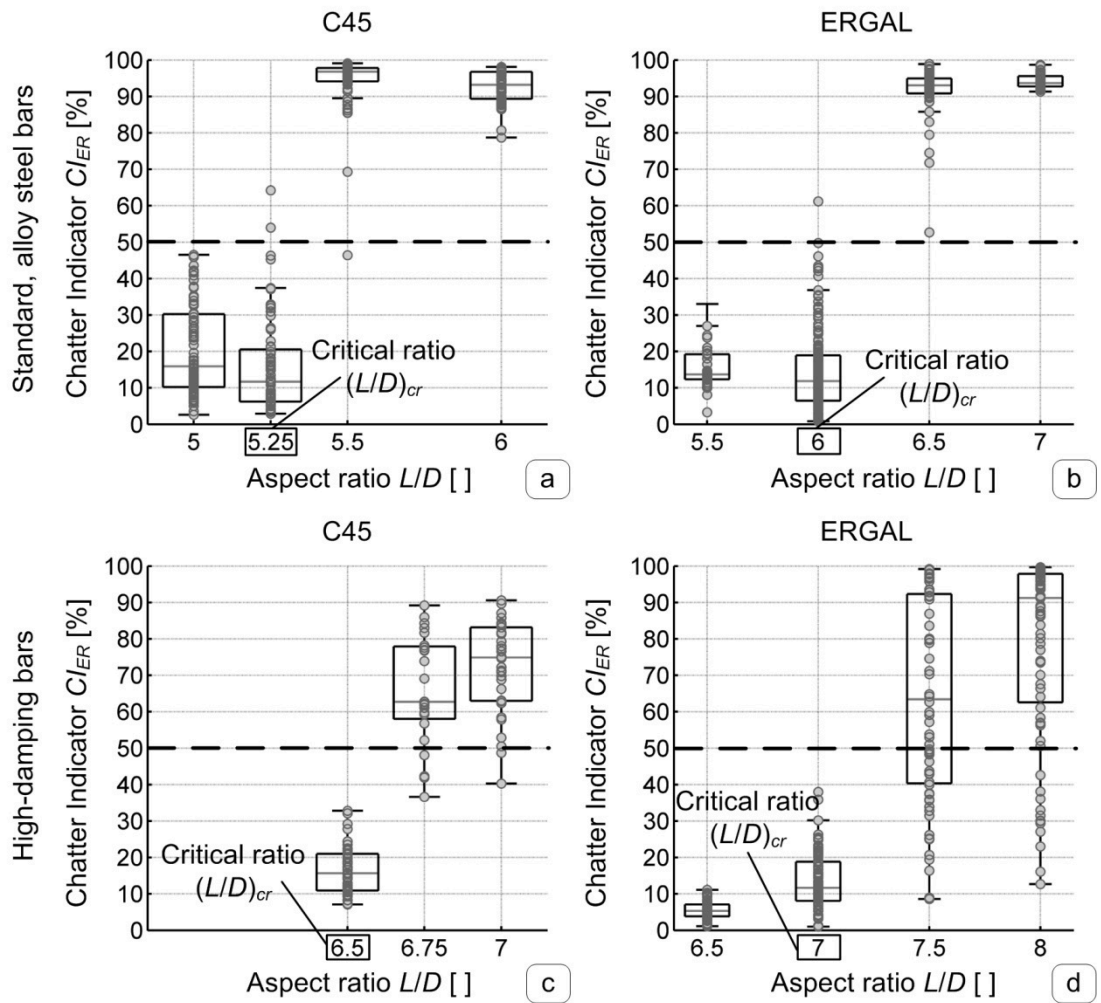
Fig. 4.12 Identification of the critical aspect ratio based on chatter indicator CI_{ER} computation (D=16mm, r_ε=0.2mm) [42]
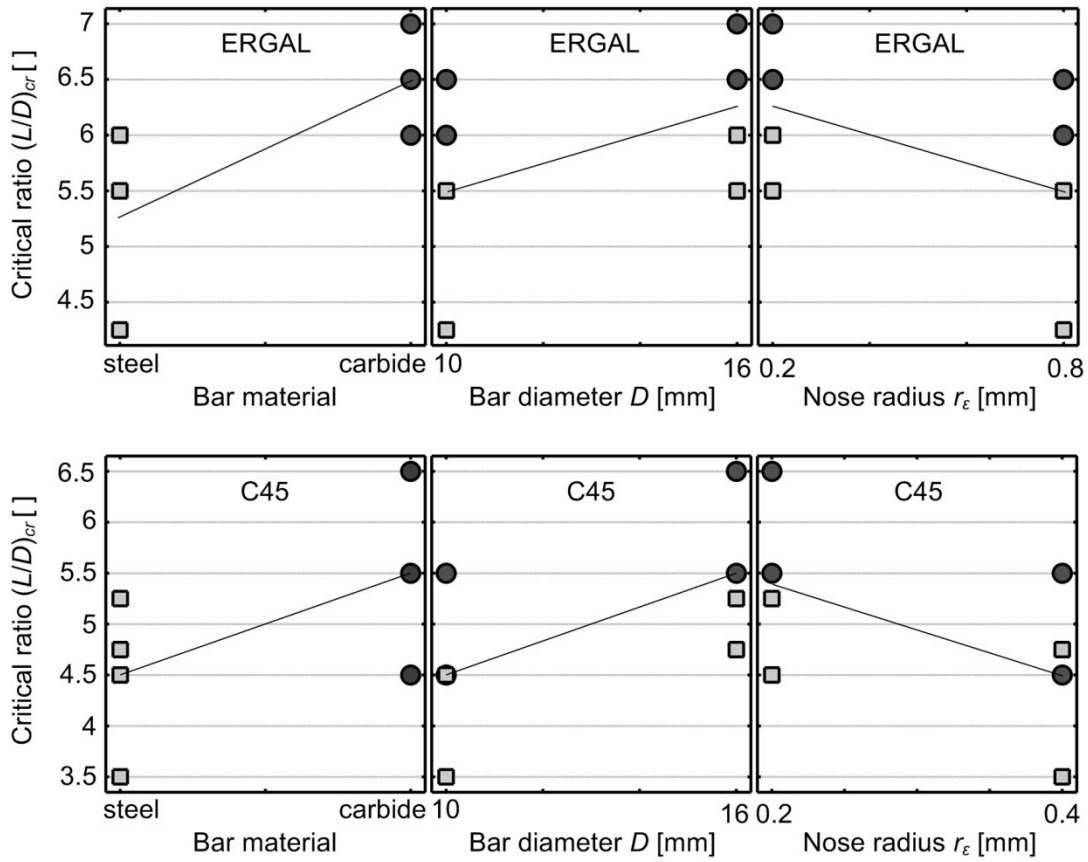
Fig. 4.13   Scatter plot diagram of $(L/D)_{cr}$ against input factors [42]
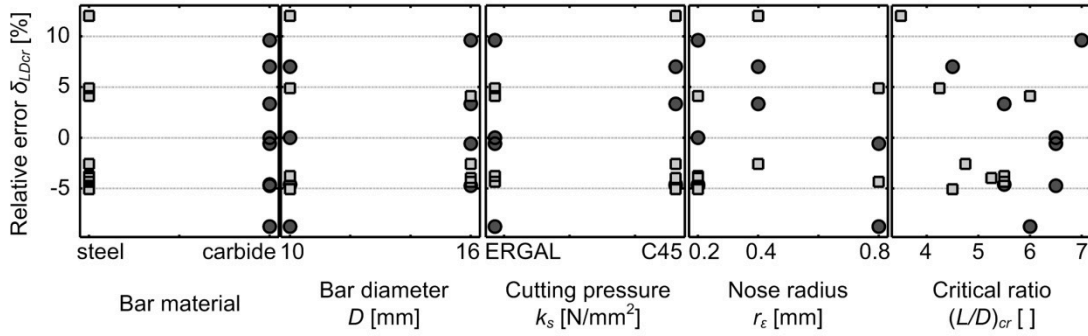
Fig. 4.14   Relative errors of the model against input factors [42]
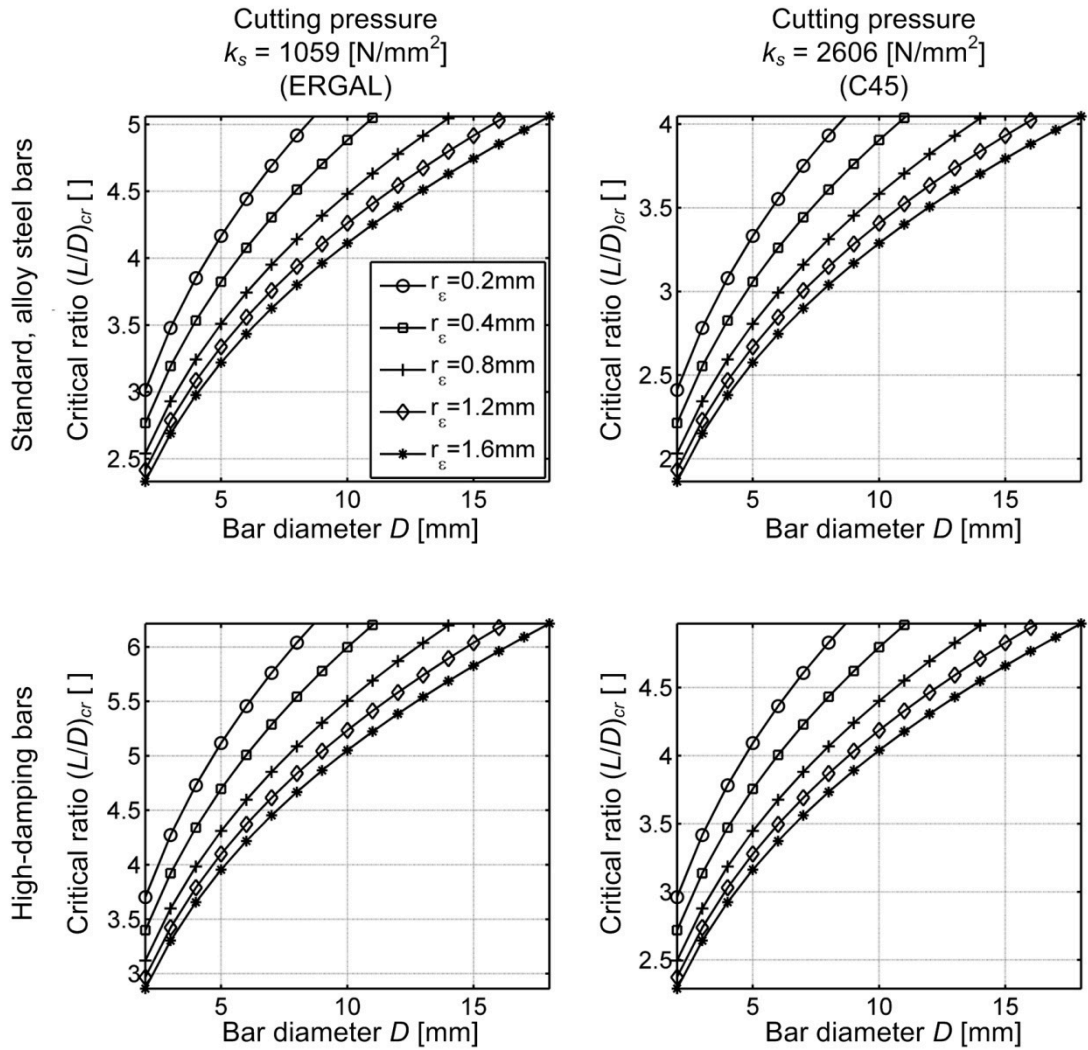
Fig. 4.15 Proposed stability charts to select proper tooling system against bar diameter and material, workpiece material and nose radius [42]

4.4.5 Conclusions about chatter avoidance strategy in internal turning

According to the considerations and experimental results presented, the following conclusions may be drawn.

- Regenerative radial cutting force coefficient k_τ represents the strength of tool tip–workpiece dynamic interaction; it was numerically evaluated from Shearing and Ploughing cutting force coefficients derived in Chapter 3;
- The radial regenerative cutting force coefficient k_τ mainly depends on cutting pressure k_s and tool nose radius, whereas the sensitivity to cutting parameters (cutting speed v_c, depth of cut a_p and feed f) is negligible in first approximation when performing internal turning finishing operations;
- The only recommended robust stable region was that below the stability lobes minima, denoted by the critical value of regenerative radial cutting force coefficient $k_{\tau,cr\ min}$;
- Based on the preliminary observations, a mathematical model of the critical ratio $(L/D)_{cr}$ – maximum boring bar aspect ratio assuring a stable cutting process for almost all cutting conditions – was proposed;

- Input factors of the predictive model were bar material, bar diameter D, cutting pressure k_s, tool nose radius r_ε, whereas the influence of cutting parameters (a_p, v_c, f) were considered negligible;
- Experimental cutting tests confirmed that a given machining system configuration (characterized by bar material and diameter D, aspect ratio L/D, workpiece material and nose radius) was either mostly stable or unstable, independently of cutting parameters, proving that the critical ratio $(L/D)_{cr}$ was well defined;
- By performing a statistical analysis on the obtained experimental results, it emerged that $(L/D)_{cr}$ was higher when using high damping carbide boring bars or higher bar diameters D, while it was smaller when considering higher cutting pressure or tool nose radius;
- Model coefficients were determined by performing multiple linear regression on the experimental data;
- Model accuracy was very high (relative standard deviation about 6%) and no clear trends emerged from the analysis of residues.

4.5. Robust stability analysis

In the previous paragraphs, an hybrid analytical-empirical approach was established for the preliminary selection of stable tooling system configurations in internal turning. Such approach was calibrated by means of direct experimentation on the tooling systems under interest. Although this methodology is very general and it can be easily extended to other machining systems and workpiece materials, some preliminary experimental trials are recommended for model re-calibration, when new tooling systems, cutting tools or workpiece materials are involved.

In order to provide an approximate but prudential estimate of $(L/D)_{cr}$ without performing several additional tests in the shop-floor, a predictive approach was recently developed in [59]. It is based on a robust analysis of stability, which takes into account model coefficients uncertainties. It has to be pointed out that chatter prediction algorithms found in literature are generally deterministic., i.e. their predictions are derived from the nominal values of model coefficients, whereas the uncertainties affecting model coefficients are usually neglected, although they may have a great impact on the stability analysis.

Hence, in order to be thorough, in this section, a probabilistic approach is outlined, which considers stochastic models for representing machining dynamics and tool-workpiece interaction. The main goal is to estimate system's probability of instability for a given cutting process configurations, including tooling system properties, workpiece material and cutting parameters. By so doing, robustly stable tooling system configurations and cutting conditions may be identified in a preliminary production planning phase.

Concerning the internal turning process, a scheme of the procedure for robust stability analysis is shown in Fig. 4.16.
The methodology is centred on the preliminary estimation of the modal parameter of the tooling system, i.e. static compliance G and damping coefficient ξ, and on the identification of the regenerative radial cutting force coefficient k_τ, representing the dynamic force interaction between cutting tool and workpiece during chatter vibrations. These quantities can be evaluated by applying the semi-empirical approach proposed in this Chapter.
By modelling all model coefficients as random variables with their own probability density functions, the effects of model uncertainties and stochastic process behaviour are taken into account when performing the stability analysis.
Accordingly, robust analysis of stability is performed by evaluating the stability of the cutting process for each admissible combination of model parameters, taking into account their probability of occurrence.
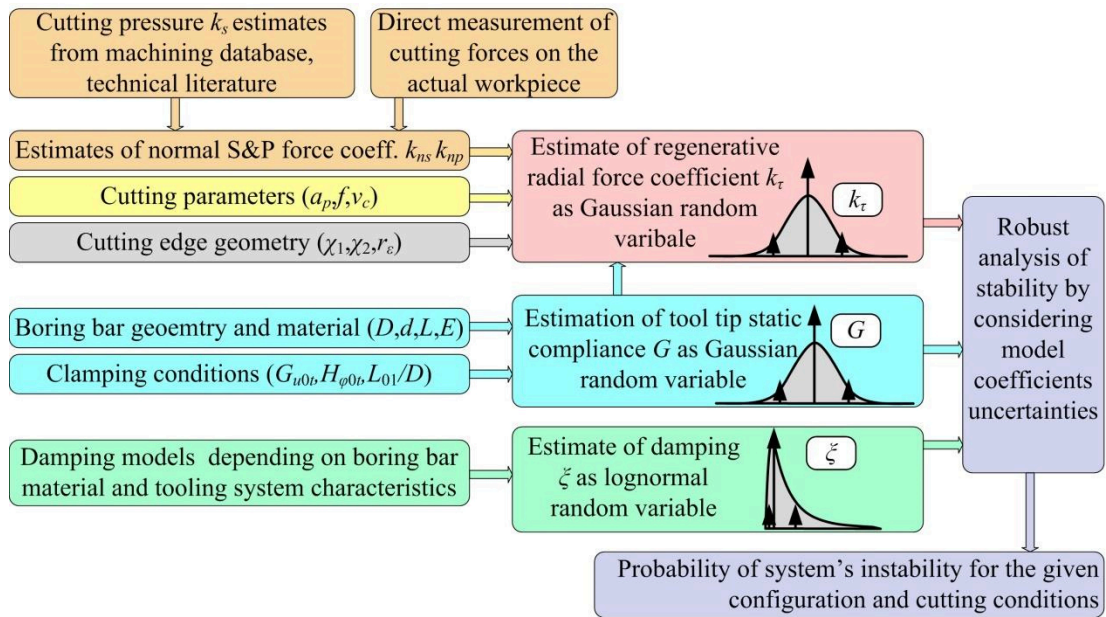
Fig. 4.16 Robust stability analysis procedure [59]

4.6. General conclusions

Self-excited vibrations negatively affect part precision and surface quality, since they are unstable and chaotic. Also, they can cause abnormal tool wear, tool breakage, damage of the tooling structure and of the spindle bearings. Such unstable vibrational phenomena typically arise when the overall machining system stiffness is relatively low, such as in the case of internal turning or peripheral milling operations performed with slender tooling system.

Therefore, chatter avoidance is crucial in high precision manufacturing of mechanical components. In literature, several approach are reported, based on chatter detection or chatter suppression: they operate when chatter phenomena have already originated during machining. On the contrary, several predictive models are developed aiming at the prevention of chatter onset.

This Chapter focuses on the analysis and prevention of the secondary chatter phenomenon, paying attention to the internal turning operation. The cutting process under analysis is generally characterized by difficulties in the preliminary selection of stable tooling system configurations for a given workpiece material, since in literature available data are often incomplete or inapplicable, especially for modern boring bars made of high-damping carbide.

Firstly, a theoretical background of the stability analysis in turning operation is recalled: it includes the analytical formulation of the regenerative effect, which is the main mechanism that causes secondary chatter.

Then, the dynamic interaction of cutter-workpiece in internal turning is investigated. The regenerative radial cutting pressure k_τ strongly affects the stability of the cutting process: an analytical formulation was derived and subsequently estimated following the Shearing and Ploughing theory.

By performing the stability analysis of the process, a hybrid semi-empirical predictive model was derived: it formulates the critical aspect ratio of the boring bar - maximum boring bar aspect ratio assuring a stable cutting process for almost all cutting conditions – as a function

59

of boring bar material and geometry, of workpiece material properties and of cutting tool geometry. The model was experimentally calibrated and validated, joining the analysis of cutting forces, the study of the dynamics of the tooling system and the evaluation of the stability of the cutting process considering different workpiece materials, several tooling system configurations and diverse cutting parameters combinations.

The proposed model can be practically applied for optimal selection of stable tooling system configurations in internal turning. Moreover, scientific findings of this research work can represent a starting point for developing a robust chatter prediction method in internal turning. Robust chatter prediction approach, as outlined in the last section, can be suitable in estimating system's probability of instability for a given cutting process configurations. It overcomes the intrinsic limit of conventional predictive models which are generally derived from the nominal values of model coefficients, neglecting the possible uncertainties affecting the model parameters, although they may have a great impact on the stability analysis.

In conclusion, it has to be emphasized the importance of chatter prediction methods. Predictive models can be preliminary applied, for example for the optimal selection of the tooling system configuration as highlighted in this Chapter. Furthermore, they can be integrated in more advance on-line control system, to perform active or adaptive control of the cutting process.

Chapter 5.

OPTIMIZATION OF MACHINING OPERATIONS ON ADVANCED DIFFICULT-TO-CUT MATERIALS

Optimization of machining process is usually aimed at maximizing productivity or minimizing production costs, by concurrently assuring a given product quality – i.e. surface quality and geometrical and dimensional tolerances.
Optimization is strictly related to the experimental study and modelling of the physical interaction of the cutting tool and the workpiece.

In this Chapter, the concept of machinability of a cutting material is illustrated and some general guidelines for facing machinability problems and for optimizing machining operations on difficult-to-cut materials are outlined. Basing on these indications, a systematic procedure is developed and applied in order to analyse and optimize a turning process on the sintered Molybdenum in dry condition. The research work was recently published in the *Journal of Materials Processing Technology* [60].

5.1. Introduction

Machinability of a material can be defined as its attitude to be machined. Unfortunately, it is very difficult to express this property numerically, since it depends on several factors.
In the past, several methods were proposed to evaluate machinability. For instance, a common machinability indicator is the ratio between the cutting speed corresponding to an average tool life of 20 min when machining the considered workpiece material under given cutting conditions and the cutting speed corresponding to the same tool life when machining a reference workpiece material (AISI B 1112 for Fe-based material), in the same cutting conditions, i.e.

$$I = \frac{v_{c,T20}}{v_{c,T20,AISIB112}} < 1 \tag{5.1}$$

Following this definition, Fe-based material with $I < 1$ shows better machinability rather than reference material. The same interpretation is valid for non ferrous-based materials, by changing the reference workpiece material.
Low machinability of a material could cause poor quality of the machined surface, high cutting forces and instability of the process, irregular chip formation, premature tool wear and short tool life.
Machinability is directly affected by cutting material properties and cutting conditions. Important characteristics to be taken into account are:

- *Chemical composition*: some alloy elements can ease or worsen the machinability of the cutting material. For example Lead acts as lubricants, reducing friction coefficient between tool and workpiece material; it promotes also chip fragmentation, reducing cutting forces and the tool wear rate; Bismuth is also used as a substitute of Lead;

Manganese or Calcium sulphides reduce ductility of material and improve chip breaking; on the contrary, other elements create metallic carbide causing tool wear: for example Al or Si can form oxide inclusions with detrimental effects on machinability;

- *Microstructure and grain size*: metallographic properties of a material can be analysed after chemical etching of a polished sample; generally, the grain size affects the deformation behaviour of the material, so the chip formation mechanism [61];

- *Manufacturing (mechanical) processes applied on the raw workpiece before machining*: methodologies such as hot or cold rolling, cold drawn casting, or forging can affect metallographic characteristics of the material as well as its physical and mechanical properties (ductility, strength, hardness); consequently, they can change the machinability of the workpiece material;

- *Thermal treatments*: they are carried out to improve final product characteristics in the perspective of final application, by influencing physical an mechanical properties (like grain size, hardness, yield strength); as a consequence, they may strongly affect machinability;

- *Physical properties of workpiece material*: Young's modulus, thermal conductivity, thermal expansion and other features could significantly influenced machinability; for example a material with low thermal conductivity will cause high cutting temperatures, which could imply premature tool wear; in adding, ductility is another important characteristic affecting the chip formation mechanism;

- *Work hardening*: while cutting, some material hardness increases due to internal stresses created by the cutting tool action on the machined surface.

Moreover, process configuration, i.e. cutting parameters, tool and toolholder and cutting conditions (dry cutting or with coolant supply) influence the machinability of a material. Indeed, cutting parameters selection (depth of cut, feed rate and cutting velocity) strongly influences the chip formation mechanism, whereas the combination of cutting tool and toolholder geometries, together with the cutting edge characteristics, can affect cutting forces during machining. Finally, cutting environment plays a key role in machinability, since cutting fluids have the function of cooling workpiece, chip and tool, reducing friction, of carrying chips away from cutting area and helping in surface finishing.

Functionalities and properties of the final product planned at the design stage can be satisfied by the selection of advanced or exotic engineering materials. Generally, desired characteristics are high surface hardness, mechanical strength, toughness, and even corrosion and oxidation resistance. An high ratio strength/weight is also required. In particular, these properties shall not change with temperature. For instance, the family of High Strength Super Alloy (HRSA) and refractory materials exhibit these properties. They are indeed selected in aerospace or automotive applications, where operating temperatures may be very high [62]. Unfortunately, these materials are difficult to cut since the high resistance at high temperature implies, cutting forces and cutting temperature, thus requiring special tools.

5.2. Literary review

Several research works dealing with machinability problems were found in literature (Tab. 5.1- *Part a* and *Part b*).

Machinability analysis is based on the study of cutter-workpiece interaction. For this purpose, scientific researches apply several strategy for the evaluation of the most relevant physical quantities related to cutting mechanics and tool wear evolution, such as cutting forces, shear stress, equivalent friction coefficient, cutting temperature analysis, surface roughness and chip morphology and feature, as highlighted in Tab. 5.1. Moreover, chemical analysis of tool rakes and chip is often performed in order to identify the dominant tool wear

mechanism. The selection of the controlled process outputs can depend on the cutting operation under analysis. For example, in the case of drilling operations, typical control strategies can involve torque measurement, monitoring power consumption of machine tool and burr formation [63] [64].

In literature, the influence of cutting temperature on machinability is often investigated, as highlighted by many authors [65] [66] [67] [68] [64]. At the contact point, high temperatures are generated due to the great cutting energy required to the process and by the typical low heat diffusion coefficient of materials, like super alloys. The temperature plays a key role for most of wear mechanism such as abrasion, adhesion and oxidation. For this reason, several studies compare process performance under different lubrication conditions: dry cutting, conventional lubrication, minimum quantity lubrication or cryogenic lubrication [69] [70] [71] [72].

The most studied materials are super alloys, which comprise Nickel-based alloy and Titanium alloy. Further experimentations regard Aluminium alloy. For example, Elgallad et al. [63] studied the machinability of Al-alloy to understand the influence of chemical elements, whereas Armendia et al. [73] Ho et al. [74] and Arrazzola et al. [75] analysed the behaviour of several Ti-alloy, comparing different chemical compositions. Also stainless steel or hardened steel are frequently studied: Ebrahimi et al. [76] compared machinability of micro-alloyed steel and heat treated alloy steel with same hardness, Suresh et al. [77] studied hardened steel AISI 4340, whereas de Carvalho [69] focused on ASTM grades 2 and 3 austempered ductile iron. Within Nickel alloy classes, Inconel 718 is the most analysed cutting material [61] [66] [78] [79].

Finally, other research works focus on the influence of tool coatings for machining a given material [80] [81].

Tab. 5.1 Experimental investigation on machinability: Literary review (*Part a*)

Ref.	Cutting process	Main Goal	Criteria of analysis	Cutting material Cuttingcondition
[63]	Drilling Tapping	Compare machinability of different Al-alloys	Total cutting force Torque Tool life	Material: Al - alloys Coolant: yes
[73]	Turning	Compare machinability of different Ti-alloys	Tool wear Wear mechanism Chip morphology Cutting forces	Material: Ti - alloys Coolant: yes
[74]	End mill	Compare machinability of different Ti-Sn alloys	Cutting length Surface observation Chips morphology	Material: Ti–Sn Coolant: No
[75]	Turning	Compare machinability of different Ti-alloys	Cutting forces Chip morphology Tool wear	Material: Ti - alloys Coolant: Yes
[76]	Boring	Compare machinability of microalloyed steel and heat-treated alloy steels;	Flank wear Chip thickness Chip morphology	Material: Steel Coolant: No
[77]	Turning	Investigate machinability of hardened steel using coating carbide inserts	Cutting forces Surface roughness Tool wear Chip morphology	Material: Hardened steel Coolant: No

Tab. 5.1 Experimental investigation on machinability: Literary review (*Part b*)

Ref.	Cutting process	Main Goal	Criteria of analysis	Cutting material Cuttingcondition
[65]	Milling	Investigate machinability of Ti alloy considering cutting temperature;	Cutting temperature	Material: Ti - alloys Coolant: No
[80]	Face milling	Compare performance of PVD and CVD coated inserts machining Ti-alloy	Cutting forces Roughness Chip morphology Tool wear Wear mechanism	Material: Ti - alloy Coolant: No
[66]	High speed turning	Investigate machinability of Inconel 718 in high speed machining	Cutting forces Cutting pressure Cutting temperature Tool wear Surface finishing Chip morphology Microstructure material	Material: Ni - Alloy Coolant: No
[82]	Drilling	Investigate machinability of RR1000 nickel based superalloy in drilling	Integrity of surface Roughness Tool wear	Material: Ni - alloy Coolant: emulsion
[78]	Turning	Relationship between tool wear and cutting forces behaviour	Cutting forces Tool wear	Material: Ni - Alloy Coolant: No
[67]	Turning	Study of machinability of special Ti-alloy	Heat conductivity Chip morphology Hardness of chip Shear band	Material: Ultra fine grained Ti alloy Coolant: No
[81]	Turning	Machinability of hardened steel with coated and uncoated insert	Chip morphology Tool wear Quality surface	Material: Hardened AISI 52100
[68]	Turning	Study machinability of high temperature aluminized steel using WC tool	Tool wear Roughness Tool temperature Tool wear	Material: Steel Coolant: No
[64]	Drilling	Evaluate influence of cutting parameters and coated insert selection	Tool wear Burr size Torque Power consumption Feed force Tool temperature	Material: Al 7075-T6 Coolant: No
[83]	Turning	Evaluate machinability of Al pure and Al-Si alloy with different coated insert	Chip form Tool wear Cutting force Roughness	Material: Pure Al, Al - alloy Coolant: No
[69]	Turning	Evaluate machinability of ASTM grades 2 and 3 austempered ductile iron	Tool life Cutting forces Surface finishing Chip morfology	Material: ASTM 2 and 3 austempered ductile iron Coolant: Dry condition (cutting force) Wet condition (Tool wear)

5.3. Experimental methodologies for machinability analysis

In the light of the research works dealing with machinability issues and of the personal experience acquired in this field, some general guidelines for facing machinability problems and for optimizing machining operations on difficult-to-cut materials are outlined in this section.

The cutting process can be interpreted as a very complex dynamical system whose stochastic outputs depend on several inputs. Some inputs are determined by the considered machining operation and have to be considered as fixed (for instance, the machine tool, the workpiece material and geometry of the final product), while others can be varied by the engineer in order to optimize the cutting process (typically, the cutting tool and the cutting parameters). Moreover, the cutting process may depend on other uncontrolled and usually unknown inputs, which may increase process variability.

In a preliminary stage, it is fundamental to identify and understand the chemical, physical, mechanical and metallographic properties of the workpiece material. Material characterization can be carried out considering several aspects, such as:

- Chemical composition, evaluable by Optical Emission Spectograph or by EDAX technique (see Fig. 5.1 as example).
- Microstructure of the material which can be analysed by Electron Probe Micro Analyser, by TEM technique, or by micrograph analysis using optical microscope, also advantageous for grain size measurement; besides, X-ray diffraction analysis can be applied for identifying the phases of material.
- Abrasiveness of the material, which can be derived from the microstructure analysis: it is related to the amount of carbides and oxides.
- Porosity of the material which can be determined using X-ray technique.
- Thermal conductivity evaluation.
- Hardness and microhardness measurements.
- Yield strength which is related to the material hardness; it gives a value of the material deformation resistance and cutting resistance; generally, low yield strength is favourable for machining, except for ductile material.
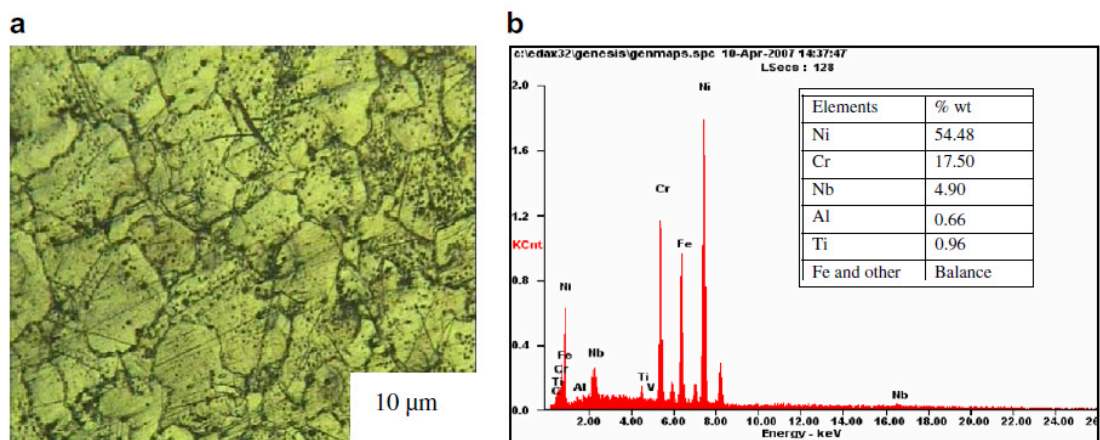
Fig. 5.1 Example of microstructure (a) and EDAX analysis (b) of Inconel 718 [66]

Besides workpiece material properties and other known and fixed process inputs, it is important to identify and register the following input data:

- cutting tool material (bulk composition and microstructure, coating characteristics);
- geometry of the cutting insert, especially chip-breaker shape, tool nose radius and edge radius; effective cutting geometry should be identified: it is due to the combination of cutting insert and tool-holder;
- description of tooling system components;
- type of lubrication (dry cutting, conventional lubrication, MQL - Minimum Quantity Lubrication or cryogenic process), chemical composition of the lubricant and process parameters such as lubricant pressure and flow;
- cutting parameters such as cutting speed v_c [m/min], spindle speed n [rpm], feed rate f [mm/rev], depth of cut a_p [mm].

In the perspective of studying the machinability of a given workpiece material or to compare the cutting performances obtained with different cutting tools, the following process outputs may be of major interest:

- *Cutting mechanics such as cutting forces and adsorbed cutting power, shear stress, equivalent friction coefficient*: high cutting forces and subsequently absorbed cutting power, elevated friction coefficients and great shear stress are symptoms of low machinability of the cutting material.
- *Process vibrations*: they are generated by very high cutting forces and they influence the accuracy of the workpiece.
- *Surface profile / undulation parameters:* low machinability of the cutting material can cause dimensional and geometrical errors, leaving technical tolerances defined by design department.
- *Surface quality*: low machinability generally gives poor surface quality.
- *Surface integrity*: low machinability can generate defects such as microcracks, or residual stress affecting micro and nano scale surface characteristics.
- *Chip properties like aspect, shape, length, chip compression ratio*: they are strongly influenced by ease in cutting material; as an example, highly ductility promotes extensive plastic deformation of the chip during cutting; plastic deformation increases heat generation and cutting temperature resulting in a long and continuous chip which in turn causes frictional heat; a difficult to cut material often exhibits long, curly and irregular chips.
- *Tool wear evolution and tool life*: low machinability negatively affects cutting mechanics which in turn influence tool life; for example increasing in power consumption or in friction coefficients increase heat generation, which raises tool temperature and lowers its resistance wear.
- *Tool wear mechanisms*: its analysis is useful to understand the properties of the cutting material in combination with cutting tool characteristics in order to optimize cutting process.

It has to be recalled that a satisfactory machinability is obtained only when the desired product quality is achieved by concurrently assuring a reasonable production time, productions costs and a sufficiently long tool life. The optimal cutting conditions correspond to a good compromise aimed at satisfying these contrasting principles.

Joined analysis of multiple process outputs may be necessary. The most employed sensors and instruments for monitoring cutting process outputs are collected in Tab. 5.2. In the following, methodologies for the evaluation of each process outcome are explained, giving

an overview of the possible inspection and monitoring techniques useful in machining analysis. Basing on this study, an experimental procedure was developed and applied on the case study illustrated in the next section.

Tab. 5.2 Process outputs analysis: most common inspection approaches and instruments adopted

Process output	Parameter	Sensor / Instrument
Mechanics of cutting process	Cutting forces	Strain gauge Dynamometer
	Temperature	Thermocouple Pyrometer
	Power consumption	Wattmeter Current consumption
Stability of the process	Cutting forces	Dynamometer
	Acceleration	Accelerometer
	Acoustic emission	AE sensor
Accuracy of workpiece	Dimension and shape	CMM 3D Laser scanner Profilometer
Surface roughness	$R_a, R_t, R_z, R_{sk}, R_{sm}\ldots$	Surface tester Optical microscope
Surface integrity	Material variations Residual stress Micro defects	Optical microscope SEM Diffractometer Microhardness tester
Tool life	Flank wear VB Crater wear KT	Optical microscope Digital micrometer
Tool wear	Wear mechanism	Optical microscope SEM EDAX
Chip morphology	Chip length Chip curvature Chip thickness Chip compression ratio Chip mechanical properties	Optical microscope SEM Hardness and microhardness tester

5.3.1 On-line monitoring techniques

Aiming at monitoring cutting mechanics and stability of the cutting process, a best practice is the implementation of a multisensors approach: several sensors or instruments can be located on the machine tool in order to monitor cutting process by on-line technique. Achieving a good process monitoring, some rules shall be followed:

- Sensor position has not to interfere with tool change or pallet movement;
- Sensor has not to reduce stiffness of the machine tool or tooling system;
- Sensor has not to limit in process parameters selection (workpiece dimension, tool dimension and geometry…);

- Sensor location has to be as close as possible to the process in order to reach high sensitivity of signal outputs with respect the process variation;
- The monitoring system has to be insensitive to the noise of the environment.

One possible strategy on cutting forces measurement is by applying strain gauges on flexible mechanical element of the machining system or by using piezoelectric sensors embedded on the machining system. Generally, strain gauges based sensors are affected by low stiffness and limited frequency bandwidth. A good compromise between stiffness and bandwidth is achieved by piezoelectric dynamometer.

A further monitored cutting mechanic is the power consumed: it can be measured by a wattmeter system located at the spindle [84] or by evaluating the current consumption of the machine tool servo system.

Evaluation of the cutting forces allows the analytical formulation of the friction coefficient. This cutting mechanics parameter is very useful in understanding machinability of a cutting material: it is velocity dependent since increasing speeds yields lower friction; it represents a heat source at the contact point between tool and workpiece, influencing the cutting temperature. Friction coefficient is simply given by the ratio of the friction force and the normal force [85] [86], such as:

$$\mu = \frac{F_n + F_c tan(\gamma)}{F_c - F_n tan(\gamma)} \ [\ ] \tag{5.2}$$

where γ is the rake face angle of the cutting insert whereas F_c and F_n are the main and the normal cutting forces, respectively. Force components can be estimated by applying cutting force model, as explained in Chapter 3. The formulation of Eq. 5.2 is applied in the next section for evaluating friction coefficient of the cutting material under investigation.

Stability of the cutting process can be monitored by applying several sensors, such as, dynamometer, accelerometers or AE sensors. Signal outputs of first two measurement systems are similar in the behaviour: they are periodic if the process is stable and manifest anomalies in unstable conditions. On the other hand, accelerometers signals have a wider spectra than the cutting force signals, therefore they are suitable for monitoring chatter onset [58]. Unfortunately, placing accelerations probes requires prior knowledge of the dynamic behaviour of the machine tool. Acoustic emission signals are periodic in the time and show irregular peaks not directly related to instability of the process: in milling, for example, irregular peaks are detectable when tooth enters or leaves the workpiece. Consequently, chatter identification is more difficult using AE sensor than accelerometers or dynamometer. On the other hand, AE sensors can be also used for monitoring tool wear and severe plastic deformations [66].

Further process outputs monitored by on-line approach are heat generation and the local temperature at the contact point between cutting tool and workpiece: as outlined yet, temperature plays a key role during machining, since it affects chip formation mechanism and can promote some tool wear mechanisms; in particular, high cutting temperature can induce a variation on the material characteristics and can reduce tool wear resistance. For this purpose, typical monitor techniques include thermocouple systems or the application of pyrometers.

5.3.2 Off-line inspection techniques

Inspection techniques of surface integrity (including surface quality), geometrical and dimensional accuracy of the workpiece and cutting tool integrity (tool wear and tool life) are generally conducted following the off-line approach at the end of the cutting process. For each process output, several inspection methods can be followed.

Geometrical and dimensional accuracy of workpiece can be controlled by CMM systems, profilometer, surface scanner 3D; moreover, roughness tester can be used also for the evaluation of the waviness of the surface.

The *surface integrity* discipline includes all possible surface alterations produced in a surface layer during machining, considering also their effect on the material properties and the changing of the required performances of surface in service. Therefore, evaluating surface integrity means analysing surface roughness, surface topography and surface metallurgy, considering macrostructure, microstructure and microhardness alterations [85]. The inspection can be performed following several methods, applying specific instruments:

- Surface roughness measurement by surface tester or micro-topographic map evaluation;
- Macroscopic examination by optical microscope at magnification 10x or less in order to identify cracks or surface defects;
- Microscopic examination of the altered cross-section, using SEM technology (Fig. 5.2) or optical microscope with magnification at 1000x: it is possible to identify microcracks, plastic deformations, phase transformation, intergranular attack, inclusions, metallurgical transformation and heat affected zone;
- Microhardness evaluation;
- Evaluate surface texture by SEM technique;
- Residual stress profile or distortion measurement applying the X-ray diffraction technique.
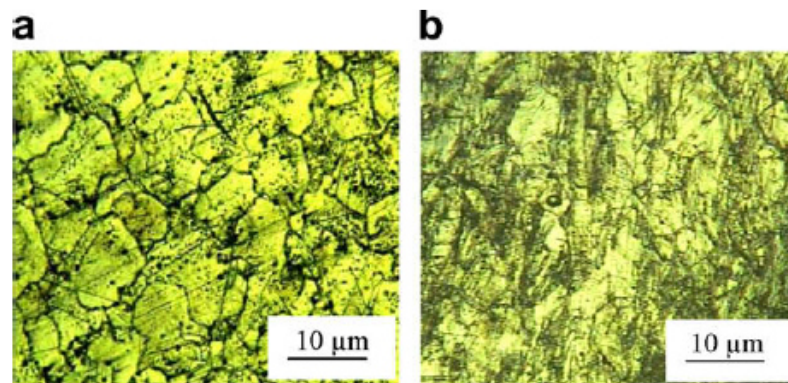
Fig. 5.2 SEM analysis of microstructure variation of Inconel 718 due to different cutting speeds [66]

Chip analysis includes the study of chip morphology by macro-scale and micro-scale observations. Generally, chip length, chip curvature and chip thickness are carefully evaluated because they are affected by cutting process behaviour. For example, chip length can be influenced by cutting parameters, such as feed rate and depth of cut, since a localized increasing of temperature improves ductility of material [67]. Also curly chips can be generated by high temperature in cutting process, resulting in large plastic generation [79]. Micro-scaling analysis performed by SEM technique (Fig. 5.3) are useful for evaluating inhomogeneities like chip shear bands, flow layers and small cracks. Furthermore, chip hardness is often studied for evaluating material changes due to cutting temperature: generally, measurements are performed at more than one point of inspection, for example, at the tool edge, at a centered point of the chip and at cutter tool edge.
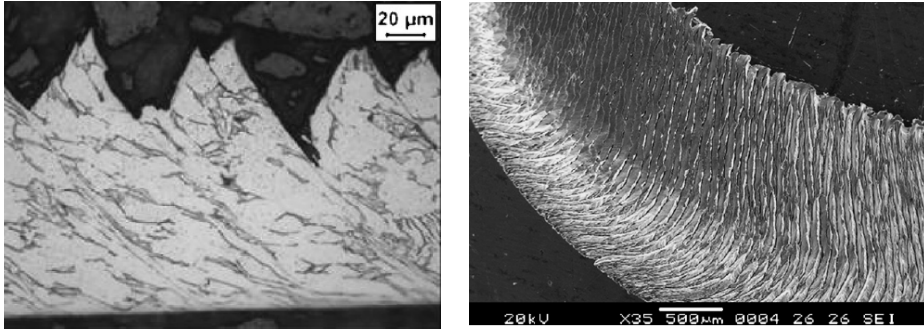
Fig. 5.3 SEM images for chip morphology analysis: cross section and chip segmentation [73]

Chip compression ratio can be computed in order to define material plastic deformation rate in the chip formation zone during cutting process. It is given by the relation [87]:

$$\zeta = \frac{h}{h_0} \ [\ ]$$
(5. 3)

where h is the chip thickness after machining, whereas h_0 is the uncut chip thickness.
In order to evaluate experimentally the value of h, the following procedure can be performed:

1. Estimation of the chip length by analytical evaluation, known the helix radius and the axial height of the chip element;
2. Measurement of the chip width by stereomicroscope observation of the cross-section;
3. Weighing of the chip using a high precision balance;
4. Calculus of the volume, known the density value of the material;
5. Evaluation of the third dimension, i.e. the chip thickness.

Unfortunately, chip morphology often shows complex shape and the evaluation of the length is very difficult. Therefore a further approach can be applied for the evaluation of the chip thickness: it includes the observation of the chip section by stereomicroscope. By applying a software for image analysis, it is possible measuring chip width and chip thickness (see Fig. 5.4). This methodology was applied for chip compression ratio estimation in the case study explained in the next section. Alternatively, chip thickness can be measured by digital micrometer, even if the evaluation can be difficult in the case of irregular chip formation.

The evaluation of the chip compression ratio allows the determination of cutting mechanics parameters, such as the shear angle and shear stress. Shear angle φ is computable by the expression:

$$tan(\varphi) = \frac{cos(\gamma)}{\zeta - sin(\gamma)}$$
(5. 4)

where γ is the rake face angle of the cutting tool.
The shear stress formulation is:

$$\tau_s = \left(F_c cos(\varphi) - F_n sin(\varphi)\right) \cdot \frac{sin(\varphi)}{b \cdot h_0} \ [MPa]$$
(5. 5)

where F_c and F_n are the main and the normal forces, respectively, whereas b is the chip width.
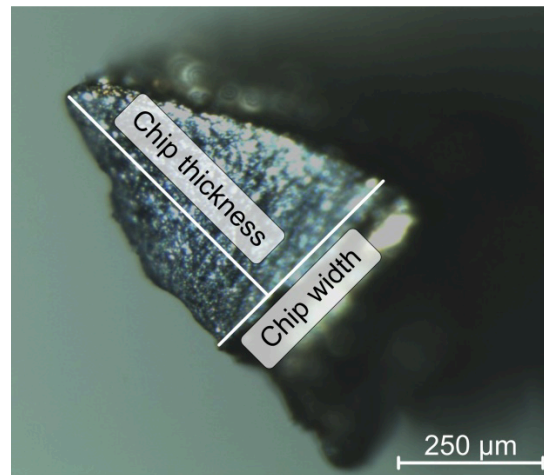
Fig. 5.4 Chip thickness evaluation by stereomicroscope observation and image analysis

Tool life generally depends on cutting parameters, working material and cutting environment. It is also affected by tool chipping, tool fracture and surface roughness.

The measurement of the flank wear *VB* and of the crater wear *KT* are typical criteria for determining cutting tool life. The former is the most applied since easier in evaluation. Measurements of flank wear can be performed by optical microscope and image analysis or by digital micrometer. In the case of single point turning machining, the standard ISO 3685:1993 [88] can be followed: it defines a maximum value of *VB* which determines the end of the cutting tool life.

Tool wear is inversely proportional to the tool life. By observing tool characteristics it is possible analysing tool wear mechanism: it can be performed by macroscopic and microscopic analysis. Optical microscope can be adopted to observe wear, to identify eventual heat altered zone, notching, chipping and Built-Up Edge. Microscopic investigations include topography maps analysis, Scansion Electron Microscope and EDAX analysis. SEM is often adopted for analysing and illustrating tool wear mechanisms, determining the surface profile of tool face and coating removal. Generally, wear of the cutting tool is observed before and after application of the etching technique: it is useful for the removal of adhered workpiece material and for the observation of erosion marks, crater formation or coating removal. EDAX analysis is used as a qualitative identification of chemical elements on the faces and edges of the tool (see Fig. 5.5): it is useful on the identification of the composition of adhered material and for differentiating chemical elements of the bulk of tool rather than adhered material or tool coating elements. Moreover, eventual chemical reactions can be hypothesized: they are principally caused by the high cutting temperature.

71
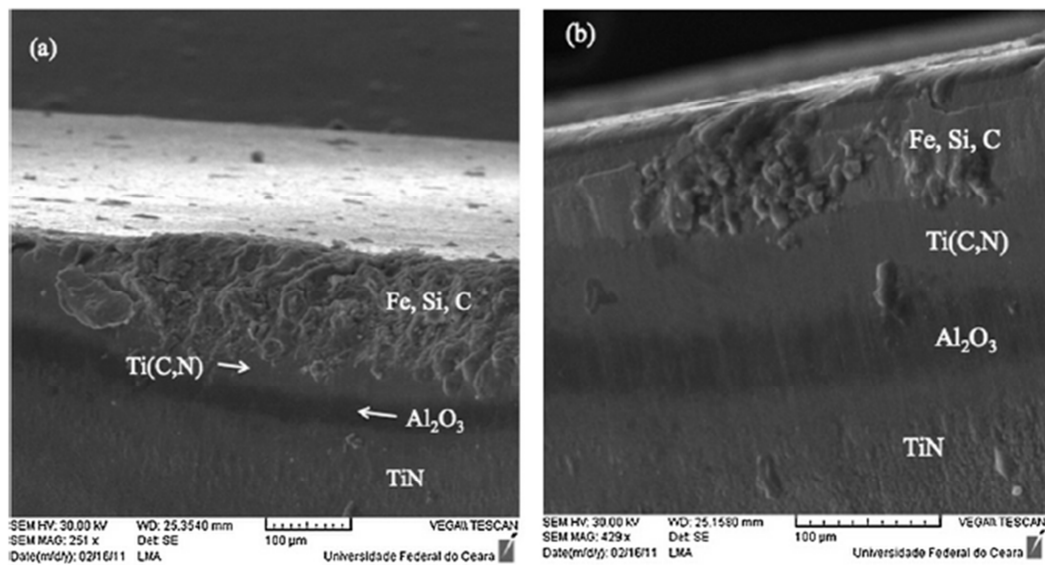
Fig. 5.5 SEM images of tool wear and chemical element identification by EDAX analysis [69]

5.4. Machinability study on dry turning of sintered Molybdenum

Basing on the indications afore mentioned about analysis methodologies of cutting process outputs and of material properties, a systematic procedure was applied in order to investigate on the machinability of a pure sintered Molybdenum in dry turning process. This cutting material was not analyzed in previous scientific research works and only few indications about its machinability are given from material supplier and tool manufacturers.

The research work was recently published in the *Journal of Materials Processing Technology* in 2013 [60].

5.4.1 Cutting material characteristics

Molybdenum is a refractory metal with body-centered cubic crystal structure with high atomic number and density [89].

Molybdenum based alloys are mainly fabricated by powder metallurgy and arc-casting methods. In both cases, the obtained billets or ingots are generally hot-worked by applying bulk deformation processes such as forging, rolling, extrusion and drawing. Eventually, they undergo specific thermo-mechanical treatments in order to achieve a semifinished product, which can be further processed through machining operations.

Physical and mechanical properties of (almost pure) sintered Molybdenum are summarized in Tab. 5.3. Except the considerably higher Young modulus, its mechanical properties are comparable to those of conventional carbon steels. However, key features of Molybdenum are its higher mechanical strength and hardness at higher temperatures, especially when considering sintered Molybdenum alloys with dispersed particles, see Takida et al. [90]. This is due to the very high melting point ($2620 \circ$C) and recrystallization temperatures of sintered Molybdenum, which are comparable to those of Inconel 718 [91]. Of course, mechanical properties of sintered Molybdenum are also influenced by grain dimension and structure, as well as by the adopted sintering procedure, as shown by Srivatsan et al. [92]. Also, Molybdenum exhibits low thermal expansion, high thermal conductivity, and low heat capacity in comparison with most ferrous materials. Besides, it has high corrosion resistance to molten glass and metals, which are desirable characteristics for several engineering applications.

Tab. 5.3 Chemical and physical characteristics of Molybdenum and other references material [60]

Property	AISI 1045 (Ck45)	Inconel 718	sintered Mo
Chemical composition [% in weight]	C0.42-0.50; Si≤0.40; Mn 0.65; Cr≤0.40; Ni≤0.40; Mo≤0.10; Cr+Mo+Ni≤0.63	C≤0.08; Mn≤0.35; Si≤0.35; Cr 17-21; Ni 50-55; Mo 2.8-3.3; Nb+Ta 4.75-5.50; Ti 0.65-1.15; Al 0.2-0.8; Co≤1; Fe(balance)	Mo 99.97
Density at 20 °C [g/cm³]	7.85	8.20	10.28
Melting point [°C]	1350	1336	2620
Recrystallization temperature [°C]	540-675 °C	>850°C	800÷1200
Young Modulus E [GPa]	210	205	340
Yield strength Y [MPa]	300-450	550-1000	350-700
Tensile strength R [MPa]	570-800	800-1450	450-850
Brinnell Hardness [HB]	170-230	250-400	200-230
Elongation A [%]	16	5-20	<30
Coefficient of linear thermal expansion at 20 °C, [µm/(m K)]	11.5	13.0	5.2
Thermal conductivity at 20 °C [W/(m K)]	46-52	11.2	140
Specific heat capacity at 20 °C [J/(kg K)]	480	435	254
Cutting pressure k_s [MPa]	2000-2600	2500-5000	2500-4500
Recommended cutting speed v_c [m/min] in finish turning	350-500 (cemented carbides); 400-650 (cermets)	40-90 (cemented carbides); 150-220 (ceramics or cBN)	<140 (cemented carbides)
Approximate relative cost [ ]	1	≈ 25	≈ 65

Specifically, tested material is a sintered pure molybdenum (Mo > 99,97%) with average Brinnell Hardness of 201HB.

In order to analyse the microstructure of the material, two polished, chemical etched samples, were analysed by metallographic microscope. One sample related to the cross section (Fig. 5.6 (a)), while the second one related to the longitudinal section of a cylindrical element (Fig. 5.6 (b)). Analysis in cross-section highlighted irregular grains: their size ranging from about 2 to 15 µm. From longitudinal section, long and thin grains of about 50 µm were observed, in a consequence of the process fabrication of the material. Finally, a porosity of 5% was estimated.
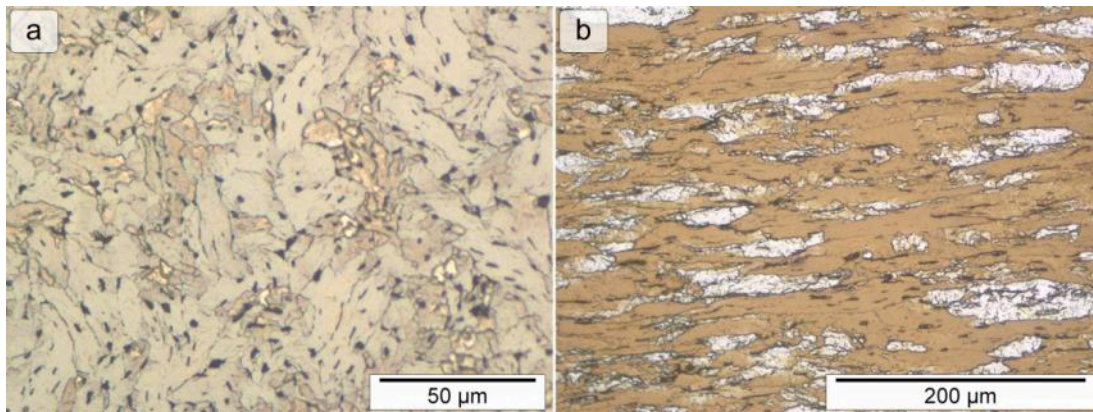
Fig. 5.6 Microstructure after Murakami etching: cross-section (a) and longitudinal section (b) [60]

Sintered molybdenum is considered a material difficult-to-cut because its tendency to adhere to the rake face of the tool causing tool wear like build up edge and short tool life. Moreover, generally, poor surface finishing is achieved and machined surface is affected by work hardening.

Some guidelines are reported in literature [93] and by tools manufacturers [89] to work molybdenum:

- sharp tool are generally preferred;
- the workpiece should be steadily chucked and tools rigid enough to avoid vibrational phenomena;
- low cutting speeds ($v_c < 140$ m/min) are suggested to avoid excessive tool wear;
- cutting process with copious supply of coolant shall be provided, even if it could be toxic; in add, it could be absorbed by porous on the surface, representing a danger for health of operators.

5.4.2 Experimental set-up

Turning tests were performed in a CN multifunction machine tool Okuma Multus B300W (see Fig. 5.7). Dry external turning process on sample with length L of 150 mm and initial diameter D of 80 mm were carried out.

Following the guidelines for machinability evaluation, as outlines in the previous section, multiple process outputs analysis was performed.

In this study, surface quality was evaluated by a portable roughness tester Mitutoyo Surftest SJ-201 (Fig. 5.7 – b): it allows the surface evaluation without removal of workpiece from the machine tool, avoiding errors in workpiece repositioning. Other non-compliances of the machined surface such as chatter marks or microchips were assessed by direct visual inspection.

Cutting forces were measured close to the tool tip in the three cutting direction by the special tri-axial turning dynamometer developed by Totis et al. [38]: it is composed by a commercial toolholder in which are located three piezoelectric probes to evaluate the main cutting force F_c, the back force F_p and the feed force F_f, with cross-talk effects negligible.

Cutting process vibrations were measured by means of a piezoelectric uniaxial accelerometer Kistler 8705B50 installed at the machine tool head along the longitudinal feed direction Az.

For automatic tool inspection during tool wear tests a digital microscope mounted to a special fixture attached to the opposing spindle of the CN lathe was applied (see Fig. 5.7 – c).

A Leica M165C stereomicroscope was used for direct visual inspection of worn tools and chip morphology analysis. Finally SEM investigation was performed to understand tool wear mechanisms.

All sensor signals were sampled at 20kHz by using a National Instruments device (cDAQ-9178) connected via USB to PC. Analysis was performed in MathWorks Matlab environment.
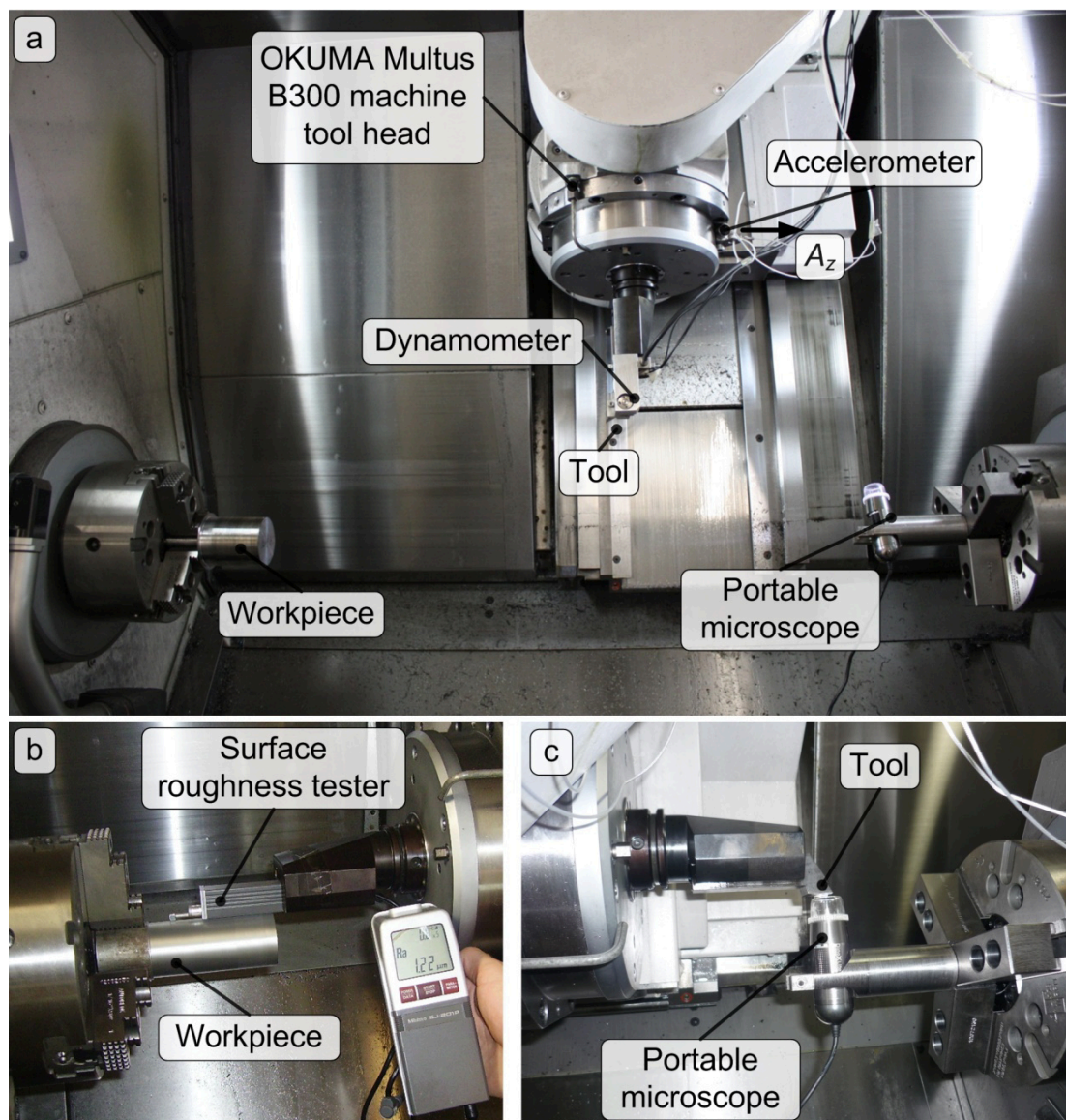
Fig. 5.7 Experimental set-up

Aiming at studying machinability of sintered Molybdenum in dry finishing external turning, a list of suitable cutting tools were selected (see Tab. 5.4): cutting tests were performed in order to evaluate their performance and assess the machinability properties of the cutting material. The common characteristics of the selected tools were the rhombic geometry, with tool included angle β equal to 55°, nose radius r_ε equal to 0.4mm and entering angle χ equal

to 93°. A great variety of tool geometries and materials were selected, which were inspired by literature and by tool manufacture recommendations. Negative basic-shape cutting inserts type DNGA1506, DNGA1504, DNMG1506 and DNMG1504 mounted on Sandvik DDJNR2525M15-2 toolshank as well as positive-basic shape insert type DCMT11T3 and DCGT11T3 mounted in Sandvik SDJCR2525M11 toolshank were selected. Ceramic (CER), CerMet (CMT), cemented carbide (WCN and WCP), both coated and uncoated were tested (Tab. 5.4).

Tab. 5.4 Characteristics of the cutting tools applied in cutting tests [60]

Code	Tool shape	Core composition	Coating	Coating thickness [µm]	Cutting edge inclination λ [deg]	Chamfer γ_1 x L_1 [deg x mm]	Normal rake γ [deg]	Rounded cutting edge r_n [µm]
CER1	DNGA1504	Al_2O_3 + TiCN	PVD_1	1	-7°	-26°x0.1	-6°	20
CER2	DNGA1506	Al_2O_3 + TiC	PVD_1	1	-7°	-31°x0.15	-6°	20
CMT1	DNMG1504	TiC(>50%), WC(28.3%), Co(8%)	PVD_2	5.5	-7°	/	4°	25
CMT2	DNMG1506	TiC, TiN and WC; Co(15%)	Uncoated		-7°	-2°x0.07	11°	35
CMT3	DNMG1506	TiC, TiN and WC; Co(18%)	PVD_3	3	-7°	-2°x0.07	11°	50
WCN1	DNMG1504	MGS WC(85%), Co(9.5%); γ-phase (5.5%)	CVD_1	7.5	-7°	/	9°	30
WCN2	DNMG1504 (with wiper)	MGS WC(88.5%), Co(5.8%); γ-phase (5.7%)	CVD_1	21.5	-7°	/	4°	50
WCN3	DNMG1506	UMGS WC(89%), Co(10%); γ-phase (1%)	PVD_4	4.5	-7°	/	7°	35
WCN4	DNMG1504	MGS WC(91.3%), Co(6.5%); γ-phase (2.2%)	CVD_2	5.5	-7°	/	9°	20
WCN5	DNMG1504	MGS WC(91.3%), Co(6.5%); γ-phase (2.2%)	CVD_2	5.5	-7°	/	6°	30
WCN6	DNMG1506 (with STTS)	UMGS WC(83.5%), Co(15.5%); γ-phase (1%)	PVD_4	4.5	-4°	/	9°	35
WCN7	DNMG1506 (with STTS)	UMGS WC(89%), Co(10%); γ-phase (1%)	PVD_4	2.25	-4°	/	9°	30
WCN8	DNMG1506	UMGS WC(89%), Co(10%); γ-phase (1%)	PVD_4	2.25	-7°	/	7°	30
WCN9	DNMG1504	MGS WC(93.6%), Co(6%); γ-phase (0.4%)	PVD_5	3.5	-7°	/	14°	20
WCN10	DNMG1504	MGS WC(93.6%), Co(6%); γ-phase (0.4%)	PVD_5	5.5	-7°	/	6°	5
WCN11	DNMG1506	WC(81%), Co(9%); γ-phase (10%)	CVD_1	15	-7°	-2°x0.07	11°	50
WCN12	DNMG1506	UMGS WC(89%), Co(10%); γ-phase (1%)	PVD_4	4.5	-7°	/	7°	40
WCP1	DCMT11T3	UMGS WC(83.5%), Co(15.5%); γ-phase (1%)	PVD_4	4.5	0°	/	6°	35
WCP2	DCMX11T3 (with wiper)	UMGS WC(83.5%), Co(15.5%); γ-phase (1%)	PVD_4	4.5	0°	0°x0.07	18°	30
WCP3	DCMT11T3	UMGS WC(93.6%), Co(6%); γ-phase (0.4%)	PVD_5	3.5	0°	/	5°	25
WCP4	DCGT11T3	UMGS WC(89%), Co(10%); γ-phase (1%)	Uncoated, polished		+5°	/	26°	5
WCP5	DCMT11T3	UMGS WC(83.5%), Co(15.5%); γ-phase (1%)	PVD_4	4.5	+4°	7°x0.15	15°	50
WCP6	DCGT11T3	MGS WC(94%),Co(6%)	Uncoated		+10°	/	15°	10
WCP7	DCGT11T3	MGS WC(94%),Co(6%)	Uncoated, polished		+8°	/	28°	5

PVD_1 = TiN; PVD_2 = TiN-TiCN-TiN; PVD_3 = TiCN; PVD_4 = TiAlN; PVD_5 = AlTiN; CVD_1 = TiN-TiCN-Al_2O_3; CVD_2 = TiN-TiCN- Al_2O_3-TiCN-TiN; MGS = fine grain (grain dimension≈1µm); UMGS = ultra-fine grain (grain dimension < 1µm); SCBG = Chipbreaker with special geometry

5.4.3 Preliminary cutting tests

Preliminary cutting tests were performed in order to evaluate a suitable range of cutting parameters for turning with dry conditions. Afterwards, analyzed cutting tool were compared in terms of surface roughness, chip control, cutting forces and resistance to tool breakage or tool wear, in order to identify the best cutting tools for the final phase, i.e. the tool wear tests.

Influence of cutting speed

Aiming at investigating on the influence of cutting speed on the machinability of sintered Molybdenum in longitudinal finishing turning, depth of cut a_p was fixed to 0.3mm, whereas feed rate f had to be about 0.11mm/rev in order to achieve desired quality surface. Therefore, cutting speed v_c was the main factor in the design of experiments described in Tab. 5.5.
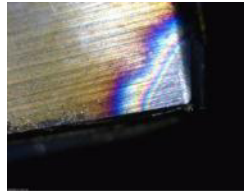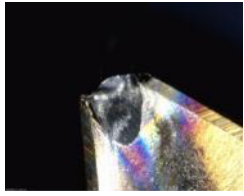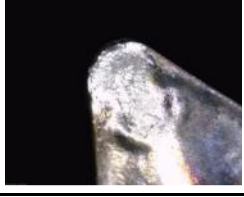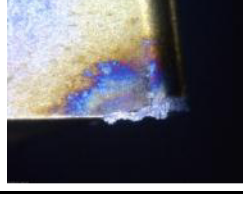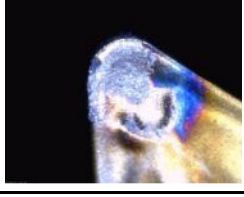
The considered process outputs were main cutting force F_c, machine tool head acceleration in feed direction A_z and surface quality R_a. Cutting force signal was low-passed filtered by applying a cut-off frequency of 500 Hz, whereas the acceleration signal was filtered by applying band-pass filter with bandwidth from 100 to 4000 Hz, in order to remove the dynamic disturbances affecting the measuring chain.

Tab. 5.5 DOE for analyzing influence of cutting speed on cutting process [60]

Factor	Level	Values
Cutting tools	24	See Tab. 5.4
Cutting speed v_c [m/min]	6	$50 \div 300$
Feed f [mm/rev]	1	0.11
Depth of cut a_p [mm]	1	0.3
Replication		1 or 2

By performing these experimental investigations, it was first observed that several cutting tools were not adequate for machining sintered Molybdenum, because of sudden tool tip breakage, rapid flank wear, land progression or premature cutting tool edge cracking. Low performances were attributed to several causes, such as brittle material of the core of the tool, inadequately tool coating or tool geometry (see Tab. 5.6 for ceramic and CerMet cutting insert, Tab. 5.7 relating to cemented carbide tools). These cutting inserts were excluded from following experimental phases.

Tab. 5.6   Inadequate tools after preliminary cutting tests and possible reasons of failure
(Ceramic and CerMet cutting inserts)

Code	Notes	Primary flank 1 mm	Rake face 1 mm
CER1	Tool breakage due to very large negative rake angle, and ceramic brittle tool core material		
CER2	Tool breakage due to very large negative rake angle and ceramic brittle tool core material		
CMT1	Rapid flank wear and cutting edge cracking causing poor surface quality due to brittle core material		
CMT2	Rapid flank wear and cutting edge cracking causing poor surface quality due to brittle core material		
CMT3	Rapid flank wear and cutting edge cracking causing poor surface quality due to brittle core material and high rounded cutting edge		

Tab. 5.7   Inadequate tools after preliminary cutting tests and possible reasons of failure
(cemented carbide cutting inserts)

Code	Notes	Primary flank 1 mm	Rake face 1 mm
WCN1	Flank wear causing poor surface finishing, due to inadequate CVD coating		
WCN2	Rapid flank wear and cutting edge cracking causing very poor surface quality due to very thick CVD coating, large rounding cutting edge and wiper geometry		
WCN6	Tool tip breakage due to special sharpening		
WCN7	Tool tip breakage due to special sharpening		
WCN9	Tool tip breakage due to brittle material and high positive normal rake angle		
WCN10	Tool tip breakage due to brittle material and very sharp cutting edge		
WCN11	Rapid flank wear and cutting edge cracking due to thick CVD layer and large cutting edge radius		

Experimental trends measured with the other cutting tools are shown in Fig. 5.8 for negative basic-shape inserts type DNMG, and Fig. 5.9 for positive basic-shape inserts type DCMT/DCGT.

From the analysis of the results, all the considered process outputs were strongly affected by cutting speed v_c. In particular, surface roughness R_a was significantly reduced when cutting speed v_c was increased. A satisfactory surface quality was achieved when cutting speed was greater or equal to 150 m/min. Likewise, the average main cutting force F_c components, as well as the energy of machine tool head vibrations (given by the standard deviation of the accelerations signal) were greatly reduced when cutting speed was increased above the limit of 150 m/min. Moreover, built up edge (removed material stick to the rake face of the tool) was observed especially at low cutting speeds. Accordingly, built up edge formation is responsible for a non-stationary and anomalous chip formation at lower cutting speeds. This was further confirmed by analyzing the ratio of cutting forces fluctuations with respect to the average main cutting forces ($\sigma(F_c)/\mu(F_c)$), which was decreasing as the cutting speed increased.

It should be highlighted that some positive shape-base cutting inserts (type DCGT, WCP4, WCP6 and WCP7) showed a better behavior in the whole cutting speed range, including low cutting speeds.
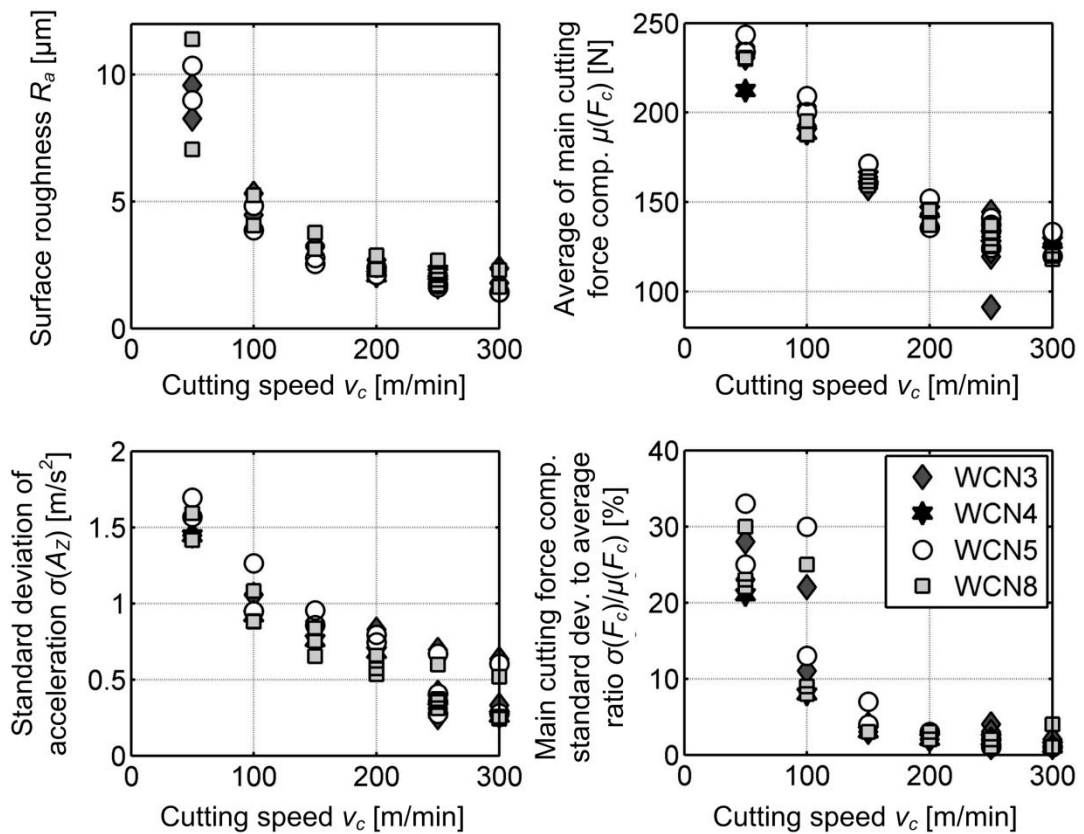
Fig. 5.8 Influence of cutting speed on outputs of cutting process for negative basic-shape cutting inserts [60]
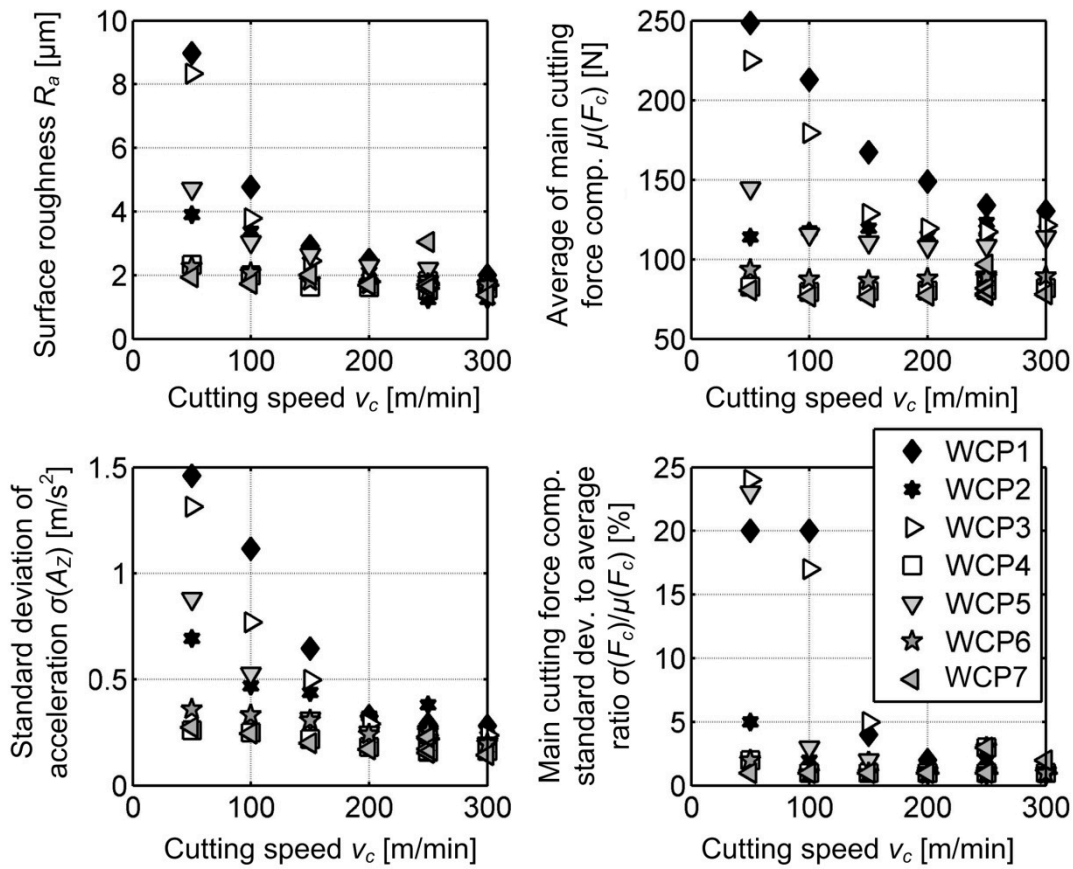
Fig. 5.9 Influence of cutting speed on outputs of cutting process for positive basic-shape cutting inserts [60]

For each applied cutting speed, visual inspection of the machined surface was also carried out. In Fig. 5.10 the workpiece surfaces machined by two reference cutting tools called WCN8 and WCP4 are shown. It is evident that quality surface for a given v_c, was improved applying a positive basic shape cutting tool instead of a negative basic-shape insert. Moreover, experimental evidences derived from data analysis were confirmed by visual inspection: surface quality increased when cutting speed was increasing.
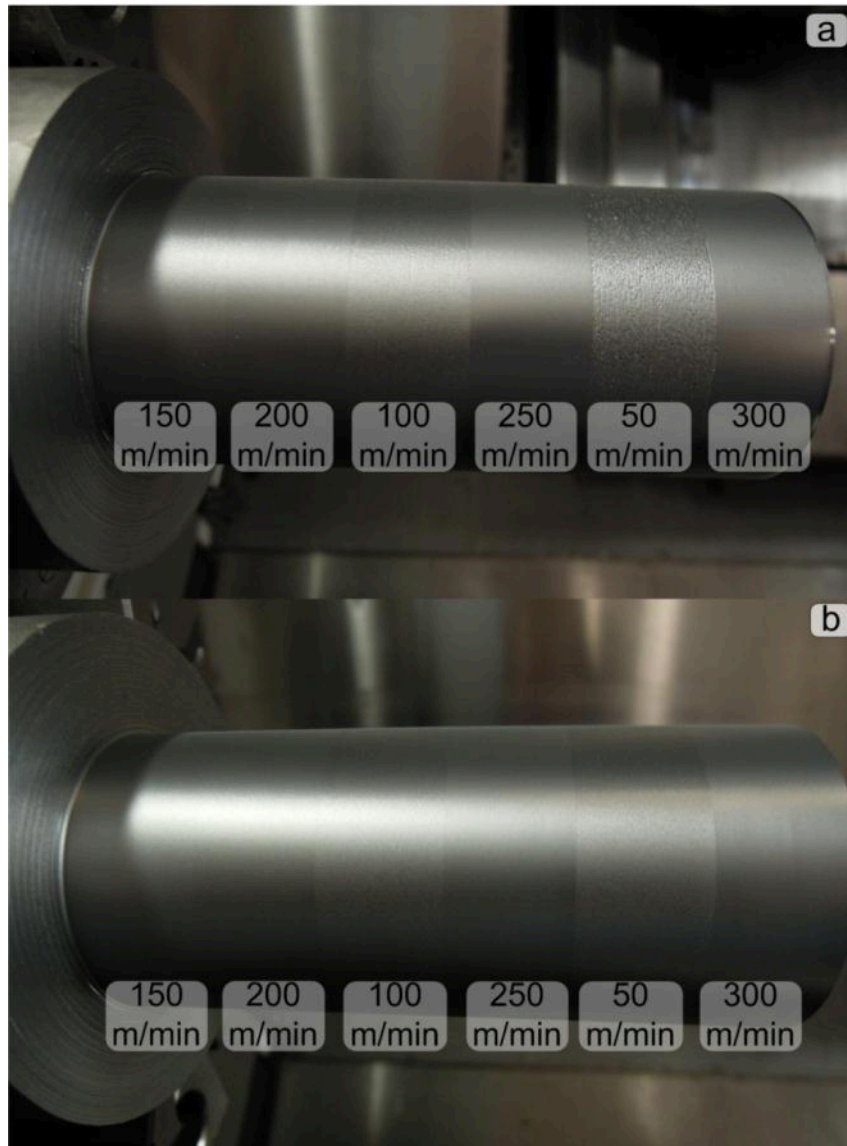
Fig. 5.10 Machined surface at various cutting speeds v_c for negative basic-shape cutting tool WCN8 (a) and positive basic-shape cutting tool WCP4 (b) (f=0,11 mm/rev, a_p=0.3mm)

Chip form was also analyzed by considering two representative cutting inserts, the WCN8 and the WCP4 (see Fig. 5.11). Short or medium washer-type helical chips were obtained by applying WCP4 cutting insert. At microscopic level, by stereomicroscope inspection, chip form was rather regular, except with v_c equal to 50 m/min. Regarding WCN8 cutting tool, loose or connected arc chips were observed at lower cutting speed, whereas washer-type helical chips were observed at higher cutting speed. However, at microscopic level, chips were more irregular than those of WCP4, suggesting that WCN8 was affected by a worse, non-stationary chip formation mechanism.

Aiming at understanding the influence of cutting speed on chip formation, chip compression ratio ζ was also measured, see Fig. 5.12. Chip compression ratio ζ was defined by Zorev [87] as the ratio of chip thickness to uncut chip thickness, as explained in the previous section. Experimental values of chip compression ratio increase up to a maximum value and then they considerably decrease as cutting speed in further increased. The observed behavior is qualitatively similar to that reported by Zorev [87] for a conventional carbon steel, ad it is in

83

accordance with the hypothesis of build-up edge formation promoted by low cutting temperatures and high plastic shear deformations observed at low/medium cutting speeds. In addition, it was noticed that chip compression values of negative-shape cutting insert WCN8 were significantly higher than those obtained by applying positive basic-shape cutting insert WCP4. Besides, maximum chip compression ratio was observed at 150 m/min in the case of WCN8, whereas it was observed at 100 m/min in the case of WCP4.

Better experimental results obtained with positive basic-shape cutting inserts WCP4, WCP6 and WCP7 are probably due to their highly positive geometry and to the characteristics of tool rake face (uncoated and polished), which promoted a regular chip formation by concurrently reducing of cutting forces.
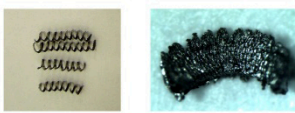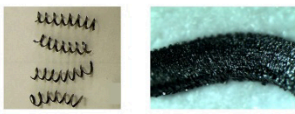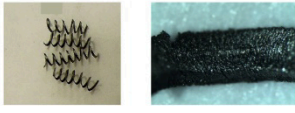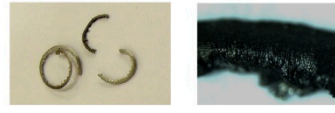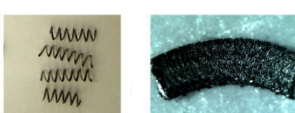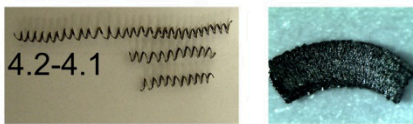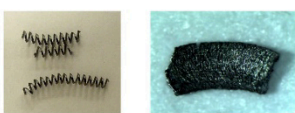
Fig. 5.11 Influence of cutting speed on chip form for WCP4 and WCN8 (f=0,11mm/rev, a_p=0.3mm); chip forms according to ISO3685 (1993): 4.1 = long washer-type helical chips; 4.2 = short washer-type helical chips; 4.3 = snarled washer-type helical chips; 6.1 = connected arc chips; 6.2 = loose arc chips) [60]
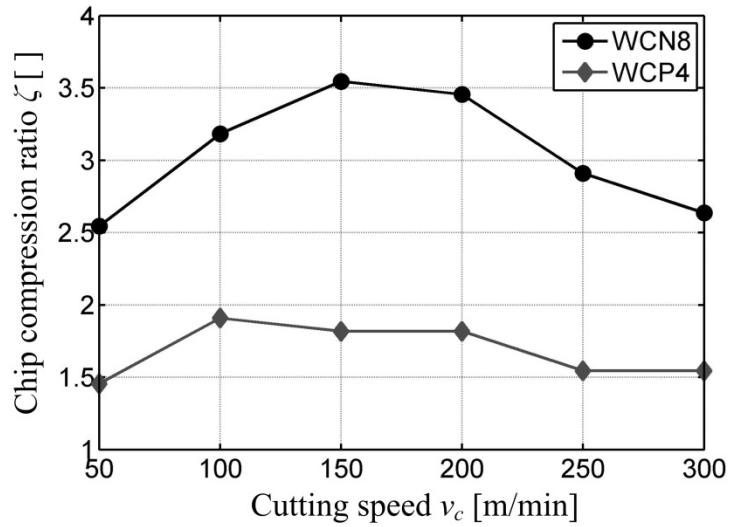
Fig. 5.12 Influence of cutting speed on chip compression ratio for WCP4 and WCN8 (f=0,11mm/rev, a_p=0.3mm) [60]

After that preliminary considerations, it was establish that there are a significant benefits in terms of surface quality and chip formation by applying a cutting speed greater than 150 m/min in dry cutting condition. Therefore, following investigations was carried out in the cutting speed range between 180 and 320 m/min.

Machined surface quality

In order to analyze the effect of cutting parameters on surface quality and chip control, design of experiments, reported in Tab. 5.8, was carried out.

Tab. 5.8 DOE to investigate influence of cutting parameters on surface quality [60]

Factor	Level	Values
Cutting tools	12	WCN3, WCN4, WCN5, WCN8, WCN12, WCP1, WCP2, WCP3, WCP4, WCP5, WCP6, WCP7
Cutting speed v_c [m/min]	3	180, 250, 320
Feed f [mm/rev]	4	0.075, 0.11, 0.14, 0.175
Depth of cut a_p [mm]	1	0.3
Replication	2 or plus	

Experimental surface roughness R_a showed a parabolic trend as feed rate f was increased, see Fig. 5.13. Also the effect of cutting speed on surface roughness was significant. For most of cutting insert, surface roughness linearly decreased as cutting speed increased.
From these experimental findings, a simple mathematical model to estimate R_a for each cutting tool was proposed.

$$R_a = k_0 + k_1 f + k_2 f^2 + k_3 \cdot v_c + k_4(f \cdot v_c) + k_5(f^2 \cdot v_c) \tag{5.6}$$
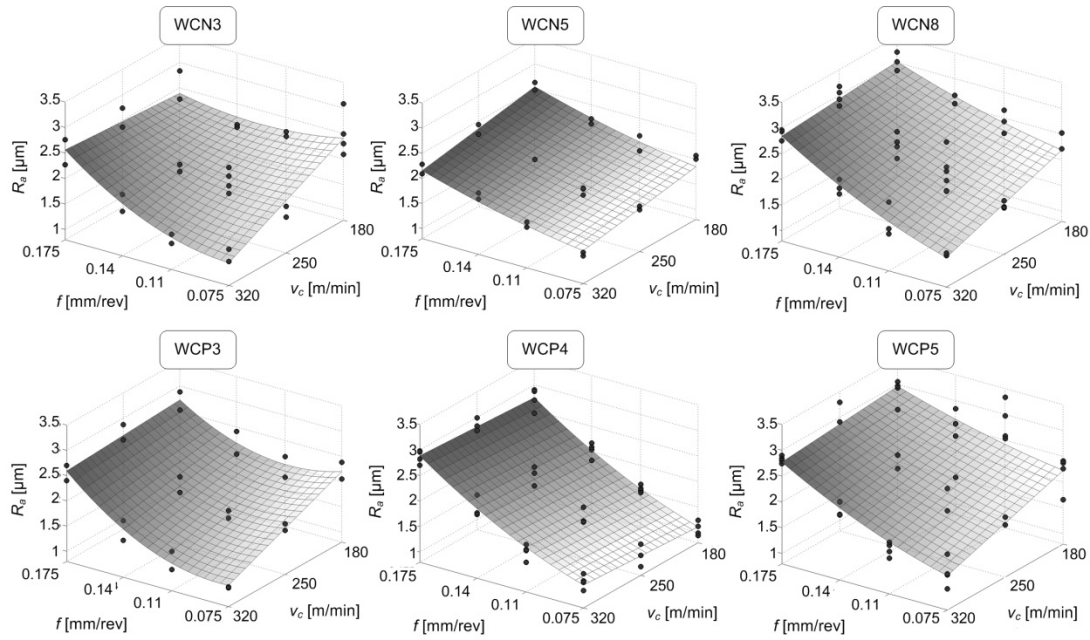
Fig. 5.13 Surface roughness R_a model and experimental values for some of most representative cutting inserts (a_p=0.3mm) [60]

Unknown coefficients were estimated by applying the stepwise regression technique in order to exclude the coefficient related to a non-influence factor. It shall be pointed out that model structure varies a lot from tool to tool. Therefore, the surface roughness is strongly influenced by the interaction between tool geometry and cutting parameters.

In order to ease cutting insert comparison, a reference surface roughness value $R_{a,ref}$, predicted by the model applying v_c equal to 250m/min and f equal to 0.11mm/min are listed in Tab. 5.9.

For evaluating the repeatability of surface quality results, experimental data dispersion was estimated by computing the standard deviation $\sigma_{\varepsilon Ra}$ of relative errors, defined as:

$$\varepsilon_{Ra} = \frac{R_{a,exp} - R_{a,mod}}{R_{a,mod}} \ [\%] \tag{5.7}$$

where $R_{a,mod}$ and $R_{a,exp}$ are average values predicted by model and experimental points, respectively.

Cutting inserts affected by the highest values of experimental data dispersion, i.e. WCN4, WCN12, WCP5, WCP7, were discharged, since they were considered unreliable for assuring repeatable surface quality. Insert WCP6 was also discharged since the chip breaker was not working properly for any feed levels.

Tab. 5.9 Experimental results of surface roughness and model parameters [60]

Tool code	Surface roughness R_a model							$R_{a,ref}$ [μm]	Surface quality [%]	Chip control (f_{min})
	k_0	k_{vc}	k_f	k_{fvc}	k_{f2}	k_{f2vc}	$\sigma_{\varepsilon,rel}$ [%]			
WCN3	5.20	-1.04E-02	-1.73E+01	/	/	3.81E-01	10.8	1.84	96	fair (0.11)
WCN4	3.44	-6.00E-03	/	/	/	1.34E-01	19.7	2.35	92	good (0.075)
WCN5	2.20	-2.80E-03	/	/	2.80E+01	/	5.9	1.83	96	good (0.075)
WCN8	3.23	-6.83E-03	/	/	/	1.83E-01	8.9	2.08	96	fair (0.11)
WCN12	/	/	2.81E+01	-4.08E-02	/	/	27.4	1.98	83	good (0.075)
WCP1	3.06	-5.76E-03	/	/	/	1.50E-01	8.0	2.07	96	good (0.075)
WCP2	3.01	-6.23E-03	/	/	/	/	9.2	1.45	92	fair (0.11)
WCP3	5.94	-1.15E-02	-4.49E+01	6.03E-02	1.57E+02	/	8.5	1.68	96	good (0.075)
WCP4	0.57	9.82E-04	/	/	6.55E+01	/	8.6	1.60	96	good (0.075)
WCP5	3.20	-6.35E-03	/	/	/	1.63E-01	16.6	2.11	88	good (0.075)
WCP6	0.74	/	/	/	8.00E+01	/	11.0	1.71	92	poor in the whole range
WCP7	0.82	/	/	/	8.24E+01	/	20.3	1.82	92	good (0.075)

Cutting force analysis

In order to compare the residual cutting inserts in terms of cutting process mechanics, cutting force measurements were carried out applying the design of experiments illustrated in Tab. 5.10.

Tab. 5.10 DOE to investigate influence of cutting parameters on cutting force model coefficients [60]

Factor	Level	Values
Cutting tools	7	WCN3, WCN5, WCN8, WCP1, WCP2, WCP3, WCP4
Cutting speed v_c [m/min]	3	180, 250, 320
Feed f [mm/rev]	4	0.075, 0.11, 0.14, 0.175
Depth of cut a_p [mm]	5	0.1 ÷ 0,5
Replication	2	

From experimental investigations, trends of main cutting force F_c, feed force F_f and back force F_p were derived against cutting parameters. In Fig. 5.14 are reported experimental mean value of the measured forces applying the negative basic-shape cutting tool WCN8 and the positive basic-shape cutting insert WCP4. In general, it emerged that positive basic shape tool, like WCP4, exerts minor cutting forces in comparison with negative basic shape inserts, thanks the positive shape of the rake face. Moreover, main cutting force and feed force increased with depth of cut and feed values, whereas they decreased if cutting speed was

increased. These effects are more evident analyzing experimental trends of WCN8. Back force was not affected by depth of cut, but it increased if feed rate was increasing.
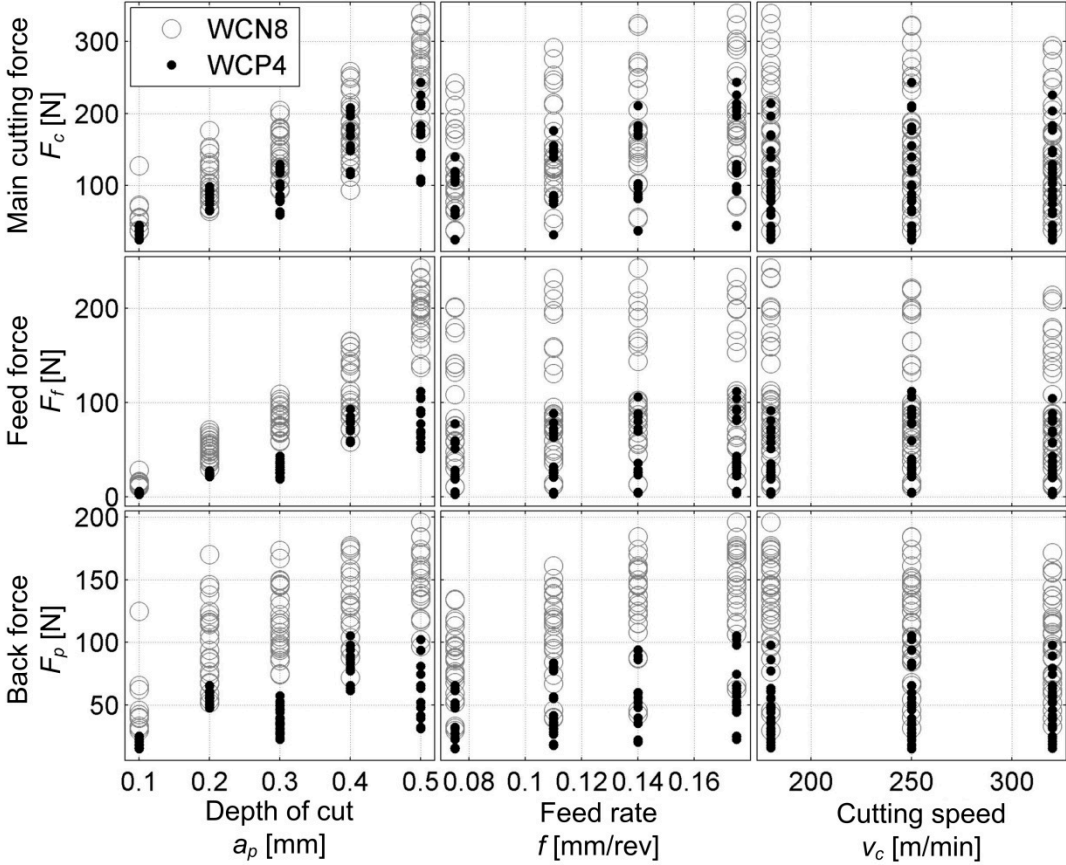
Fig. 5.14 Scatter plot diagram of cutting forces against cutting parameters for tools WCN8 and WCP4

By applying the Shearing and Ploughing cutting forces model, presented in Chapter 3, cutting forces were modeled; cutting force model coefficients, model adequacy and the observed state of the cutting edge at the end of these tests are listed in Tab. 5.11. In Fig. 5.15, average cutting forces, at reference cutting conditions are reported.

In general, the proposed cutting force model demonstrated good interpolation capabilities, since model errors were moderate for all the cutting inserts.

Tab. 5.11   Cutting force model coefficients, model adequacy and tool wear *VB* [60]

Code	k_{cs} [N/mm²]	k_{cp} [N/mm]	k_{ns} [N/mm²]	k_{np} [N/mm]	$\sigma_{\varepsilon F}$ [%]	VB [mm]
WCN3	2411	95.3	1711	157	11.7	0.1<*VB*<0.2
WCN5	2400	96.4	1750	148	9.93	0.1<*VB*<0.2
WCN8	2524	92.2	1806	157	11.8	0.1<*VB*<0.3
WCP1	2098	144	1517	190	9.96	Broken
WCP2	2691	60.9	1728	110	9.96	*VB*>0.3
WCP3	2080	135.2	1589	168	9.15	Broken
WCP4	2267	32.1	932	58.9	8.71	0.1<*VB*<0.2

Cutting coefficients were slightly different among the tested cutting tools, even if the cutting force measured at the reference cutting conditions were about the same for most of cutting tools. This can be explained by considering that shearing coefficients (k_{cs} and k_{ns}) variations between two cutting inserts were partially counterbalanced by opposite variations of the corresponding ploughing coefficients (k_{cp}, k_{np}).

Analyzing the results, it has to be highlighted that WCP4 cutting insert was characterized by significantly smaller S&P coefficients (precisely, k_{cp}, k_{ns} and k_{np}) and by smaller cutting forces at reference cutting conditions. This behaviour can be simply explained by the normal rake geometry of the WCP4 which was considerably greater in comparison with all the other cutting inserts.
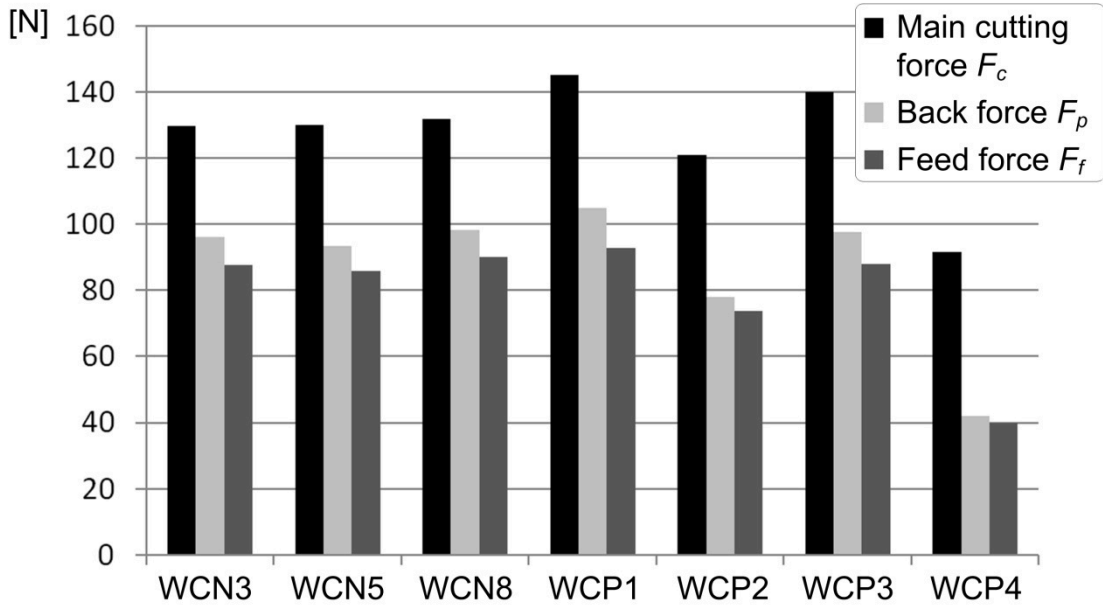
Fig. 5.15   Average cutting forces components (v_c=250m/min, f=0.11mm/rev, a_p=0.3mm) [60]

By applying the standard relations of orthogonal cutting [86], shear angle ϕ of about 40° was estimated from the normal rake angle γ and from the chip compression ratio ζ obtained with WCP4 at cutting speed equal to 250 m/min, feed equal to 0.11 mm and depth of cut equal to 0.3 mm. An equivalent friction coefficient μ of about 1.5 was determined, applying Eq. 5.2,

by comparing the main and normal cutting force components dF_c and dF_n, and by taking into account the normal rake angle γ. Finally, the chip flow stress τ_s on the shear plane was estimated, as explained in the previous section, yielding 670 MPa in the case of WCP4 cutting insert. These calculations were repeated for the other inserts (characterized by smaller normal rake angles), yielding an average shear angle ϕ of about 22°, an average equivalent friction coefficient of about 1.25, and an average chip flow stress τ_s of about 700 MPa. It is worth noting that the average chip flow stress τ_s determined for the sintered Molybdenum considered in this research is very similar to the chip flow stress reported by Micheletti [86] for a conventional AISI 1045 steel (about 660 MPa). This result should not be unexpected, if we consider the hardness of sintered Molybdenum, which was about that of AISI 1045 steel. However, a greater average equivalent friction coefficient μ was observed with sintered Molybdenum than the average value provided by Micheletti for conventional steels ($\mu \approx 1$), confirming the stronger tendency to adhesion of the considered material to the normal rake, which was responsible for heavy plastic shear at the chip – normal rake interface.

As reported in Tab. 5.11, cutting inserts WCP1, WCP2 and WCP3 were affected by tool tip breakage or excessive tool wear at the end of the tests. Accordingly, they were discharged, leaving WCN3, WCN5, WCN8, WCP4 as the only candidates for the final tool wear tests.

5.4.4 Tool wear tests

Tool wear tests were finally carried out on the remaining cutting tools, following the design of experiments illustrated in Tab. 5.12.

Tab. 5.12   Design of experiments for tool wear tests [60]

Factor	Level	Values
Cutting tools	4	WCN3, WCN5, WCN8, WCP4
Cutting speed v_c [m/min]	2	215, 285
Feed f [mm/rev]	4	0.11
Depth of cut a_p [mm]	5	0.3
Replication	2	
Additional cutting tests		v_c=180 m/min for WCN3, WCN5, WCN8 v_c=320 m/min for WCP4

The maximum width of the tool flank wear land VB_{max} were measured during the tool wear tests to monitor tool wear progression. Tool life was defined by applying the criterion of VB_{max} = 0.3mm. Surface quality was also monitored, by measuring absolute roughness R_a and by visual inspection of the machined surface.

Giving a direct comparison of the wear resistance of the applied cutting inserts, tool wear curves versus machining time are shown in Fig. 5.16 for a reference value of cutting speed equal to 215 m/min and in Fig. 5.17 considering v_c=285m/min. As expected, tool life decreased when cutting speed was increasing. This behavior was more evident for negative basic-shape cutting insert (WCN3, WCN5, WCN8). Tool wear resistance was significantly higher in the case of WCP4.
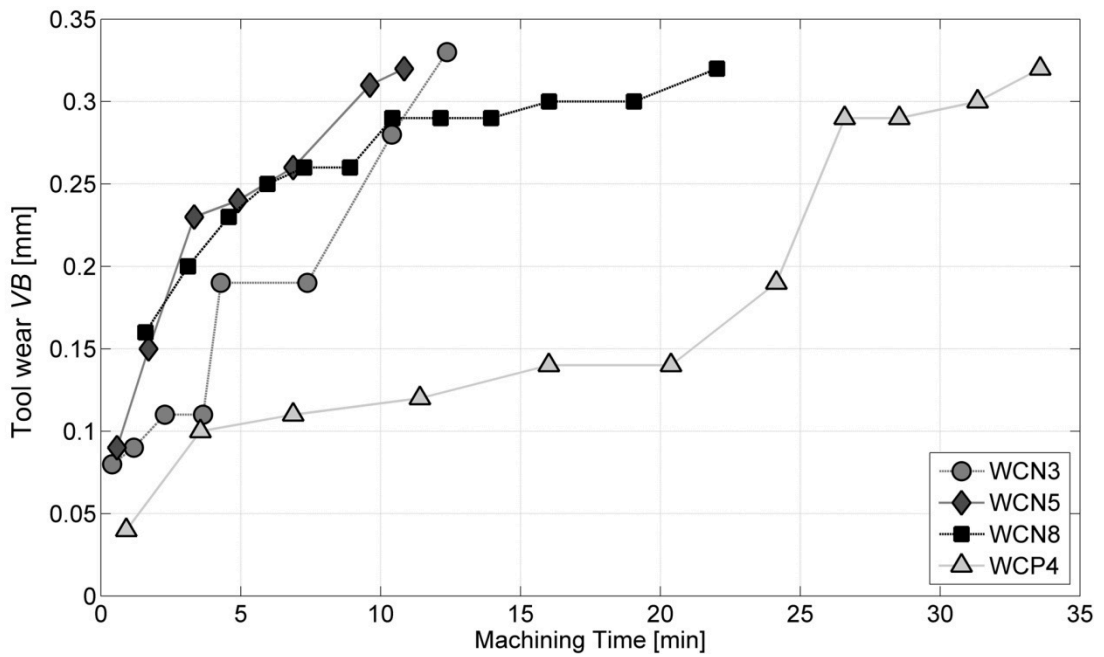
Fig. 5.16 Comparison of tool wear progression curves at reference cutting speed v_c=215m/min, for the tested tools
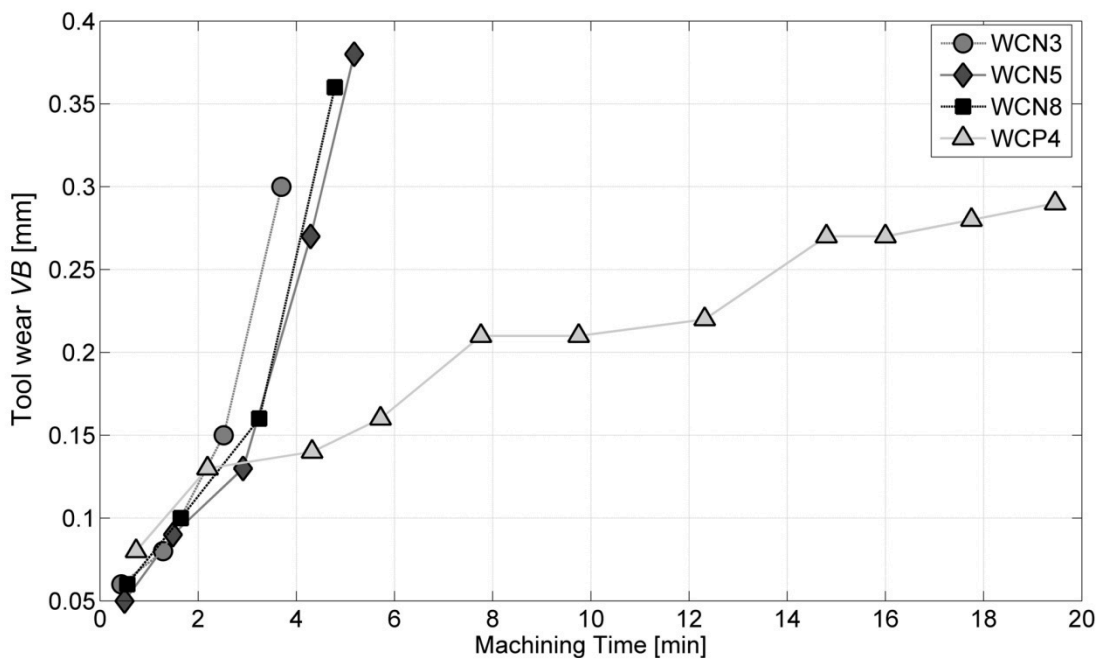
Fig. 5.17 Comparison of tool wear progression curves at reference cutting speed v_c=285m/min, for the tested tools

From Tab. 5.13 to Tab. 5.16 some images about primary flank wear, rake face wear and secondary flank wear are collected: it is evidenced the damages of various cutting inserts in machining Molybdenum in dry turning. The measured VB and R_a are reported at the end of tool life and at the halfway instant. All inserts exhibited an heat affected zone due to the high temperature because refractory characteristic of Molybdenum. Moreover, stick cutting

material on insert faces was detected. Flank wear was observed for all cutting inserts; in the case of WCP4 cutting insert, also notch wear was supposed.
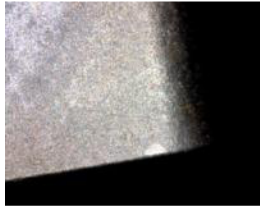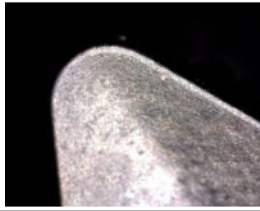
Tab. 5.13 Tool wear progression for WCN3 (v_c=215m/min, a_p=0.3mm, f=0.11mm/rev)

WCN3 1 mm	$T = 0$ min $VB = 0$ mm	$T = 4.3$ min $VB = 0.14$ mm $R_a = 3.26$ µm	$T = 12.4$ min $VB = 0.33$ mm $R_a = 3.48$ µm
Primary flank			
Rake face			
Secondary flank			
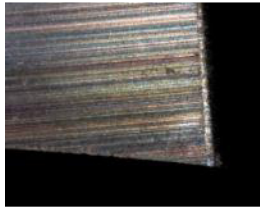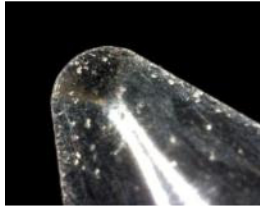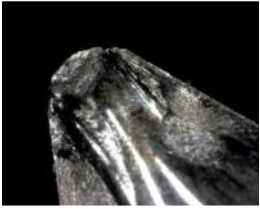
Tab. 5.14 Tool wear progression for WCN5 (v_c=215m/min, a_p=0.3mm, f=0.11mm/rev)

WCN5 1 mm	$T = 0$ min $VB = 0$ mm	$T = 4.9$ min $VB = 0.24$ mm $R_a = 3.17$ µm	$T = 9.16$ min $VB = 0.31$ mm $R_a = 4.58$ µm
Primary flank			
Rake face			
Secondary flank			

Tab. 5.15 Tool wear progression for WCN8 (v_c=215m/min, a_p=0.3mm, f=0.11mm/rev)

WCN8 1 mm	$T = 0$ min $VB = 0$ mm	$T = 4.6$ min $VB = 0.23$ mm $R_a = 2.72$ µm	$T = 22$ min $VB = 0.32$mm $R_a = 4.79$ µm
Primary flank			
Rake face			
Secondary flank			

Tab. 5.16 Tool wear progression for WCP4 (v_c=215m/min, a_p=0.3mm, f=0.11mm/rev)

WCP4 1 mm	$T = 0$ min $VB = 0$ mm	$T = 3.6$ min $VB = 0.1$ mm $R_a = 2.59$ µm	$T = 33.6$ min $VB = 0.32$ mm $R_a = 5.75$ µm
Primary flank			
Rake face			
Secondary flank			

The behaviour of the surface roughness R_a against tool wear VB_{max} was strongly dependent on the considered cutting inserts, see Fig. 5.18. In general, surface roughness increased with tool wear. On the average, better surface quality was achieved with WCN3 and WCN8 cutting inserts, showing almost linear trends with respect to VB_{max}. The behaviour of the WCN5 insert was less satisfactory. More scattered results were obtained by applying the cutting tool WCP4: it is not recommended if quality surface has to be taken carefully under control.
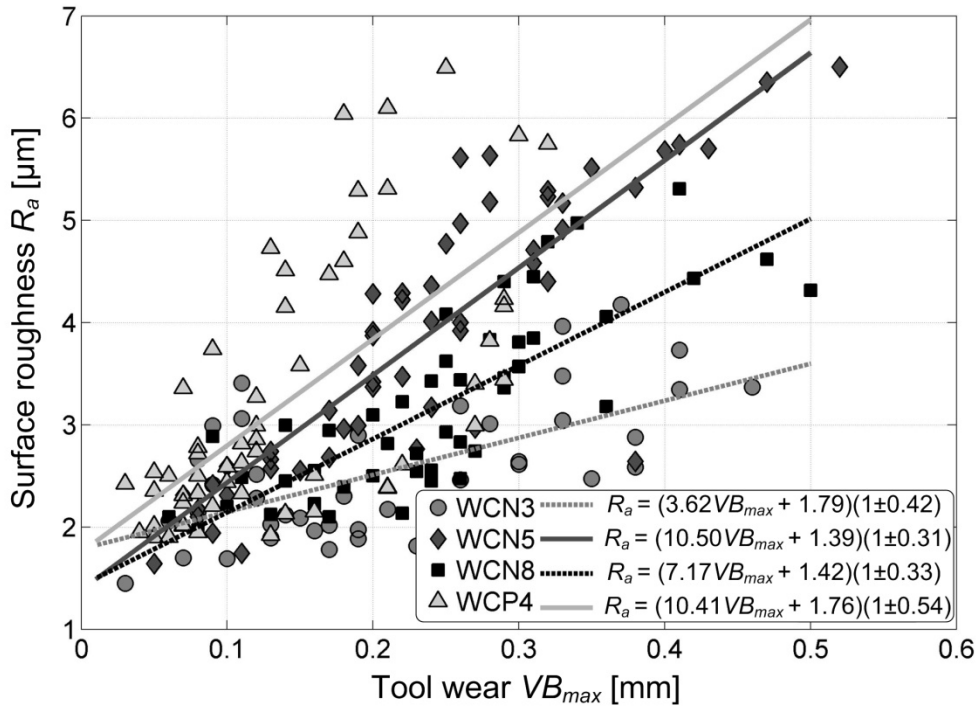
Fig. 5.18 Surface roughness R_a behaviour against tool wear VB and interpolating linear models [60]

In order to compute tool life, Taylor's approach was applied. Accordingly, tool life expectancy is defined by the relationship:

$$v_c T^n = C \qquad (5.8)$$

Where n and C are unknown coefficients dependent on tool characteristics and workpiece material: they have to be estimated experimentally.

Tool life curves were computed by only considering the data obtained with cutting speed levels of 215 and 285 m/min, determining the Taylor's model (Fig. 5.19). WCP4 was characterized by considerably higher tool life and by smaller data dispersion in comparison with the other three cutting inserts. Since the cost of each cutting insert was similar, the economic cutting speed, i.e. the optimal cutting speed according to economic criteria, of WCP4 is higher than the other economic cutting speed of the other inserts. Accordingly, it was decided to carried out additional experimental tests, at 180 m/min with WCN3, WCN5 and WCN8 and at 320 m/min with WCP4. The aim was evaluating the reliability of the obtained Taylor's curves.

In general, there is a satisfactory agreement between Taylor's curves and additional experimental points, partially validating the Taylor's model outside the investigated cutting speed range.
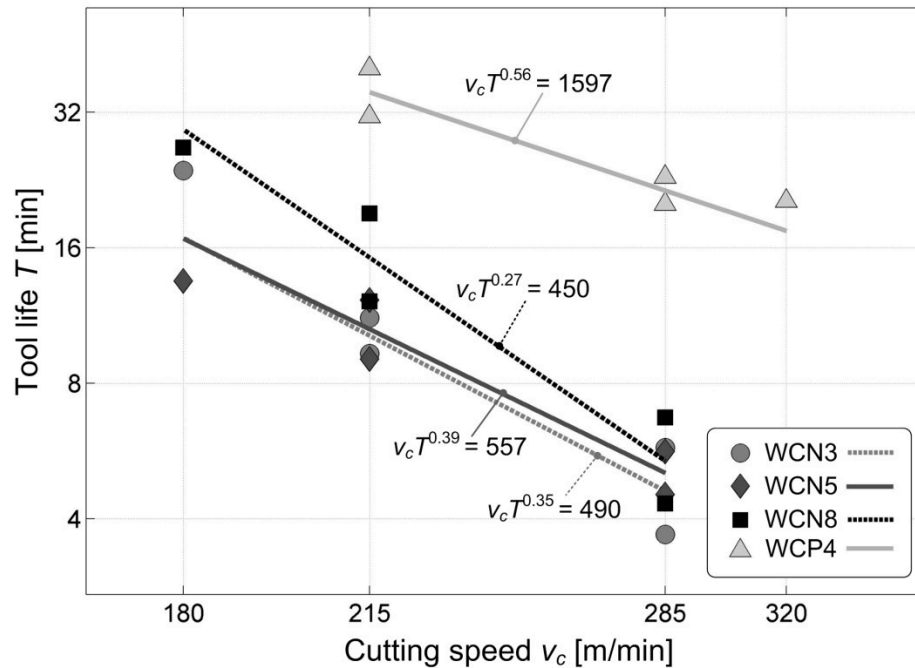
Fig. 5.19 Experimental tools life and Taylor's curves [60]

Finally, tool wear mechanisms were investigated by acquiring high-definition images by means of Scanning Electron Microscope (Fig. 5.20). SEM images of worn tool WCN3, WCN5 and WCN8 (Fig. 5.20 – a, c and e) before chemical etching revealed a thick built up edge on the rake face, whereas thinner layer of Molybdenum was stuck on WCP4 cutting tool. A possible reason of that can be explained by the higher normal rake angle combined with a better surface quality of the insert achieved by polishing treatment.

After chemical etching (Fig. 5.20 – b, d, f and g), worn tool WCN3, WCN5 and WCN8 were affected by large flank wear land, due to mechanical abrasion of cutting material. Deep notches were also clearly visible both on flank and rake face suggesting that oxidation had been an important tool wear mechanism. This hypothesis was confirmed by performing the chemical analysis by EDS procedure, in the surrounding of notches, which revealed the presence of various type of oxide. Specifically, Oxygen in combination with Molybdenum was found on all cutting inserts; Oxygen in combination with Titanium or Aluminum was detected on WCN3 and WCN8, whereas Oxygen in combination with Tungsten was observed on the uncoated positive insert WCP4. Local cutting edge breaking were also observed ((Fig. 5.20 – d and f), probably due to thermo-mechanical stresses. In addition, small craters were detected on the rake face, likely due to the adhesion mechanism connected to built up edge formation.

Considering the positive basic-shape cutting insert WCP4, the flank wear land was narrow, except at the lateral borders of the area, where deep notches were present. Such notches continued on the rake face. Moreover, the highly sharp cutting edge suffered of chipping and local cracking, causing a premature worsening of surface quality in some cases. No crater on the rake face was observed, suggesting that oxidation was the dominant tool wear mechanism for WCP4. The effects of direct mechanical abrasion were indeed less dramatic for this cutting insert, while the effects of adhesion were not observed at all.

Following these considerations, main cause of tool wear was the high temperature characterizing machining of refractory materials, like Molybdenum. Indeed, mechanical stresses were of secondary importance, since cutting forces were not considerably greater

95

than conventional materials, such as carbon steel. In addition, cutting material adhesion on rake face may influence the cutting process and the tool wear progression, especially when inadequate tool geometries or cutting parameters are adopted.
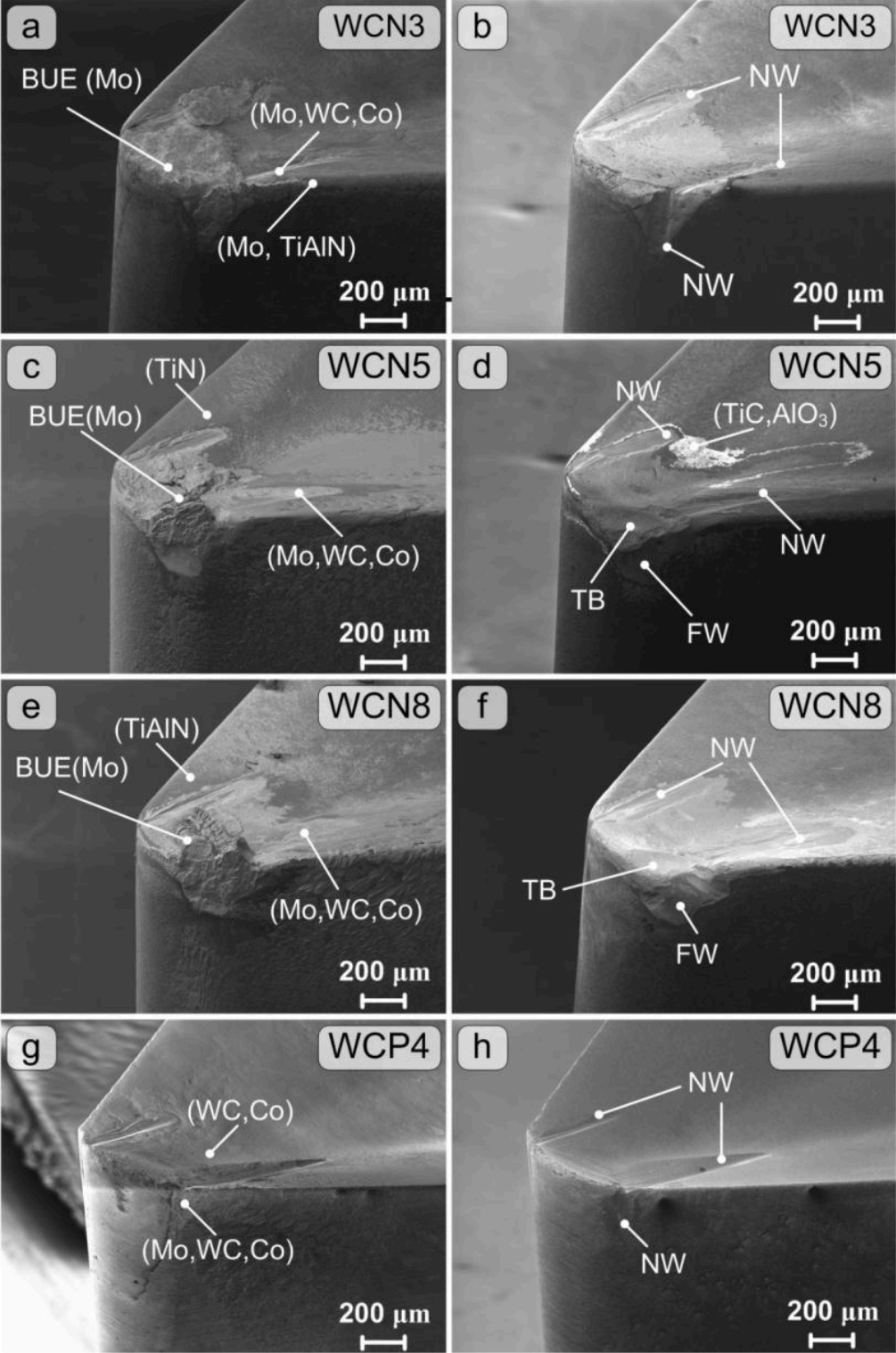
Fig. 5.20 SEM images of worn tool before (a, c, e, g) and after (b, d, f, h) chemical etching (BUE: Build-Up-Edge, FW: Flank Wear, NW: Notch Wear, TB: Tool Breakage) [60]

5.4.5 Conclusions about dry turning of sintered Molybdenum

From the experimental investigation, the following conclusion may be drawn.

- There are great benefits in turning sintered Molybdenum in dry cutting conditions at relatively high cutting speed: when the cutting speed was greater than 150 m/min the cutting process was stable, surface finish was good, cutting forces and machining system vibrations were low; also, the built up edge formation was reduced at high cutting speed due to the better chip flow;
- Experimental surface roughness R_a showed a parabolic increase as feed was increased, in accordance with literature; cutting speed played an important role when machining sintered Molybdenum, in contrast with the behaviour of more conventional workpiece materials: in most cases, surface roughness linearly decreased as cutting speed was increased;
- Surface roughness was strongly influenced by the interaction between tool geometry and cutting parameters;
- In general the cutting forces were slightly higher in comparison to conventional carbon steels and were strongly influenced by the normal rake angle;
- Chip flow stress of sintered Molybdenum was analogous to that of conventional carbon steel; however, a greater equivalent friction coefficient was observed with sintered Molybdenum than that reported in literature for conventional steels, confirming the stronger tendency to adhesion and plastic shear at the chip – normal rake interface;
- Ceramic based cutting inserts were not adequate for machining sintered Molybdenum, because of their brittleness and negative geometry; similarly, CerMet grades were not suitable, probably due to their brittleness;
- The applicability of cemented carbide tools strongly depends on the interaction between tool geometry, coating characteristics and tool surface treatment;
- Most significant characteristics for a successful tool application appeared to be: medium grade Cobalt content ($\approx 10\%$), ultrafine grain size (<1 µm), positive rake angle ($\gamma \geq 6°$), small rounded cutting edge radius ($r_n \leq 35$ µm), thin coating (<6 µm), simple tool tip geometry (e.g., no wiper, no chamfer), polished surface;
- From the analysis of worn tools it emerged that oxidation was the dominant tool wear mechanism: this was due to the high temperatures achieved when turning Molybdenum, in accordance with the behaviour of most refractory metals and heat resistant superalloys;
- Workpiece material adhesion slightly affected the negative basic-shape cutting inserts WCN3, WCN5 and WCN8, as evidenced by the small craters detected on their rake faces; on the contrary, it was practically negligible in the case of positive basic-shape tool WCP4 since its higher normal rake angle and polished rake face reduced chip sticking;
- The longest tool life (32 min at 215 m/min) was observed with WCP4 cutting insert, which had highly positive geometry and polished surface, and therefore the lowest cutting forces, thus reducing the heat generation and temperature; accordingly, there were less oxidation wear and abrasion wear which are both strongly related to tool temperature.

Accordingly, it is possible to machine sintered Molybdenum in dry cutting condition at relatively high speed and obtain a good surface finish and a tool life greater than 20 min, which is still used as a reference to roughly evaluate the profitability of a machining application.

It would also be of further interest to investigate the application of alternative lubricant strategy (for example cryogenic technique or MQL strategy) for efficient machining of sintered Molybdenum.

5.5. General conclusions

Optimization of machining process is strictly related to the experimental study and modelling of the physical interaction of the cutting tool and the workpiece material. Cutting process is a very complex dynamical system whose stochastic outputs depend on several inputs. Moreover, the results obtained in slightly different experimental conditions may significantly vary from those reported in literature. Therefore, it is crucial develop effective experimental procedures for understanding and optimizing the specific machining process under analysis.

Nowadays, advanced or exotic engineered material, such as Super Alloy family or refractory materials, are often selected by the design department in order to fulfil functionalities and properties of the final product. Typical requirements are high surface hardness, mechanical strength, toughness, corrosion and oxidation resistance. The main purpose is the retention of these characteristics, also in case of high temperature in service. Unfortunately these materials are difficult to cut: the high resistance at high temperature implies high plastic deformation, high cutting forces and cutting temperature, affecting workpiece accuracy and reducing the tool wear resistance.

Aiming at studying the machinability of a given workpiece material or to compare the cutting performances obtained with different cutting tools, several process outputs should be taken into account, such as the accuracy of the workpiece, surface integrity, cutting mechanics (cutting forces, friction coefficients, stability of the process), chip morphology, tool wear and tool life. Obviously, a deep knowledge of cutting material properties and characteristics – chemical composition, microstructure, porosity, thermal conductivity, mechanical properties – is crucial for a proper selection of the tooling system, working parameters and cutting environment.

In this Chapter, an overview of the possible strategies for cutting material characterization, for monitoring cutting process and for inspecting workpiece accuracy was given: it emerged that there exist a great number of methodologies for evaluating cutting process outputs of interest.

This study was very useful in developing a systematic procedure for an experimental investigation aiming at analysing machinability problems and in optimizing cutting operations of exotic engineered materials. It was successfully applied in dry turning of sintered Molybdenum.

Thanks to the effectiveness of the applied methodology in studying machinability of sintered Molybdenum, similar strategy can be employed in analysing different difficult to cut materials as presented in [94] which analysed the performances of cutting tool during dry turning of a special-alloy Hadfield steel.

Chapter 6.

MASS FINISHING OF HIGH PRECISION MECHANICAL COMPONENTS

In high precision manufacturing, strict accuracy is required to the final product, such as very stringent dimensional and geometrical tolerances and high surface quality. To achieve these requirements, generally, conventional cutting processes, like turning, milling, grinding or lapping, are not adequate due to intrinsic limits of the cutting system. Such manufacturing processes are indeed not suitable in responding to the meso or nano-scale requirements. Moreover they may produce defects on the workpiece, such as burrs, contaminants, residual stresses that should be removed by special techniques: these defects can affect the machined surface characteristics. Consequently, specific manufacturing processes must be applied in order to perform deburring and radiusing actions, together with the improvement of the surface quality, i.e. surface roughness and surface integrity, and for polishing operations.

Mass finishing is a very common approach for improving part accuracy and surface quality and for removing small defects due to previous cutting operations. For these reason, mass finishing operations are often carried out at the final stages of the production cycle.

Moreover, mass finishing processes are relatively cheap since they permit to work a great number of workpieces simultaneously.

In this Chapter an overview of conventional mass finishing techniques will be presented. Typical edge and surface quality technical requirements in high precision manufacturing will be introduced. Later, a preliminary optimization of a conventional vibrational finishing approach will be illustrated. Eventually, an innovative dry mass finishing technique, performed using a prototype working machine, for deburring, radiusing and polishing, will be presented, together with some preliminary experimental findings.

6.1. Mass finishing processes

Mass finishing is one of the most applied technique for deburring, radiusing, polishing and for improving surface quality and surface integrity of a workpiece. Several different typologies of machines are commercially available: the equipment generally operates as a batch process or as a continuous flow process. Removal action is possible thanks the presence of abrasives, media and water compound. For this reason, these techniques have the additional advantage to machine a great number of workpieces simultaneously (hundred or thousand parts per hour) finishing the most exposed surfaces as well as edges. Since they work on masses of parts, they typically are the lowest cost processes for wide range of parts and materials, both metallic both not-metallic: for this reason they are considered as flexible working processes. Process variables are the machine size, media size, shape and material, the relative amount to part volume, abrasive compound size, material and volume, water volume and cycle time. In add, individual machine type introduces supplementary variables. Moreover, workpiece variables shall be considered for a proper process selection, such as: geometry, shape and material of the part and the required accuracy (geometrical and edge tolerances, surface quality, aesthetic aspect, burr characteristics).

In the following, main mass finishing processes will be compared and an overview about media and compound selection will be presented.

6.1.1 Mass finishing technologies

There exist several technologies to perform a mass finishing process, but the basic mechanism for any equipment involves the placement of workpieces in tubs of rotating media. The relative movement of the parts against the media scrubs the parts surfaces and edges, providing, also, an edge radiusing and a polishing effect.
Most employed mass finishing processes in the high-precision manufacturing field are [95]:

1. Rotary barrel tumbling;
2. Vibratory finishing;
3. Centrifugal barrel finishing;
4. Centrifugal disk finishing;
5. Spindle finishing.

Rotary barrel tumbling is a low pressure abrading process. It is performed by controlled sliding and rolling actions of the workpieces with media (i.e. the material used in mass finishing that actually works the piece) and water and compound (i.e. the mix of different chemicals), if present, within a barrel which rotates with a given speed. In this process, as the barrel rotates, the load moves upward in the barrel up to a turnover point; the force of gravity overcomes the tendency of the mass of staying compacted, and then the upper layer slides towards the bottom of the barrel, creating the active layer (see Fig. 6.1) where workpieces are effectively machined.
Normally, the barrel is loaded to about 60% of capacity. In the case of large or heavy workpieces the workload can reach the 80%, even if an high load reduces the force of workpiece contacts, resulting in much longer cycle. The abrading action may occur as workload rises, but about 90% of the rubbing action occurs during sliding: if workload increases, the upper layer decreases in length, therefore the rubbing action time decreases. It was estimated that the sliding actions occur only about one-third of the run time, while two-thirds of the time the workpieces are merely being rotated around the media, without sliding. Peripheral rotation speeds are generally comprised between 30 m/min and 60 m/min: higher speed can cause separation between media and workpieces, whereas lower speeds involve higher working time. The process is affected by several parameters: shape and size of the barrel, shape and size of the workpiece, selected media and its proportion in the workload, the compound used, the water level, the rotational speed of the barrel and the process time.
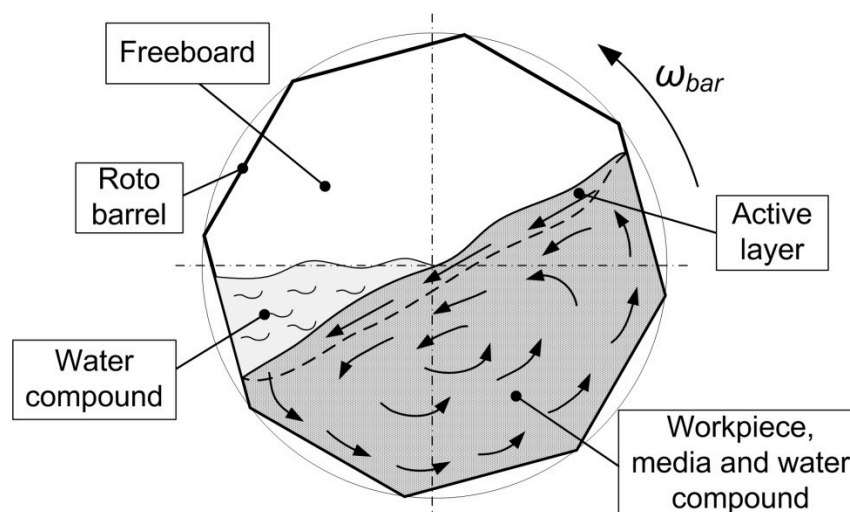
Fig. 6.1 Sketch of barrel finishing technology

Vibratory finishing is one of the most popular type of mass finishing, also for surface conditioning. It is very versatile and it is used for deburring, deflashing, edge and corner radiusing, surface finishing and stress relieving. Two basic configurations exist: rectangular tub or round blow type. The technology is based on an open-top working chamber containing the media, compound, water and workpiece, mounted on a spring system connected to a vibratory motion generator. While the chamber is vibrating, finishing is performed by the media and compound's scrubbing action on the workpieces. Vibratory finishing can provide more finishing action than barrel finishing techniques and it can process larger parts. Moreover, thanks to the open-top-chamber, in-process inspection, unloading and reloading without stopping process are possible. The tub-type machine, is generally characterized by a U-shape cross section and it is generally mounted on coil or rubber springs (see Fig. 6.2). Action of media against the workpiece takes place throughout the entire load: media rubs against parts, while entire load is turning over within the container. As a result, cycle time is shorter than that of barrel finishing. Round bowl or toroidal vibratory finishing machine has a doughnut-shaped working chamber, permitting a continuous circular flow of media and workpieces.
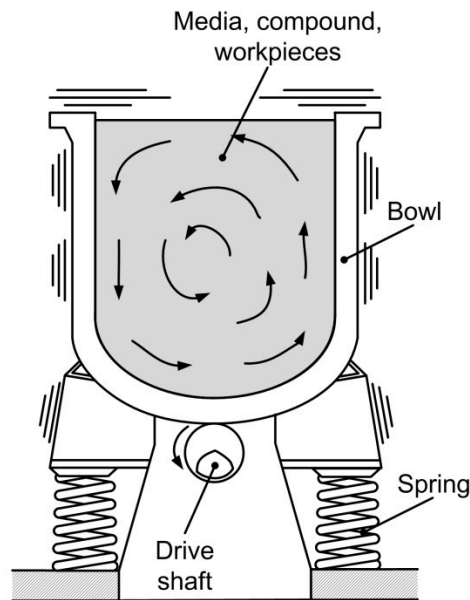
Fig. 6.2 Schematization of a tub-type vibrational finisher [95]

Centrifugal barrel finishing, like other mass finishing systems, uses media, water and compound to machine workpieces, but it takes advantage from the centrifugal motion of the mass, resulting in a very fast working process. It is called also mass orbital barrel finishing and permits a smooth rubbing action with little or none workpiece impingement, producing fine finishing on precision and fragile parts. A number of drums are mounted on the periphery of a turret, which rotates in one direction while drums rotate at slower speed on the other direction (see Fig. 6.3). Rotation can be in a horizontal or vertical axis, even if the first option is the most preferred one. Drums are loaded with similar rules to those of a normal barrel finishing: about 60% - 80% of each drum volume are filled with media, water, compound and workpieces. Turret rotation creates a high centrifugal force: this force compacts the load within the drums preventing hits between components. Rotation of the drums creates the sliding of media around the workpieces with finishing effect. This technology is characterized by very fast cycle time, 20-50 times faster than conventional vibratory finishing, and its results are generally consistent and reproducible, close tolerances can be maintained and very smooth surfaces can be realized.
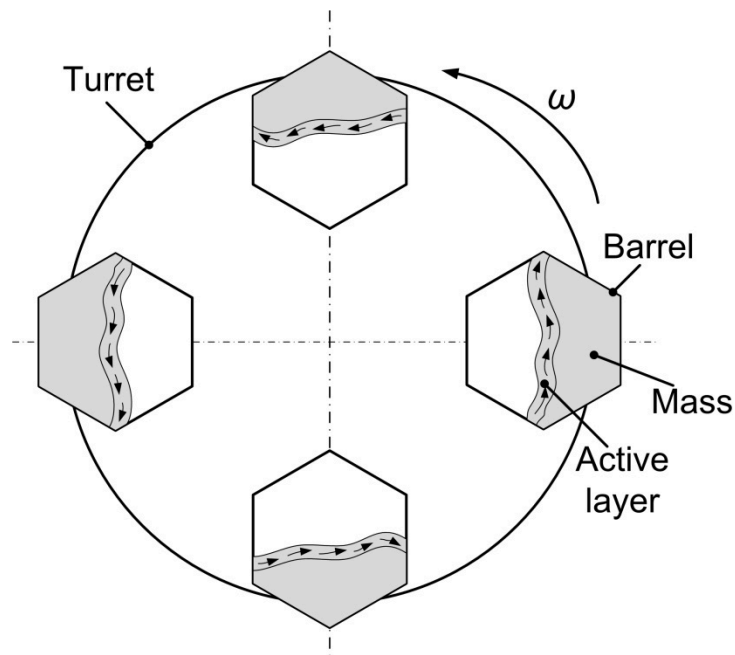
Fig. 6.3 Schematization of a centrifugal barrel finisher [95]

Centrifugal disk finishing (Fig. 6.4) is the most recent high-energy mass finishing process. It is based on a bottom disk that rotates with high peripheral velocity (> 600 m/min): the mass within the working chamber is accelerated outward. When the loaded mass touches the stationary sidewalls of the chamber, they act as a brake and the load starts in decelerating as it is forced upward by the mass behind it. Consequently, mass rises the top of the load, the flow goes toward the center of the working chamber and finally downwards toward the disk. This mass motion provides a smooth parts and reduces the impingement between workpieces. Energy created within the working chamber is greater than that obtained by conventional vibratory systems, reducing cycle time, even if the equipment cost is about five time that of vibratory ones. Unfortunately, this process cannot handle a huge variety of workpieces as barrel, vibratory or centrifugal barrel processes. For example, large parts cannot be machined using finishing system currently available, whereas very small parts or media cannot be easily handled because the system requires a small gap between the disk and the static sidewalls.
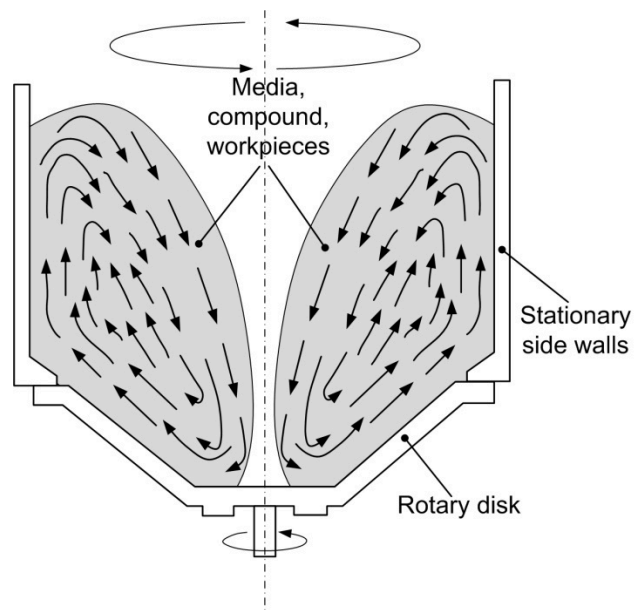
Fig. 6.4 Schematization of centrifugal disk finisher [95]

Spindle finishing consists of a circular rotating tub which contains the media and one or more rotating spindles on which workpieces are held and immersed on the media (Fig. 6.5). Abrasive action is performed by the rotation of the tub in a direction and the high speed rotation of the workpiece in the opposite direction. Processing cycle rarely exceeds few minutes and are frequently in the seconds-scale. The drawback is that workpiece shall be individually mounted on the spindle. Spindles generally rotate between 10 and 3000 rpm, even if, in add, working strategies using stationary or oscillating spindle are adopted. The tubs are generally stationary, but they can also rotate and vibrate. Spindle location is adjustable to vary the results of finishing operation: for a maximum action, spindles are located close to the periphery and to the bottom of the rotating tub, where the media action is more energetic. This approach is applied for finishing cylindrical-shape components, such as gear, pump, rotor: they are easy to fix and the media action is uniform over all surfaces.
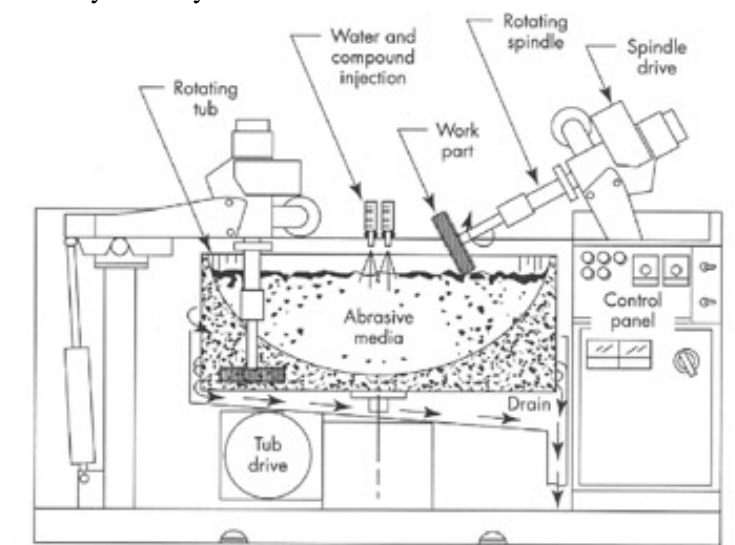
Fig. 6.5 Spindle finishing technique schematization [95]

As it can be deduced, all these conventional finishing techniques differ one each other for the equipment, cycle time, typology of media to be adopted and workpiece characteristics that can be processed. Summarizing, a comparison of outlined mass finishing approaches is reported in Tab. 6.1.

Tab. 6.1 Comparison of mass finishing process

Mass finishing approach	Equipment cost	Cycle time	Media characteristics	Workpiece characteristics
Rotary barrel	Low	Slow	All sizes	Small and medium sizes
Vibratory tub	Low	Medium	Medium size	Small, medium, large or long size
Vibratory bowl	Medium	Medium	Medium size	Small, medium, large size No cavities
Centrifugal barrel	High	Fast	Small size	Precision and fragile parts No long size
Centrifugal disk	High	Fast	Small size	No very small component
Spindle finishing	High	Fast	Very small size	No small or very long size Cylindrical shape

6.1.2 Media and chemical compound in mass finishing

Media refers to the abrasive or not-abrasive consumable elements in a mass finishing processes. The function of media is machining workpieces in order to reach desired accuracy. Moreover, media reduces or avoids impingement between parts and it operates as a carrier for the compound used. The factors that shall be considered in media selection are composition, size, shape and weight, whose selection depends on the shape and dimension of workpieces; in add, finishing requirements and the characteristics of the adopted mass finisher are issues to be taken into account.

Media composition defines the intent of media, that can be produced for cutting or finishing action: cutting type of media contains abrasives, whereas finishing type of media is abrasives-free or it is characterized by very fine abrasives. Considering the cutting type media, higher the abrasive content, faster is the finishing process. Media with aggressive cutting capabilities are suitable for large burrs removal, while for smooth surface, finishing type shall be preferred. Media composition determines its weight that affects the rate of the process: heavier media exerts more pressure on the workpiece rather than lighter media. Most common media compositions are:

o Ceramic media: it is the most used and it is generally composed with up to 50:50 ratio of abrasive to clay. Hard ceramic media generally cuts slower than soft ceramic, which allows the clay to wear and expose more grains of abrasive. Harder media are generally used in high-energy finishing processes.

o Plastic media: it is sometimes selected for mass finishing, even if its performance is not comparable with ceramic media due to the lower weight and faster wear rate: typically it is employed in surface finishing for not-hardened metals (brass, aluminum).

o Metallic media (typically stainless steel or copper): it is heavier than ceramic media and it does not contain abrasives; it can be adopted for work hardening, polishing, or to abrade workpiece material if mixed with abrasive powders.

Shape of media (see Fig. 6.6) depends on the workpiece shape and geometry, considering the possibility to machine all the surfaces, to avoid the lodging in holes or cavities and to permit easily separation from the parts at the end of the cycle. Shape of media can be:

o Triangular: it provides uniform action in reaching corner and slotted area;

o Cylinders: generally, it has ends cut with a certain angle able to reach recesses more easily; this shape is also ideal for deburring holes;

o Diamond and cones: they can reach corner, recesses and holes;

o Sphere: it has good flow action and it offers a good surface contact.

The selection of the proper size of the media depends on the fact that media shall be separated from workpieces during and after finishing process; at the same time media shall be able to reach all workpiece surfaces. For this reason it has to be considered that small media helps in keeping small parts separated, but at the same time large media cuts faster and produces rougher surface finishing. For this reason, a mix of media with different size is often adopted.

Fig. 6.6 Example of media shape and dimension commercially available [96]

Mass finishing compound is added to the mass of media and workpieces in order to increase the material removal action, to inhibit corrosion onset, to cool the workload, reducing friction, and to prevent the deposition of micro-chips on workpiece surfaces. Most compounds are combination of chemical elements that dissolve in water. Compounds can be classified basing on their function, such as abrasive, descaling, cleaning, deburring or edge radiusing, burnishing and coloring. Generally, the solution includes detergents, water softener, rust inhibitor, and abrasive grains, if required.

6.1.3 Literary review

In literature, most of scientific research works refer to vibratory mass finishing strategy that is widely used in deburring, radiusing, polishing and cleaning metallic components.

Some works investigate on measurement system of impact forces and/or abrasives velocity during bulk motion (see Tab. 6.2). Difficulties in detection of bulk characteristics lie in the risk of perturbation of the bulk motion due to the presence of a probe sensor within workload.

Wang et al. [97] developed a force sensor based on strain gauges able to detect impact forces during vibrations. In add, during experimental tests, they applied an optical fiber to record images about bath motion. Authors' aim was to understand the sources in changes of roughness and hardness of the workpiece: from an experimental study it emerged that surface changes depend on lubrication condition, media roughness and media size, since they affect the interaction between media and workpiece, and hence they affect the extent in plastic deformation per impact. On the other hand, authors observed that impact force parameters, such as average and maximum force and impulse, did not vary with lubrication condition, so they concluded that hardness and roughness changes depend on smaller-scale differences in the impact conditions. Moreover, they noted that parts resulted in contact with media for approximately 30% of the total finishing time: from the analysis of videotape frames, it emerged that media was loosely-packed as it flowed past the workpieces, creating a gap in the packing near the surfaces of component.

Similar analysis was performed by Yabuki et al. [98] which applied a special force sensor embedded to a freely moving workpiece to measure simultaneously normal and tangential forces exerted by media. Experimental observations were conducted also by a micro-video camera to record the motion of media as it collided on the workpiece surface; furthermore, electron micrographs of impact craters were analyzed to determine the contact mechanisms of media. Authors found that largest normal impact forces were associated to a particular media contact mechanism which verified itself when a piece of media was stationary on the workpiece surface while adjacent media rolled over it. Moreover, they observed that most of the applied type of media did not slide on the workpiece in the dry condition, therefore they concluded that sliding action was more common in water-wet finishing, in which maximum impact force and frequency of impact occurrence were lower. Using these experimental findings, Baghbanan et al. [99] studied the behavior of energetic tub-type vibratory finishing process; authors correlated forces with the resulting changes in surface roughness, hardness and material loss, as well as with residual curvature of aluminum workpieces. Authors deduced that principal variables of the process were the degree of lubrication, cycle time and workpiece material and that vibratory finishing approach for the process analysis was not specific to a particular machine, frequency or amplitude, but generally applicable.

Ciampini et al. [100] utilized a force sensor to detect impact velocity distributions, impact frequencies and impact power per unit of area. The sensor was fixed to a stiff support in order to provide impact velocity data independently on workpiece size, shape and material. Moreover, sensor was used to quantify the effect of media type, finisher amplitude and location within chamber on the probability distribution of the particles impact velocity normal to surface of workpiece. Authors, by experimental observations, found that a more aggressive process was arising reducing the media amount and moving the media closer to the wall due to an increasing in contact frequency, total energy flux and impact velocities; furthermore, they discovered that contacts occur periodically with finisher's driving frequency. Later, same authors [101] proposed the Almen system to characterize the effect of varying parameters of vibratory finishing process for the purpose of process development and control. They obtained the saturation curves by mass finishing of two aluminum Almen strips and, using experimental observations of previous work [100], they provided an

apparatus able to simulate normal impacts in the vibratory finishers. This approach was then applied in a further research [102] in order to provide a predictive model of saturation curves of Alman strips for characterizing the effect of media impact velocity on residual stress formation during vibratory finishing.

More recently, Hashemnia et al. [103] developed a laser displacement probe to measure impact velocity. The aim of the research was to achieve the analysis of the motion of a vibrating particle by the contact of the vibrating sensor window. In add, sensor outputs were used to measure bulk flow velocity and a method for measuring the media packing was provided.

Tab. 6.2   Analyzing bulk motion characteristics: Literary review

Ref.	Aim	Finishing strategy	Media/ Workpiece	Sensors
[97]	Analyze impact parameters effect on workpiece changes and bulk motion	Bowl-type vibratory finisher	Ceramic/ Al-alloy	Strain gauge Video camera Profilometer Hardness tester SEM microscope
[98]	Analyze bulk characteristic (impact forces, crater formation, media contact mechanism)	Bowl-type vibratory finisher	Ceramic/ Al-alloy	Micro-camera Force sensors SEM microscope
[99]	Analyze bulk characteristics	Tub-type vibratory finisher	Ceramic/ Al-alloy	Accelerometers Profilometer Micro-hardness tester Force sensors Micro-camera SEM microscope Alman strips
[100]	Analyze bulk motion properties	Tub-type vibratory finisher	Ceramic and steel/ None	Force sensor
[101]	Simulate the vibrational finisher properties by Almen system	Tub-type vibratory finisher	Steel / Al-alloy	Almen strips Strain gauge
[103]	Provide a laser sensor probe for bulk characterization	Tub-type vibratory finisher	Ceramic and steel / None	Accelerometers Laser displacement sensor

Scientific researches mentioned so far allow the comprehension of the mechanisms which underlie the mass finishing phenomena. Unfortunately, these works do not furnish practical tool to select proper working conditions to achieve optimization of mass finishing process. Even today, the trial and error approach is one of the most applied for selecting working parameters: both in scientific both in industrial literature, few works focus on modelling finishing processes and most of them are based on empirical approach and on experimental observations. Some of research aiming on mass finishing modelling are listed in Tab. 6.3.

A pioneer in providing vibratory finishers fundamentals was Hashimoto [104]. He proposed simple but effective predictive analytical models for controlling process outputs such as surface quality and material removal. Author, moreover, gave a formulation for optimization of cycle time of a vibratory finishing process.

In a more recent work, Naeini et al. [105] developed a discrete elements model in order to predict granular flow in a two-dimensional vibratory system. Model simulated the collisions

and resulting velocities of the media on the working chamber side walls and on the workpiece.

Mohajeriani et al. [106] presented a numerical modelling of edge rounding for brittle materials, which are not commonly studied such as ductile materials. Authors, basing on experimental observations by a previous research [107] provided a prediction method for the evolution of edge profile, considering different initial edge shapes. The model was useful to understand the effect of the initial edge chamfer geometry and the distribution of impact forces on edge wear and surface topography. Cariapa et al. [108] presented a material removal model in a centrifugal disk mass finishing machine, filling the gap in literature and industrial research about this mass finishing approach. Authors modelled the workload motion basing on fluid-dynamic theory and numerical analysis; material removal model was defined as a function of the ratio of the density and hardness of metal workpiece and of ceramic media.

Tab. 6.3   Predictive models in mass-finishing approach: Literary review

Ref.	Aim	Finishing strategy	Media/ Workpiece	Sensors
[104]	Provide an analytical prediction model for surface quality and material removal	Bowl-type vibratory finisher	Not specified/ Steel	Surface tester SEM microscope
[105]	Provide a predictive empirical model for granular flow behaviour	Tub-type vibratory finisher	Steel/ None	Camera Accelerometers
[106]	Provide a predictive numerical model for vibratory finishing of brittle material	Tub-type vibratory finisher	Steel and ceramic/ Borosilicate glass	None (data from previous research)
[108]	Provide a numerical predictive model for material removal in centrifugal disk finishing approach	Centrifugal disk finisher	Ceramic / Steel, Al-alloy, Brass	Accelerometer Force sensor SEM microscope

6.2.   Edge requirements: burrs issue

Satisfying strict edge technical requirements represents one of the most critical aspect in high-precision mechanical manufacturing. Due to cutting operations, in semi-finishing and finishing stages, edges of workpiece generally present defects such as burrs: they affect functionalities of the components or may cause difficulties in the assembly stage. Indeed, burrs increase stress concentration, reducing structure resistance and fatigue life and, if detachable, they may contaminate system in which component is assembled; moreover they can interfere with proper setting of mechanical fasteners or clamping components. In the worst case burrs can undermine safety during handling of component.

For example, it reports the case of the workpiece in Fig. 6.7. Specific element is a component of an injector system for automotive engine: its edges are characterized by micro-scaling burrs due to the previous grinding operation. The risk of burrs presence is related to the possibility of contamination of the assembly during functioning. Indeed, a high-pressure fluid will pass through the burred small hole in the picture: if burrs are not pre-emptively removed, the flow might detach and transport them within system causing the failure of the engine.
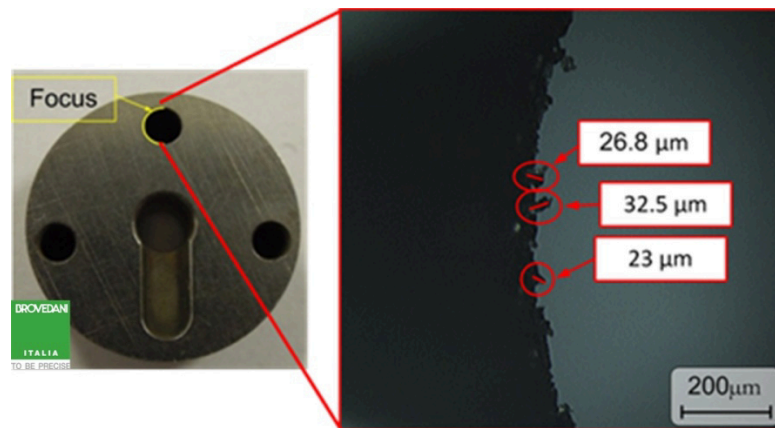
Fig. 6.7 Micro scale burrs after grinding operation (Courtesy of Brovedani SpA)

In order to prevent or minimize burrs formation, several aspects of cutting process set-up shall be taken into account, such as:

- Tooling system selection and condition: selection of proper tool properties (coating, bulk material and geometry) in compliance with workpiece characteristics is crucial; moreover tool wear or tool damages may affect burr formation mechanism (see for example Fig. 6.8)

- Analysis of workpiece material and of the desired final geometry;

- Selection of process conditions such as cutting parameters and lubricating strategy;

- Manufacturing strategy, such as the sequence of the cutting operations or the proper tool path planning for each operation.

However, burr formation cannot be often avoided, therefore burrs must be removed by supplementary machining operations affecting the total production costs to 30% [95]. Due to economic advantages of mass finishing technique, these approaches are commonly preferred in deburring action.
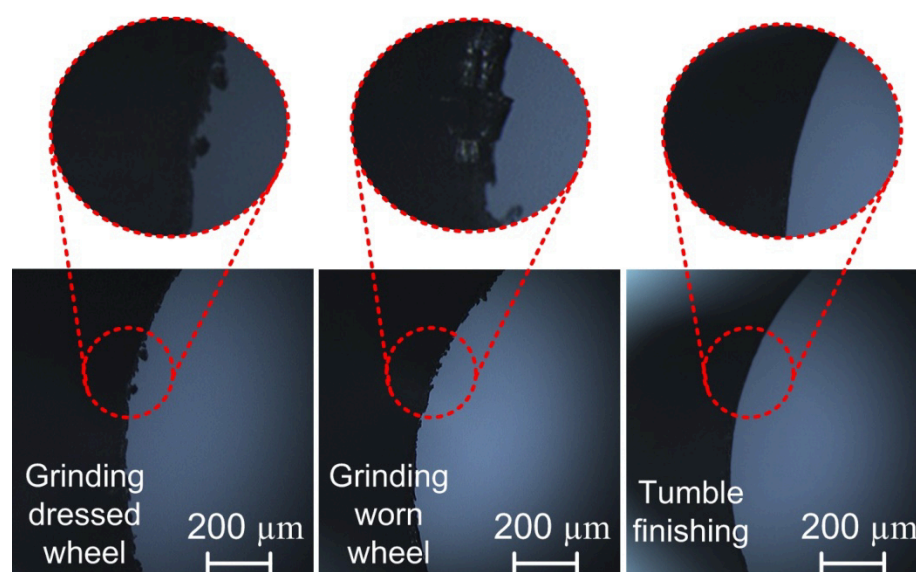
Fig. 6.8 Different characteristics of burrs due to grinding dressed wheel and grinding worn wheel and typical edge after burrs removal

6.2.1 Definition of edge quality requirements

In the past, technical drawings gave only the representation of the ideal geometric shape of the component, without any deviations. Since the burr phenomenon represents today a critical aspect in manufacturing due to the required high quality standards of the components, in technical documents, the caption "burr free" or other specific geometrical indications are often found. Providing clear communication of the desired edge conditions is a low cost method for reducing deburring actions and finishing costs. Examples of edge quality requirements are listed in Tab. 6.4.

Tab. 6.4   Example of edge quality requirements [95]

Class	Grade	Radius tolerance	Instruments for quantitative evaluation	Typical application
E0	Exceptional high quality edge	0.1 – 0.2 µm	Interference microscope, SEM	Diamond micro cutting tool
E1	High quality edge	0.3 – 5 µm	Profile measurement machine, metallographic analysis, surface roughness tester	Edge of cutting tools
E2	Sharp edge	8 –30 µm	As above	Hydraulic orifice edge
E3	Rounded edge	0.08 – 0.3 mm	Stereo microscope	Mechanical parts
E4	Chamfered edge	0.4 – 0.6 mm	Optical comparator	Mechanical parts
E5	Dull edge		Sharpness gage	Some automotive parts

Unfortunately, describing edge requirements is not so simple since several burr definitions exist; the caption "burr free" is meaningless without references, especially for the definition of the geometry of the edge and for the proper selection of the inspection technique.

In order to determine edge characteristics, standards, such as ISO 13715 [109] or DIN 6784 [110], are considered as reference: they define a burred edges of a workpiece if it has an overhang greater than zero. In literature, Schafer, as reported by Aurich et al. [111], defined burr as the part of workpiece which produced through manufacturing process on an edge or on a surface and which lie outside the desired geometry. While Scahfer's definition includes burrs on surfaces, that can derive from casting or welding operations, DIN or ISO standards restrict the definition only to the workpiece edges (see Fig. 6.9).
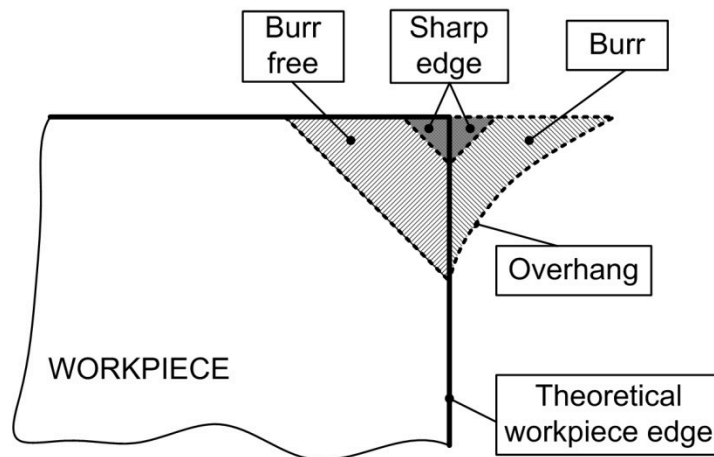
Fig. 6.9 Sketch of machined edge [109]

Common indications about edge geometry follow the standard references, indicating the minimum and/or maximum dimension in deviating from the ideal shape of edge. To respect these geometrical requirements, a further dilemma can be encountered: defining burrs geometries, and so edge dimensions, can be carried out following several approaches.

In literature, burr definition is based on the length profile and the cross-section characterization. Length profile shows the shape of the burr along the edge, and the only available geometrical information is the burr length, whereas in cross-section definition, burr shall be characterized by several measure, such as (see Fig. 6.10):

- Burr root thickness b_r;
- Burr height h_0: the distance between the ideal edge and the highest point in the cross sectional area;
- Burr root radius r_f: determined by positioning a circle to the burr root;
- Burr thickness b_g that is the thickness parallel to the burr root area at a distance of r_f.
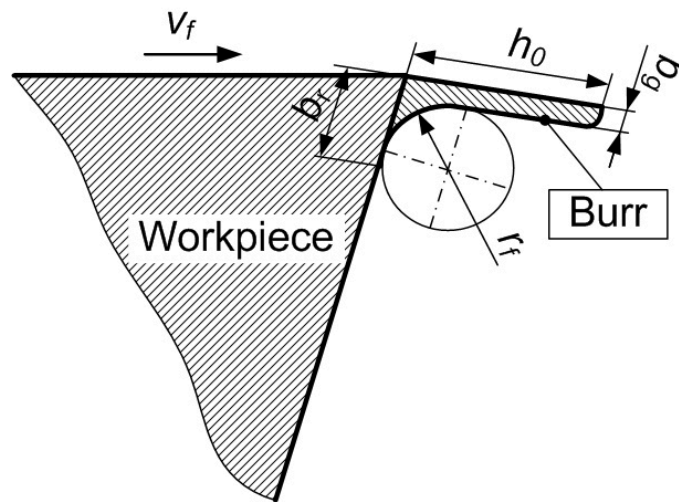
Fig. 6.10   Characterization of cross section of a burr [111]

Contrary to the Schafer's definition and characterization of burr geometry, DIN and ISO standards consider only one dimension to describe burr, i.e. the deviation from the ideal geometrical outline of the edge (Fig. 6.11). It shall be measured from the burr tip perpendicular to the workpiece surface from which the burr is protruding. This is the faster approach to characterize burr size, especially using simple contact measurement method, like profilometer.
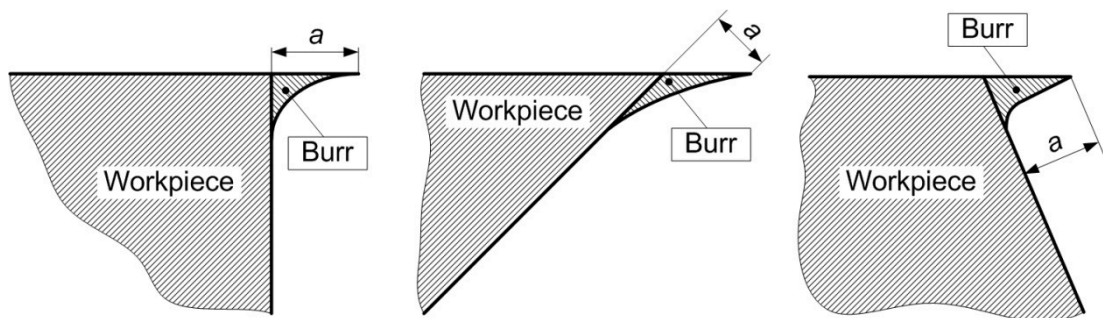
Fig. 6.11   Burr geometry definition by DIN 6784 [110]

6.3. Surface requirements

A further purpose of mass finishing of high precision components is the surface conditioning: these approaches, typically, realize smoother surfaces and, at the same time, they are able to polish and to clean them by removal defects and residuals deriving from previous cutting process or from surface treatments. Therefore, surface conditioning does not refer only to an improvement in surface roughness: its meaning is certainly wider.

Surface finish is generally referred to the surface texture, that is characterized by four aspects [95]:

- *Roughness*, that is the uniform fine irregularities in texture deriving from previous cutting process;
- *Waviness*, that is the undulation topology of much coarser frequency than roughness;
- *Lay*, that is the direction at which irregularities occur;
- *Flaws*, that are irregularities that have no uniform pattern, including cracks, pits, scratches etc.

Defining proper surface quality requirements and reaching them by surface conditioning techniques are crucial if high performance of mechanical component is required. Surface conditioning, indeed, contributes in increasing service life and functioning of the parts, especially if severely stressed in service. It includes also the creation of isotropic surface textures, replacement of positive skewed surface profile with negative or neutral skew and developing compressive stresses.

Surface quality requirements, evaluated by the roughness parameters R_a, R_t and R_z, guarantees a better fatigue life: it affects the strength of a part subjected to fatigue loading since notch patterns left by the machined operation, in which cracks can nucleate. Moreover poor surface finish may introduce millions of points for crevice corrosion on surface; in adding, if the components shall be assembled, it may reduce the contact points between surface, giving higher and very localized contact stress.

It has to be pointed out that component life and its performance are not achieved defining only these general requirements of roughness. Surface skewness, i.e. the surface profile symmetry, is a further crucial aspect to be considered. Generally, unfinished parts or workpiece surface machined by conventional cutting process, show positive skewed surface: it has an undesirable effect on bearing ratio of surface and it can have a negative impact on part performance where the contact between surfaces is necessary.

Surface texture plays a key role in part functionalities: the texture created by conventional machining is generally aligned to the tool direction. Part life can be improved if surface texture is altered in a random nature: isotropic condition of surface improves part wear, fracture and fatigue resistance.

Surface integrity is a further important characteristic of surface accuracy: it can be modified by several phenomena, such as plastic deformation, recrystallization, surface hardness, microcracking, high tensile residual stresses, untempered martensite formation, stress corrosion. One of the most common defect is given by the residual tensile stress which is caused by machining operations: it makes components susceptible to premature failure, especially if repeatedly stressed. Surface conditioning helps in replacing residual tensile stress with uniform residual compressive stress.

Therefore, achieving high surface accuracy is very important to resist wear and fatigue, to favour lubricating conditions, to decrease friction and/or abrasion with mating parts and to resist corrosion.

Mass finishing process is one of the most applied approaches for surface conditioning, especially in high energetic strategy. Unfortunately, even if these techniques help in improving surface quality, without affecting lay or waviness of workpiece in general, they can cause a variety of flaws that negatively affect accuracy. Flaws, like nicks, do not affect average roughness of surface, whereas scratches can negatively influence roughness measurement. Therefore, it is important defining how much these defects are important beside roughness value.

Mass finishing processes can improve surface quality below 0.02µm; on the other hand, they can be adopted to roughen surface to provide better adhesion. Typically, surface of 0.4-0.8µm are obtained by deburring operations. Centrifugal barrel tumbling or centrifugal disk finishing techniques produce mirror surface quality, in the order of 0.02-0.04µm. The key point is the proper selection of media, compound and process parameters. For example, working parameters suitable for deburring or edge radiusing are not always appropriate for surface quality improvement.

6.4. Optimization of vibratory mass finishing process

Main goal of this section is the optimization of the cycle time of a mass finishing strategy (using conventional finishers), by applying the predictive analytical model proposed by Hashimoto [104]. Mathematical optimization method is based on the idea that the surface of a workpiece is characterized by an inherent surface texture with a constant roughness, called roughness limitation Dr. Moreover, it considers that the cycle time of mass finishing process is affected by the initial value of the workpiece surface roughness Ir: the greater the difference between Ir and Dr, the faster is the rate of roughness change. Considering the absolute average value R_a of surface quality, an expression in time domain was proposed by the author:

$$R_a(t) = (Ir - Dr) \cdot e^{-\frac{t}{T}} + Dr \qquad (6.1)$$

where T is defined as the time constant of the vibratory finishing system: its value gives an indication about effectiveness of the mass finishing apparatus. Time constant T can be evaluate by the process time t when the surface quality reaches the value $R_a(T)$ given by the expression:

$$R_a(T) = (Ir - Dr) \cdot e^{-\frac{T}{T}} + Dr \qquad (6.2)$$

Therefore, defining the target value of desired surface quality Ar, optimum cycle time can be estimated from the Eq. (6.1) substituting t with T_{opt} and considering $R_a(t)$ equal to Ar, such as:

$$T_{opt} = -T \cdot ln\frac{(Ar - Dr)}{(Ir - Dr)} \qquad (6.3)$$

6.4.1 Application of the optimization approach: Experimental set-up and data analysis

In this thesis, the proposed approach was applied in order to predict an optimized cycle time of a mass-finishing strategy in order to fulfill surface quality of an automotive component. This analysis was conducted at the Brovedani SpA company.

The workpiece under analysis is a component for the high pressure pump assembly for automotive engine. It has got an axial symmetric geometry, with 50mm length, and two characteristic external diameters, d equal to 5mm and D equal to 9mm (see Fig. 6.12). It is

made of hardened bearing steel, with hardness about 60 HRC; following its production cycle, the surfaces must be coated by DLC technique after the manufacturing process. In order to perform DLC coating with optimal result, surface quality shall be controlled carefully. Specifically, technical requirements about surface accuracy is defined in R_a minor than 0.1 µm.
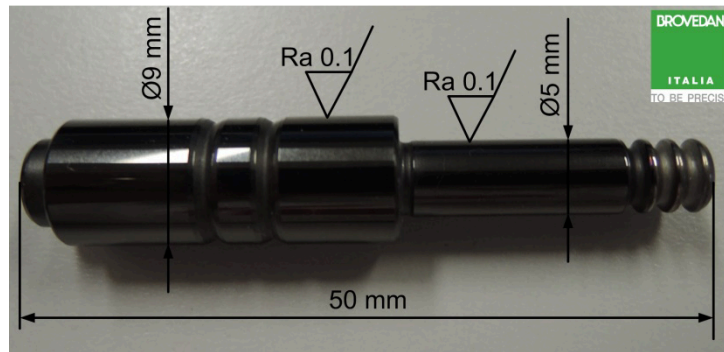
Fig. 6.12 Workpiece geometrical characteristics

Basing on the previous experiences of technicians at the company, a proper mass finishing strategy was characterized by three cycles with different mass finishers and/or working parameters, as listed in Tab. 6.5. The preliminary finishing operation, which will be called "Rough finishing", and a subsequent finishing cycle called "Intermediate finishing", were carried out by a bowl-type vibratory finisher. The final stage, named "Super-finishing", was defined by a super-finishing cycle using a centrifugal disk finisher in order to reach the desired surface quality. For all processes, an amount of 40% of workpiece and 60% of media and water compound was adopted in order to avoid impingement between parts and for guaranteeing a good finishing accuracy even the complex shape of the component, characterized by cavities and chamfered edges. The selected geometry of the media was a cylindrical shape with oblique cutting for all finishing processes because it was considered appropriate not only for surface finishing, but also to remove eventually burrs or contaminants on cavities and chamfered edges (see Fig. 6.13).

Optimization procedure starts with preliminary mass finishing tests, for each finishing stages, in order to determine the parameters necessary in prediction of optimal cycle time, i.e. the initial roughness Ir, the roughness limitation Dr of the workpiece, and the constant time T typical of the finisher system.

Tab. 6.5 Preliminary finishing strategy

Finishing process	Machine type and parameters	Media	Chemical compound function	Abrasive powder
Rough finishing T=180min	Vibrational finisher Polyservice P60 fz=50Hz, ω=3000rpm	Ceramic with medium grade L=10mm, d=3mm	Degreasing	Aluminum oxide (grit size: 4-6µm)
Intermediate finishing T=180min	Vibrational finisher Polyservice P60 fz=50Hz, ω=3000rpm	Ceramic with medium grade L=7.5mm, d=4mm	Corrosion inhibitor	None
Super-finishing T=180min	Centrifugal disk finisher Polydisc P35 ω=220rpm	Ceramic with low grade L=10mm, d=3mm	Corrosion inhibitor	None

114
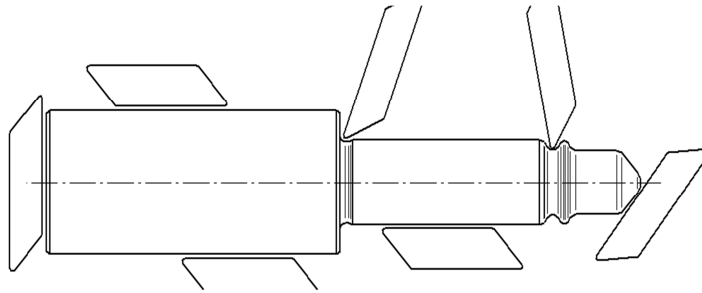
Fig. 6.13 Selection of proper media shape for mass finishing basing on the workpiece geometry

In this study, unfinished workpieces were characterized by two different initial surface qualities due to the previous grinding operation carried out applying different material removal rate: in the following, these different conditions will be identify as *Status 1* and *Status 2*.

Surface quality was analyzed by a surface tester Taylor Hobson mod. Form Talysurf 120i, evaluating the roughness parameters R_a. Measurements were performed on ten workpieces before each finishing stage, for estimating the initial roughness *Ir*, every 60 minutes to verify the improvement of the surface accuracy, and at the end of each finishing cycle for defining the roughness limitation *Dr*. Indeed, the cycle time of 180 minutes established for each finishing process was considered suitable to reach the limit value of surface quality. Moreover, desired surface quality *Ar* was quantified in order to reach a final surface roughness about half of the technical requirements.

Trends of the average surface roughness R_a are shown in Fig. 6.14 and in Fig. 6.15, from which it is possible to note the well-known asymptotic behavior of surface roughness during a finishing process.

Characteristic of each mass finishing processes are derived from the observation of the graphs, and value are collected in Tab. 6.6.
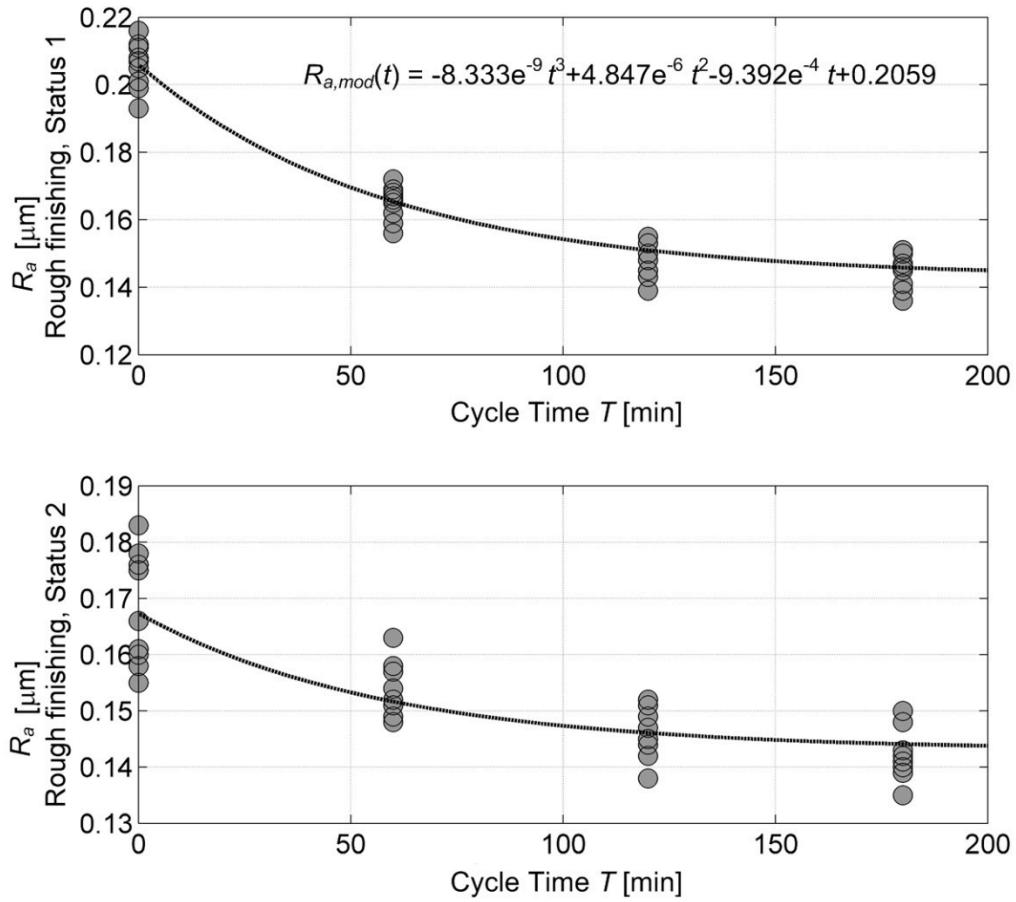
Fig. 6.14 R_a measurements during the rough finishing process for workpieces with *Status 1* (on the top), and *Status 2* (on the bottom)

The equation shown in the top plot:

$$R_{a,mod}(t) = -8.333e^{-9}\,t^3 + 4.847e^{-6}\,t^2 - 9.392e^{-4}\,t + 0.2059$$
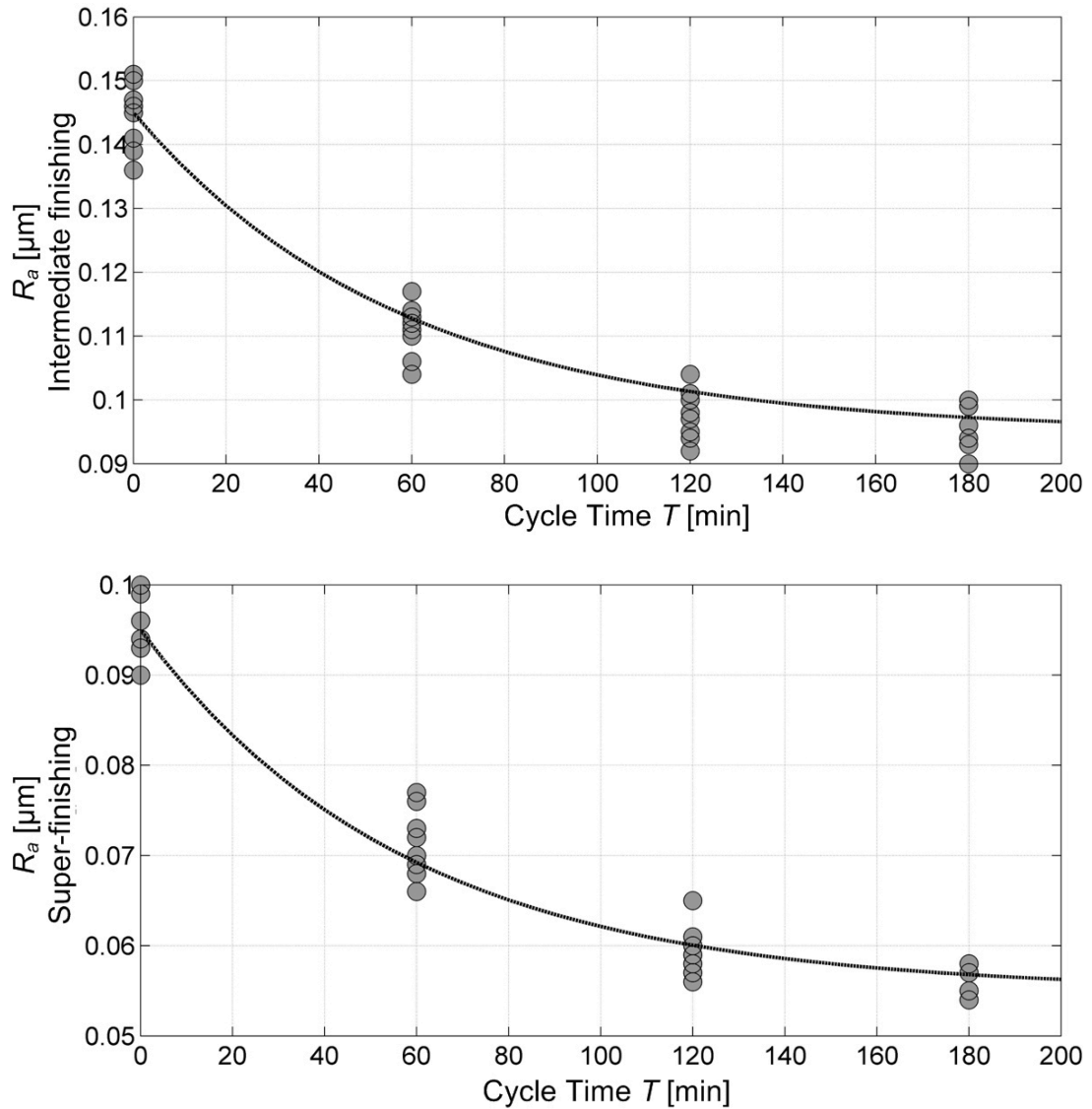
Fig. 6.15 R_a measurements during the intermediate finishing process (on the top) and the super-finishing process (on the bottom)

Tab. 6.6 Characterization of mass finishing processes

Mass finishing process		Ir [µm]	Dr [µm]	Ar [µm]
Rough mass finishing	Status 1	0.2059	0.143	0.150
	Status 2	0.1673		
Intermediate finishing		0.1453	0.095	0.10
Super-finishing		0.096	0.055	0.06

For evaluating the time constant T of each mass finishing system, the trend of average roughness R_a of unfinished workpiece with initial *Status 1* was considered. It is well interpolated by a cubic curve fitting (see Fig. 6.14).

Imposing $R_{a,mod}(t) = R_a(t)$ in Eq. 6.1, T was found equal to 58 minutes.

Substituting $T = 58$ min in the Eq. 6.1, the expression of R_a for the first mass finishing process, was derived as:

$$R_a(t) = (Ir - 0.143) \cdot e^{-\frac{t}{0.967}} + 0.143 \qquad (6.4)$$

Considering the two initial roughness conditions, model well represents experimental data, with an error about 0.7295% for *Status 1* and 0.7728% for the *Status 2*.
In the same manner, for the intermediate finishing stage, the derived model interpolates with a relative error of 1.6954% and the formulation was:

$$R_a(t) = (Ir - 0.095) \cdot e^{-\frac{t}{0.90}} + 0.095 \qquad (6.5)$$

Super-finishing process was performed by a centrifugal disk finisher, which differs from the vibration mass finishing in functioning principles. By the way, applying the proposed approach for modelling R_a, the gap between model and experimental data was found very small, equal to 3.2798%; therefore the mathematical model adequacy was acceptable. The derived expression is:

$$R_a(t) = (Ir - 0.055) \cdot e^{-\frac{t}{1.05}} + 0.055 \qquad (6.6)$$

Modelling parameters evaluated for each mass finishing stage are collected in Tab. 6.7.

Tab. 6.7   Model parameters

Mas finishing process		Dr [μm]	Time constant T [min]	Standard relative error σ [%]
Rough mass finishing	Polyservice P60, medium abrasive ceramic media, L=10mm, d=3mm	0.143	58	0.7295 (Status 1) 0.7728 (Status 2)
Intermediate finishing	Polyservice P60, medium abrasive ceramic media, L=7.5mm, d=4mm	0.095	54	1.6954
Super-finishing	Polydisc P35, low abrasive ceramic media, L=10mm, d=3mm	0.055	63	3.2798

According to the optimization procedure, known the model parameters, it is possible apply Eq. 6.3 to estimate the optimized process cycle curve in function of the initial roughness Ir for each finishing stage (see graph in Fig. 6.16 for the rough finishing process).
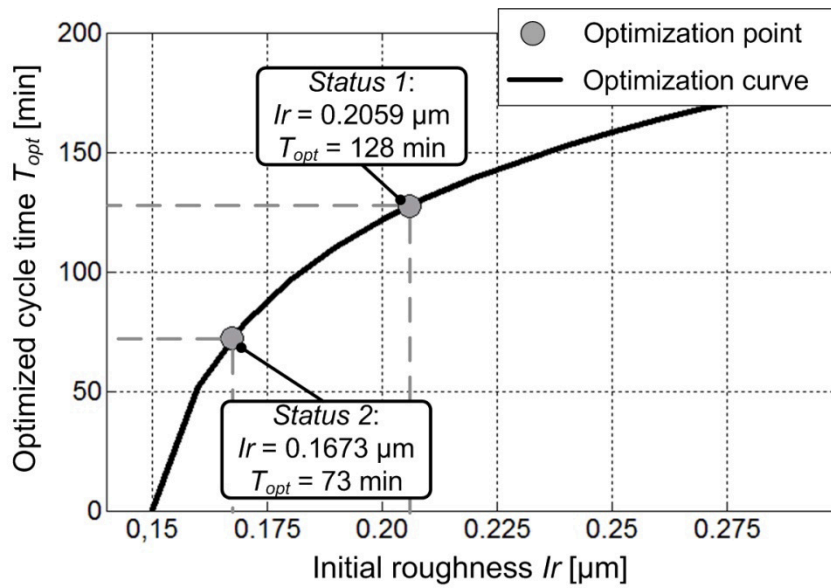
Fig. 6.16 Optimization curve for rough finishing conditions

Results of the analytical optimization approach are shown in Fig. 6.17, where it is noticed the possibility of reduction of cycle times in comparison with those preliminary applied. For example, considering the workpieces with *Status 1*, total cycle time can be set to 404 min instead of 540 minutes, whereas if *Status 2* is analyzed, optimized cycle time will be equal to 348 minutes. Overall optimized parameters for the considered mass finishing strategy are collected in Tab. 6.8.
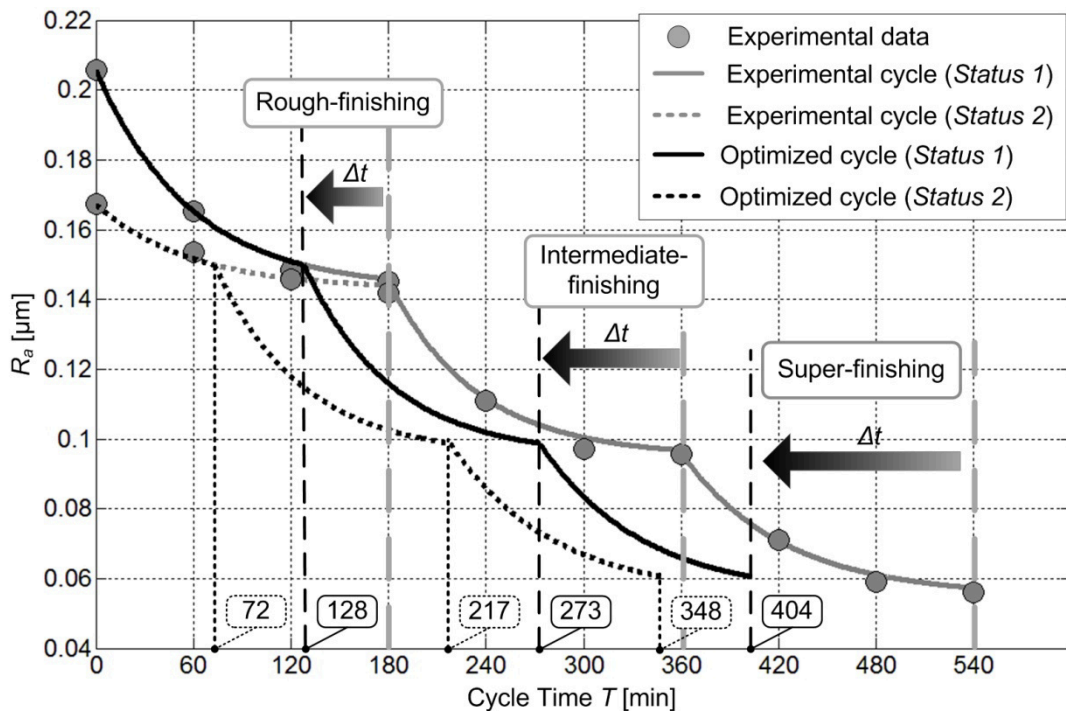
Fig. 6.17 Mass finishing strategy optimization

Tab. 6.8 Optimized mass-finishing parameters

Mass finishing process		Initial Roughness Ir [µm]	Limit roughness Dr [µm]	Desired roughness Ar [µm]	Current cycle time T [min]	Optimized cycle time T_{opt} [min]	Gap Δt [min]
Rough-finishing	*Status 1*	0.02059	0.143	0.150	180	128	52
	Status 2	0.1673	0.143	0.150	180	73	107
Intermediate finishing		0.150	0.095	0.10	180	145	35
Super-finishing		0.10	0.055	0.06	180	131	49

Analyzing Fig. 6.17 it emerges that, if raw workpieces have a better initial surface quality (*Status 2*), the cycle time of the first mass finishing stage is very low. Therefore, it can be supposed that only two cycles of mass finishing process, i.e. the Intermediate and the Super-finishing stages will be suitable to reach desired accuracy of workpiece. By this optimization strategy, the overall cycle time will be further reduced to 274 minutes, Fig. 6.18.
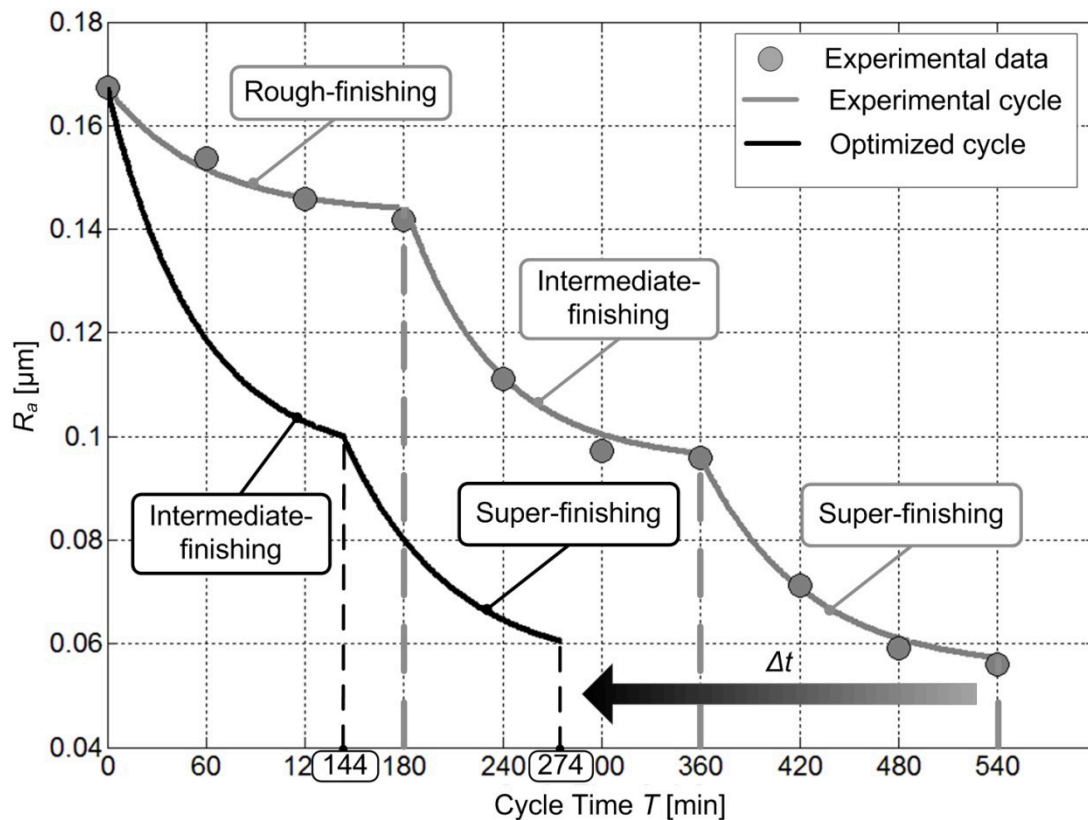
Fig. 6.18 Optimization of mass finishing strategy for workpieces of *Status 2*

6.4.2 Conclusions

Mass finishing approaches are generally employed by the trial and error approach. In this section, an analytical predictive model for the optimization of the cycle time in mass finishing was applied. The optimization strategy requires a preliminary experimental phase, where a mass finishing strategy was performed, including three different mass finishing

processes. This step was fundamental in order to define the characteristic parameters (*Ir*, *Dr* and *T*) of each mass finishing stage. It was derived that cycle time is strictly related to the initial surface quality: if poor surface quality characterized the component, a longer process time is needed. Considering different initial surface qualities of the workpiece, optimal cycle times were predicted by applying the analytical approach: for the initial *Status 1*, T_{opt} was estimated in 404 minutes, whereas with *Status 2* T_{opt} was derived equal to 348 minutes. Furthermore, with better initial surface quality, a new finishing strategy was proposed, reducing mass finishing stages: by performing only two processes instead of three steps the estimated T_{opt} was decreased to 274 minutes.

6.5. A new mass finishing approach: the dry technology

Nowadays, dry solutions for barrel or vibratory finishing are the challenge for manufacturing companies. Dry finishing strategy can avoid the production of effluent, limiting the issue of waste management, that is very expensive. Applying dry solution, indeed, only abrasive powder will be generated by working process: fines treatment may be up to ten times less heavy than wet sludge management; moreover, dry fines are considered not dangerous for environment.

In the past, Davidson and Massarsky proposed a dry finishing technique based on the principle of spindle finishing, called turbo-abrasive machining [112] [113]. Barletta et al., as will be exposed in the next Chapter, applied the concept of fluidized bed in order to perform a new system for dry finishing [114] [115] [116] [117]. Moreover, further solutions are commercially available: they use modified conventional vibratory finishers in order to carry out a mass finishing process without water and chemical compounds.

In the following, an innovative dry mass finishing system, based on the barrel finishing principle, will be presented. The developed prototype mass finishing machine will be employed to finishing workpieces with different geometries and initial characteristics for deburring and radiusing of edges and for improving surface accuracy.

6.5.1 Dry mass finishing working machine prototype

Dry mass finishing prototype was designed by University of Tor Vergata (Rome) basing on specific requirements of some unfinished automotive mechanical components manufactured at the Brovedani SpA company. Finishing tests were carried out at the Brovedani SpA, in which plant the machine was installed. Analysis was performed by experimental observations of mass finishing performance on workpieces currently produced by the company, since advanced instruments or sensors for evaluating specific process characteristics, such as impact forces or impact velocity of media, were not available.

Referring to Fig. 6.19, the specific machine tool is composed by a roto-barrel in which are loaded abrasive media and workpieces. The motion of the batch is given by the rotation of the barrel in clockwise or counter-clockwise directions by an engine with 1.8kW power, by regulating the rotation speed ω_{bar}; an air flow is supplied by an high pressure centrifugal fun with 1.5kW of power and pressure of 250 mmH$_2$O, working at room conditions (1atm, 21°C). The air flow rate is regulated by the velocity of rotation ω_{blo} of the air blower; it enters in the working chamber passing through a sandwich grid with internal pore size of 50µm. Moreover, the barrel can be tilted to prevent amass of media and workpiece on the internal side wall, giving a better motion of the batch. Air flow, mixed with micro-chips and abrasives powders exits from the top of the barrel.

Being a dry system, water compound is not adopted in this mass finishing process. Abrasive action, in order to perform deburring, edge radiusing and polishing, is given only by the selected media.
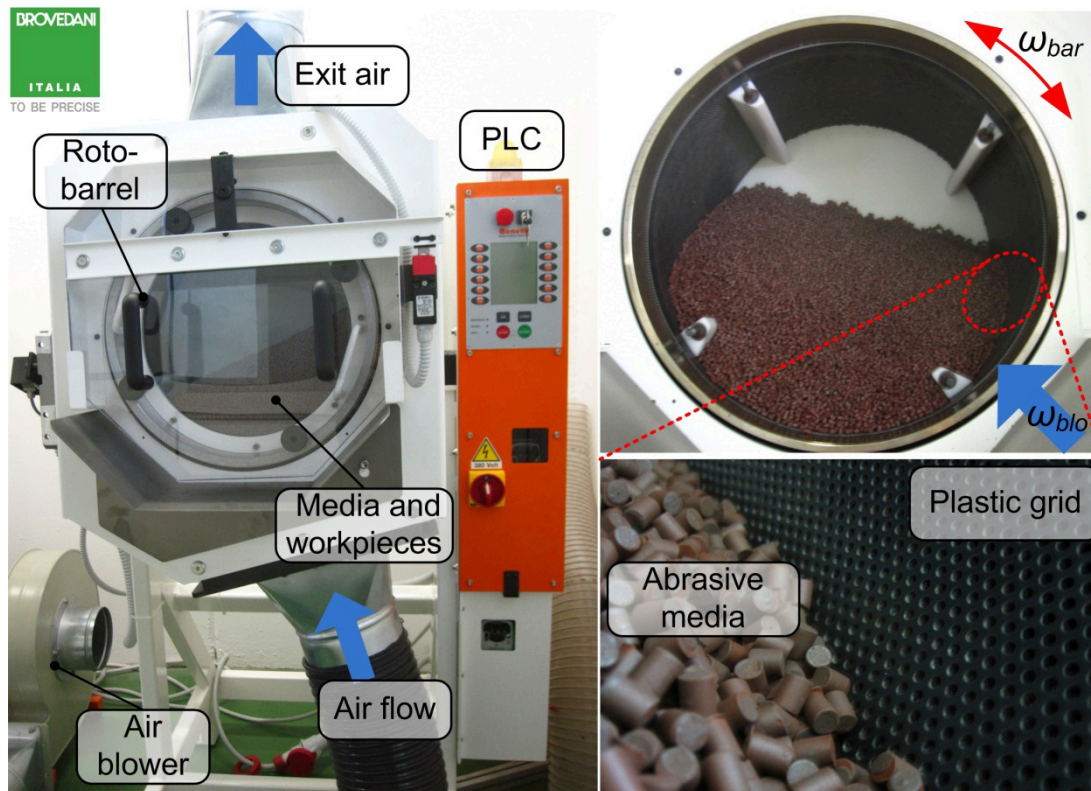
Fig. 6.19   Machine tool for dry deburring and radiusing (courtesy of University of Tor Vergata and Brovedani SpA)

6.5.2 Defining working parameters

In order to define the working parameters, bath motion was experimentally observed. The process factors were identified in the air flow rate and the barrel rotational speed. Aiming at determining suitable working regimes, the basic notions of conventional barrel finishing are considered from literature, since specific studies are not available.

Conventional barrel finishing, as outlined in the previous section, is characterized by the motion of the mass upwards to a turnover point in the barrel; sliding action occurs on the upper layer of the workload and the force of gravity overcomes the tendency of the mass to be aggregated; then the upper layer slides on the bottom of the rotating barrel. The mix of media, water compound and workpieces can be assimilated to a granular fluid, which characteristics depend on the physical and geometrical properties of the granular fluid itself: so, it is very difficult in identifying bath properties.

Bath motion and action are affected by the dimension of solid elements, the friction force entity and the amount of fluid in the roto-barrel. The wide range within parameters defines great differences in the granular fluid behaviors. During rotation, motion can be similar to the movement of solid elements or typical of viscous fluids.

If an half-filled barrel rotates at low rotation speed, the mix of material tends to move compact and stick to the internal wall rising up to a certain quota; then it slides downward in an inclined plane with an angle θ_m (motion angle): at this angular value, friction and inertial forces cannot prevail on the direction of the motion of the weight. If the barrel is pulled up, the batch places in the working chamber with an inclined configuration, characterized by the

angle θ_r (repose angle). The difference between the two angle is the relax angle δ (see Fig. 6.20).
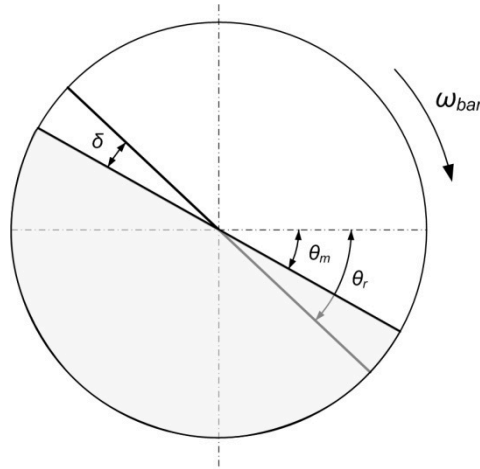
Fig. 6.20 Characterization of bath motion in barrel finishing

A classification of bath motion, generally applied in barrel finishing analysis, includes (Fig. 6.21):

- *Slipping*: particles place in a stable configuration with small repose angle; since low rotation speed of the barrel are applied, slipping motion is not suitable in finishing processes because it can be a time-consuming regime;

- *Slumping*: motion is characterized by interchanging of configuration with repose angle and motion angle; so free surface has oscillations with amplitude equal to the relax angle; it is typical of low gradient of speed and it is not suitable for finishing;

- *Rolling*: it is the more effective motion and it is characterized by an active layer with constant inclination;

- *Cascading*: it is similar to the previous motion, but the active layer create a S-shape;

- *Cataracting*: cohesion forces between particles are won by centrifugal forces and the elements are throw in a projectile motion; this causes impingement of workpieces and for this reason, generally it is not adopted in finishing;

- *Centrifuging*: elements in the batch adhere to the internal wall of the barrel while rotation; in this situation relative speeds are quite null and so material removal is very low.
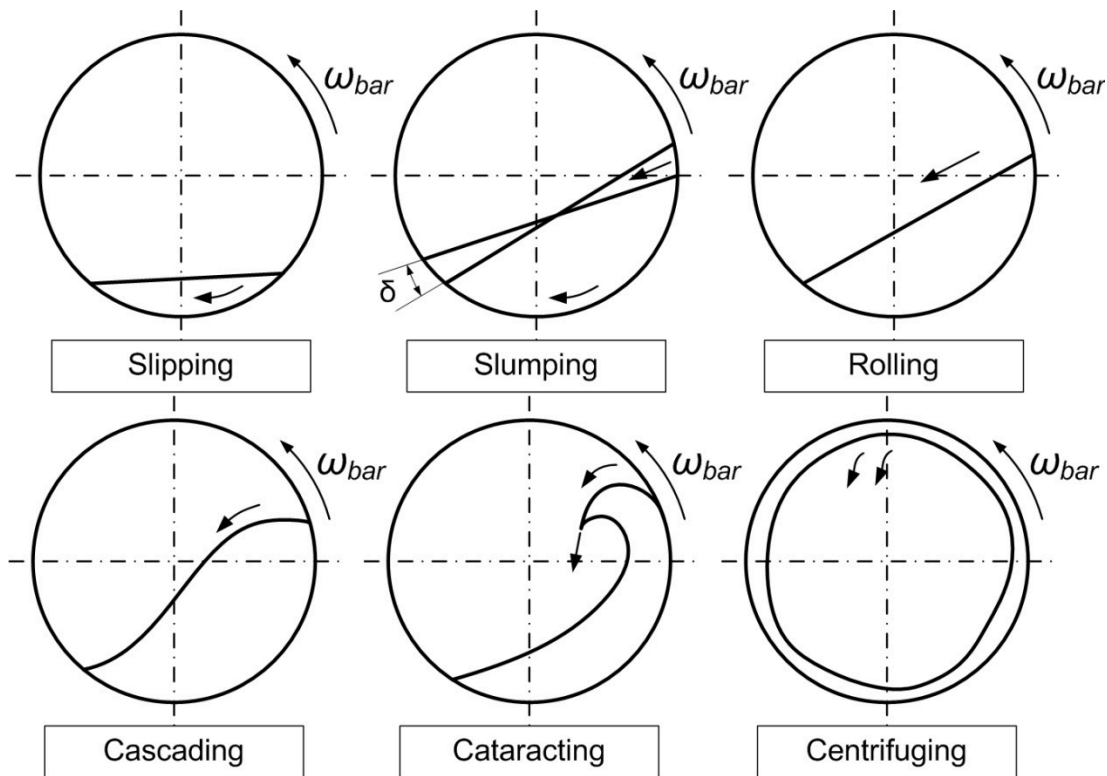
Fig. 6.21 Sketch of barrel motion regimes classification

Aiming at understanding the bath behaviour of the dry mass finisher, different levels of barrel and fun rotation speed were applied, following the DOE in Tab. 6.9. Bath motion was observed to understand its behaviour comparing it with typical regimes found in conventional barrel finishing processes.

The study was conducted considering three levels for each factor, the high level, the low level and the medium one. Barrel rotational speed levels were defined considering the speed limits of the machine ($10\ rpm\ \leq \omega_{bar} \leq 50\ rpm$), whereas for the air flow rate, the low level was defined in order to obtain a minimum motion of the bath whereas the high level was selected for giving a vigorous regime. In adding, the bath behaviour without air flow was observed. It shall be pointed out that applying ω_{bar} = 50 rpm, structural vibrations occur, so the high level was decreased to 45 rpm.

Tab. 6.9 Bath motion behaviour: DOE

Factor	Level	Values
Blower rotational speed ω_{blo} [rpm]	4	0, 2300, 2700, 3100
Barrel rotational speed ω_{bar} [rpm]	3	10, 30, 45

Without air flow rate and selecting a barrel rotation speed of 10 rpm, a regime of cascading was observed: increasing the speed the cascading phenomenon is more and more evident (see Fig. 6.22 for the counterclockwise direction and Fig. 6.23 for clockwise direction of the barrel). With higher rotational speed the mass tends to separate, due to the mass-breakers within the barrel: in this situation the motion is very energized, with a regime that can be assimilated to the cataracting one; at this regime, impingement of workpieces may occur causing damages of workpieces.
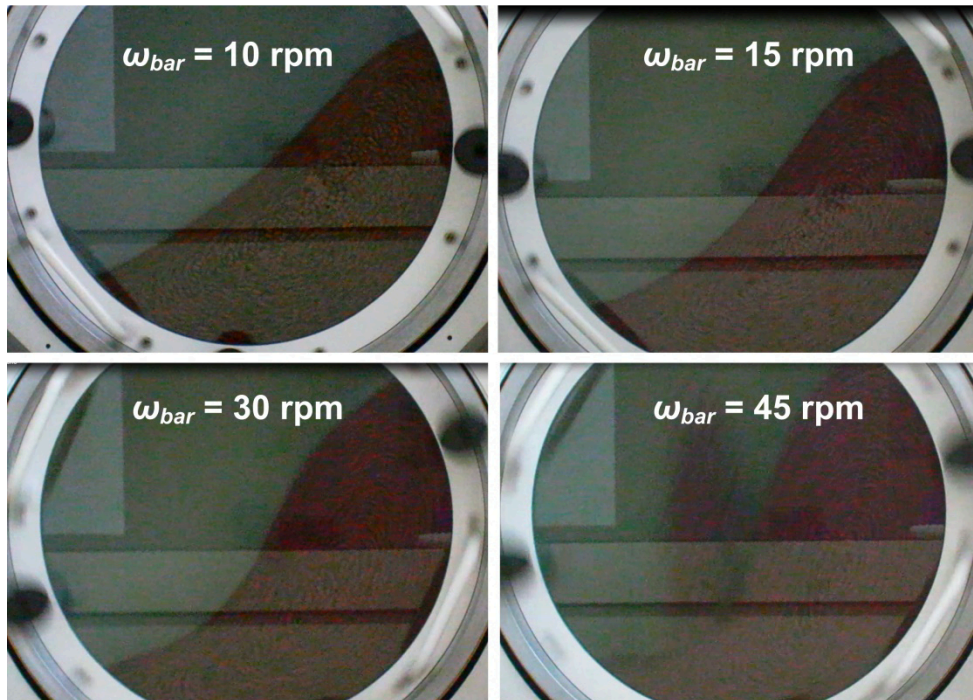
Fig. 6.22   Bath motion varying barrel rotational speed (ω_{blo} = 0 rpm, Counterclockwise direction)
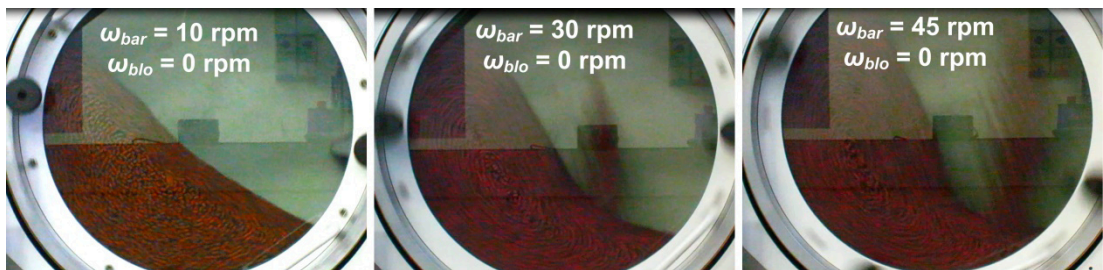
Fig. 6.23   Bath motion varying barrel rotational speed (ω_{blo} = 0 rpm, Clockwise direction)

In order to analyse the effect of the flow rate, bath motion was observed at low barrel rotational speed (see Fig. 6.24 for the counterclockwise direction and Fig. 6.25 for the clockwise regime). Bath has a slight expansion in volume and setting a low air flow rate the S-shape of the bath tends to flatten. If air fun speed increases, the air flow generates preferential paths to pass through the mass: media has a chaotic motion, especially in the case of clockwise direction of rotation. This effect is due to the structural characteristic of the machine prototype since air flow direction is not aligned with the vertical axis of the barrel (see Fig. 6.19): if counterclockwise direction is selected, air flow enters in the barrel where the most amount of media is located, so media motion will be less energetic; on the contrary, during a rotation with clockwise direction, most of amount of media will amass on the left side of the chamber, whereas input of air occurs on the right side: therefore, air flow will apply a thrust force to a minor volume of media, distancing it with a vigorous force from the rest of the mass. These observations suggest that bath motion behaviour changes if clockwise or counterclockwise direction is selected; in adding, the combination of working parameters plays a fundamental role.

Experimental observation of bath regimes had suggested that the selected levels of process factors would be appropriate in an empirical analysis of the effectiveness of the innovative mass finishing system as explained below.
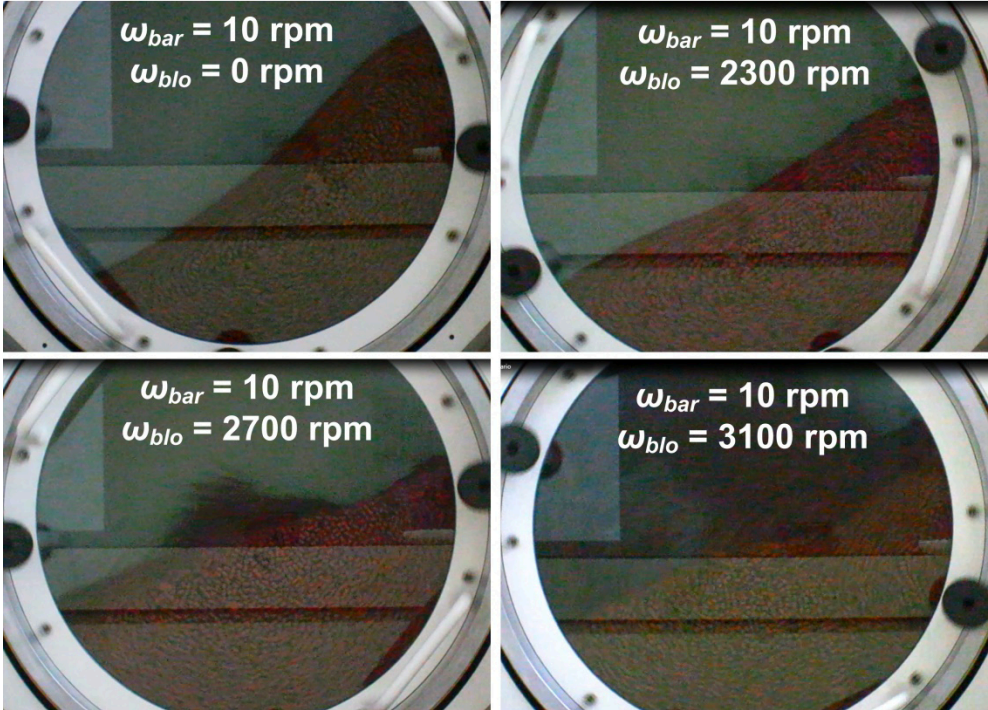
Fig. 6.24   Bath motion varying air flow rate (Counterclockwise direction)
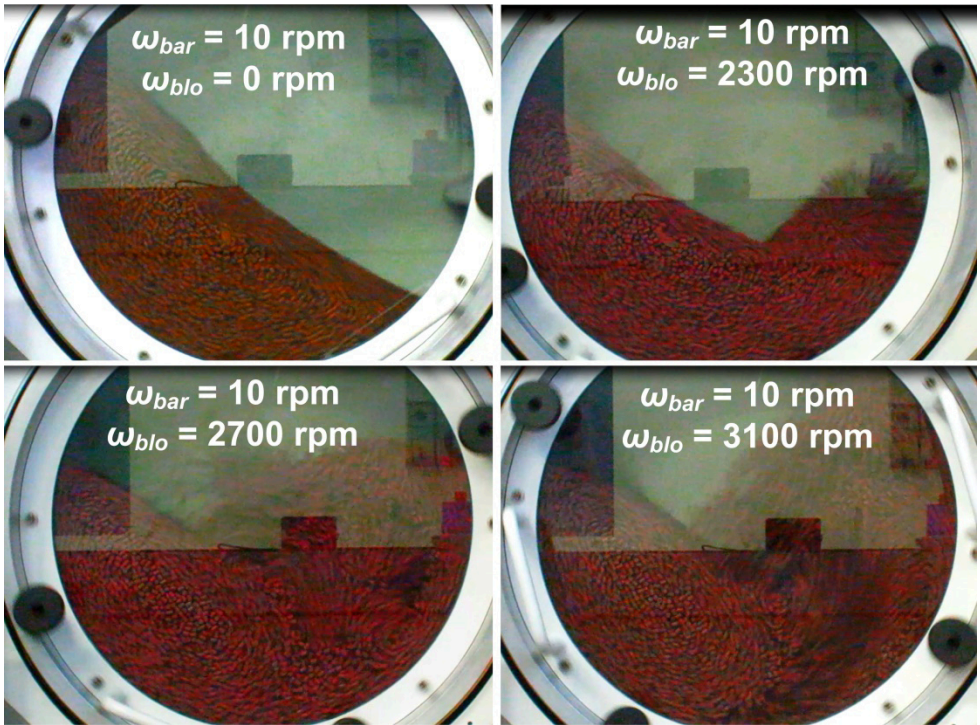
Fig. 6.25   Bath motion varying air flow rate (Clockwise direction)

6.5.3 Experimental procedure and set-up

Main purpose of the experimental investigation was understanding the competitiveness of dry technology than conventional mass finishing approach. For this purpose, several aspects shall be considered: deburring action, removing contaminants due to previous machining processes (cutting oil and micro-chips deriving from grinding operation) and radiusing effect.

The prototype behaviour was analysed performing mass-finishing on a small ground component for diesel injector system. The component is currently manufactured at the Brovedani SpA company. The workpiece is made of a stainless steel Nickel-based. Its geometry is characterized by internal diameter of 22mm and thickness about 3mm (see Fig. 6.26). Edges have to be burr-free and their dimensional tolerance dictates the maximum value of the edge in 0.15mm in both longitudinal and axial direction. Dents are not admitted. Purposes of mass finishing process were deburring (burrs are generated by previous grinding process), chips and oil removal and radiusing the edges.

This component was a good candidate for testing the machine behaviour thanks the simple shape. Moreover, the stainless steel material avoids the corrosion onset, so workpiece could be handled without specific expedients.
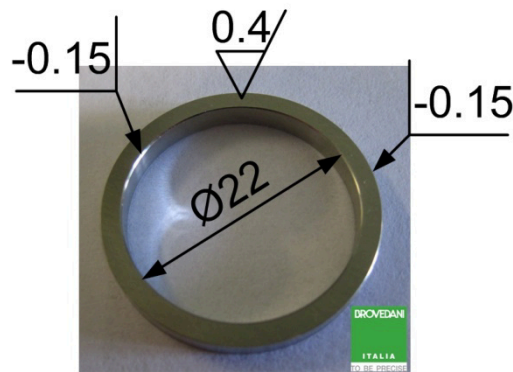
Fig. 6.26   Automotive component for testing prototype machine (Courtesy of Brovedani SpA)

In order to evaluate the functionality of the machine tool to finish the specific workpiece, and understand proper working parameters, a preliminary DOE was adopted (Tab. 6.10).

Tab. 6.10   Preliminary finishing tests: DOE

Working parameter	Levels	Values
Bolwer rotational speed ω_{blo} [rpm]	3	$2300 \div 3100$
Barrel rotational speed ω_{bar} [rpm]	3	$10 \div 45$
Barrel rotation direction	2	Clockwise, Counterclockwise
Barrel tilt [deg]	1	2
Cycle time [min]	1	120
Repetition		1 or 2
Total tests		30

A batch of eleven ground components was applied, in order to avoid impingement between workpiece; parts were analysed before and after the process.

Referring to specific quality requirements, several process outputs should be considered for evaluating the accuracy of workpiece:

1. Completely burr removal from edges;
2. Radiusing of edges;
3. Absence of dents.

For sake of simplicity, in the preliminary stage, cleanliness of the components was evaluated only by a visual control whereas geometrical tolerances were not considered: the aim was to verify the ability of the process in deburring and material removal.

The inspection strategy adopted before and after the mass finishing process is collected in Tab. 6.11. Experimental data were processed in Mathworks Matlab environment.

Tab. 6.11 Inspection strategy for preliminary tests

Evaluated factor	Instrument	Sample analyzed	Control each sample
Edge geometry	Profilometer Mahr MarSurf CD120	3	16 measurements max.
Presence of burr	Stereomicroscope Leica M165C	3	8 pictures max.
Surface quality	Roughness tester Taylor Hobson Form TalySurf 120i	1	4 measurements max.
Dents	Stereomicroscope Leica M50	1	Overall sample by visual inspection

The selected abrasive media was the OTEC TZM with cylindrical geometry. The grain length was about 4 – 5 mm whereas the diameter was 3 mm. It was made of plastic material with SiC particles and it was suitable to work elements susceptible to dents like the workpiece under testing. Obviously, due to the geometry, the media cannot work adequately parts with small holes, undercuts or small groves.

Abrasives dresses themselves removing worn part and allowing the new abrasive. Dressing occurs by the removal of a slice in the cross-section (Fig. 6.27). In add, media surface showed abrasive particles in SiC with micro metal chips due to the material removal held back by its soft polymeric matrix.
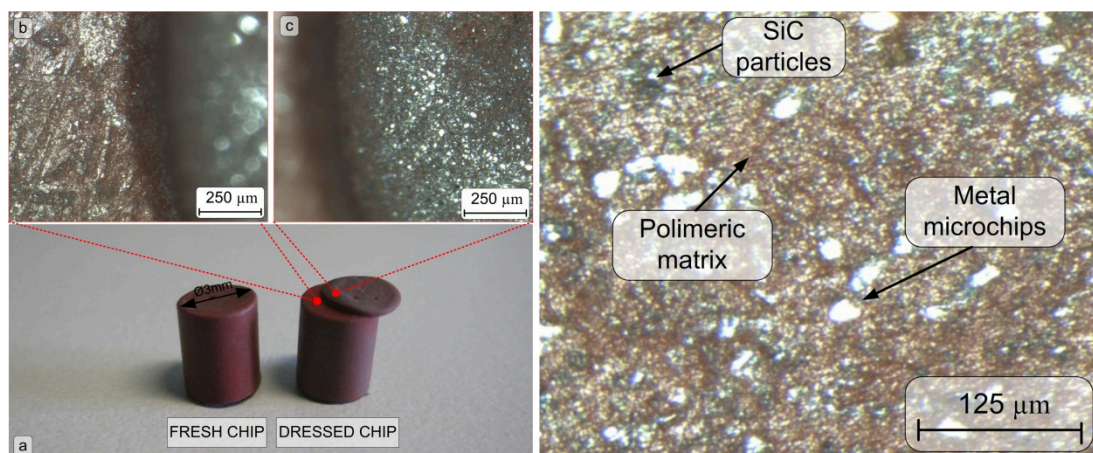
Fig. 6.27 Fresh and dressed OTEC abrasive chips (a) and difference between dressed surface (b) and worn surface (c) by stereomicroscope

6.5.4 Deburring action: Data analysis and discussion

Considering the effectiveness of the dry process in deburring, three workpieces for each combination of working parameters were controlled by a stereomicroscope before and after the process; each workpiece was observed at four different inspection points (see Fig. 6.28 as an example).
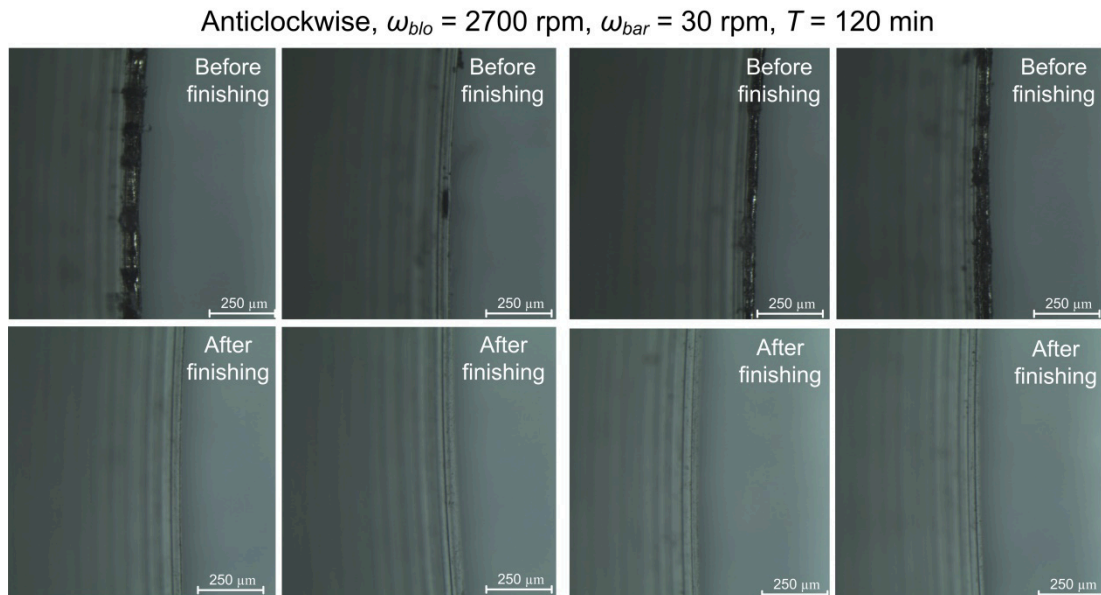
Fig. 6.28   Comparison of edge status of a workpiece at four inspection points before and after mass finishing process

Therefore, observing images, a qualitative evaluation of the accuracy of the edge was given by numerical value (see Fig. 6.29) as follow:

- *Level 1*: Huge burr dimension
- *Level 2*: Medium burr dimension
- *Level 3*: Slight burr dimension
- *Level 4*: Perfectly deburred.
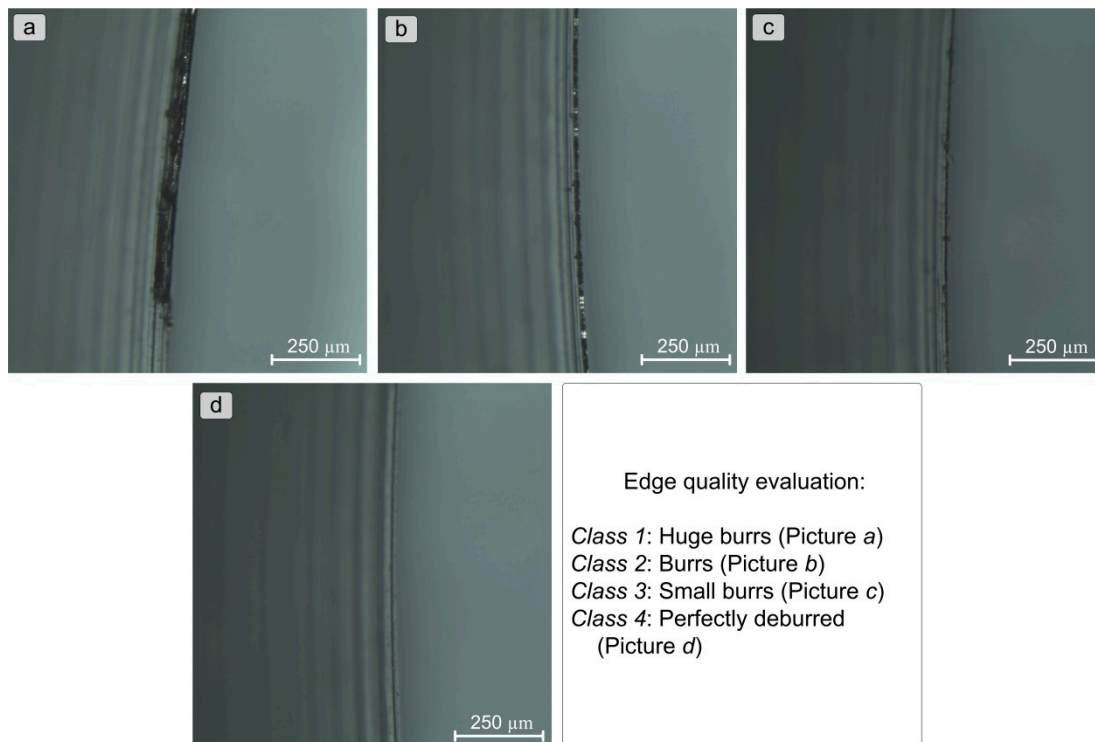
Fig. 6.29 Edge cleanliness evaluation

Each workpiece was characterized by the mean value of the quality levels assigned to the four inspection points. The effectiveness of the deburring action was evaluated as the difference between quality levels after and before mass finishing.

Analyzing scatter diagrams in Fig. 6.30, unfortunately it is not possible to identify linear trends of deburring action against working parameters.
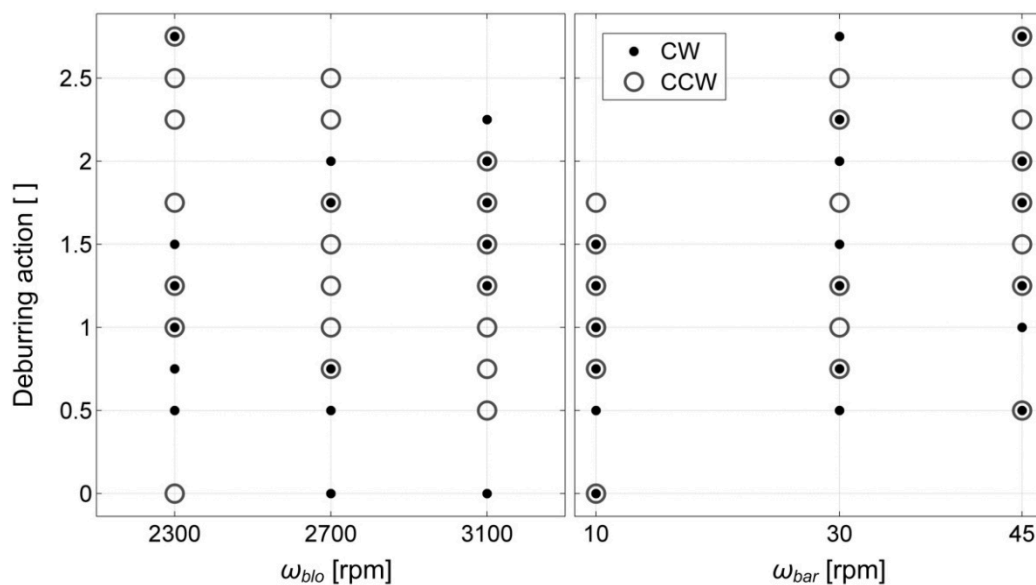
Fig. 6.30 Scatter diagrams of deburring qualitative evaluation against working parameters
(CW: Clockwise barrel direction, CCW: Counterclockwise barrel direction)

From the analysis of variance (Tab. 6.12) it is deduced that only the rotation speed of the barrel affected the deburring action of the dry mass finishing process.

Tab. 6.12   Analysis of variance of experimental data

Parameter	Sum of square	dof	Mean square	F-statisic	p-value
rot	0.7824	1	0.78241	2.1	0.1554
ω_{blo}	0.294	2	0.14699	0.39	0.677
ω_{bar}	5.9606	2	2.98032	7.99	0.0012
$rot*\omega_{blo}$	0.9745	2	0.48727	1.31	0.2823
$rot*\omega_{bar}$	0.0856	2	0.04282	0.11	0.8919
$\omega_{blo}*\omega_{bar}$	1.4421	4	0.36053	0.97	0.4367
Error	14.9282	40	0.37321		
Total	24.4676	53			

A simple mathematical model was proposed to predict the deburring action *Deb* of the finishing process; for sake of simplicity rotation directions of barrel were computed singularly. Model coefficients were estimated by applying the regression technique on the means of experimental values.

$$Deb_{mod} = k_0 + k_1\omega_{bar} + k_2\omega_{blo} + k_3\omega_{bar}^2 + k_4\omega_{blo}^2 + k_5\omega_{bar} \cdot \omega_{blo} \qquad (6.7)$$

Interpolating surfaces are shown in Fig. 6.31 together with experimental points; model coefficients and coefficients of determination *R* squared are collected in Fig. 6.13 together with standard deviation of relative errors between experimental data and the model estimates, calculated as:

$$\sigma_{mean} = std\left(\frac{Deb_{mod} - Deb_{exp,mean}}{Deb_{exp}}\right) \cdot 100\ [\%] \qquad (6.8)$$

Furthermore, in order to verify the repeatability of the deburring action for a given process configuration, experimental data dispersion was estimated by computing the standard deviation $\sigma_{\varepsilon Deb}$ of the of the relative error:

$$\varepsilon_{Deb} = \frac{Deb_{mod} - Deb_{exp}}{Deb_{mod}} \cdot 100\ [\%] \qquad (6.9)$$

where Deb_{exp} are the quality level values assigned to the three workpieces for each parameters combinations, whereas Deb_{mod} is the average value predicted by the model, respectively. Analyzing results of Eq. 6.9, which are listed in Tab. 6.13, it has to be pointed out the high dispersion of experimental data.

Tab. 6.13   Coefficients of model parameters, correlation and relative errors

Rot.	k_0	k_1	k_2	k_3	k_4	k_5	R^2 [%]	σ_{mean} [%]	$\sigma_{\varepsilon Deb}$ [%]
CW	12.16	-0.0089	0.0308	1.65e-6	-5.82e-4	9.57e-6	86.43	17.01	43.16
CCW	-2.50	0.0012	0.2150	5.43e-19	-6.75e-4	-5.88e-5	92.71	18.17	45.98
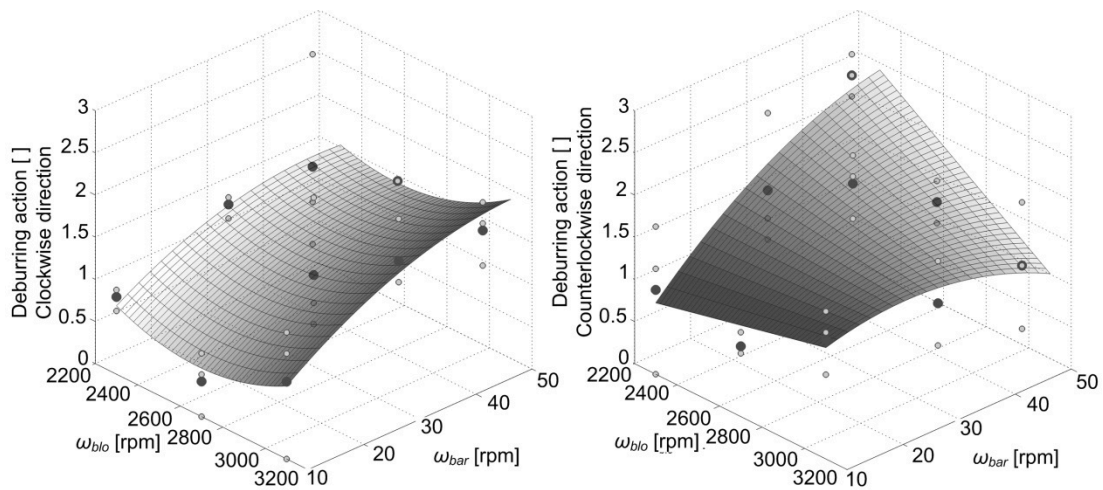
Fig. 6.31 Modelling the deburring action of the dry mass finishing technique

6.5.5 Radiusing action: Data analysis and discussion

In order to evaluate effectiveness of the mass finishing process in radiusing of edges, the geometry of internal and external edges was measured considering 16 inspection points for each workpiece. Measurements were performed by a Taylor Hobson profilometer before and after machining, see Fig. 6.32. An example of measurement is shown in Fig. 6.33 where it can be notices the increment, i.e. a radiusing action, of the dimension along *x-* and *y-axis*, which refer to the ground plane and the turned plane, respectively.
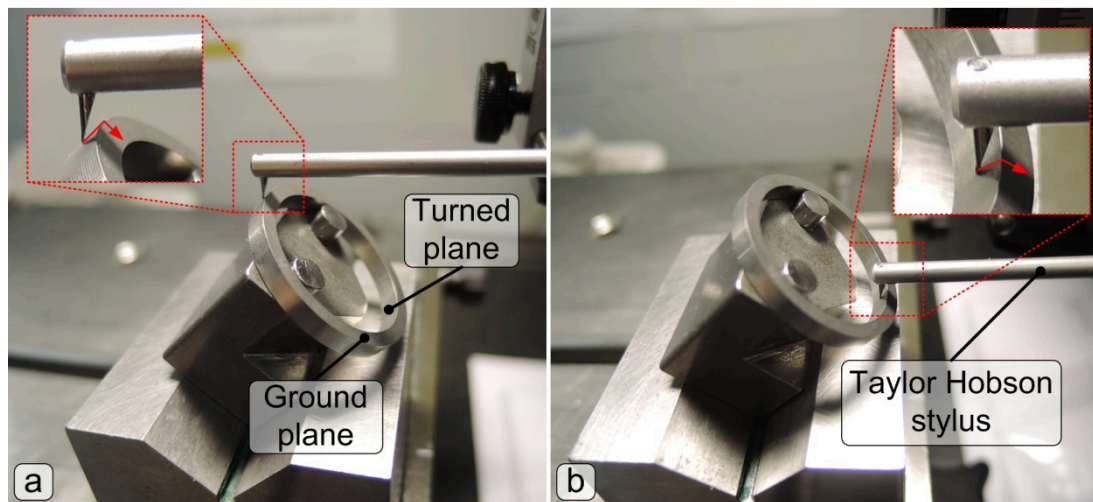
Fig. 6.32 Edge profile measurements by Taylor Hobson profilometer: External edge (a) and internal edge (b)

Before finishing

x_1=0.0916 mm

y_1=0.0973 mm

Ground plane

Turned plane

After finishing

x_2=0.1091 mm

y_2=0.1055 mm
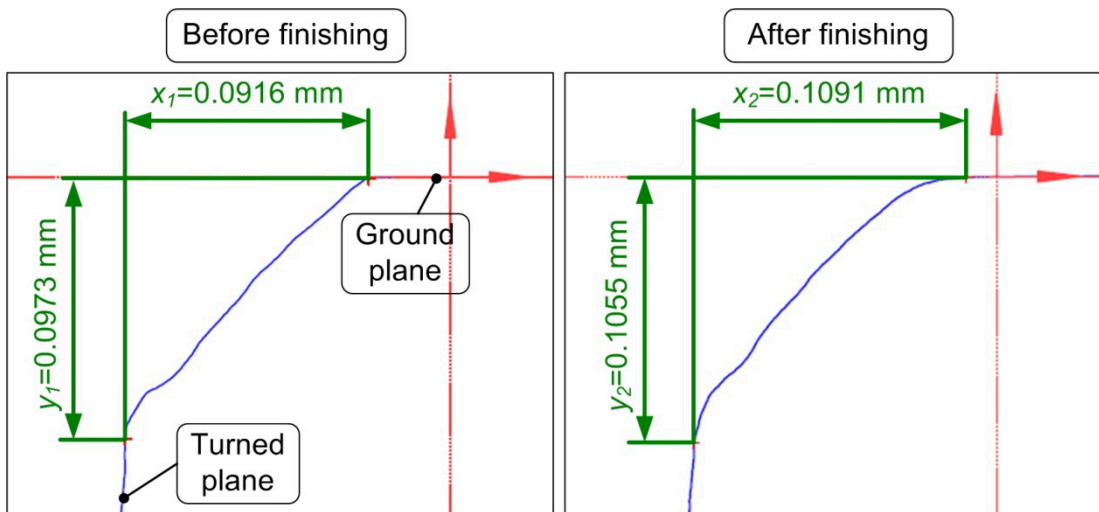
Fig. 6.33 Comparison edge profile before and after dry mass finishing process (Rotation: Clockwise, ω_{blo} = 3100 rpm, ω_{bar} = 30 rpm)

In Fig. 6.34 a measurement of a burr, in agreement with the standard DIN 6784 [110] is shown: after finishing, the burr was not detected, therefore working process removed it successfully, reaching also a radiusing effect of the edge.

Before finishing

0.0181 mm

x_1=0.0035 mm

y_2=0.0554 mm

After finishing

x_2=0.0409 mm

y_2=0.0193 mm

Ground plane
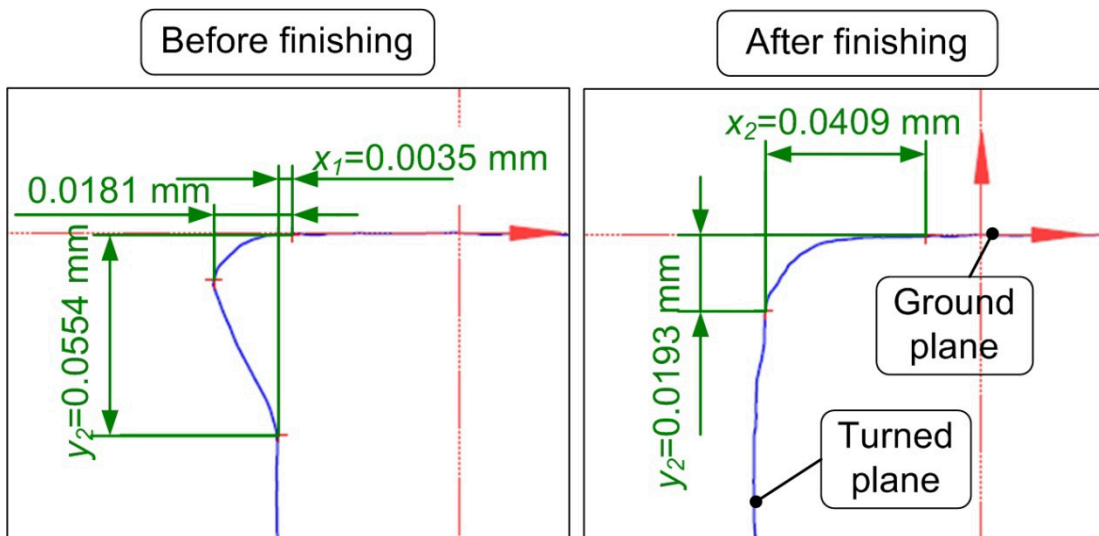
Turned plane

Fig. 6.34 Deburring by dry mass finishing process (Rotation: Clockwise, ω_{blo} = 3100 rpm, ω_{bar} = 30 rpm)

An example of the overall measurements for a single workpiece is shown in Fig. 6.35, where profiles along ground and turned planes, before and after the mass finishing process, are collected. Thanks to the radiusing effect of the process, dimensions after the process were greater than those before machining.
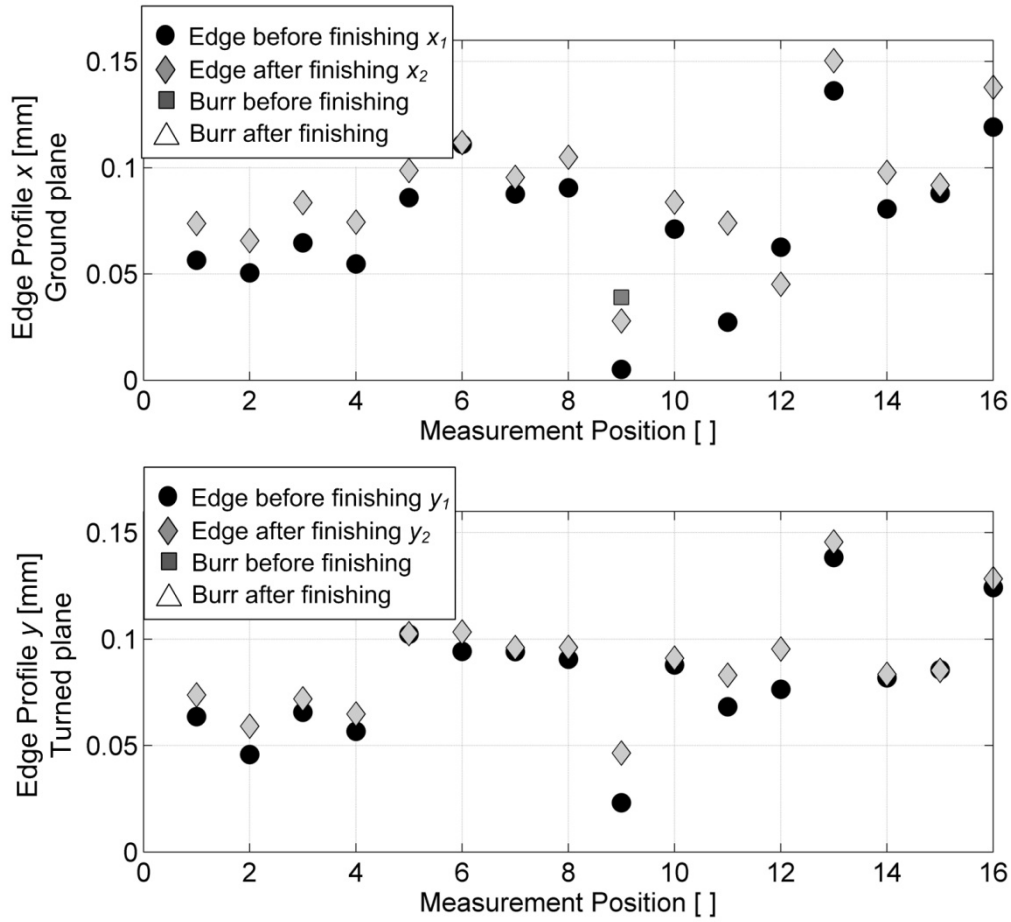
Fig. 6.35 Edge profile measurements before and after dry finishing process (Rotation: Clockwise, ω_{blo} = 2300 rpm, ω_{bar} = 30 rpm)

Aiming at analyzing the radiusing effect, the material removal rate *MRR* was evaluated. It has to be pointed out that in literature *MRR* states the volume of material removal per unit of time [mm^3/min] [85] [3]. In this work, for sake of simplicity, *MRR* represents a linear quantity expresses in [mm]. It is given by the absolute differences between the edge dimension after and before mass finishing process (see Fig. 6.33 as reference):

$$MRR_{Ground\ Plane} = x_2 - x_1\ [mm] \tag{6.10}$$

$$MRR_{Turned\ Plane} = y_2 - y_1\ [mm] \tag{6.11}$$

MRR values were observed by scatter diagram to understand the influence of working parameters on the process behavior, Fig. 6.36. It is evident that the rotation of barrel affects the material removal rate, especially for the clockwise rotation direction: greater the level of ω_{bar}, greater is *MRR*, for both ground and turned planes. The comprehension of the influence of ω_{blo} is more difficult because it is not possible to define a specific trend of the experimental data.
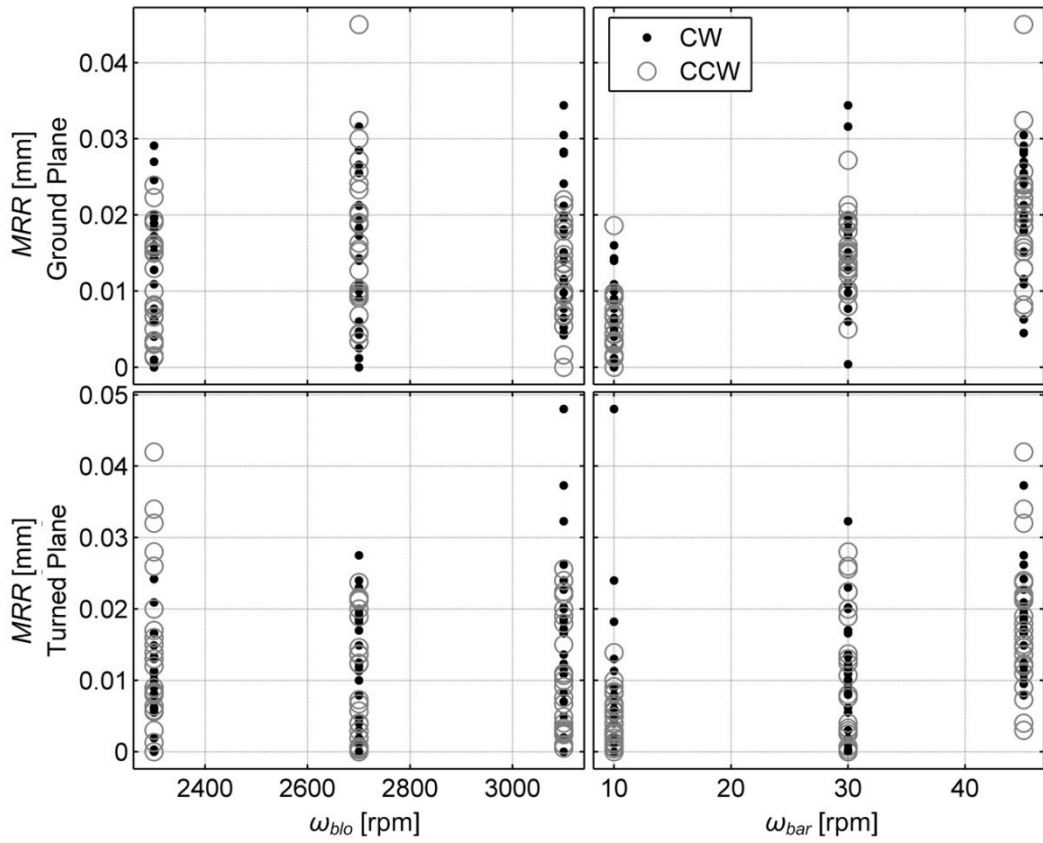
Fig. 6.36 Scatter diagram of the material removal against working parameters

Therefore the analysis of variance of mean value of *MRR* for each workpiece was carried out to understand whose working parameters, i.e. air flow rate, rotation speed and rotation direction of barrel, strongly affect process behavior; in the analysis, profiles along the ground plane (Tab. 6.14) and the turned plane (Tab. 6.15) were considered separately. It emerged that only rotation speed of the barrel strongly affects the material removal capacity of the dry system, for both ground and turned plane.

Tab. 6.14   Analysis of variance for *MRR* of ground plane

Parameter	Sum of square	dof	Mean square	F-statisic	p-value
Rotation direction *rot*	0.00001	1	0.00001	1.17	0.3013
ω_{bar}	0.00066	2	0.00033	52.07	0
ω_{blo}	0.00002	2	0.00001	1.53	0.2563
Error	0.0008	12	0.00001		
Total	0.00076	17			

Tab. 6.15 Analysis of variance for *MRR* of turned plane

Parameter	Sum of square	dof	Mean square	F-statisic	p-value
Rotation direction *rot*	0.00001	1	0.00001	1.37	0.2637
ω_{bar}	0.00041	2	0.0002	18.88	0.0002
ω_{blo}	0.00003	2	0.00002	1.48	0.2664
Error	0.00013	12	0.00001		
Total	0.00058	17			

In the light of outlined observations, a simple mathematical model was proposed to predict the material removal *MRR*, for sake of simplicity considering the rotation directions of barrel singularly. Model coefficients were estimated applying the regression technique on the mean value of experimental values.

$$MRR_{mod} = k_0 + k_1\omega_{bar} + k_2\omega_{blo} \tag{6.12}$$

Interpolating surfaces are shown in Fig. 6.37, whereas model coefficients and coefficients of determination *R* squared are collected in Tab. 6.16 together with standard deviation of relative errors between experimental data and the model estimates, calculated as:

$$\sigma_{mean} = std\left(\frac{MRR_{mod} - MRR_{exp,mean}}{MRR_{mod}}\right) \cdot 100\ [\%] \tag{6.13}$$

Furthermore, in order to verify the repeatability of the material removal rate for a given process configuration, experimental data dispersion was estimated by computing the standard deviation $\sigma_{\varepsilon MRR}$ of the of the relative error:

$$\varepsilon_{MRR} = \frac{MRR_{mod} - MRR_{exp}}{MRR_{mod}} \cdot 100\ [\%] \tag{6.14}$$

where *MRR_{exp}* are the experimental points and *MRR_{mod}* is the average value predicted by the model, respectively. Analyzing results of Eq. 6.14, listed in Tab. 6.16, it has to be pointed out the high dispersion of experimental data.

Tab. 6.16 Coefficients of model parameters, correlation and relative errors

	Rot.	k_0	k_1	k_2	R^2 [%]	σ_{mean} [%]	$\sigma_{\varepsilon MRR}$ [%]
Ground plane	CW	-0.0041	4.469e-4	2.291e-6	97.13	11.83	51.64
	CCW	-0.0029	3.968e-4	1.875e-6	79.70	19.95	45.76
Turned plane	CW	-0.0120	2.674e-4	6.465e-6	65.14	25.76	74.01
	CCW	0.0133	3.7693e-4	-4.721e-6	93.23	28.74	82.03
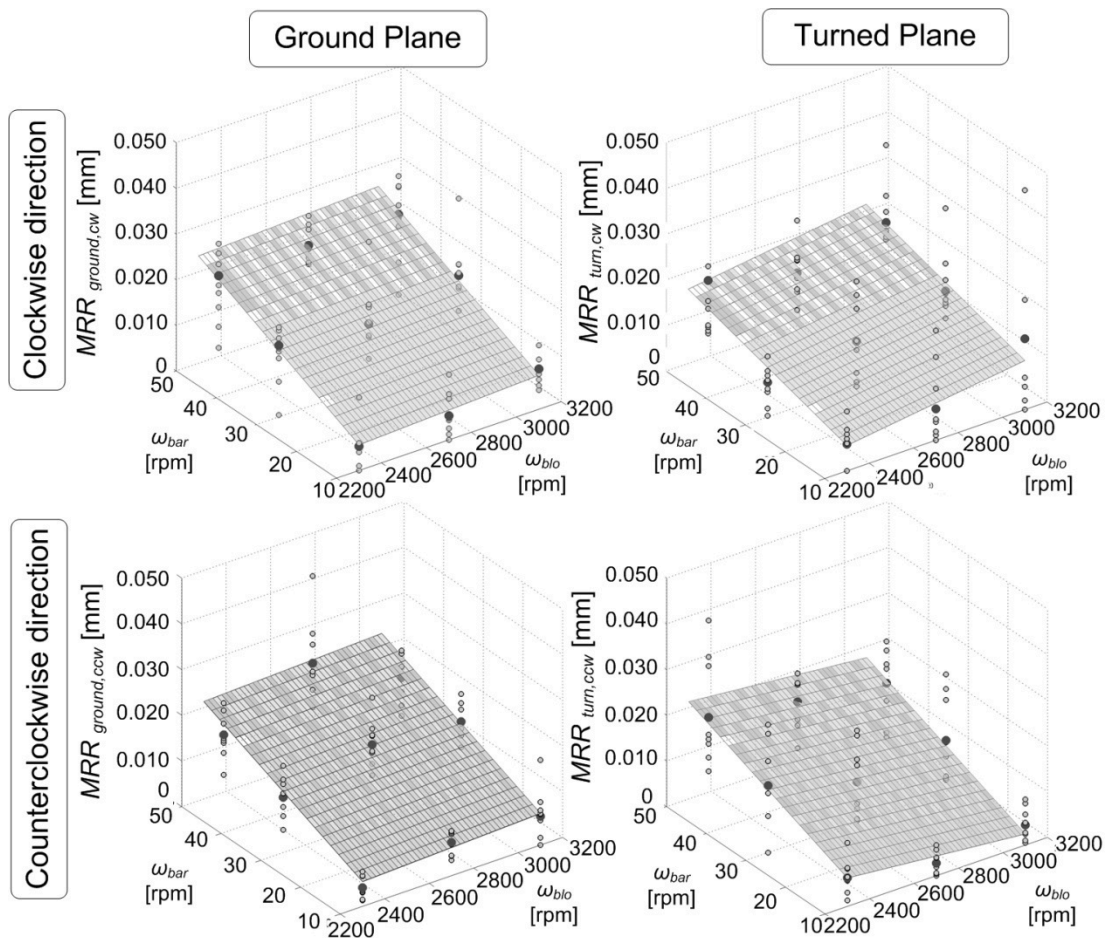
Fig. 6.37   Modelling of experimental *MRR*

6.5.6 Final observations about finishing by the innovative dry system

From experimental evidences about dry mass finishing prototype, it emerges that the process could be applied in deburring and radiusing of workpieces. However, for a given a combination of working parameters, the process is not robust both in deburring both in radiusing actions, since high dispersion of data was observed. On the other hand, it has to be pointed out that the evaluation of the two analyzed finishing actions differs basing on the edge requirements that are considered. Deburring action cannot be considered effective, since edge should be perfectly deburred: this result was rarely observed on the machined workpiece. On the contrary, the radiusing action performed by the dry mass finishing process can be acceptable, since radiusing aims at increasing the edge dimensions, without exceeding a maximum value defined by the design department. For this reason, even if the machine does not assure repeatability on the edge geometry, the only crucial aspect to be taken into account is to verify if the dimensional and geometrical tolerances are fulfilled.

Among the working parameters, barrel rotation speed strongly affects the accuracy of the workpiece. Also the rotation direction seems to influence workpiece quality, probably due to the different interaction with the air flow rate, which enters into the barrel with an inclined direction respect to the vertical axis of symmetry of the machine.

The air flow rate represents the factor that differentiates the prototype rather than a simple dry barrel finishing technology. By performing specific tests without air flow rate, it emerges that gas flow limits the action of abrasive media: air flow reduces the sliding action of

abrasives due to the chaotic bath motion resulting in a longer cycle time. On the other hand, air flow guarantees the removal of contaminants (micro-chips and abrasive powders) from the working chamber, avoiding re-depositions on the workpieces surfaces; it can create a greater number of point of contact between parts and media, thanks to the abrasive bed expansion (only if proper rate is selected, i.e. a medium air flow rate); moreover, it generates a cushion-effect limiting the impact energy between media and workpieces.

Furthermore it shall be noticed that damages on workpiece edges were not detected: dents can be originated from impingement of parts or by the contact of workpiece with grains. This aspect was avoided by selecting a very small batch and by using abrasives grains with soft matrix. It was demonstrate, indeed, that ceramic media: this is caused by the ceramic matrix which is harder than the plastic one.

6.6. Super-finishing by dry mass finishing equipment

Further purposes in using mass finishing process are fine polishing or removing contaminants due to previous surface treatments or machining process from workpiece surfaces. Therefore dry mass finishing system, exposed in the previous section, was tested in order to verify the possibility in adopting the new approach in a super-finishing process.

6.6.1 Case study and experimental set-up

The workpiece under investigation is an hardened stainless steel component for automotive application; it is manufactured at the Brovedani SpA company. After cutting processes it is subjected to a nitro-carburizing hardening treatment in order to improve its anti-scuffing properties, the adhesive wear resistance and the corrosion resistance. Unfortunately, heat treatment produces residuals that make the surface accuracy not admissible because contaminants may affect final functionalities of the part (see Fig. 6.38 - a): for this reason, a fine polishing process based on centrifugal finishing strategy is currently adopted, which results in a polished surface as shown in Fig. 6.38 - b. The selected mass finishing process has to improve surface accuracy without modifying geometry and shape of workpiece.

Fig. 6.38   Workpieces status after heat treatment (a) and after current polishing strategy (b)

The aim of fine polishing tests using dry mass finishing system was to verify the possibility in substituting current mass finishing strategy in order to reduce the high costs in waste treatment that the company has to incur.

A specific DOE (Tab. 6.17) was adopted. Combinations of working parameters were selected basing on the bath motion observation outlined in the previous section (see Fig. 6.39). Firstly, in order to perform a fine polishing of workpieces a regime of sliding (ω_{bar} = 30 rpm) with high air flow rate (ω_{blo} = 3100 rpm) was adopted in order to intimate as long as possible the contact between media and workpieces: the expansion of the bath, due to the hair flow rate, allows the media movement below the active layer, performing more abrasive action on the surfaces. Then, a regime of cataracting (ω_{bar} = 45 rpm) with medium air flow rate (ω_{blo} = 2700 rpm) was set, because in the previous experimental analysis it had been observed as one of the most effective regime in working components. Lastly, an intermediate regime (ω_{bar} = 30 rpm and ω_{blo} = 2700 rpm) was selected to avoid impingement of workpieces, typical of cataracting regime; lower air flow rate was selected in consciousness that air flow rate may limit the abrasive media action. The remaining combination of parameters (ω_{bar} = 45 rpm and ω_{blo} = 3100 rpm) was not chosen because the bath motion might be too chaotic and not effective for fine polishing process.

Tab. 6.17   DOE for super-finishing process by dry mass finishing strategy

Factor	Level	Values
Rotation speed of barrel ω_{bar} [rpm]	2	30,45
Rotation speed of air blower ω_{blo} [rpm]	2	2700,3100
Cycle time T [min]	2	60, 120
Combination of parameters ω_{blo}- ω_{bar}	3	3100-30 2700-45 2700-30
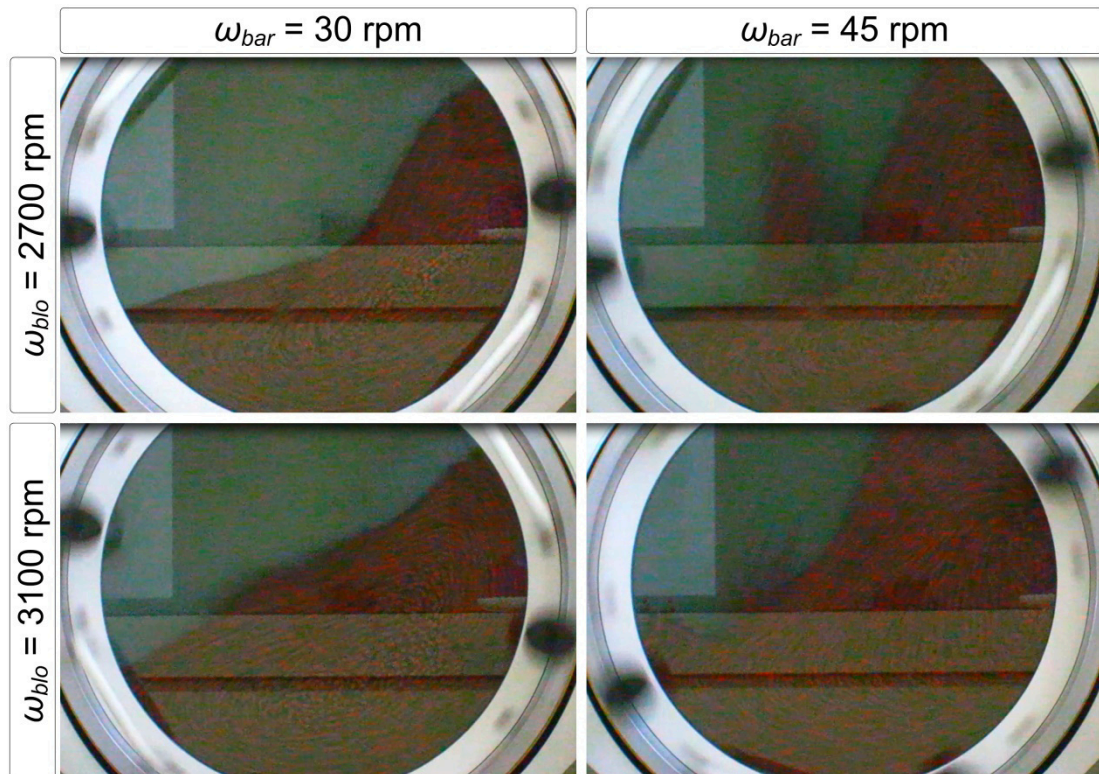
Fig. 6.39   Bath motion regimes for fine-polishing tests

Analysis of machined workpieces was performed by visual inspection, in order to identify homogeneity on the surface aspect; experimental surface quality was compared with surface aspect derived from current finishing strategy.

6.6.2 Experimental results and discussion

Fine polished workpieces are shown in Fig. 6.40. It emerges that the first combination of working parameters (ω_{bar} = 30 rpm and ω_{blo} = 3100 rpm) was not so effective, considering both cycle times tested: by comparing results to workpieces machined with the other regimes, some defects are evident in surface accuracy, see Fig. 6.40 (a) and (b). Also in the case of bath motion given by the combination ω_{bar} = 30 rpm and ω_{blo} = 2700 rpm, the cycle time equal to 60 minutes was not sufficient in a completely removing of heat treatments residuals (Fig. 6.40 – e), whereas surface quality was acceptable applying a cycle time of 120 minutes. The cataracting regime was the most effective one, thanks to the high energetic motion of the bath, both for T = 60 min both for T = 120 min. In particular, setting a cycle time of 120 minutes, roughness peaks due to the previous turning process were smoothed (see Fig. 6.41 – a), with an improvement in service life of components. Unfortunately, this regime caused impingement between workpieces: this critical aspect would be more evident if the batch of working machine is greater than those was selected for this preliminary study. Indeed, dents were detected on the edges of workpieces (see Fig. 6.41 – b): these defects are not admissible by the workpiece final accuracy requirements. For these reasons, cataracting regime should be applied only if dents are admitted by technical specification; alternatively, applying lower cycle time can reduce the probability of impingement of parts.

Accordingly, aiming at performing a fine-polishing by a dry mass finisher, a proper bath regime should be the sliding one, with an intermediate air flow rate: it promotes the sliding action of sliding regime on the abrasive active layer avoiding the limitation that higher air flow rate creates in abrasion.

In conclusion, dry mass finishing is a promising techniques in fine polishing, since surface quality is comparable, and even better than those is achieved by current mass finishing strategy. Unfortunately, these conclusions were not confirmed by a deeper analysis, for example by working a greater batch of workpieces. So, further tests should be performed in order to verify the capability of the process.
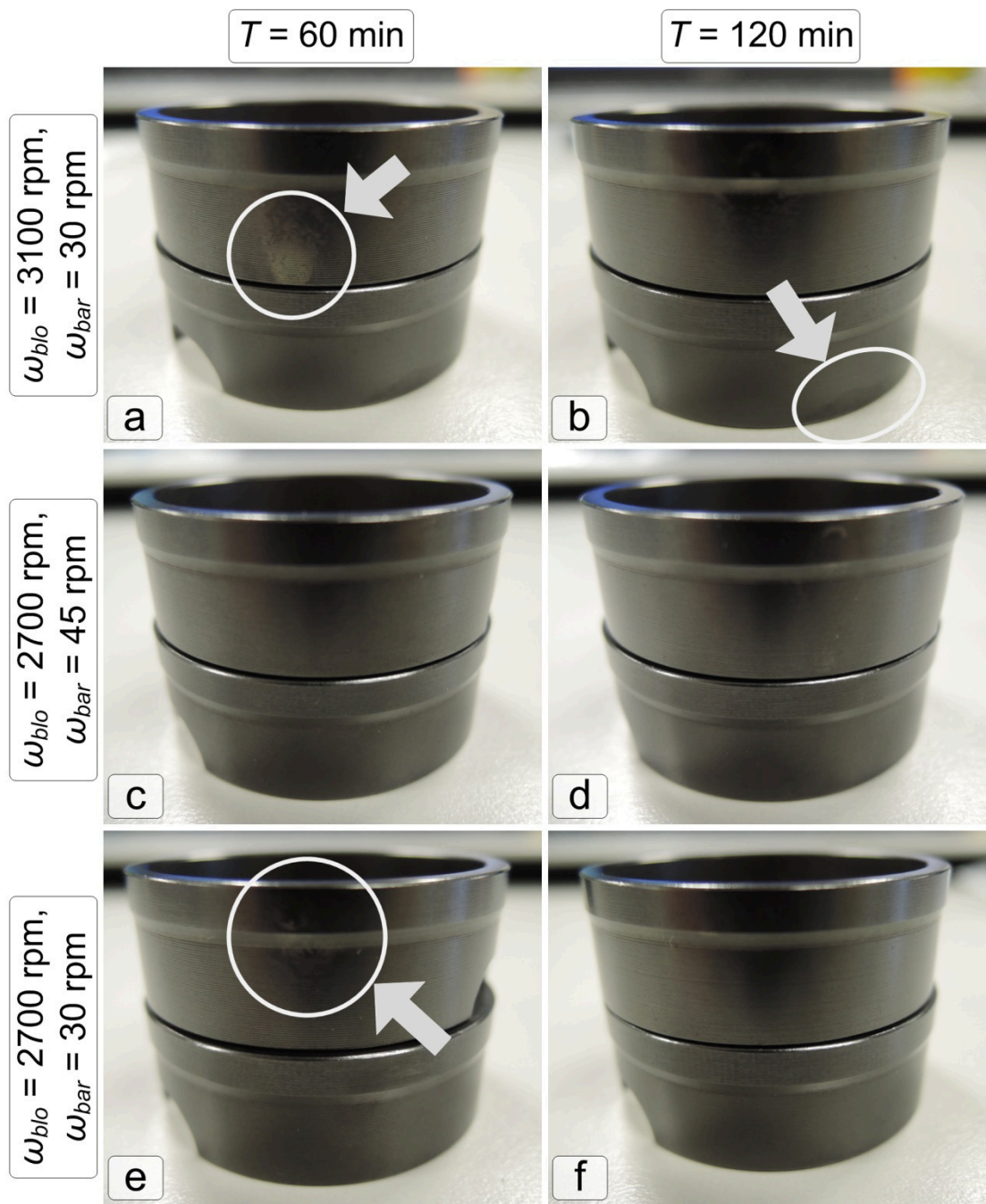
Fig. 6.40 Visual inspection of workpieces after dry mass finishing process
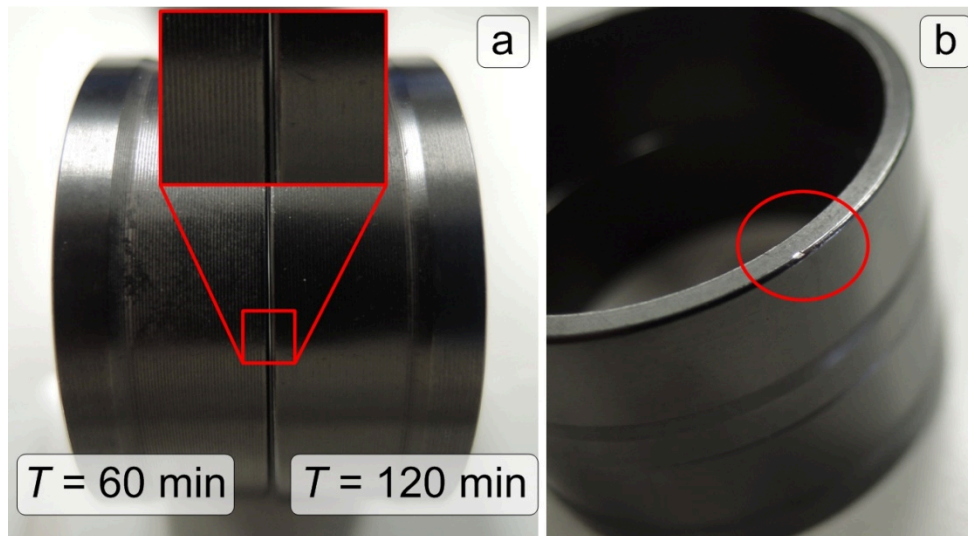
Fig. 6.41 Workpieces after dry mass finishing (ω_{blo} = 2700 rpm, ω_{bar} = 45 rpm): comparison of smoothness of surface (a), detected dent after T = 120 min (b)

6.7. General conclusions

In high precision manufacturing, strict accuracy is required to the final product, such as very stringent dimensional and geometrical tolerances and high surface quality, including surface integrity.

Conventional manufacturing processes or heat treatments can generate defects on the workpiece such as burrs, damages of surface texture or presence of contaminants. These damages can be often limited but are rarely completely avoided: they have to be removed by specific processes, since they may affect the required final functionalities of the workpiece.

The mass finishing technique is a well-known method for achieving this goal.

Unfortunately, there are still huge gaps in the technical literature and a strong need for structured methodologies for enhancing process performance. Most common approach – especially in industry – is based on trial and error method, since instruments or sensors for a scientific characterization of the process behaviour are very difficult to design; moreover, only a few specialized analytical models for accuracy prediction were found in literature.

In this Chapter, an overview of the most applied mass finishers was presented. Afterwards, the edge and surface requirements were highlighted.

A predictive analytical approach based on a previous research work was applied to a mass-finishing strategy in order to define the optimal cycle time. Then, an innovative mass finishing prototype, working in dry conditions, was tested in order to evaluate its effectiveness in deburring, radiusing and super-finishing.

Main conclusions of this research work are given below.

Optimization of vibrational mass finishing strategy:

- Following the analytical predictive model proposed by Hashimoto [104], the optimal cycle time for mass finishing strategy was predicted; the aim of the mass finishing was the improvement of surface quality (R_a) of ground workpieces manufactured at the Brovedani SpA company;

- Surface quality was analysed by roughness measurements; unfinished workpieces were characterized by two initial surface roughness due to different grinding processes: *Status 1* with higher R_a and *Status 2* with lower R_a;

- By performing a preliminary experimentation, which included three mass finishing processes, characteristic parameters (i.e. initial roughness of the workpiece *Ir*, roughness limitation of the workpiece *Dr* and time constant of the finisher *T*) were defined considering each finishing technology;

- The cycle time is strictly related to the initial surface quality: if poor surface quality, a longer process time is needed;

- Optimal cycle times were predicted depending on the initial surface accuracy of the workpiece: for the *Status 1*, T_{opt} was estimated in 404 minutes, whereas with *Status 2* T_{opt} was derived equal to 348 minutes (preliminary mass finishing was performed with T=540 min);

- In the case of *Status 2*, thanks the good initial surface quality, a new finishing strategy was proposed, reducing mass finishing stages in only two processes: in this case, the estimated T_{opt} was decreased to 274 minutes.

Dry mass-finishing technique:

Two experimental investigations were conducted aiming at analysing performance of the dry mass finishing technology: the former study focused on deburring and radiusing action, whereas the latter scientific investigation was focused on fine-polishing of surfaces. Experimental tests were performed at the Brovedani SpA company using a prototype designed by the University of Tor Vergata.

➢ Deburring and radiusing actions

- The dry mass finishing technology could be applied in deburring and radiusing of workpieces; however, the process is not robust both in deburring both in radiusing actions, since high dispersion of data was observed.

- Deburring is not effective since the desired edge quality, i.e. completely absence of burrs, was never fulfilled;

- Barrel rotation speed is the most important factor influencing the accuracy of the workpiece, whereas the effect of the other process parameters is limited;

- Interpolating mathematical models represent the trend of mean values with good accuracy, considering both deburring both radiusing action; however experimental data show a great dispersed distribution, so the analyzed working process was difficult to control;

- The air flow rate differentiates the prototype functioning than a simple dry barrel finishing technology;

- Air flow reduces the sliding action of abrasives due to the chaotic bath motion, resulting in a longer cycle time; on the other hand, air flow guarantees the removal

of contaminants (micro-chips and abrasive powders) from the working chamber, avoiding re-depositions on the workpieces surfaces; it can create a greater number of point of contact between parts and media, thanks to the abrasive bed expansion; it generates a cushion-effect limiting the impact energy between media and workpieces.

- Damages on workpiece edges were not detected: dents could be originated from impingement of parts or by the contact between workpiece and grains. This aspect was avoided by the selection of a small batch and by using abrasives grains with soft matrix. By performing further tests with ceramic media, which has an harder matrix than polymeric grains, damages on edges were observed.

➢ Super-finishing action:

- The purpose was the removal of heat treatment residuals from surfaces of an stainless steel component for automotive; the process should not modify workpiece shape and geometry;
- Three bath regimes were selected; regimes are given as the combination of the barrel rotation speed ω_{bar} and the air flow rate ω_{blo};
- Best results were achieved with medium flow rate (ω_{blo}=2700 rpm) and high rotation speed of barrel (ω_{bar}=45 rpm), for both considered cycle times, T=60 min and T=120min; imposing T=120min, smoothness of surface was observed; however, impingement of workpieces is possible due to the regime of bath motion: indeed, dents were detected;
- Applying high flow rate (ω_{blo}=3100 rpm) with medium rotation speed of barrel (ω_{bar}=30 rpm) surface accuracy was not excellent; higher ω_{bar} was not tested because bath motion was considered too energetic;
- Good accuracy of workpiece surfaces was achieved with medium levels of air flow rate and rotation speed of barrel, i.e. ω_{blo}=2700rpm and ω_{bar}=30rpm, and T=120 min, reaching surface quality better that those realized by current finishing process, applied by the company.

➢ Dry mass finishing is a promising technology for deburring, radiusing and fine polishing of workpieces; further investigations should be performed aiming at improving the capacity of the process, also considering abrasive media with different characteristics. It has to be pointed out that dry finishing requires higher cycle times comparing with conventional mass finishing strategy: the competitiveness of this innovative strategy lies in avoiding the problem of waste treatments that is very expensive and difficult in management.

Chapter 7.

CLEANLINESS OF HIGH PRECISION MECHANICAL COMPONENTS

7.1. Why cleaning mechanical components

In high precision mechanical manufacturing, especially for automotive, aerospace, microelectronics and biomechanical applications, cleanliness of the part is a crucial requirement to fulfill desired functionalities.

Cleaning of components means the removal of undesired contaminants to a wanted preset level. The preset level is normally defined as the minimum level at which no adverse effects take place in a subsequent operation.

The need for higher cleanliness levels derives from the rapid advancements in current technologies; in adding, the trend in miniaturizing of components dictates more strict requirements in cleanliness.

Contaminants – included also detachable burrs - can affect functionality of the part or of the assembly component. For example, in automotive systems, a foreign body can circulate in several parts composing the engine, such as pumps, injectors or transmissions, causing severe damages. In particular, in an injector design, mechanical clearance are in micro-scale (about 100 – 200 µm): a contaminant can clough up the movable element or obstruct the small exit hole. Moreover, contamination can drastically alter surface properties such as wettability, adhesion, optical or electrical characteristics.

Nowadays, design of automotive and aerospace engine requires increasingly high accuracy due to different aspects to be fulfilled:

- Requirements in extreme performances with an evolution of components design, often reducing part dimensions and/or selecting high performance materials: for example, injectors exit holes are dimensioned to reach higher fluid pressure;
- Demand for ever minor environmental pollution released by internal combustion engines.

As will be exposed in following sections, cleanliness requirements are identified by several methods, even if the most applied is the indication of the maximum acceptable contaminant dimension.

In the light of developments of design requirements for improving engine performance, cleanliness requirements became more stringent in the last decade. In particular, if cleanliness demand was simply the absence of chips and oil or grease in the begin of the XXI century, in the last period, cleanliness requirements deny the presence of contaminants greater than 400 µm; moreover, the current trend is to reduce the allowable contaminant dimension up to 200 µm max (Fig. 7.1).
Generally, further requirements complete the specification, such as the state of the surfaces of the workpiece: they have not to show haloing, pitting, or spot.

To satisfy the cleanliness requirements, several washing technologies are available. In this Chapter, wet methodologies to wash mechanical components will be presented and

techniques to evaluate cleanliness level will be exposed considering automotive field. Finally, a new technique for cleaning a specific engine element will be presented. All these sections are realized thanks to the courtesy of the Brovedani SpA company.
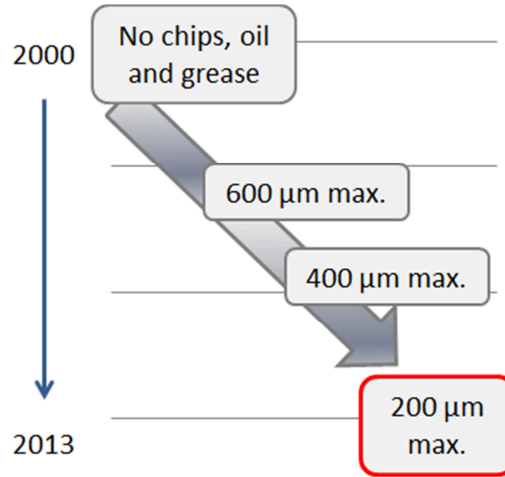
Fig. 7.1 Cleanliness requirements evolution concerning maximum acceptable contaminant dimension

7.2. Cleaning technologies

A classification for wet washing methods is based on the nature of the cleaning media, which is the active element on the bath in removing contaminants. Washing approaches can be:

- aqueous washing approach, which includes immersion and spraying washing technique;
- solvent–based washing approach, generally not applied for spraying techniques.

The selection of a cleaning media (aqueous or solvent-based) depends on the contaminants, that can be organic or inorganic. In other words, the choice depends on the water solubility of the contaminants. Organic contaminants in most of the cases are hydrophobic, like oil, grease, waxes, polymers coating, whereas most of inorganic contaminants are insoluble in solvents (metal or plastic chips, paste, calamine).

Aqueous media can be alkaline, neutral or acid, depending on the nature of contaminants. It is generally preferred in applications requiring cleaning of very large volumes of parts or fine-cleaning. Effectiveness of the media is based on an organic and inorganic builder and surfactants. The latter are able to insert themselves between surface and contaminants, dislodging non-polar contaminations (oil and grease), as well as polar contaminant (emulsion, particles, salts). Other function of builders is to provide a buffer of pH lending material without changing the desired pH of the bath. Surfactants are long chain of organic molecules with polar or non-polar sections in their chain; they can be ionic or non-ionic nature based on the type of functional group. If diluted in water, surfactants form aggregates called micelles at a level above their critical micelle concentration (CMC). Surfactants are able to emulsify an organic oil soil into the aqueous medium and/or to increase the degree of wettability of the surface, which permits the cleaner to penetrate and remove the soil. Wettability is the ability of a liquid to stay in contact with a surface. It is defined by the Young's equation (see Fig. 7.2) [118]:

$$\gamma_{sb} cos\vartheta = \gamma_{wb} - \gamma_{sw}$$

(7. 1)

146

where:

ϑ is the wetting angle;

γ_{sb} is the surface tension between bath and soil;

γ_{wb} is the surface tension between workpiece surface and soil;

γ_{sw} is the surface tension between soil and workpiece surface.

To increase wettability, the wetting angle shall decrease.
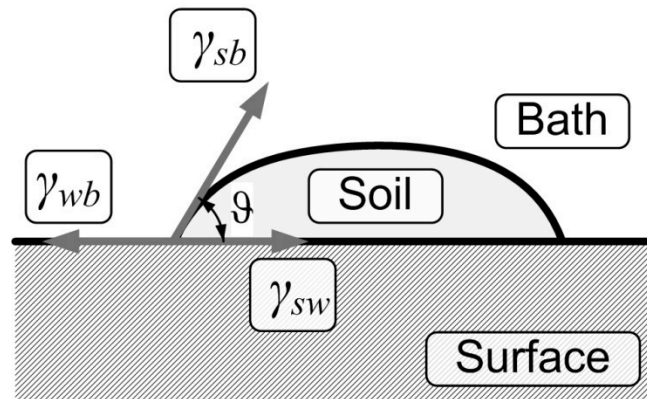
Fig. 7.2 Definition of wetting angle

Further elements commonly present in a aqueous-based bath are [119]:

- *Dispersants*: they avoid re-adhering to cleaned parts;

- *Corrosion inhibitors*: they avoid oxidation effect of the material that otherwise occurs due to the ionic nature of the bath;

- *Defoarmers*: they avoid the formation of foam which can cause cavitation on the recirculation pump as results of air presence in the line; moreover foam tends to cling to surface.

Solvent cleaning operates following the principle "like dissolves like". They are most effective in dissolving and removing organic material, like grease and oil and are used in concentration of 100%. Close attention needs to be given to emission and/or flammability concerns. For this reason, solvents are never used in a spraying cleaning technique. A common solvent-based technique is the vapor zone cleaning approach. It is founded on boiling or heating organic solvent vapor which migrates upward to the workpiece. Vapor is able to penetrate the tight spaces in parts surfaces, improving efficiency. This approach can be enhanced using ultrasonic or spray-under immersion systems.

7.2.1 Immersion and spray washing techniques

A further distinguish of washing wet technique, typically applied in automotive and aerospace fields, is basically based on the geometry of the workpiece [120]:

- *Immersion cleaning*: workpieces are immersed and, eventually, sprayed within cleaning liquid in a proper tank; it is generally suitable for various simple and complex workpiece shapes; the adhering contaminants are removed primarily through the chemical cleaning effects of the cleaning media employed [121];

- *Spray cleaning*: workpieces are in an air environment (for example in a tunnel) and they are washed by a spray flow of cleaning liquid through a nozzles with pressure starting

from 6-8 bar for conventional system; contaminants are partially removed or emulsified by the chemical effect of the media and partially sprayed off by the high kinetic energy of the jet; the method is not suitable for workpiece with deep holes, cavities, undercuts and so on.

Considering cleaning immersion approach, washing techniques can be classified according to the bath motion approach. Static solution, indeed, is rarely effective in cleanliness: the purpose is to create a continuous relative movement between workpiece and liquid in order to facilitate the soils removal. A typical bath motion may consist in the mechanical movement of the workpiece, for example in up&down motion of the pallet in which are located workpieces, or through the rotation of a barrel; moreover, a system based on jets within the bath which create liquid currents and turbulences can be employed, or a forced recirculation of the bath is applied. However, one of the most applied and investigated agitation technique in precision mechanical components is the ultrasonic approach.

In ultrasonic technique, the cleaning action occurs in water solutions due to different physical mechanisms [122]:

- Chemical reactions between the soluble impurities and the cleaning agents diluted in the water;

- Dissolution of impurities from surface into solution and the products of the chemical reactions between impurities and solution;

- Ultrasonic cavitation phenomenon which removes the insoluble impurities from the surface of the object to be cleaned.

Cavitation effect is the only physical phenomenon that enhances the removal of impurities: it consists of the creation in a liquid of very small vacuum bubbles, filled to a certain degree with vapor; bubbles under certain conditions implode. The implosion releases energy that dislodges impurities off the surface of the workpiece. The effectiveness of the cleaning action depends on the number of bubbles imploded and on the implosion force, which is subjected to the quantity of vapor and gas in each bubble. Implosion is more powerful if low vapor quantity is on the bubble. Frequency of ultrasonic energy represents the most crucial aspect: low frequencies provide more aggressive cleaning action and produce large cavitation bubble, so this type of configuration is not applied for precision cleaning. Frequencies between 72 and 100 kHz are the most employed.

Also the temperature of the bath affects the number of liquid bubble: it increases with temperature of the liquid, therefore cavitation should be more effective. On the other hand, if temperature increases, the liquid has a higher vapor pressure, so the gas content in the bubble becomes higher, reducing implosion force. For same reason, gas content in the fluid shall be removed by degassing procedure. Furthermore, implosion force depends on the level of the liquid in the bath: maximum power is reach if the height of liquid column is a multiple of the ultrasonic wavelength. Unfortunately, ultrasound wavelength varies with temperature.

A variant of the ultrasound technique is the megasonic cleaning system, which adopts frequency between 700 kHz and 1.2 MHz, generated by ceramic, piezoelectric crystal, which is excited by high frequency AC voltage. Megasonic cavitation occurs with smaller bubbles compared with ultrasonic, resulting in lower local energy released in implosion. This reduces the risk of damages of the surfaces.

Ultrasound washing machine can be mono-tank or multi-tank to perform more than one washing cycle in series, changing working parameters and/or bath components if necessary.

Fig. 7.3 Particular of multi-tank washing machine based on U.S. technique (Courtesy of Brovedani SpA)

Spraying system can be considered as a further technique for creation motion within the bath, both in immersion both in air environment. The most critical aspect is the proper design and location of the nozzles system because the washing machine shall fulfill three tasks:

- Flood the surface with detergent solution to remove oil-based soils (and render them water soluble, miscible or compatible): it requires a modest fluid throughput since all surface shall be covered; in this phase, impact pressure is irrelevant;

- Impact of the mix of water and detergent to soften soil material and to remove them from the surface: this function requires high pressure stream of fluid focused at the zones of parts where the level of soil is highest; it is not necessary to impact all component surfaces;

- Rinse the debris from the parts which will be subsequently dried and inspected: it requires the highest volume of fluid to displace debris and dilute dirty cleaning fluid retained over all part surface; pressure level is relevant only to provide the volume of fluid needed.

Generally, spraying system in air environment is installed in a tunnel washing machine, to have the movement through the machine of the parts thanks a belt conveyor.
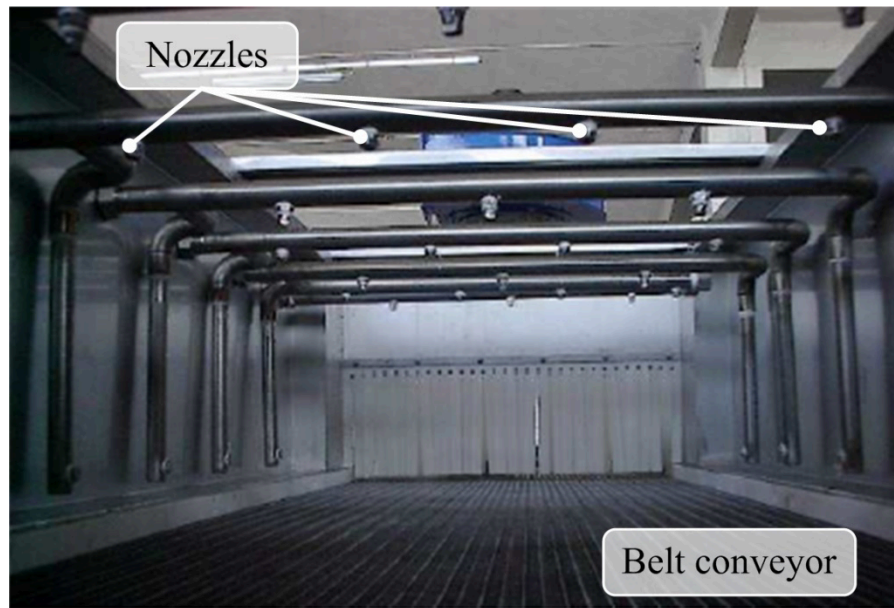
Fig. 7.4 Tunnel washing machine (Courtesy of Brovedany SpA)

Lastly, a further washing technique is the carbon dioxide cleaning: it can be applied in immersion or sprayed systems thanks to the fact that CO_2 can be used in three different states:

- in liquid form, where CO_2 performs surface cleaning and degreasing;
- in gas state, injecting as a "snow" from special nozzles;
- in a super critical state for extraction of liquid by chemical phenomenon.

Carbon dioxide cleaning method is commonly applied to remove organic soils, but is not suitable to rust, scale, and most inorganic compounds.

7.2.2 Washing technologies

From the technological point of view, washing system can be split in four categories:

- *Multi-tank washing machine* (see Fig. 7.3): It works following the immersion approach and it is suitable for a finishing washing; normally, its technological limit is related to a maximum measurable particle of size 300÷400 µm; the effectiveness of cleaning action is affected by shape and geometry of the workpiece, that in general are placed on pallets; it is technologically advanced and it permits a flexibility in configuration of working parameters: each tank can contain different detergent (type and concentration), different temperature of liquid and diverse bath motion strategy, such as ultrasound, mechanical movement of workpiece, injection flood; it has a medium productive and it is demanding in maintenance;

- *Tunnel washing machine* (see Fig. 7.4): It is generally applied for rough washing, for example intermediate cleaning action between cutting processes, since a minimum contact between bath liquid and the workpiece; its technological limit is evaluated in maximum particle size of 400÷600 µm; the effectiveness of washing action depends on the geometry and the shape of the workpiece: component position is fundamental aspect; the tunnel technology allows high productive and easy maintenance thanks the simple design;

- *Solvent washing machine*: it works generally in immersion for cleaning oxidable workpieces with complex shape; it is suitable for mass treatment, especially to remove cutting oil; the technological limit is close to 400 µm max of particle size; moreover, it is easy and economical for maintenance, guarantying a constant bath quality; it has to be pointed out the necessity in paying attention to the toxicity of solvent products;

- *Aqueous mono-chamber washing machine* (see Fig. 7.5): it is adopted generally for workpieces with medium-complex shape from which cutting oil shall be removed; principles of its washing action is very similar to whose of the multi-tank technology; in add, this washing machine offers protective action by corrosion inhibitor; it has a compact design; the technological limit is evaluated in particle size of 300÷500 µm max.

Fig. 7.5 Aqueous mono-chamber washing machine (Courtesy of Brovedani SpA)

7.2.3 Washing mechanical components: Literary review

In literature, few scientific research works focus on the cleanliness issue of mechanical components. Most of researches investigate on ultrasounds washing technique in immersion approach aiming at understanding its properties varying working parameters, in providing new sensors to monitor washing action or in analyzing the possible damages on the washed surface (Tab. 7.1).

Niemczewski [122] investigated on the influence of the height of the liquid column on the cavitation – temperature interaction. Author considered a medium size industrial ultrasonic cleaner with tap water, under typical industrial condition. He concluded that intensity of tap water cavitation was highest at temperature below 20°C but a single value of optimal temperature could not define because cavitation was affected by the amount of liquid in the

cleaning tank and by air content. Later, same author [123] studied the cavitation intensity depending on the concentration of chemical elements in an alkaline solution for ultrasound cleaning. He confirmed that cleaning substances concentration had a deleterious influence on the cavitation intensity. Author suggested a concentration of 8-10% of cleaning substances to reach higher cavitation intensity.

In a previous research, Maisonhaute et al. [124] analyzed the forces acting on an adsorbed particle located on a surface. Authors found that shear stress involved during the collapse of the bubbles was an important factor. Moreover, efficiency of the ultrasonic cleaning was strongly depended on the size of the adsorbed particle to be removed. Thiemann et al. [125] provided a systematic characterization and comprehension of different structures of bubbles, considering the acoustic cavitation from the applied sound field to the microscopic cavitation effects.

Jueschke et al. [126] provided a quantitative evaluation of cavitation intensity for ultrasonic cleaning vessel using different sensor techniques. Authors in their experimental tests, considered controlled environmental conditions in a wider range of parameters. By experimental results and observations, in subsequent work, same authors [127] presented a statistical method for describing a cavitation process.

Zeqiri et al. [128] studied a new sensor for monitoring spatial distribution of cavitation activity in megasonic vessel cleaning technique. The sensor was able to associate the megahertz acoustic emissions produced by the cavitating bubbles with specific regions of space within the vessel. Applying the new sensor, authors confirmed that spatial distribution was related to the cleaning ability of the system. Also Jenderka et al. [129] analysed the spatial distribution of cavitation activity by a new pressure sensor. Authors experimentally determined the spatial distribution of sound field parameters, such as: positive and negative peak pressure, amplitudes of fundamentals, harmonics and sub-harmonics as well as the energy density and the spectral density in several frequency ranges.

Further research works investigated on surface damages caused by ultrasonic action. Unfortunately, ultrasound cleaning may cause damages on the workpiece if it is not well calibrated. Just thinking to a porous material like aluminium alloy: the bubble penetrating in pores can cause an enlargement of them due to the cavitation effect. Moreover, if cavitation frequency is close to the resonance pulsation of the part, worse damages may occur, as analysed by James et al. [130], in medical application. Ultrasonic action may cause harmonic oscillation and fatigue damages in small structure: in few cases further cleanliness technologies should be adopted. Also Steblenko et al. [131] conducted a research dealing with ultrasounds damages. Authors analysed the effect of ultrasound cleaning action on the surface of Si-wafer: cavitation might produce damages on the component due to cleaning forces which action is not selective: they attack contaminants together with surface material.

Tab. 7.1   Ultrasound cleaning technique: Literary review

Ref.	Purpose	Washing process	Instruments / Sensors
[122]	Investigate on the influence of temperature, liquid level and gas content on the cavitation intensity	U.S. cleaning with tap water	Branson cavitation meter
[123]	Investigate on the effect of cleaning media concentration on the cavitation intensity	U.S. cleaning with tap water	Branson cavitation meter
[124]	Analyse the forces acting on an adsorbed particle located on a surface	U.S. cleaning with water and detergent	Atomic force microscope Nano scope
[125]	Analyse the bubble structure behaviour in a sound field	U.S cleaning with no-degassed water	Optical hydrophone probe (acoustic meas.) High speed camera
[126]	Provide different sensors for quantitative measurement in U.S. cleaning vessel:	U.S. cleaning vessel with deionised water	Current probe Temperature meas. O2 concentration meas. Cavitation indicator sensors
[128]	Provide a new sensor for evaluating the spatial distribution of cavitation activity	U.S. cleaning vessel	Power analyser Bacofoil release non-stick foil Hanna instrument (for T and %O2)
[129]	Provide a new sensor for evaluating the spatial distribution of cavitation activity	U.S. washing with deionized water	Temperature meas. Interferometer
[130]	Investigate on the U.S. damages in small medical devices	U.S. washing	SEM microscope
[131]	Investigate on the U.S. damages on Si-wafer surface	U.S. with distilled water	Spectrometer X-ray diffractometer

7.3.   Cleanliness strategy

In literature review, it is very difficult to get information about cleanliness strategy to be adopted for cleaning high precision mechanical components; few informations can be found from indications of washing machine manufacturers': however these informations are generally related to a specific components and/or to a specific cleanliness requirements.

Therefore, the purpose of this section is to provide general indications for a proper selection of washing technique basing on the geometry of the workpiece considering the nature of contaminants on it. This analysis was conducted with the fundamental collaboration of technicians at the Brovedani Group SpA company.

Fig. 7.6 Selection of proper cleanliness technology

7.3.1 Criteria for a proper selection of the cleanliness strategy

In order to fulfill cleanliness requirements, in selecting a proper washing strategy, several aspects shall be considered and analyzed:

- Workpiece dimensions, shape (presence of holes, undercuts, etc.), and material (for example common or stainless steel, aluminum alloy etc.);
- Type of contaminants on the workpiece surface;
- Surface quality requirement and cleanliness specification;
- Required productivity: considering the possibility to clean workpieces with different shape, material and contaminants using the same washing machine.

Contaminants are several in nature and they depend on the applied production process of the workpiece and on the environmental quality. They can be classified as:

1. Synthetic or organic cutting oil, emulsifiable or not, deriving from cutting operations (turning, milling, drilling, grinding): higher the viscosity of the oil, more difficult is the elimination of the greasy element;
2. Chips, which can be metallic or made of other cutting material, for example polymers (see Fig. 7.7);
3. Microchips due to grinding operation;
4. Abrasive pastes deriving from lapping or polishing operations (Fig. 7.8);
5. Abrasives used in finishing processes, like grinding, sanding or barrel finishing: they can nullify subsequent coating or can affect super-finishing process;

154

6. Water-based residual due to mass finishing (water-compound);
7. Calamine due to electro deburring actions;
8. Oxides due to thermal treatments (like quenching), laser cutting or electro-deburring;
9. Fibers.

Fig. 7.7 Rough or semi-finishing machining contaminants, which in general are cutting oil and metal or plastic chips: they can obstruct holes or can remain in cavities (Courtesy of Brovedani SpA)
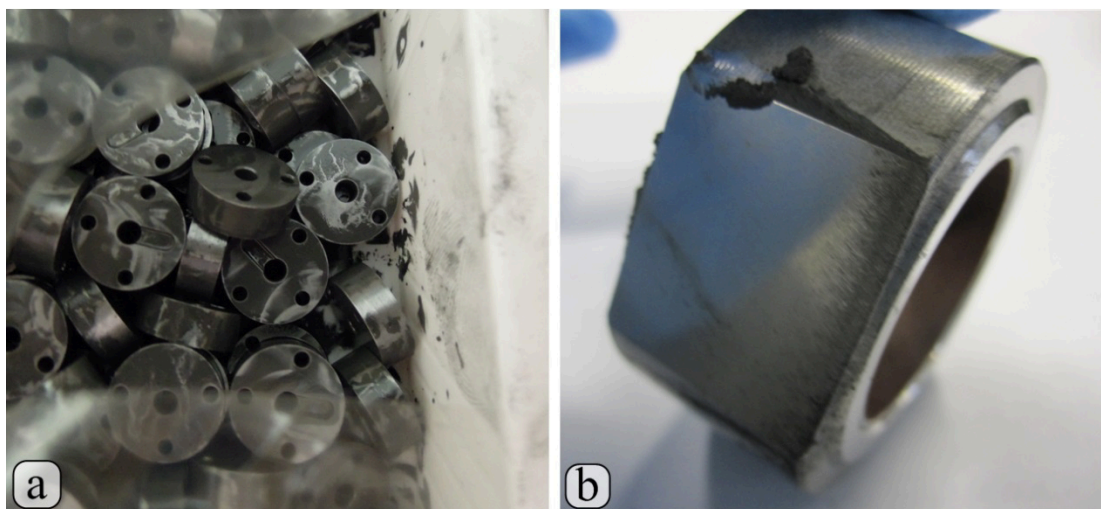
Fig. 7.8 Lapping (a) and polishing (b) contaminants (Courtesy of Brovedani SpA)

The combination of these information represents the one of the input factor for a proper process selection, that shall take into account different characteristics on the cleaning technology (Fig. 7.6), such as:

- Cleaning media, which selection depends on the workpiece material and observed contaminants;

- Bath motion technology, based on the shape and dimension of the workpiece and on the adopted cleaning media; in adding, cleanliness requirements play an important role in the selection of the bath motion technique;

- Machine type, that is related to the bath motion technology and the required productivity;

- Loading and unloading system of the washing machine, that depends on the machine type and on the workpiece characteristics: for example parts can be loaded in a roto-

155

barrel with jumble configuration if components are not subjected to dents; otherwise pieces can be placed on a conveyor or in pallets if avoiding damages is crucial;

- Drying technique, that is typically defined by washing machine technology and not selectable: drying stage is fundamental to avoid haloing and pitting on the surface, that are not generally admissible.

Once the selection of the washing strategy is carried out, other factors shall be taken into account. Firstly, working parameters shall be defined, such as characteristics of the detergent and its concentration within the bath, the necessity of corrosion inhibitors, especially in the case of Fe-based steel, the liquid temperature, the ultrasound power or the pressure value of spraying system and, finally, the cycle time. Working parameters can change during the washing process, so a proper monitoring system shall be adopted: for example a thermocouple to evaluate the temperature, a system for monitoring the pH of the bath, a meter to control the liquid level on the tank in case of immersion technique.

A method for a proper filtration of the bath shall be considered to avoid the saturation of the bath by contaminants and re-deposition of soils on the workpiece: effectiveness of the washing action is strictly related to the purity of the bath. For this reason, in some cases, a system for isolating oil and grease (skimmer system) can be implemented. This system is also useful to separate light contaminants, like polymeric soils, which float on the bath surface due to the low specific weight.

7.3.2 Proposed cleanliness strategy

In the following, hypothesis of cleanliness strategy will be proposed (Tab. 7.2). The analysis was conducted considering wet technologies commonly adopted in automotive application. The input parameters are the shape of the workpiece and the cutting processes carried out before of washing stage: they define probable contaminants on the surface of component. For simplicity, workpiece is considered made of stainless steel.

If workpiece has not a complex shape, i.e. without holes, undercuts or cavities, difficulties in cleaning are due only to the nature of contaminants deriving from the previous cutting process. However, sensitiveness of the workpiece to dents formation has to be considered: for example a part with sharp edges shall be handled with more attention than element with chamfered edges. In particular, components with sharp edges shall be loaded on the washing machine positioned on pallets, avoiding contacts between workpieces; chamfered parts can be loaded in random position, for example in roto-barrel for a mass treatment.

If workpiece is roughly machined or semi-finished (turning, milling or grinding processes) the most probable contaminants are metallic or polymeric chips and organic or synthetic cutting oil. Therefore, a proper washing strategy can use solvent or aqueous-bath cleaning media, with spraying or immersion system.

If component is machined by a mass finishing process, contaminating it with water compound and abrasive powders, the washing technique shall be based on aqueous solution, because solvents cannot remove the water based contaminant on the surface of the workpiece. It has to be pointed out that if workpiece has to be machined by a mass finishing process, also a pre-washing is needed: cutting oil and chips deriving from previous cutting process (for example turning or milling) may affect the abrasive action in finishing stage. Similar washing strategy shall be followed in the case of lapping or polishing action, where sludge of abrasive paste is present on the surface: it is suggested in removing it by aqueous-based approach in immersion technique, with U.S. action or other bath movement techniques.

Washing strategy selection becomes more complex if holes or cavities characterized workpiece shape.

In the case of through holes, the washing strategy is defined by the hole diameter. Specifically, if it is big enough, spray technique can be adopted; otherwise, if its dimension is not sufficient to be completely cleaned by a pressure flow of liquid, immersion technique shall be suggested. The selection of aqueous-based or solvent cleaning media depends on the nature of contaminants on the workpiece surfaces: if workpiece has been machined by mass finishing or lapping processes, aqueous solution shall be preferred in order to remove the water compounds or abrasive paste residues, whereas in the case of cutting oil, chips or microchips, the solvent solution may be adopted.

In the case of blind holes (or cross-sections holes), solvent-based cleaning media has to be selected if possible: solvent is a volatile element and it can be removed successfully during the drying stage from the bottom of the hole without particular actions. If solvent base system is not possible, immersion technique shall be adopted, selecting suitable bath movement (for example, workpiece rotation, ultrasound technique, spraying, if hole diameter is big enough, and so on) in order to reach all surfaces of the hole. In adding, if the blind hole is contaminated by sludge of abrasive paste due to a lapping process, a focused washing strategy shall be preferred: typically, workpieces are placed in a fixed position in order to facilitate the contact between liquid and internal surfaces; bath movement shall be energetic enough to remove contaminants, for example using spraying high pressure system or mechanical movement of workpiece.

In conclusion, considering a component made of stainless steel, which does not required particular expedients in washing, cleaning media will have to be selected basing on the contaminants nature, whereas the washing machine technology will have to be defined in order to intimate the contact between bath and workpiece surfaces (external or internal), choosing the proper bath motion (spraying, high pressure flooding of the bath, ultrasounds) and/or the correct mechanical movement of the workpieces (pallet in rotation or up&down movement). Finally, the strategy will have to consider the ability of the washing system in drying the component completely, without haloing or spots.

Tab. 7.2 Possible washing strategies adoptable in wet cleaning of automotive high precision mechanical components

			MANUFACTURING CYCLE and TYPICAL CONTAMINANTS			
			1. Rough machining 2. Final washing	1. Rough machining 2. Grinding process 3. Final washing	1. Rough machining 2. Pre-washing 3. Mass finishing 4. Final washing	1. Rough machining 2. Polishing or Lapping 3. Final washing
			• Cutting oil • Metal or plastic chips	• Cutting oil • Micro-scale chips	• Water compound • Abrasives powder	• Sludge • Abrasive paste
GEOMETRICAL CHARACTERISTICS OF AXIALSIMMETRIC WORKPIECE	No hole		Media: Aqueous solution, Solvent Bath motion: US, Spray, Rotation, Recirculation Technology: Tunnel, Multi-tank, Mono-chamber	Media: Aqueous solution or Solvent Bath motion: US, Spray, Injection flood, Recirculation Technology: Tunnel, Multi-tank, Mono-chamber	Media: Aqueous solution Bath motion: US, Spray, Mechanical movement Technology: Multi-tank	Media: Aqueous solution Bath motion: US, Spray, Mechanical movement Technology: Multi-tank
	Through hole		Media: Aqueous solution, Solvent Bath motion: US, Spray (if possible), Rotation, Recirculation Technology: Tunnel, Multi-tank, Mono-chamber	Media: Aqueous solution, Solvent Bath motion: US, Spray (if possible), Injection flood, Recirculation Technology: Multi-tank, Mono-chamber	Media: Aqueous solution Bath motion: US, Spray (if possible), Mechanical movement Technology: Multi-tank	Media: Aqueous solution Bath motion: US, Spray (if possible), Mechanical movement Technology: Multi-tank
	Blind hole		Media: Aqueous solution, Solvent Bath motion: Immersion, Spray high pressure (if possible), Rotation, Recirculation Technology: Multi-tank, Tunnel, Mono-chamber	Media: Aqueous solution, Solvent Bath motion: US, Spray (if possible), Injection Flooding, Mechanical movement Technology: Multi-tank, Mono-chamber	Media: Aqueous solution Bath motion: US, Spray (if possible), Mechanical movement Technology: Multi-tank	Alternative solution is recommended
	Cross-section hole		Media: Aqueous solution, Solvent Bath motion: Immersion with a relative movement between bath and workpiece, Spray (if possible) Technology: Multi-tank, Mono-chamber	Media: Aqueous solution, Solvent Bath motion: Immersion with a relative movement between bath and workpiece, Spray (if possible) Technology: Multi-tank, Mono-chamber	Media: Aqueous solution Bath motion: US, Spray (if possible), Mechanical movement Technology: Multi-tank	Media: Aqueous solution Bath motion: US, Spray (if possible), Mechanical movement Technology: Multi-tank

7.4. Cleanliness specifications and inspection techniques

Generally, customers of high precision mechanical components define cleanliness specification: it is based on the mechanical properties and required functionalities of the parts or of the assembly in which the part will be mounted.

Following specific standards, like International Standard ISO 16232 [132] for automotive components, cleanliness limits can be expressed as:

1. Maximum admissible dimension of the contaminants, as outlined above;

2. Maximum number of contaminant particles allowed, considering several dimensional of class of particles;

3. Maximum acceptable weight of particles, defined by the gravimetric analysis.

These limits are commonly distinguished basing on the nature of the contaminants, metallic or not-metallic. In general, for each class of particles, requirements are different: more stringent demands regard metallic elements, whereas for not-metallic particles, or fibers, major tolerance is typically given.

A further aspect that can be involved in cleanliness requirements is the magnetization level of the component: if the workpiece is not demagnetized, not only difficulties in assembly or disassembly can occur, but also during washing process, metallic particles can attach to the surface with failure of the cleaning action.

In order to define and characterize contamination level on a workpiece, several approaches are reported in the ISO standard 16232:2005 for automotive application [132].

Basically, the already washed workpiece is manually cleaned yet, following specific procedure, in order to verify the presence of residual contaminants. The most applied methods in automotive field are listed below. The number of the components under analysis shall be defined in order to collect a significant quantity of contaminants.

- *Pressure rinsing technique*: using micro-filtered clean fluid under pressure, all surfaces of the component are manually rinsed to remove residual contaminants; the pressure of the liquid shall be adjusted in order to obtain a jet with sufficient power to remove particle without damages of surfaces; extraction liquid and particles shall be carefully collected in a proper containers; finally, the collection equipment shall be carefully rinsed to collect the accumulate contaminants in a clean sample container;

- *Ultrasonic technique*: component is re-washed by ultrasonic technique with temperature and power of U.S. defined by cleanliness specification; once the ultrasonic actions are completed, component is rinsed following the pressure rinsing method; rinsed liquid together with the volume of liquid bath of U.S. action shall be carefully collect;

- *Test bench technique*: extraction of contaminants occurs by a functional test bench; the test fluid circulating within the system under pressure or under vacuum conditions;

- *Agitation technique*: component is partially filled by a known volume of extraction liquid; after, it is sealed and then agitated in all possible direction in order to extract contaminants; particles remain suspended on the test fluid, that will be analyzed;

- *Gravimetric analysis*: it is applied to define the mass of contaminants, which are separated from extraction liquid by a filtering action; after weighting contaminant mass, gravimetric concentration is given by the ratio between the weight and the relevant unit (i.e. wetted volume, wetted surface, number of components);

In order to analyze the collected extraction fluid by pressure rinsing, ultrasonic, agitation or test bench techniques, liquid has to be filtered by a vacuum system: it passes through a

membrane with pore size of 5 - 8µm for separating residual contaminants from the liquid. Cleanliness filter has to be analyzed in order to verify the presence of contaminants: this operation can be performed by an automatic scansion system able to detect the dimension and the nature of particles (see Fig. 7.9 for the case of pressure rinsing inspection technique). In Fig. 7.10 are shown possible contaminants observable by a filter analysis.
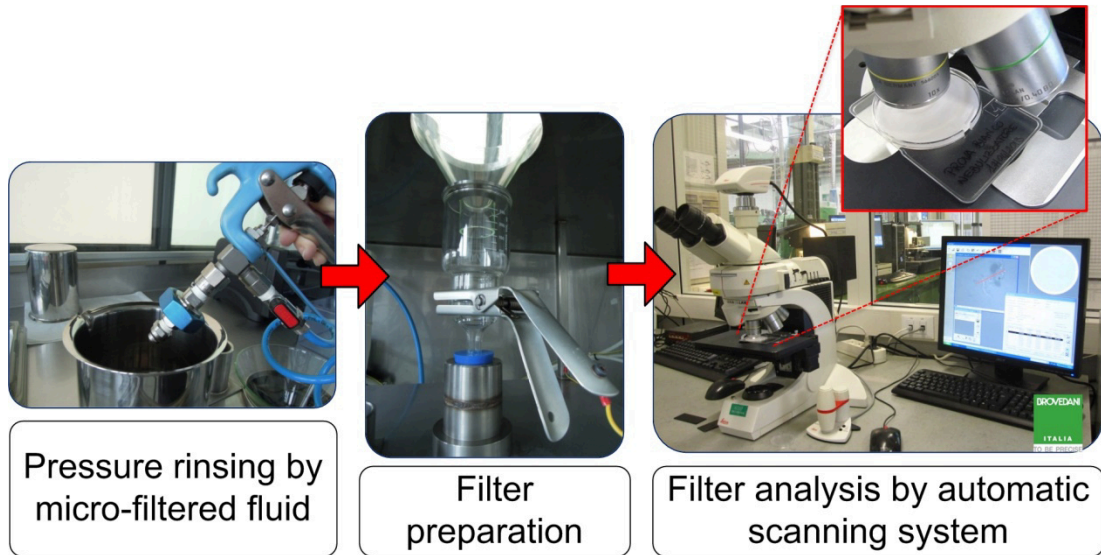
Fig. 7.9 Cleanliness inspection: Pressure rinsing method

It has to be pointed out that all inspection stages must be preceded by the blank tests: the overall equipment for cleaning tests is analyzed without workpiece in order to verify the cleanliness level. The procedure is typically defined by standards or customers instructions. Generally, blank test is carried on by pressure rinsing, where all tanks, handling systems and the vacuum apparatus are cleaned by filtered liquid. The liquid passes through the membrane filter to separate contaminants and the filter is analyzed by the scanning system. Contaminants shall not exceed the 10% of expected contaminants in workpiece cleaning tests, or shall be lower than a specified number of observable particles. This result assures that following cleaning tests will be not affected by soils already present on the cleaning test apparatus.

The effectiveness of the mentioned inspection techniques depends on several factors, that are controlled or defined by procedures specific for each products. For example, considering the pressure rinsing method, liquid pressure, flow rate, distance between nozzle and workpiece and dimensional characteristics of the nozzle shall be considered; in case of U.S. approach also ultrasound power, temperature of bath and cycle time shall be defined.
Moreover, liquid used in inspection tests shall be compatible with the workpiece material, with the liquid that will be adopted in final application of the part and with test equipment. Generally, it is recommended a fluid with low viscosity and with the capability to remove or degrease oil and grease.

160
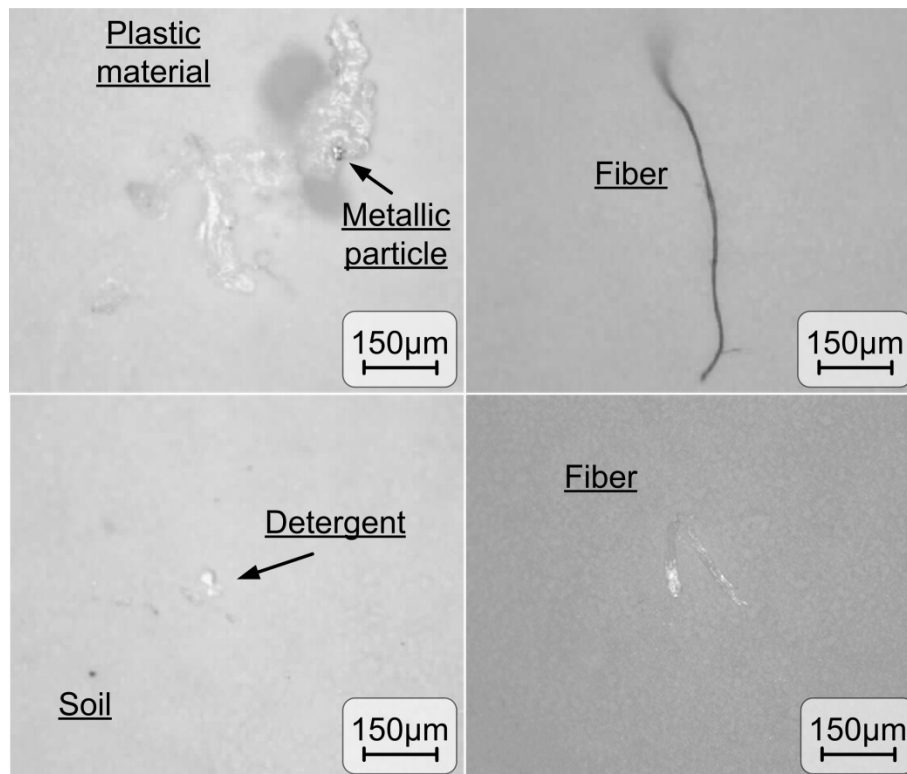
Fig. 7.10 Images from scanning microscope for cleanliness inspection

7.5. Cleanliness mechanical parts by FBM technique

In this section, an innovative wet washing system will be presented. It is based on the fluidized bed principle and it was implemented in a prototype washing machine designed by University of Tor Vergata basing on specific requirements of the company Brovedani SpA.

7.5.1 The Fluidized Bed Technology

The principle of Fluidized Bed Machining was developed by Barletta et al. at University of Tor Vergata, basing on the principle of turbo-abrasive machine presented by Massarsky and Davidson in the '80s and '90s [113] [133]. It is centered on finishing or super-finishing of mechanical components by fluidization (i.e. suspension) of abrasive powders in a special working chamber. Therefore the technology can be considered as a dry or wet washing process based on mechanical actions given by abrasives motion.

A typical apparatus is composed principally in four sections (Fig. 7.11):

1. An air blower which supplies a fluid flow to the bed in order to create the fluidization of abrasives; typically, the blower supplies air flow at low or moderate pressure since small abrasives (0.2 – 2 mm) shall be suspended;

2. A bed column, in which homogenization of the incoming flow occurs in order to generate smooth fluidization regimes of the abrasives in the main chamber;

3. A porous plate located at the bottom of the bed column that allows the homogenization of the fluid;

4. A recirculation system which allows the recovery of abrasives entertained in the fluid flow at the highest fluidization speeds; it permits also the collection of most of the fines produced during process.

161
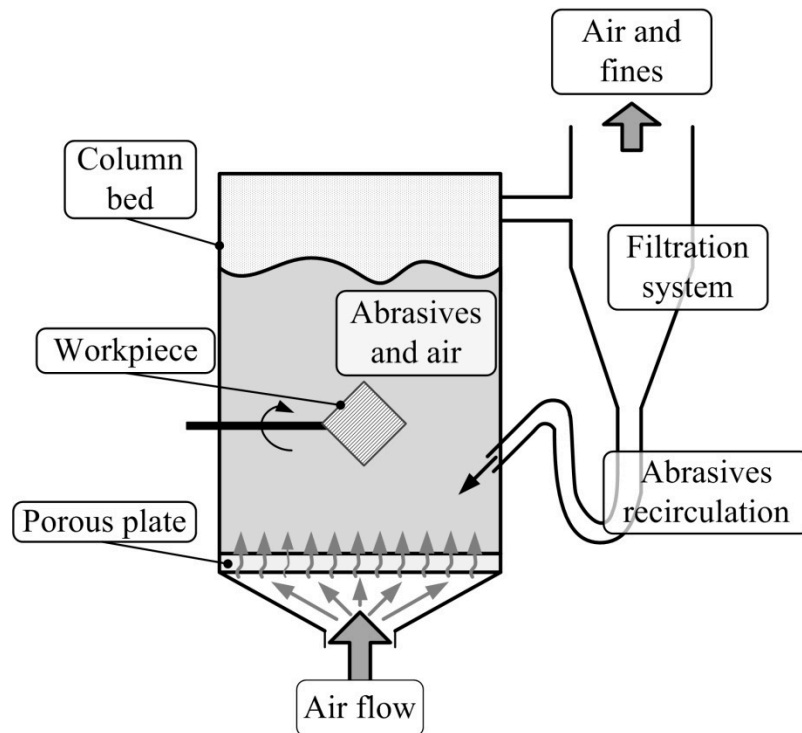
Fig. 7.11 Schematization of the apparatus for fluidized bed machining [116]

The effectiveness of the machining process is defined by different factors: the relative impact speed, the number and the angle of impacts of fluidized abrasives on the workpiece surface. The flow rate plays a fundamental role because it dictates the fluidization regime within the bed. Fluidization regime defines, in turn, the capacity of material removal or contaminant displacement from a machined surface.

The workpiece is subjected to repeated impacts thanks to the motion of suspended abrasives. Abrasive motion is characterized by moderate pressure and variable speed: increasing the flow rate changes the fluidization regime. Especially, when the flow rate is too low to counterbalance the weight of the abrasives bed, the particles are motionless (Fig. 7.12 – a). There exists an air flow rate able to generate a hydrodynamic push which counterbalances the abrasives weight: under these conditions, the fluidized bed is said to be in minimum fluidization regime and the abrasives move like an isotropic emulsion (Fig. 7.12 – b). This regime is very unstable: it can evolve to a bubble bed (Fig. 7.12 – c), by a slow increasing of flow rate, or it can re-convert in a fixed bed. The bubbling regime is the first one suitable for projecting abrasives on a surface: the impact speed is typically very low (less than 1 m/s). Due to axial segregation along the vertical direction of the fluidization column, the workpiece is preferentially machined in the main direction of the fluid flow: for this, workpiece rotation or motion is preferred to create an uniform performance of the washing process. Increasing flow rate, the dimension and shape of bubbles change. Firstly bubbles tend to increase their dimension as large as the characteristic dimension of the fluidization column (slug regime, Fig. 7.12 - d); turbulent regime (Fig. 7.12 – e) occurs with a further increasing of the flow rate: bubbles stretch along the main flow direction and the impact between abrasives and workpiece surface is more violent. The pneumatic regime (Fig. 7.12 – f) is characterized by the disappearance of bubbles and an uniform emulsion is formed.
It shall be pointed out that increasing flow rate does not change the operating pressure once the abrasive bed is suspended.
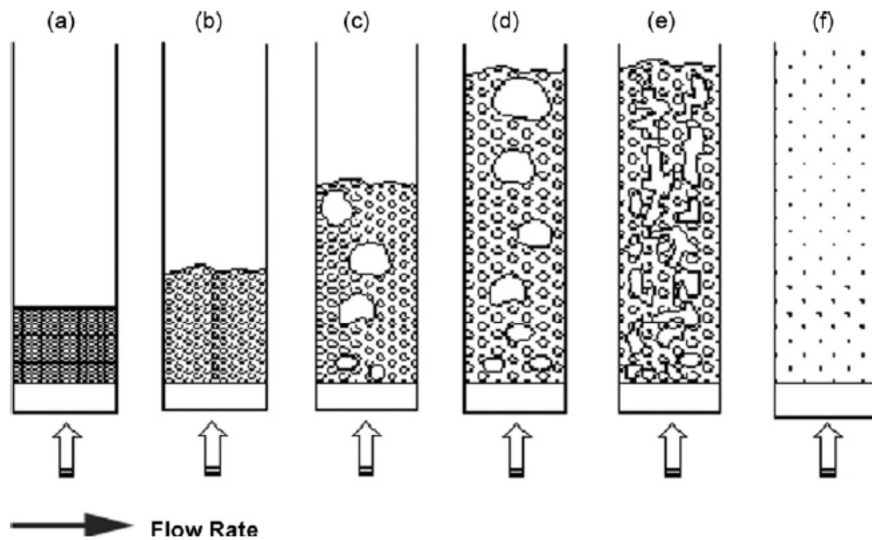
Fig. 7.12   Fluidized bed regime schematization [116]

In literature, several scientific research works were presented by Barletta et al. applying the Fluidized Bed Machining technology with different purposes, as listed in Tab. 7.3. Unfortunately, in their scientific researches, authors tested the Fluidized Bed Technology only by applying finishing or washing in dry condition.

This methodology was never carried out in wet condition to perform a washing process of a component, aiming at removing chips and inorganic contaminants; eliminating the greased components on the surface is very difficult by dry strategy; moreover, typically, the application of detergents or solvent is needed.

For this, the University of Tor Vergata designed a wet washing machine basing on the experiences of the fluidized bed theory: the purpose was to overcome the challenge in applying fluidization technique to a liquid bath. The washing prototype machine, was designed thinking to specific issues of workpieces machined at the company Brovedani SpA where the prototype was placed.

In the following, the washing machine will be presented and an experimental research in its cleanliness effectiveness of a specific workpiece will be carried out.

Tab. 7.3   Fluidized bed machining: Literary review

Ref	Purpose	Technology / Abrasives	Workpiece	Controlled parameters
[114]	Analyze influence of abrasive types and process parameters on finishing of complex shape workpiece	Fluidized bed machining / SiO2, Al2O3	AA 2024 O AA 20204 T3	Roughness Material removal Surface topography
[134]	Finishing internal surface of narrow and long workpiece by an innovative machine	Fluidized bed assisted abrasive jet machining / Al2O3	SS 316L	Roughness Waviness Surface morphology
[115]	Finishing tubular workpiece by fluidized bed assisted abrasive jet machining	Fluidized bed assisted abrasive jet machining / Al2O3	AA 6082 T6	Material removal Roughness Surface morphology
[116]	Analyze influence of working parameters on finishing and superfinishing by Fluidized bed machining	Fluidized bed machining / Al2O3	Brass Aluminum WC-Co coating	Surface morphology Roughness Material removal Oil removal
[117]	High speed finishing by fluidized bed machining	Recirculating fluidized bed machining / Al2O3, hazel nut	CuZn15	Surface morphology Roughness Surface integrity

7.5.2 Washing machine prototype

The washing machine prototype (Fig. 7.13) was adopted to clean a specific mechanical components at the Brovedani SpA company.

In order to understand the potentiality in cleaning of the innovative system, the investigation was based on experimental observations of the bath behaviour and on evaluation of the cleanliness quality of the workpiece. Unfortunately, in the period of experimental tests and analysis and during the writing of this thesis, no data or information about this new approach were available from literature.

Following the Fluidized Bed Machining theory see Fig. 7.13, an air flow is generated by an air blower characterized by power of 4.5 kW, a maximum flow rate up to 500 m^3/h and a flow pressure up to 600 mmH$_2$O. Suction conditions are at room temperature (21°C) and with ambient pressure (1atm).

The air flow passes through a porous plate made of PTFE, with pores dimensions of 0.2 μm: homogenization of the gas occurs in the fluidized bed column, which is filled by liquid bath (detergent and deionized water) and, eventually, not abrasive media. Media can be adopted in order to create a mechanical action for contaminants removal thanks the impact between grains and the surface of workpiece. Liquid is extracted from a tank with overall capacity of 25 l, by a suction pump (1.8 kW). Temperature of the bath is defined by PLC and monitored by a thermocouple.

Workpieces are fixed on shafts within the fluidized bed column: during washing, they rotate as a satellite.

During machining, a slight recirculation of liquid bath from the operating column to the tank takes place following the communicating vessel principles; reintegration of the bath occurs by the suction pump, passing through a filter element.
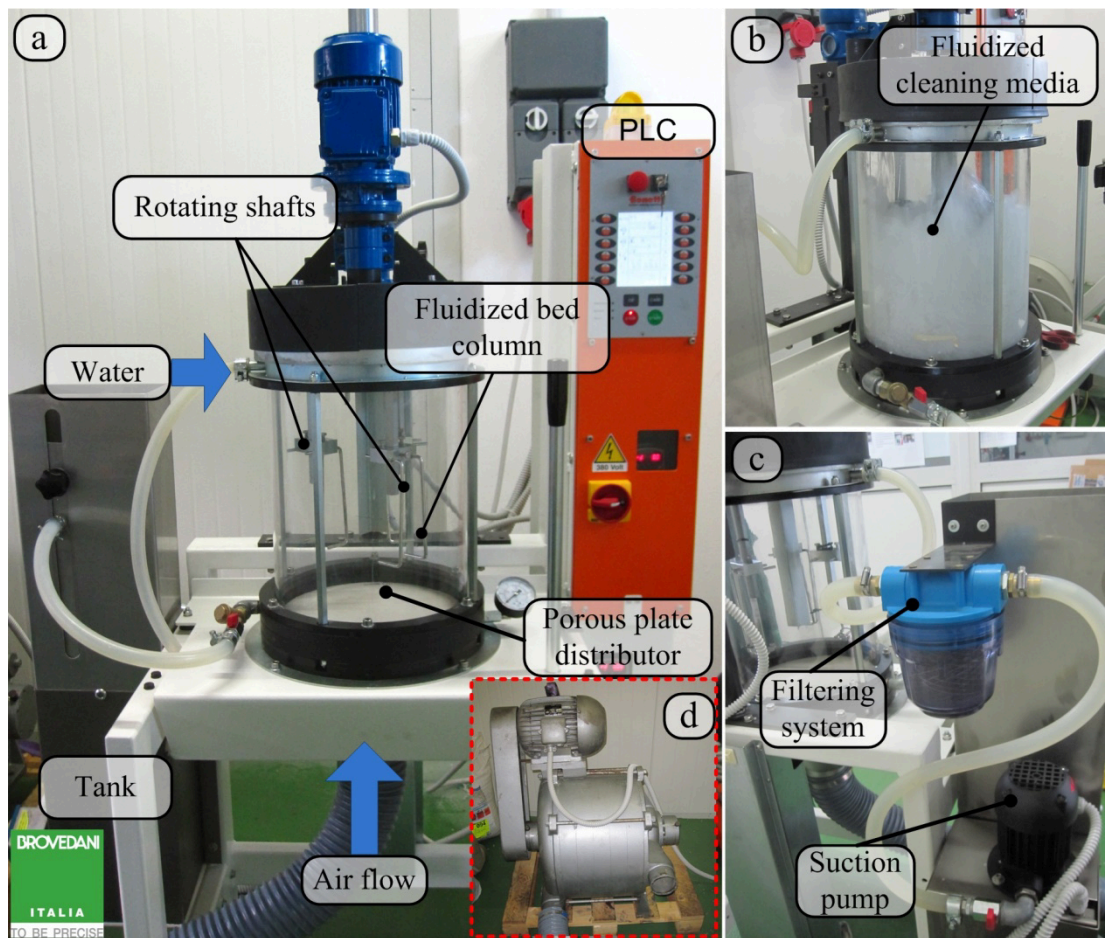
Fig. 7.13 Prototype Fluidized Bed Machining for washing mechanical components: (a) overview of the apparatus, (b) fluidized cleaning media within the bed column, (c) back side of the washing machine with suction pump and filtering system of liquid bath, (d) air blower for supplying gas flow (courtesy of University of Tor Vergata and of Brovedani SpA)

In Fig. 7.14, the development of the fluidization of the liquid bath is shown. The bed column is filled with a fixed level of deionized water (about 4 liters in volume) without air flow (a). When air flow (ω_{blo} = 2100 rpm, Q = 170 m^3/h) starts entering in the column through the porous septum, fluidization takes place and the bath tends to blow up (b – c) until reaching a steady state: the level of the bath is more or less constant, probably due to the fact that the number of imploded bubbles is compensated by the generation of new bubbles by the air flow.

At this point, in order to analyze the regimes which characterized the fluidized bed column composed by deionized water, different flow rate Q, between 116 m^3/h and 265 m^3/h, (ω_{blo} = 1800 ÷ 2600 rpm) were applied (Fig. 7.15). Observing the liquid bath motions it emerges that applying low flow rate (under 150 m^3/h) liquid level is higher rather than the cases of high Q: it can be explain from the fact that bath motion is less energetic and the generated air bubbles are more populous than the imploded ones.

However, if detergent is added to the deionized water, the formation of foam changes the bath behavior (see Fig. 7.16, where bath was deionized water, detergent and solid not-abrasive media). At low air flow rate, foam formation is favored, probably due to low energetic bath motion which cannot destroy bubbles; however, increasing Q, foam brings. Nevertheless, considering constant liquid level in the working chamber and applying higher

flow rate (over $Q = 270$ m^3/h), the bath motion becomes more energetic: from previous observations, it is expected that bath level decreases, but the fluidized bed expands. This phenomenon can be explained by the fact that the number of new generated bubbles overcomes the imploded ones.

Therefore, low flow rates Q (less than 150 m^3/h) cannot be suitable for fluidization due to the foam formation. Foam must be avoid because it can cause difficulties in controlling washing process, it can re-contaminate workpiece, hold back contaminants and can generate problems in the filtration system.

On the contrary, higher values of ω_{blo} may create bath motion regimes difficult in controlling due to the bed column expansion.

Following these observations, the suitable air flow range applicable in washing tests was defined in $\omega_{blo} = 2000 \div 2600$ rpm, with the purpose of understanding its influence on cleaning effectiveness.
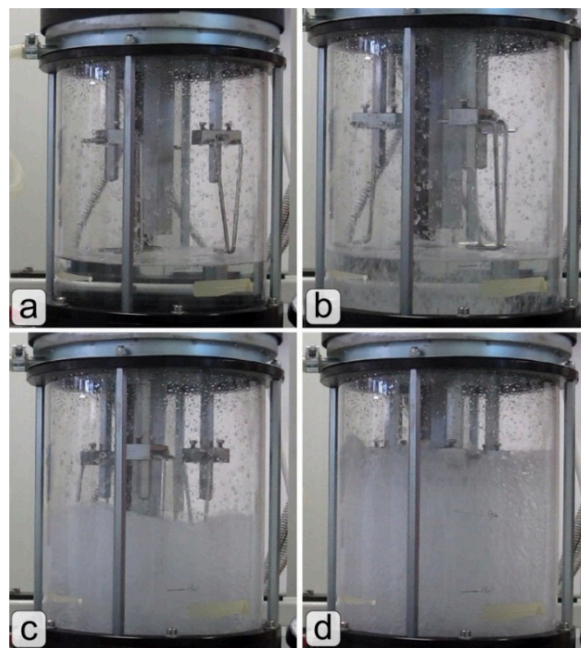
Fig. 7.14 Fluidization evolution in FBM machine: (a) air flow off, (b) starting fluidization, (c) increasing bath level, (d) steady state of fluidization ($\omega_{blo} = 2100$ rpm, $Q = 170$ m^3/h)
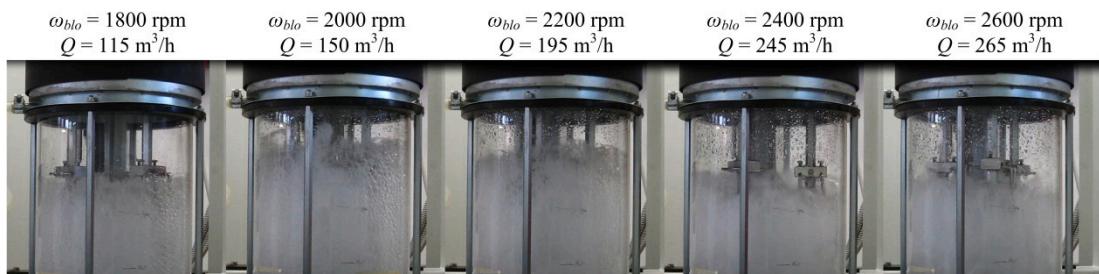
Fig. 7.15 Observable fluid regimes varying air flow rate (only deionized water)

ω_{blo} = 2000 rpm $\quad$ ω_{blo} = 2200 rpm $\quad$ ω_{blo} = 2400 rpm $\quad$ ω_{blo} = 2600 rpm
Q = 145 m³/h $\qquad$ Q = 175 m³/h $\qquad$ Q = 215 m³/h $\qquad$ Q = 255 m³/h
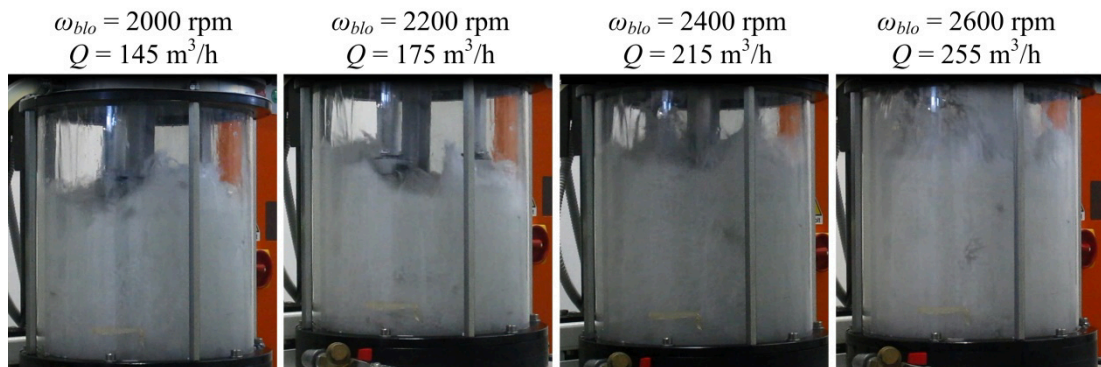
Fig. 7.16   Bath regimes with detergent and deionized water

7.5.3 Case study and experimental set-up

The workpiece to be cleaned by the FBM washing machine is a component of the common rail pump for diesel engine machined at the Brovedani SpA company (Fig. 7.17). It is a ring with two external plane faces; its characteristic dimensions are the external diameter of 47mm and height of 25 mm; plane faces are 20 mm length. The component is made of tempered bearing: therefore it is vulnerable to pitting on the machined surfaces.
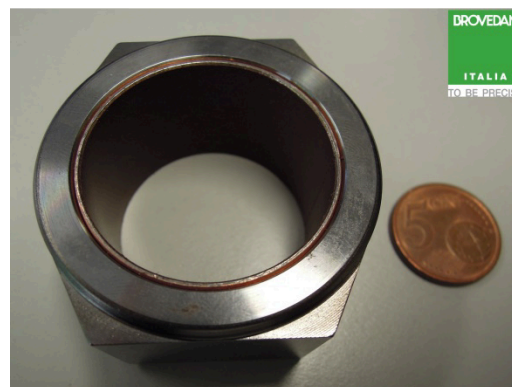
Fig. 7.17   Workpiece under cleaning analysis by FBM system

After an hard turning process, it is polished on the flat faces in order to obtain a flatness minor than 0.5 µm. Polishing process is performed using abrasive paste that is composed by organic grease and oxide of aluminum. The paste is very difficult to remove by conventional washing approaches, like spraying or U.S. techniques, due to the greasy component.

Currently, the workpiece is washed at Brovedani SpA, by an ultrasound technique in a multi-tank washing machine (see Tab. 7.4): washing cycle comprises three stages of ultrasound actions with different ultrasound powers, different detergent typologies and bath concentrations. A rinsing stage separates the three washing tanks. Further steps are two stages of rinsing in immersion with mechanical up&down motion and a final air drying phase. The component is subjected to corrosion, so inhibitor is added within baths in all tanks.
In spite of this complex washing strategy, workpiece is not always perfectly cleaned since difficulties in bath re-generation. For this reason, the washing machine prototype was tested to verify if the new washing strategy can be a valid alternative to the U.S. approach.

In order to evaluate effectiveness of the washing action, in comparison with the current washing strategy, the cycle time of the active removal stage was considered constant and equal to 15 minutes. Since the prototype was designed only for the active removal stage of contaminants, the rinsing and drying phases were carried out in the pluritank washing machine followed current strategies.

Tab. 7.4   Adopted washing cycle at Brovedani SpA

Washing cycle phase	Parameters	Values
Tank 1: Washing	Ultrasound, three transducers	1 – 10 W/l 2 – 18 W/l 3 – 11.5 W/l
	Temperature	70 ° C
	Cycle time	7 min
Tank 2: Washing	Ultrasound, three transducers	1 – 17 W/l 2 – 18 W/l 3 – 19 W/l
	Temperature	65°C
	Cycle time	5 min
Tank 3: Rinsing	Temperature	30°C
	Cycle time	50 sec
Tank 4: Washing	Ultrasound, two transducers	1 – 20W/l 2 – 16 W/l
	Temperature	60°C
	Cycle time	4 min
Tank 5: Rinsing	Temperature	30°C
	Cycle time	40 sec
Tank 6: Rinsing	Ultrasound	12 W/l
	Temperature	35°C
	Cycle time	35 sec
Tank 7: Rinsing	Temperature	35°C
	Cycle time	35 sec
Tank 8: Air drying	Temperature	125°C
	Cycle time	5 min

Typical contamination status of workpiece is shown in Fig. 7.18: generally, one of the two plane surfaces is more dirty than the other due to the adopted polishing technology.
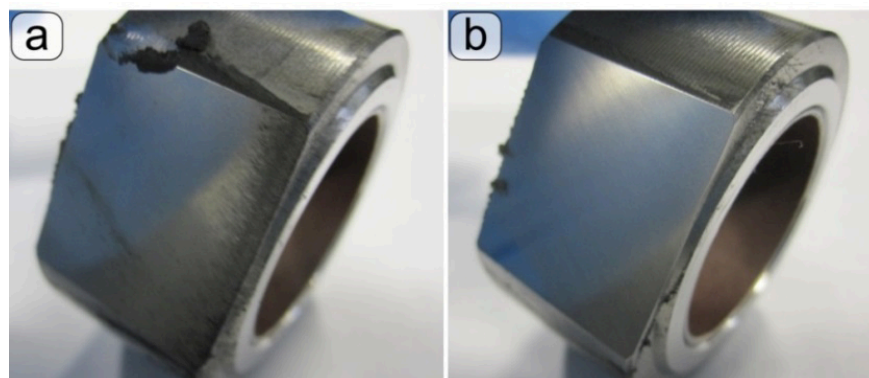
Fig. 7.18   Polishing paste on the two flat faces of the workpiece: a surface will be more dirty (Side A – Picture a) than the other surface (Side B – Picture b) due to the polishing system
(Courtesy of Brovedani SpA)

In order to wash the workpiece under analysis, the washing bath of the Fluidized Bed Washing Machine was composed by deionized water (conductibility < 1 µS/cm) and neutral detergent at 4% of concentration. The detergent, which contains an inhibitor product to avoid corrosion onset, was the Henkel P3 Neutracare 3300: it is suitable for spray and high pressure cleaning techniques. It does not represent the first option for abrasive paste removal by conventional immersion washing technique, due to its chemical composition, but its selection was imposed by the needs to avoid foam that might be create by air flow.

A specific Design of Experiment (Tab. 7.5) was applied in order to understand suitable working parameters and effectiveness of the washing technique.

Tab. 7.5 DOE for washing by Fluidized Bed Machining

Parameter	Level	Value
Batch [pcs]	1	1
Detergent	1	P3 Neutracare 3300 (4%)
Solid media	1	Polymeric spheres (d=3mm)
Bath temperature	1	60°C
Blower rotation speed ω_{blo} [rpm]	4	2000 ÷ 2600
Shaft rotation speed ω_{sha} [rpm]	3	20 ÷ 40
Cycle time [min]	1	15

By adopting the selecting range of rotation speed of air blower, the air flow rate Q was comprised between 145 m^3/h and 255 m^3/h.

Contaminated workpieces were fixed at the rotating shafts of the machine with the two contaminated surfaces in vertical direction, in order to facilitate the cleaning action. The bed column was filled with about four liters of liquid (detergent and de-ionized water) and a similar volume of solid plastic elements was added in order to increase the mechanical removal actions of contaminants by their motion within the liquid bath, see Fig. 7.19. In same figure is also shown the desired cleaning quality output, derived from the cleanliness level obtained by the ultrasonic washing strategy adopted at Brovedani SpA.
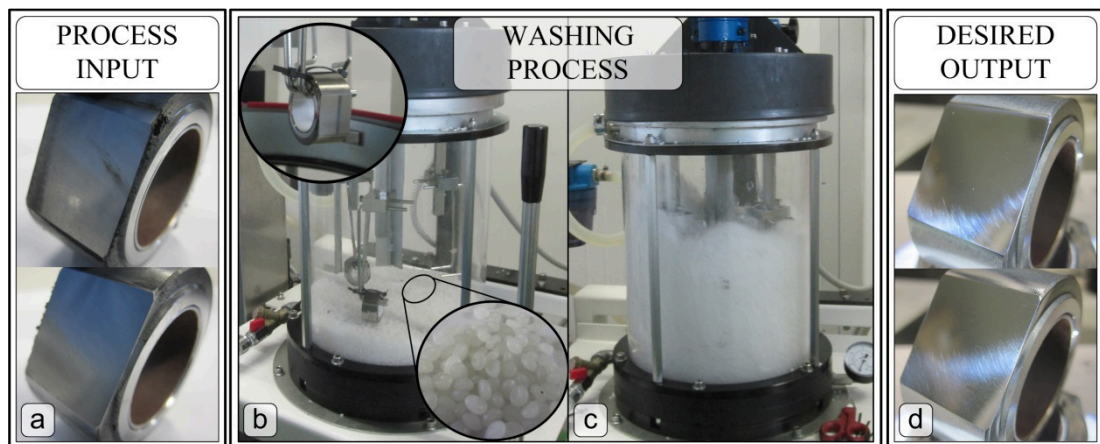
Fig. 7.19 Washing by FBM technology: Initial status of workpiece (a), machine set-up (b), cleaning action (c), desired quality output (d)

Cleanliness quality is finally evaluated by visual inspection, following the actual inspection procedure followed at the company. Surfaces are analyzed under a microscopic cold light source Leica CLS 150LED able to highlight eventual not-removed haloing due to greasy

component of the abrasive paste. Haloing must be avoided following the customer cleanliness specification.

7.5.4 Experimental results

In order to evaluate effectiveness of the washing process, qualitative cleaning level were defined from experimental results, see Fig. 7.20:

- *Class 1*: Workpiece extremely dirty
- *Class 2*: Workpiece very dirty
- *Class 3*: Workpiece dirty
- *Class 4*: Workpiece slightly dirty
- *Class 5*: Workpiece perfectly clean, desired output

It shall be pointed out that quality of cleaning comprises between *Class 1* and *Class 4* are not admissible; only cleaning level of *Class 5* reaches the cleanliness specifications of the workpiece.
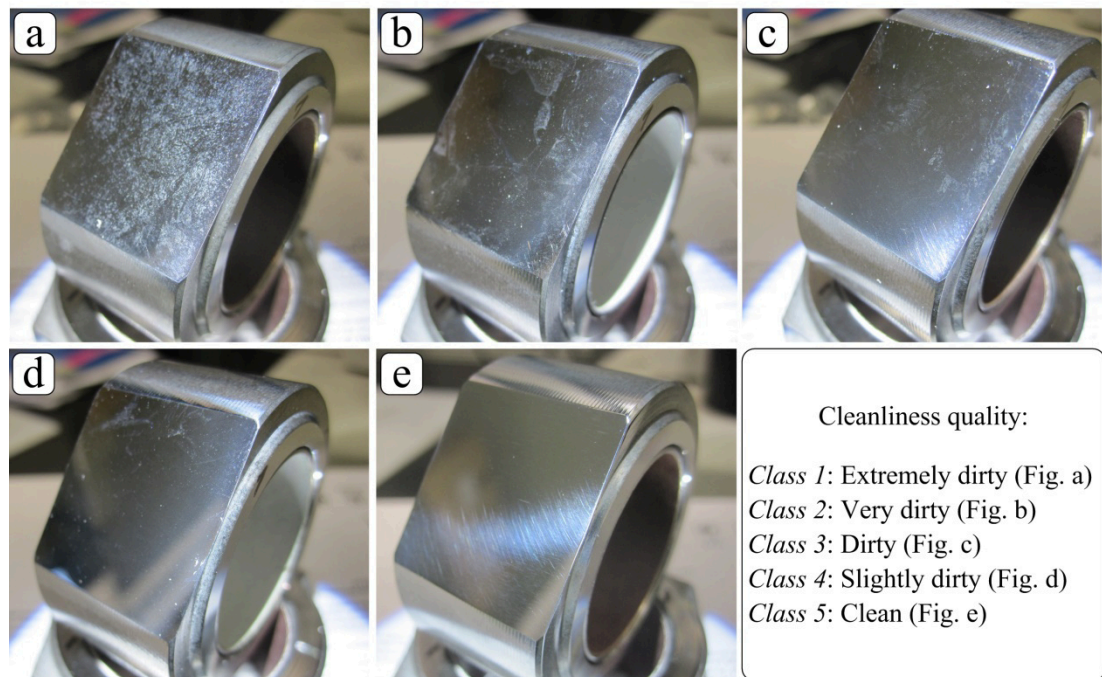
Fig. 7.20   Qualitative cleanliness evaluation adopted in data analysis

After washing tests, following the DOE, each cleaned workpiece were observed and the qualitative cleanliness class was assigned as the consequence of the cleanliness effectiveness of the prototype machine: results are shown in a scatter diagram in Fig. 7.21.
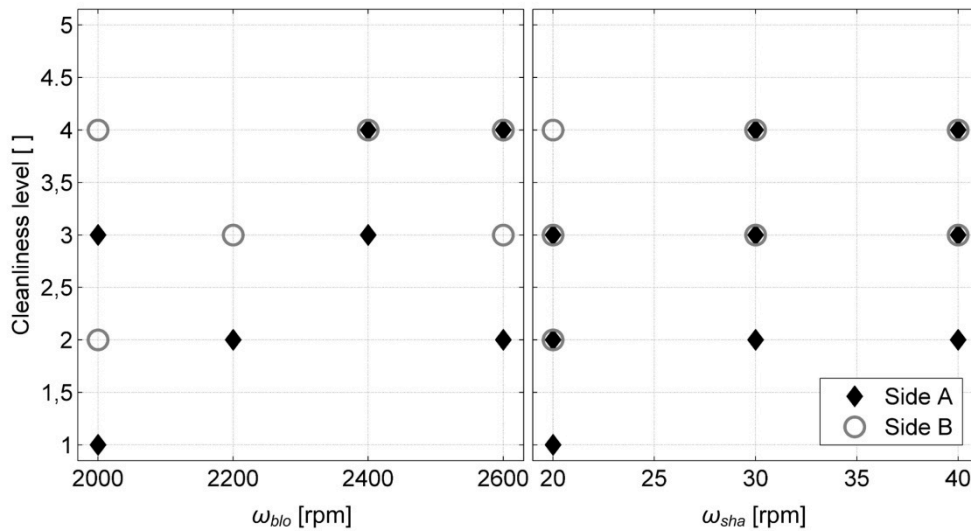
Fig. 7.21   Scatter diagram of washing tests results

From the scatter diagram analysis, it shall be highlighted that no perfectly cleaned workpiece (quality level of *Class 5*) were observed after the experimental washing process. Moreover, no definite trend can be found. However, it shall be supposed that increasing the air flow rate and the rotation speed of shafts, a more effective washing action could be performed. It has to be pointed out that the cleaning quality was affected by the initial contamination level of the surfaces: the process was more effective if the surface was less dirty (Side B).

Performing the analysis of variance (Tab. 7.6), it emerges that all process factors are significant: air flow rate and rotation speed of shafts have a strong influence on the results. Moreover, initial status of contaminated surfaces cannot be neglected.

Tab. 7.6   Analysis of variance

Factor	Sum of square	dof	Mean square	F statistic	p-value
Air flow rate	6.6667	3	2.22222	8.1	0.0014
Rotation speed of shafts	5.3333	2	2.66667	9.71	0.0015
Initial contamination level	2.6667	1	2.66667	9.71	0.0063
Error	4.6667	17	0.27451		
Total	19.3333	23			

Therefore, from the analysis of the experimental results, the effectiveness of washing process can increase selecting medium flow rate (ω_{blo} = 2400 rpm) and medium/high rotation speed of shafts (ω_{sha} = 30 – 40 rpm). Considering as an important aspect the energy consumption, it can be concluded that the combination of ω_{blo} = 2400 rpm and ω_{sha} = 30 rpm shall be selected as one of the best washing performance, even if the quality was not identical to the desired one. However, this combination of parameters can be promising because it is comparable with cleanliness quality observed after the first ultrasound washing stage of the washing cycle currently adopted on the company: the comparison is shown in Fig. 7.22.
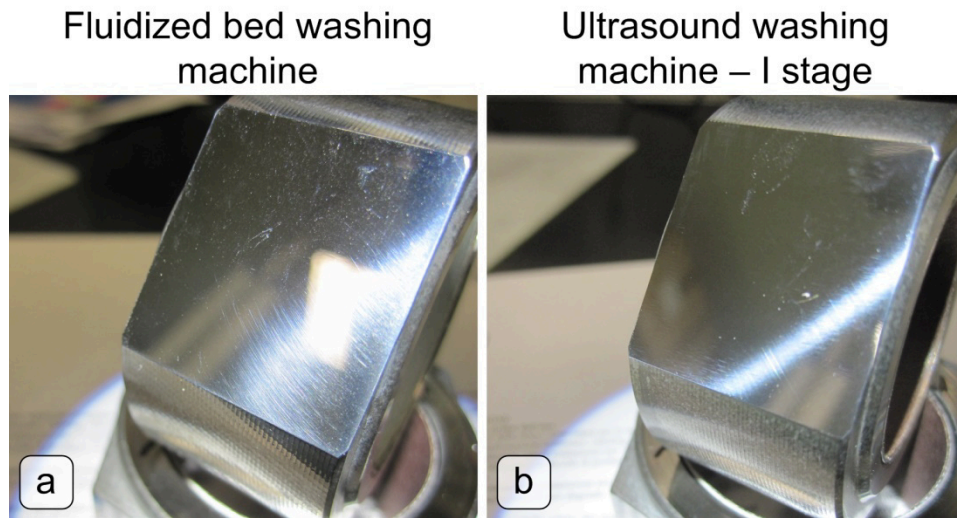
Fig. 7.22 Comparison of cleanliness result of washing machine prototype (a) and after the first stage (Tank 1) of the ultrasound washing action

7.5.5 Improving the potentiality of the washing prototype: Further experimental tests

Once defined a proper combination of working parameters, further experiment tests were carried out aiming at understanding the potentiality of the prototype washing machine. Firstly, the effect of solid plastic element added within the bath on the mechanical removal action was investigated, following the DOE in Tab. 7.7.

Tab. 7.7 Influence of solid media on the effectiveness of washing action

Parameter	Level	Value
Batch [pcs]	1	1
Detergent	1	P3 Neutracare 3300 (4%)
Solid media	2	Polymeric spheres (d=3mm) None
Bath temperature	1	60°C
Blower rotation speed ω_{blo} [rpm]	1	2400
Shaft rotation speed ω_{sha} [rpm]	1	30
Cycle time [min]	1	15

Result of the tests, is shown in Fig. 7.23, where it is evident that the solid elements motion within the bath was fundamental to obtain contaminants removal.
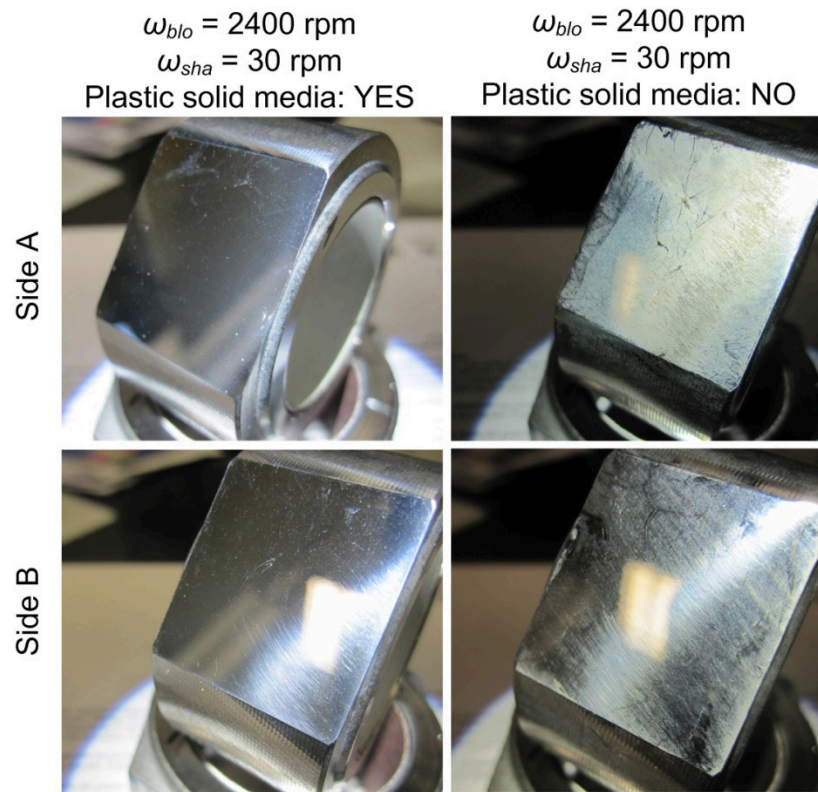
Fig. 7.23   Effect of the solid media on the mechanical removal action

From experimental tests it emerges that the effectiveness of the washing machine prototype was not suitable to reach the desired cleanliness quality by a single washing stage. Therefore, following the strategy of multiple washing actions, further tests were performed, as reported in Tab. 7.8.

Tab. 7.8   Further experimental tests: DOE

	Parameter	Level	Value
	Washing strategy	3	FBM + FBM[(*)] U.S. + FBM FBM + U.S.
	Batch	1	1
Fluidized bed washing machine	Detergent	1	P3 Neutracare 3300 (4%)
	Solid media	1	Polymeric spheres (d=3mm)
	Bath temperature	1	60°C
	Blower rotation speed ω_{blo} [rpm]	1	2400
	Shaft rotation speed ω_{sha} [rpm]	1	30
	Cycle time [min]	1	15
Ultrasound washing machine	Detergent	2	HT 1401 (5%) – I tank HT 1170 (3%) – II and III tank
	Ultrasound power	3	See Tab. 7.4
	Cycle time [min]	3	See Tab. 7.4

[(*)]F.B.M. – Fluidized Bed Machining, U.S. Ultrasound technique

Firstly, two washing stages by the FBM prototype machine were performed: the intent was to understand if the washing machine is able to remove haloing on the surface after a first rough washing stage with same technique. Unfortunately, results were not satisfactory (Fig. 7.24 – a).

Therefore, a second test was planned to verify if the prototype has got the capacity in removing haloing after a first ultrasound washing stage performed by the current washing cycle. In this way, it was possible to establish if the washing technique can be implemented as a finishing cleaning stage substituting the second and the third ultrasound washing actions in the multi-tank machine: also in this case cleanliness quality was not reached (Fig. 7.24 – b).

As outlined yet, it was observed that the quality of the washing component by the first stage of the ultrasound pluritank machine is similar to the quality output from the FBM action. Basing on these evidences, a further test was carried out: rough washing was performed by the FBM technique, whereas the finishing was performed in the pluritank washing machine starting from the second stage. Cleanliness quality was better than other tests (see Fig. 7.24 - c).

From these further experimental tests, it can be concluded that the washing machine prototype is suitable for rough cleaning, but it cannot be employed for a finish cleaning due to its intrinsically limitations.
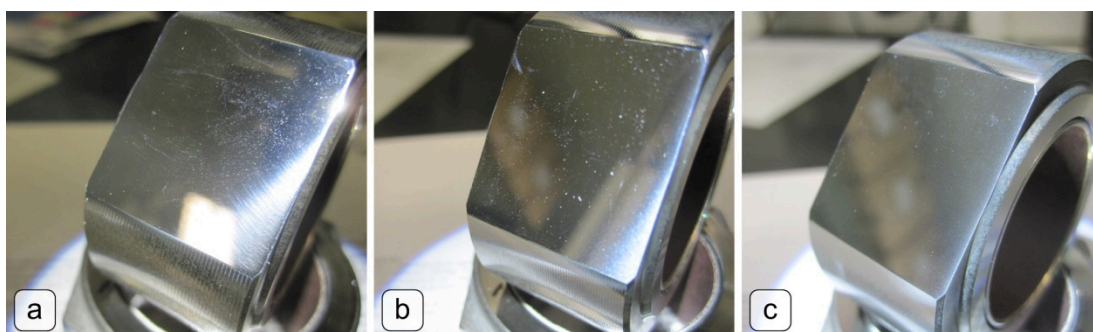
Fig. 7.24   Comparison of washing strategy results: FBM and FBM (a), U.S. and FBM (b), FBM and U.S. (c)

7.5.6 Conclusions about the Fluidized Bed washing technique

The Fluidized Bed theory was applied in order to design an innovative washing approach. The washing prototype was adopted for verifying the potentiality in removing polishing paste on the surfaces of an automotive parts manufactured by Brovedani SpA.
The experimental results were compared with cleanliness level reached by the current washing strategy based on a multi-tank ultrasound machine.

The following conclusions may be drawn:

- In general, increasing air flow rate reduces the liquid column level;

- Bath composition affects the bed column behaviour: if only deionized water is used, expansion of bath is minor rather than the case of the combination of water and detergent, especially with high air flow rate;

- Detergent suitable for spraying washing technique has to be adopted due to the tendency in foam formation;

- From experimental tests, it emerged that the washing prototype cannot reach the required cleanliness level of the workpiece: the reason can lie on the selection of the detergent that is not indicated for abrasive paste removal;

- From the analysis of variance, both working parameters (ω_{blo} and ω_{sha}) influence the washing action; moreover, the initial contamination level of the component shall be considered;

- Better cleanliness levels were achieved applying medium air flow rate (ω_{blo} = 2400 rpm) and medium rotation speed of shafts (ω_{sha} = 30 rpm);

- The presence of not abrasive media within the bath is crucial to remove contaminants as much as possible;

- Cleanliness quality was not improved performing two washing stages by the fluidized bed technology; moreover, the machine is not suitable for a precision washing;

- Cleanliness quality was improved performing a rough washing stage by the FBM and concluded the cleanliness strategy by two further washing action by U.S. technique;

- FBM prototype can be suitable for a rough cleaning since its intrinsic characteristics.

7.6. General conclusions

In high-precision mechanical manufacturing, cleanliness of a component plays a fundamental role for assuring the required accuracy of a workpiece. "Cleaning" means the removal of contaminants (chips, oil, abrasive paste, water compound, detachable burrs) from the surfaces of a workpiece, which can affect the functionality of the part or of the assembly. Nowadays, the need for higher cleanliness levels compared with past requirements, derives from the rapid advancements in various current technologies. Also the trend towards the miniaturization of components dictates highly stringent cleanliness standards.

In literature, few informations are reported about washing strategy suitable for mechanical components. Therefore, in this Chapter an overview of the wet washing approaches was presented.

Washing strategies, including the selection of washing technique and cleaning media typologies, were generated thanks the collaboration with experts at the Brovedani SpA company. The analysis was based on the workpiece geometry and on the nature of contaminants, which depend on the manufacturing processes of the component.

For the sake of completeness, cleanliness requirements indications and the techniques for cleanliness inspection – based on the ISO standard 16232:2005 for automotive components – were explained.

Finally, an innovative washing machine (designed by University of Tor Vergata) was tested for cleaning a specific automotive component at the Brovedani SpA company. The washing prototype is based on the principle of the fluidization of cleaning bed. The experimental analysis was based on the comparison of cleanliness quality of the Fluidized Based Machine with results reached by U.S. strategy in removal polishing paste. Analysing cleanliness results, it emerged that the washing prototype is suitable for rough finishing, as a spray technique, that is generally applied for intermediate washing. This limitation is related to the fluidized bed technology: due to the air flow on the liquid bath, only specific detergents can be adopted avoiding foam formation; however, in general, these detergents are not suitable in removing polishing paste.

GENERAL CONCLUSIONS

The discipline of Precision Manufacturing plays a crucial role in production of high-precision mechanical components. Such components may be characterized by complex geometry, microscopic features and they are frequently made of difficult-to-cut or exotic materials. Precision Manufacturing deals with the realization of parts by advanced production processes which require a deep knowledge on machine tools and manufacturing processes. Main targets of Precision Manufacturing are:

1. satisfying very strict workpiece requirements in terms of dimensional and form accuracy, as well as surface quality and integrity;

2. enhancing cutting tool performance (in terms of machinability/chip formation mechanisms, tool life);

3. satisfying advanced part requirements arising from Precision Design such as very stringent cleanliness levels, absence of burrs and other geometrical defects.

Main goal of the current thesis was conceiving advanced modeling techniques as well as innovative experimental methodologies aiming at these targets.

Main achievements and conclusions obtained in this research work are summarized below.

- Precision manufacturing has to guarantee all the functionalities of the final part simultaneously, such as mechanical, tribological, thermal and optical functions; they are defined by the design department. This could imply advanced specifications expressed at meso and nano scale, besides conventional requirements expressed at macro and micro scale.

- In the light of these very strict requirements, several factors may affect the accuracy of the workpiece and the optimization in general, such as the accuracy of the machine tool, static and dynamic behaviour of the cutting system, characteristics of the cutting material, tool life, finishing and superfinishing needs and cleanliness requirements.

- Regarding dimensional and geometrical workpiece accuracy, it does mainly depend on programmed tool trajectory accuracy, machine tool positioning accuracy and kinematics, undesired deflection of tool tip or workpiece. Such deflection is typically due to mechanical compliance of the machining system, differential thermal expansions, tool wear and other causes. Besides, unacceptable surface quality is mainly due to anomalous tool tip/workpiece vibrations or cutting mechanics and worn cutting edge.

Therefore, innovative methodologies for avoiding, detecting or attenuating undesired vibrational phenomena are strongly required. For achieving this purpose, the following phases play a crucial role: modeling and identification of machining system dynamics, cutting force modeling, modeling the tool-workpiece dynamic interaction.

Modeling and identification of machining system dynamics

- In this perspective, the machining system has to be ideally decomposed into different subsystems, and the most flexible elements have to be identified. Modeling efforts should focus on such elements. Different approaches are feasible: analytical, numerical and experimental.

- From the analysis of literature and from direct experience in this field, it was assessed that the best compromise between model accuracy, model simplicity and costs (time and

resources consumed for model determination) is achieved when hybrid models are considered: they are built on physical principles and FE models, but they require experimental calibration/validation.

- The application of this concept to a real case study of great industrial interest – internal turning with slender tooling systems – was proposed in the current thesis. Specifically, the following results were obtained:

  o in a first stage, modal tests were carried out at the tool tip in order to understand the dynamic behaviour of the tooling system with different configurations (different bar material and geometry and several ratio of the bar length L and bar diameter D): it emerged that the boring bar dynamics can be approximated by a single harmonic oscillator where damping values mainly depend on the boring bar ratio L/D and on bar material;

  o in order to represent the tooling system dynamics in internal turning, tooling system was successfully modelled following the hybrid approach, combining a Timoshenko FE model of the boring bar with the dynamics of toolholder experimentally evaluated;

  o improvement of the accuracy of the model was achieved by considering an additional bar overhang: it models the non-ideal constrain at the toolholder-boring bar interface; best results were achieved assuming that the ratio of the additional bar overhang to bar diameter is constant, independently from boring bar material and geometry;

  o in general, the predicted static compliances were in good agreement with experimental results (bias $|\mu_{\varepsilon rel,G}| < 2.3\%$ and $\sigma_{\varepsilon rel,G} < 7.3\%$ for both bar materials); the estimate of the main resonance frequency provided by the model was satisfactory but slightly less accurate ($|\mu_{\varepsilon rel,f}| < 1.6\%$ and $\sigma_{\varepsilon rel,f} < 8.7\%$ for both bar materials): estimates regarding boring bars of bigger diameter were affected by a greater discrepancy due to the dynamic interaction between boring bar and spindle-tool holder dynamics which cause unexpected resonance peaks that could not predicted by the model;

  o Interpolation results obtained by applying the Rayleigh model were not satisfactory; a simpler empirical model based on a smaller number of model coefficients was derived demonstrating a better interpolation capability (bias $|\mu_{\varepsilon rel,log\xi}| < 3.2\%$ and $|\sigma_{\varepsilon rel,log\xi}| < 20.3\%$ for both bar materials).

Modeling of cutting forces and tool-workpiece dynamic interaction

- From the analysis of state of the art it was assessed that cutting forces are mainly modelled following analytical and semi-empirical mechanistic approaches; the former are generally inaccurate because of the strong (often unrealistic) simplifications they are based on; the latter is widely employed and can overcome the limit of the purely analytical models.

- In this thesis a mechanistic model was proposed for describing the cutting forces in turning operations: it includes the effect of the tool geometry and of the cutting parameters; by so doing, the cutting forces are modelled as a function of the instantaneous contact length and uncut chip section area.

- By performing cutting tests, it was demonstrated that the proposed model was in good accordance with experimental data (bias $|\mu_{\varepsilon F}| < 3\%$ and $|\sigma_{\varepsilon F}| < 20.1\%$ for Ergal material and $|\mu_{\varepsilon F}| < 9\%$ and $|\sigma_F| < 22.3\%$ considering the C45 cutting material).

- During machining, the dynamic interaction between tool and workpiece can be described by the regenerative radial cutting force coefficient k_τ. Such coefficient is used for estimating radial cutting force variations due to tool tip vibrations experienced by the tool

in the actual and previous workpiece round. The analytical approach used in literature for estimating such coefficient is inaccurate for general internal turning applications.

- Here a numerical approach was applied, which was based on cutting force measurements. From the analysis of numerical computations it was assessed that the radial regenerative cutting force coefficient k_τ mainly depends on cutting pressure k_s and tool nose radius, whereas the sensitivity to cutting parameters is negligible in first approximation when performing internal turning finishing operations.

Development of practical method for selection of stable tooling systems

- Chatter prediction methodologies require several experimental tests for calibrating and validating the algorithms they are based on; however, from the analysis of the state of art, it was pointed out that only a few experimental tests are reported in literature, especially in the case of internal turning. On the contrary, the accent is mostly placed on numerical simulation of cutting process dynamics.

- Concerning finishing internal turning operation, the only recommended robust stable region was that below the stability lobes minima, denoted by the critical value of regenerative radial cutting force coefficient $k_{\tau, cr\ min}$;

- A semi-empirical predictive model of the critical ratio $(L/D)_{cr}$ – maximum boring bar aspect ratio assuring a stable cutting process for almost all cutting conditions – was proposed with a relative standard deviation about 6%: input factors were the bar material, the bar diameter D, the cutting pressure k_s, the tool nose radius r_ε; the influence of cutting parameters (a_p, v_c, f) were considered negligible: it was confirmed by performing cutting tests with different machining system configurations, i.e. boring bar material and geometry, workpiece material and tool nose radius;

- The proposed hybrid analytical-empirical approach can be adopted for the preliminary selection of stable tooling system configurations in internal turning, since data available in literature are often incomplete or inapplicable, especially for modern boring bars made of high-damping carbide.

- Experimental results and the developed model can be integrated in a new and robust chatter prediction method for internal turning operations: it provides an approximate but prudential estimate of $(L/D)_{cr}$ without performing several additional tests in the shop-floor. The method is based on a probabilistic approach, which considers stochastic models for representing machining dynamics and tool-workpiece interaction.

Optimization of machining process is usually aimed at maximizing productivity or minimizing production costs, by concurrently assuring a given product quality. Therefore, enhancing high cutting tool performance, in terms of machinability of the material, tool life and tool wear play a key role.

- The cutting process is a very complex dynamical system whose stochastic outputs depend on several inputs. Unfortunately, it may depend on several uncontrolled and usually unknown inputs, which may increase process variability. The results obtained in slightly different experimental conditions may significantly vary from those reported in technical literature. In other words, the reliability of the results and guidelines found in technical literature is very limited. Therefore, it is crucial to develop and apply effective experimental procedures for understanding and optimizing the machining process under analysis.

- For this purpose, it is fundamental to identify most significant process inputs, such as the cutting material properties (chemical composition, microstructure and grain size,

porosity, physical and mechanical properties) and the cutting process configuration, i.e. cutting parameters, cutting tool and tool holder characteristics and cutting environment.

- Moreover, in addition to conventional process outputs representing process performance, other process outputs should be measured in the perspective of cutting tool comparison and process optimization. Cutting forces, power consumption, cutting temperature and vibrational phenomena can be successfully monitoring by applying on-line control strategies, also with a multi-sensor approach. Their measurements allow the evaluation of further process outputs of interest, such as the friction coefficient. On the contrary, off-line control strategies can be carried out for the inspection of the dimensional and geometrical accuracy of the workpiece and its surface integrity, but also for analysing the chip morphology, including the estimation of the chip compression ratio, together with the investigation of the tool wear mechanism and the evaluation of the tool life.

- An innovative experimental methodology for investigating machinability problems and for optimizing cutting operations of difficult-to-cut material was conceived. The proposed methodology was successfully applied in dry turning of sintered Molybdenum. From the research work emerged that:

    o great benefits in turning sintered Molybdenum in dry cutting conditions were achieved at relatively high cutting speed: when the cutting speed was greater than 150 m/min the cutting process was stable, surface finish was good, cutting forces and machining system vibrations were low; also, the built up edge formation was reduced at high cutting speed due to the better chip flow; this finding was in contrast with typical indications which suggest to machine Molybdenum by applying cutting speed less than 140 m/min with coolant supply;

    o cutting speed played an important role on the surface quality, in contrast with the behaviour of more conventional workpiece materials: in most cases, surface roughness linearly decreased as cutting speed was increased; in adding, surface roughness was strongly influenced by the interaction between tool geometry and cutting parameters;

    o chip flow stress of sintered Molybdenum was analogous to that of conventional carbon steel; however, a greater equivalent friction coefficient was observed with sintered Molybdenum than that reported in literature for conventional steels, confirming the stronger tendency to adhesion and plastic shear at the chip – normal rake interface;

    o ceramic based cutting inserts were not adequate for machining sintered Molybdenum, because of their brittleness and negative geometry; similarly, CerMet grades were not suitable, probably due to their brittleness;

    o a highly positive geometry and an uncoated and polished surface condition of the cutting inserts with carbide bulk material were identified as the most effective to achieve high surface quality, good chip formation control and excellent tool life also with high cutting speed (T=32 min at v_c=215 m/min), optimizing the cutting process;

    o from the analysis of worn tools by SEM technique it emerged that oxidation was the dominant tool wear mechanism: this was due to the high temperatures achieved when turning Molybdenum, in accordance with the behaviour of most refractory metals and heat resistant superalloys.

High precision mechanical components have to fulfill advanced requirements arising from Precision Design in order to satisfy the functionalities of the final product: these requirements can involve unconventional tolerances and highly surface quality. Specifically, technical specifications demand absence of burrs and other geometrical defects, improvement of the surface integrity and very stringent cleanliness level.
For this purpose, dedicated actions have to be adopted.

Mass finishing of high precision mechanical components

- Mass finishing is a very common approach for improving part accuracy and surface quality, and for removing small defects due to previous cutting operations. For these reason, mass finishing operations are carried out as the final stages of the production cycle. Mass finishing processes are relatively cheap since they permit to work a great number of workpieces simultaneously.

- From the literature, it emerged that there exist several technologies to perform mass finishing of mechanical components: the selection of the proper technique basically depends on the workpiece shape, dimensions and final required tolerances as well as on the desired cycle time. Moreover, the effectiveness of the finishing process is related to the adopted media type and to the characteristics of the water compound.

- From the analysis of the state of art, it was assessed that most of research works focused on the experimental comprehension of the motion and behavior of the workload, i.e. the mix of media, water compound and workpieces; few research works aim at developing analytical or semi-empirical models for the mass finishing process optimization, due to its complexity.

- In order to optimize a mass finishing strategy aiming at improving the surface quality of a workpiece, a scientific study was conducted at Brovedani SpA Company. The main findings are:

  o by applying an analytical approach proposed in literature by Hashimoto in 1996, it was possible predict the optimal cycle time to reach the desired surface roughness;

  o the roughness of the machined surface before mass finishing has a strong influence on the final results;

  o the mass finishing strategy, which comprised three mass finishing stages with different working machine and working parameters can be reduced at two stages of work if the initial surface quality is sufficiently high: therefore, the cycle time was considerable reduced (T=274 min instead of the initial T=540 min and rather than the optimized T=348 min considering three finishing stages).

- Furthermore an innovative mass finishing technology was tested. It was design by University of Tor Vergata (Rome), and was based on the concept of dry mass finishing approach. The prototype was experimentally tested in order to understand its effectiveness in deburring, radiusing and fine-polishing of specific case studies manufactured at Brovedani SpA company. Main scientific results are:

  o The dry mass finishing technology did not manifest a robust process neither considering deburring action nor in radiusing action; however, radiusing could be carried out considering a proper initial edge geometry;

  o Air flow tends to limit the deburring and radiusing action; on the other hand it helps in cleaning the components and mitigates the contact between abrasive granulates and workpieces avoiding damages on the parts edges;

  o Barrel rotation speed strongly affects the accuracy of the workpiece, whereas the influence of the other working parameters, such air flow rate and barrel rotation direction was limited;

  o Interpolating mathematical models represent the trend of mean values with good accuracy, considering both deburring both radiusing action: for the counterclockwise direction of the barrel, σ_{mean}=18% for the deburring action and σ_{mean}=20% for the radiusing action taking into account the ground plane; however experimental data show large dispersion around average values, estimated by the standard deviations of

181

relative errors ($\sigma_{\varepsilon Deb}$=46% and $\sigma_{\varepsilon MRR}$ =45.7% considering the counterclockwise direction of barrel for both deburring and radiusing actions and the ground plane measurements for the *MRR* evaluation): so the analyzed working process does not assure the repeatability of the results;

o Dry mass finishing was effective in improving the surface quality of a component by a polishing action: residuals from heat treatments were successfully removed by applying the proper process condition; on the other hand impingement of workpieces could occur.

Cleanliness of high precision mechanical components

• In Precision Manufacturing, cleanliness of the mechanical parts is crucial, since contaminants may affect subsequently cutting process of workpiece or can influence the functionality of the final product.

• Nowadays, cleanliness specifications tend to reduce the admissible dimension of contaminants, requiring a more advanced and sophisticated washing strategy. From the analysis of state of the art about washing technologies, some general guidelines were outlined.

• Thanks with the collaboration with Brovedani SpA company, some innovative washing strategies were elaborated. The purpose was to give practical indications for optimizing a washing process.

• An innovative washing machine was studied and tested at Brovedani SpA company. The prototype was designed by University of Tor Vergata basing on the fluidized bed principle. By experimental investigation on a specific workpiece, whose contaminants was abrasive paste, main findings are:

o The motion of the bath is strictly related to the air flow rate, and its composition, i.e. deionized water, detergent and solid media;

o Cleanliness effectiveness is strictly related to the chemical detergent: unfortunately, fluidized bed washing machine required detergents not susceptible to foam formation, which are in general not suitable in removing polishing paste;

o By performing statistical analysis of results it emerged that air flow rate and rotation speed of workpiece affected the cleanliness quality of workpiece;

o A combination of working parameters to reach a better results was experimental derived considering a medium level of air flow rate and of the rotational speed of shafts ($\omega_{blo} = 2400 \, rpm - \omega_{sha} = 30 \, rpm$);

o The washing machine was suitable for rough cleaning, but it was not possible to reach the required cleanliness quality of the workpiece.

This thesis represents a significant scientific and technical contribution for the advancement of innovative manufacturing processes of high and ultra-high precision mechanical components.

In this research work, the key factors which can strongly affect the accuracy of the part and its features in general were identified and deeply examined, by also considering critical aspects that are rarely faced in literature, such as finishing aspects and cleanliness requirements.

- General conclusions of this research work are very difficult to draw due to the heterogeneity of the aspects which have been studied. Optimization of a process in Precision manufacturing is affected by different critical aspects which require specific methodologies of analysis and exact solutions.

- The analysis of the static and dynamic behaviour of the cutting process, together with the study of the machinability of the cutting material, represent fundamental steps in order to achieve the desired workpiece accuracy and other stringent requirements. The innovative mathematical models and the general guidelines proposed in this thesis can enhance the understanding of the physical phenomena involved and they can provide effective tools for manufacturing process optimization.

- The optimization of mass finishing process and of cleaning of precision mechanical components represents a challenge. The former, principally due to the very expensive waste management of the process, the latter, due to the lack in literature of analysis of washing approaches. In the light of this, this thesis shows novel solutions by presenting a new finishing technique able to reduce waste treatments and by developing innovative washing strategies.

It would be of great industrial interest to test the practical guidelines, innovative experimental procedures and modelling techniques - successfully validated in this research work - to other manufacturing processes requiring high or ultra-high precision.

Acknowledgements

I would like to express my gratitude to my tutor and supervisor Dr. Ing. Marco Sortino, who has given me the opportunity to join his research group and work with him. He has been constantly supporting me and motivating my research work throughout my Ph.D School years.

A special thanks also to my second supervisor Dr. Ing. Giovanni Totis for his encouragement, his suggestions and advice during my research activities and the writing of this thesis. He has given me much food for thought and fruitful discussions both of which have facilitated me to achieve relevant scientific results.

I would further like to express my gratification to the Keymec, Centre for Innovation, Research and Training in the field of Mechanics in ZIPR - San Vito al Tagliamento (Italy), who have permitted me to carry out most of the research activities, as are presented in this thesis.

I would like to thank all the members of the R&D Department and within the Technical Department of Brovedani Group SpA in ZIPR - San Vito al Tagliamento, Italy. Particularly, special gratitude to Ing. Alessio Faraon and Ing. Giuseppe Mainardis, who have given me the opportunity to complete my Ph.D through the support of their company. Moreover, I would like to mention Annibale Bortolussi, Angelo Finos, Eugenio Toppan and his staff for their fundamental technical support during my research activities.

Special thanks to Sandro Belfio, Marco Nali, Daniela Barattin, Luciano Moro and Marco Gallina and many others who contributed towards my serene journey in Udine.

Finally, I want to express my gratitude to my family and to my boyfriend who have been loving and supporting me throughout this hard but gratifying experience.

Bibliography

[1] P. Schellekens, N. Rosielle, H. Vermeuelen, S. Wetzels, W. Pril, *Design for precision: Current status and trends*, Annals of the CIRP, 47 (1998), pp. 557–586

[2] *ASM Handbook, Volume 5: Surface Engineering*, (1998), ASM International

[3] F. Klocke, E. Brinksmeier, K. Weinert, *Capability profile of hard cutting and grinding processes*, CIRP Annals – Manufacturing technology, 54 (2005), pp. 22–45

[4] N.F.M. Aris, K. Cheng, *Characterization of the surface functionality on precision machined engineering surfaces*, International journal of Advance manufacturing Technology, 38 (2008), pp. 402–409

[5] L. De Chiffre, H. Kunzmann, G.N. Peggs, D.A. Lucca, *Surfaces in precision engineering, microengineering and nanotechnology*, CIRP Annals – Manufacturing technology, 52 (2003), pp. 561–577

[6] R.H. Todd, D.K. Allen, L. Alting, *Manufacturing process reference guide*, (1994), Industrial Press Inc.

[7] H.A. Youssef, H. El-Hofy, *Machining technology – Machine tools and operations*, (2008), CRC Press, Taylor & Francis Group

[8] M. Sortino, G. Totis, F. Prosperi, *Modeling the dynamic properties of conventional and high-damping boring bars*, Mechanical Systems and Signal Processing, 34 (2013), pp. 340–352

[9] I. Lazoglu, F. Atabey, Y. Altintas, *Dynamics of boring processes: Part III-time domain modeling*, International Journal of Machine Tools & Manufacture, 42 (2002), pp. 1567–1576

[10] G. Genta, *Vibration Dynamics and Control*, (2009), Springer

[11] L. Andren, L. Hakansson, A. Brandt, I. Claesson, *Identification of dynamic properties of boring bar vibrations in a continuous boring operation*, Mechanical Systems and Signal Processing, 19 (2004), pp. 869–901

[12] H. Akesson, T. Smirnova, L. Hakansson, *Analysis of dynamic properties of boring bars concerning different clamping conditions*, Mechanical Systems and Signal Processing, 23 (2009), pp. 2629–2647

[13] B. Moetakef-Imani, N.Z. Yussefian, *Dynamic simulation of boring process*, International Journal of Machine Tools & Manufacture, 49 (2009), pp. 1096–1103

[14] L. Andren, L. Hakansson, A. Brandt, I. Claesson, *Identification of motion of cutting tool vibration in a continuous boring operation—correlation to structural properties*, Mechanical Systems and Signal Processing, 18 (2004), pp. 903–927

[15] L. Houck III, T.L. Schmitz, K.S. Smith, *A tuned holder for increased boring bar dynamic stiffness*, Journal of Manufacturing Processes, 13 (2011), pp. 24–29

[16] D. Mei, T. Kong, A.J. Shih, Z. Chen, *Magnetorheological fluid-controlled boring bar for chatter suppression*, Journal of Materials Processing Technology, 209 (2009), pp. 1861–1870

[17]   M.H. Miguelez, L. Rubio, J.A. Loya, J. Fernandez-Saez, *Improvement of chatter stability in boring operations with passive vibration absorbers*, International Journal of Mechanical Sciences, 52 (2010), pp. 1376–1384

[18]   E. Budak, A. Erturk, H.N. Ozguven, *A Modeling Approach for Analysis and Improvement of Spindle-Holder-Tool Assembly Dynamics*, Annals of the CIRP, 56 (2006), pp. 369–372

[19]   A. Erturk, E. Budak, H.N. Ozguven, *Selection of design and operational parameters in spindle-holder-tool assemblies for maximum chatter stability by using a new analytical model*, International Journal of Machine Tools Manufacture, 47 (2007), pp. 1401–1409

[20]   S.S. Park, Y. Altintas, M. Movahhedy, *Receptance coupling for end mills*, International Journal of Machine Tools & Manufacture, 43 (2009), pp. 889–896

[21]   G. Catania, N. Mancinelli, *Theoretical–experimental modeling of milling machines for the prediction of chatter vibration*, International Journal of Machine Tools & Manufacture, 51 (2011), pp. 339–348

[22]   M. Wang, T. Zan, Y. Yang, R. Fei, *Design and implementation of nonlinear TMD for chatter suppression: An application in turning processes*, International Journal of Machine Tools & Manufacture, 50 (2010), pp. 474–479

[23]   M. Thomas, Y. Beauchamp, *Statistical investigation of modal parameters of cutting tools in dry turning*, International Journal of Machine Tools & Manufacture, 43 (2003), pp. 1093–1106

[24]   M.E. Merchant, *Mechanisms of metal cutting process*, Journal of Applied Physics, 16 (1945), pp. 267–275

[25]   S. Rubenstein, *A note concerning the inadmissibility of applying of minimum work principle to metal cutting*, ASME Journal of Engineering for Industry, 105 (1983), pp. 294–296

[26]   E.H. Lee, B.W. Shaffer, *The theory of plasticity applied to a problem of machining*, ASME Journal of Applied Mechanics, 18 (1951), pp. 405–413

[27]   P.L.B. Oxley, W.F. Hastings, *Minimum work as possible criterion for determining the friction conditions at the tool/chip interface*, Phil. Trans. R. Soc. Lond.,A, 282 (1976), pp. 565–584

[28]   Y. Huang, S.Y. Liang, *Cutting forces modeling considering the effect of tool thermal property – application to CBN hard turning*, International Journal of Machine Tool & Manufacture, 43 (2003), pp. 307–315

[29]   A.H. Adibi-Sedeh, V. Madhavan, B. Bahr, *Extension of Oxley's Analysis of machining to use different material models*, Transaction of the ASME, 125 (2003), pp. 656–666

[30]   B. Li, X. Wang, Y. Hu, C. Li, *Analytical prediction of cutting forces in orthogonal cutting using unequal division shear-zone model*, International Journal of Advanced Manufacturing Technology, 54 (2011), pp. 431–443

[31]   C.-S. Chang, G.-C. Tsai, *A force model of turning stainless steel with worn tools having nose radius*, Journal of Materials Processing Technology, 142 (2003), pp. 112–130

[32]   O. Kienzle, *Die Bestimmung von Kräften und Leistungen an spannenden Werkzeugmaschinen*, Z. Ver.Dtsch. Ing. (1952), pp. 299–305

[33]   H. Saglam, S. Yaldiz, F. Unsacar, *The effect of tool geometry and cutting speed on main cutting force and tool tip temperature*, Materials and Design, 28 (2007), pp. 101–111

[34]   Pohl quoted in Schröder *Die Bedeutung der Spanndicke bei Walzenfräsern*, Masch. Bau../Betr., (1934), pp. 541–548

[35]   Y. Altintas, M. Weck, *Chatter Stability of Metal Cutting and Grinding*, CIRP Annals - Manufacturing Technology, 53 (2004), pp. 619–642

[36]   J. Gradisek, E. Govekar, I. Grabec, *Using coarse-grained entropy rate to detect chatter in cutting*, Journal of Sound and Vibration, 214 (1998), pp. 941–952

[37]   F. Atabey, I. Lazoglu, Y. Altintas, *Mechanics of boring process – Part I*, International Journal of Machine Tools & Manufacture, 43 (2003), pp. 463–476

[38]   G. Totis, M. Sortino, *Development of a modular dynamometer for triaxial cutting force*, International Journal of Machine Tools & Manufacture, 51 (2011), pp. 34–42

[39]   R. Suresh, S. Basavarajappa, G.L. Samuel, *Predictive modelling of cutting forces and tool wear in hard turning using response surface methodology*, Procedia Engineering, 38 (2012), pp. 73–81

[40]   G. Bartarya, S.K. Choudhury, *Effect of cutting parameters on cutting force and surface roughness during finish hard turning AISI52100 grade steel*, Proceedia CIRP, 1 (2012), pp. 651–656

[41]   K. Bouacha, M. A. Yallese, T. Mabrouki, J.-F. Rigal, *Statistical analysis of surface roughness and cutting forces using response surface methodology in hard turning of AISI 52100 bearing steel with CBN tool*, International Journal of Refractory Metals & Hard Materials, 28 (2010), pp. 349–361

[42]   M. Sortino, G. Totis, F. Prosperi, *Development of a practical model for selection of stable tooling system configurations in internal turning*, International Journal of Machine Tool & Manufacture, 61 (2012), pp. 58–70

[43]   Y. Altintas, M. Eynian, H. Onozuka, *Identification of dynamic cutting force coefficients and chatter stability with process damping*, CIRP Annals— Manufacturing Technology, 57 (2008), pp. 371–374

[44]   G. Totis, RCPM - *A new method for robust chatter prediction in milling*, International Journal of Machine Tool & Manufacture, 49 (2009), pp. 273–284

[45]   S. Tangjisitcharoen, *In-process monitoring and detection of chip formation and chatter for CNC turning*, Journal of Materials Processing Technology, 209 (2009), pp. 4682–4688

[46]   I.N. Tansel, X. Wang, P. Chen, A. Yenilmez, B. Ozcelik, *Transformations in machining. Part 2. Evaluation of machining quality and detection of chatter in turning by using s-transformation*, International Journal of Machine Tools & Manufacture, 46 (2006), pp. 43–50

[47]   D.E. Dimla Sr., *The impact of cutting conditions on cutting forces and vibration signals in turning with plane face geometry inserts*, Journal of Materials Processing Technology, 155 - 156 (2004), pp. 1708–1715

[48]   E.C. Lee, C.Y. Nian, Y.S. Tarng, *Design of a dynamic vibration absorber against vibrations in turning operations*, Journal of Materials Processing Technology, 108 (2001), pp. 278–285

[49]   L. Rubio, J.A. Loya, M.H. Miguelez, J. Fernandez-Saez, *Optimization of passive vibration absorbers to reduce chatter in boring*, Mechanical Systems and Signal Processing, 41 (2013), pp. 691–704

[50]   A. Ganguli, A. Deraemaeker, M. Horodinca, A. Preumont, *Active damping of chatter in machine tools – Demonstration with a "Hardware in the Loop" simulator*, Proceedings of the Institution of Mechanical Engineers, Part I: Journal of Systems and Control Engineering, 219(5) (2005), pp. 359–369

[51]   A. H. El-Sinawi, R. Kashani, *Improving surface roughness in turning using optimal control of tool's radial position*, Journal of Materials Processing Technology, 167 (2005), pp. 54–61

[52]   E. Budak, E. Ozlu, *Analytical modelling of chatter stability in turning and boring operations: a multi-dimensional approach*, Annals of the CIRP, 56 (2007), pp. 401–404

[53]   L. Vela-Martinez, J. C. Jauregui-Correa, E. Rubio-Cerda, G. Herrera-Ruiz, A. Lozano-Guzman, *Analysis of compliance between the cutting tool and the workpiece on the stability of a turning process*, International Journal of Machine Tools & Manufacture, 48 (2008), pp. 1054–1062

[54]   B. C. Rao, Y. C. Shin, *A comprehensive dynamic cutting force model for chatter prediction in turning*, International Journal of Machine Tools & Manufacture, 39 (1999), pp. 1631–1654

[55]   R. Mahdavinejad, *Finite element analysis of machine and workpiece instability in turning*, International Journal of Machine Tools & Manufacture, 45 (2005), pp. 753–760

[56]   G. Urbikain, A. Fernandez, L.N. Lopez de Lacalle, M. E. Gutierrez, *Stability lobes for general turning operations with slender tools in the tangential direction*, International Journal of Machine Tools & Manufacture, 67 (2013), pp. 35–44

[57]   M. Kronenberg, *Machining science and application, theory and practice for operation and development of machining processes*, (1966), Pergamon Press

[58]   E. Kuljanic, M. Sortino, G. Totis, *Multisensor approaches for chatter detection in milling*, Journal of Sound and Vibration, 312 (2008), pp. 672–693

[59]   G. Totis, M. Sortino, *Robust Analysis of Stability in Internal Turning*, in press on the Proceedings of 24th DAAAM International Symposium, 2013, University of Zadar

[60]   M. Sortino, G. Totis, F. Prosperi, *Dry turning of sintered molybdenum*, Journal of Materials Processing Technology, 213 (2013), pp. 1179–1190

[61]   S. Olovsjo, P. Hammersberg, P. Avdovic, J.-E. Stahl, L. Nyborg, *Methodology for evaluating effects of material characteristics on machinability—theory and statistics-based modelling applied on Alloy 718*, International Journal of Advanced Manufacturing Technology, 59 (2012), pp. 55–66

[62]   E.O. Ezugwu, *Key improvements in the machining of difficult-to-cut aerospace superalloys*, International Journal of Machine Tools & Manufacture, 45 (2005), 1353–1367

[63]   E. M. Elgallad, F.H. Samuel, H.W. Doty, *Machinability aspects of new Al–Cu alloys intended for automotive castings*, Journal of Materials Processing Technology, 210 (2010), pp. 1754–1766

[64]   A. Rivero, A. Aramendi, S. Herranz, L.N. Lopez de Lacalle, *An experimental investigation of the effect of coatings and cutting parameters on the dry drilling performance of aluminium alloys*, International Journal of Advanced Manufacturing Technology, 28 (2006), pp. 1–11

[65]   M. Kikuchi, *The use of cutting temperature to evaluate the machinability of titanium alloys*, Acta Biomaterialia, 5 (2009), pp. 770 – 775

[66]   D.G. Takur, B. Ramamoorthy, L. Vijayaraghavan, *Study on the machinability characteristics of superalloy Inconel 718 during high speed turning*, Materials and Design, 30 (2009), pp. 1718–1725

[67]   R. Lapovok, A. Molotnikov, Y. Levin, A. Bandaranayake, Y. Estrin, *Machining of coarse grained and ultra fine grained titanium*, Journal of Materials Science, 47 (2012), pp. 4589–4594

[68]   T. Sasaki, T. Yakou, *Tool wear and surface roughness during machining of high-temperature aluminized steel*, Journal of Materials Processing Technology, 197 (2008), pp. 89–95

[69]   M. V. de Carvalho, D.M. Montenegro, J. de Oliveira Gomes, *An analysis of the machinability of ASTM grades 2 and 3 austempered ductile iron*, Journal of Materials Processing Technology, 213 (2013), pp. 560–573

[70]   P.S Sreejith, *Machining of 6061 aluminium alloy with MQL, dry and flooded lubricant conditions*, Materials Letters, 62 (2008), pp. 276–278

[71]   S.M. Yuan, L.T. Yan, W.D. Liu, Q. Liu, *Effects of cooling air temperature on cryogenic machining of Ti–6Al–4V alloy*, Journal of Materials Processing Technology, 211 (2011), pp. 356–362

[72]   A. Braghini Jr., A.E. Diniz, F.T. Filho, *Tool wear and tool life in end milling of 15–5 PH stainless steel under different cooling and lubrication conditions*, International Journal of Advanced Manufacturing Technology, 43 (2009), pp. 756–764

[73]   M. Armendia, A. Garay, L.-M. Iriarte, P.-J. Arazzola, *Comparison of the machinabilities of Ti6Al4V and TIMETAL® 54M using uncoated WC–Co tools*, Journal of Materials Processing Technology, 210 (2010), pp. 197–203

[74]   W.-F. Ho, S.-C. Wu, Y.-S- Hong, H.-C. Hsu, *Evaluation of the machinability of Ti–Sn alloys*, Journal of Alloys and Compounds, 502 (2010), pp. 112–117

[75]   P.-J. Arrazola, A. Garay, L.-M. Iriarte, M. Armendia, S. Marya, F. Le Maitre, *Machinability of titanium alloys (Ti6Al4V and Ti555.3)*, Journal of Materials Processing Technology, 209 (2009), pp. 2223–2230

[76]   A. Ebrahimi, M.M. Moshksar, *Study of machinability in boring operation of microalloyed and heat-treated alloy steels*, Materials Science and Engineering A, 460 – 461 (2007), pp. 314–323

[77]   R. Suresh, S. Basavarajappa, V.N. Gaitonde, G.L. Samuel, *Machinability investigations on hardened AISI 4340 steel using coated carbide insert*, International Journal of Refractory Metals and Hard Materials, 33 (2012), pp. 75–86

[78]   M. Nalbalt, A. Altin, H. Gokkaya, *The effect of coating material and geometry of cutting tool and cutting speed on machinability properties of Inconel 718 super alloys*, Materials and Design, 28 (2007), pp. 1719–1724

[79] Y. Su, N. He, L. Li, A. Iqbal, M.H. Xiao, S. Xu, B.G. Qiu, *Refrigerated cooling air cutting of difficult-to-cut materials*, International Journal of Machine Tools & Manufacture, 47 (2007), pp. 927 – 933

[80] Q. Niu, M. Chen, W. Ming, Q. An, *Evaluation of the performance of coated carbide tools in face milling TC6 alloy under dry condition*, International Journal of Advanced Manufacturing Technology, 64 (2013), pp. 623–631

[81] K. Aslantas, I. Ucun, A. Cicek, *Tool life and wear mechanism of coated and uncoated Al2O3/TiCN mixed ceramic tools in turning hardened alloy steel*, Wear, 274 – 275 (2012), pp. 442–451

[82] S.L. Soo, R. Hood, D.K. Aspinwall, W.E. Voice, C. Sage, *Machinability and surface integrity of RR1000 nickel based superalloy*, CIRP Annals - Manufacturing Technology, 60 (2011), pp. 89–92

[83] P. Roy, S.K. Sarangi, A. Ghosh, A.K. Chattopadhyay, *Machinability study of pure aluminium and Al–12% Si alloys against uncoated and coated carbide inserts*, International Journal of Refractory Metals & Hard Materials, 27 (2009), pp. 536–544

[84] N. Muthukrishnan, M. Murugan, K. Prahlada Rao, *An investigation on the machinability of Al-SiC metal matrix composites using pcd inserts*, International Journal of Advanced Manufacturing Technology, 38 (2008), pp. 447–454

[85] *ASM Handbook, Volume 16: Machining*, (1989), ASM International

[86] G.F. Micheletti, *Tecnologia meccanica 1, Il taglio dei metalli*, (1977), second ed. UTET

[87] N.N. Zorev, *Metal cutting mechanics*, (1966), Pergamon Press, Oxford, UK

[88] International Standard ISO 3685:1993: *Tool-life testing with single point turning tools*

[89] Plansee - Molybdenum. The all-rounder among the specialists, *http://www.plansee.com/en/Materials-Molybdenum-402.htm*, Plansee Se, 2014, (Page access: October 2013)

[90] T. Takida, H. Kurishita, M. Mabuchi, T. Igarashi, Y. Doi, T. Nagae, *Mechanical properties of fine-grained, sintered molybdenum alloys with dispersed particles developed by mechanical alloying*, The Japan Institute of Metals & Materials Transactions, 45 (2004), pp. 143–148

[91] Metals, Inconel Alloy 718, *http://www.specialmetals.com/documents/Inconel%20alloy%20718.pdf*, Special Metals Corporation, 2007, (Page access: October 2013)

[92] T.S. Srivatsan, B.G. Ravi, A.S. Naruka, L. Riester, M. Petraroli, T.S. Sudarshan, *The microstructure and hardness of molybdenum powders consolidated by plasma pressure compaction*, Powder Technology, 114 (2001), pp. 136–144

[93] Machinability Data Center, *Machining Data Handbook, vols. 1 and 2.*, (1980), third ed. Institute of Advanced Manufacturing Sciences, Inc., Metcut Research Associates

[94] E. Kuljanic, M. Sortino, G. Totis, F. Prosperi, *Evaluation of commercial tools for machining special-alloy Hadfield steel*, International Virtual Journal – MTM Machining Technology Material 7 (2012), pp. 96–99

[95] L.K. Gillespie, *Mass finishing handbook*, (2007), Industrial Press

[96]   Rosler   finding   a   better   way,
          http://www.rosler.it/produkte/verfahrensmittel/keramische_schleifkoerper/, Rösler
          Oberflächentechnik GmbH, 2012, (Page access: November 2013)

[97]   S. Wang, R.S. Timsit, J.K. Spelt, *Experimental investigation of vibratory finishing
          of aluminium, Wear*, 243 (2000), pp. 147–156

[98]   A. Yabuki, M.R. Baghbanan, J.K. Spelt, *Contact forces and mechanisms in a
          vibratory finisher*, Wear, 252 (2002), pp. 635–643

[99]   M.R. Baghnanan, A. Yabuki, R.S. Timsit, J.K. Spelt, *Tribological behavior of
          aluminum alloys in a vibratory finishing process*, Wear, 255 (2003), pp. 1369–
          1379

[100]   D. Ciampini, M. Papini, J.K. Spelt, *Tribological behavior of aluminum alloys in a
          vibratory finishing process*, Journal of Materials Processing Technology, 183
          (2007), pp. 347–357

[101]   D. Ciampini, M. Papini, J.K. Spelt, *Characterization of vibratory finishing using
          the Almen system*, Wear, 264 (2008), pp. 671 – 678

[102]   D. Ciampini, M. Papini, J.K. Spelt, *Modeling the development of Almen strip
          curvature in vibratory finishing*, Journal of materials processing technology, 209
          (2009), pp. 2923–2939

[103]   K. Hashemnia, A. Mohajeriani, J.K. Spelt, *Development of a laser displacement
          probe to measure particle impact velocities in vibrationally fluidized granular
          flows*, Powder Technology, 235 (2013), pp. 940–952

[104]   F. Hashimoto, *Modelling and Optimization of Vibratory Finishing Process*, Annals
          of the CIRP, 45 (1996), pp. 303–306

[105]   S.E. Naeini, J.K. Spelt, *Two-dimensional discrete element modeling of a spherical
          steel media in a vibrating bed*, Powder Technology, 195 (2009), pp. 83–90

[106]   A. Mohajerani, J.K. Spelt, *Numerical modeling of the edge rounding of brittle
          materials by vibratory finishing*, Wear, 268 (2010), pp. 1002–1012

[107]   A. Mohajerani, J.K. Spelt, *Edge rounding of brittle materials by low velocity
          erosive wear*, Wear, 267 (2009), pp. 1625–1633

[108]   V. Cariapa, H. Park, J. Kim, C. Cheng, A. Evaristo, *Development of a metal
          removal model using spherical ceramic media in a centrifugal disk mass finishing
          machine*, International Journal of Advanced Manufacturing Technology, 39 (2008),
          pp. 92–106

[109]   International standard ISO 13715:2000: *Technical drawing – Edges of undefined
          shape – Vocabulary and Indications*

[110]   Deutsche norm DIN 6784 (1982): *Edges of workpieces*

[111]   J.C. Aurich, D. Dornfeld, P.J. Arrazola, V. Franke, L. Leitz, S. Min, *Burrs—
          Analysis, control and removal*, CIRP Annals - Manufacturing Technology, 58
          (2009), pp. 519–542

[112]   D.A. Davidson, *Surface condition impact part performance: Burrs, edges can
          negatively influence function of components*, Metal finishing, 105 (2007), pp. 22–
          31

[113]   M. Massarsky, D.A. Davidson, *Turbo-abrasive finishing*, Deburring & Surface
          conditioning conference, Cincinnati, OH, October 26-27, 1993

[114]   M. Barletta, *A new technology in surface finishing: Fluidized bed machining (FBM) of aluminium alloys*, Journal of Materials Processing Technology, 173 (2006), pp. 157–265

[115]   M. Barletta, S. Guarino, G. Rubino, V. Tagliaferri, *Progress in fluidized bed assisted abrasive jet machining (FB-AJM): Internal polishing of aluminium tubes*, International Journal of Machine Tools & Manufacture, 47 (2007), pp. 483–495

[116]   M. Barletta, *Progress in abrasive fluidized bed machining*, Journal of Materials Processing Technology, 209 (2009), pp. 6087–6102

[117]   M. Barletta, S. Guarino, *High speed finishing of a CuZn15 brass alloy by Abrasive Recirculating Fluidized Bed (ARFB)*, Powder Technology, 203 (2010), pp. 591–602

[118]   Awad S., *Ultrasonic cavitations and precision cleaning*, (1996), Precision cleaning magazine

[119]   The Precision Cleaning for Advanced Technologies Technology Handbook, *http://infohouse.p2ric.org/ref/05/04280.htm*, Witter Publishing Corporation, 2000 (Page access: November 2013)

[120]   Durkee J., *Aqueous Cleaning Machines: How They Work, and Why, part I*, Metalfinishing, 2009, pp. 48–50

[121]   Durr Leading in production efficiency - Product overview, *http://www.durr.com/product-overview/cleaning-and-filtration-systems-products*, Durr AG, 2014, (Page access: November 2013)

[122]   Niemczewski B., *Observations of water cavitation intensity under practical ultrasonic cleaning conditions*, Ultrasonics Sonochemistry, 14 (2007), pp. 13–18

[123]   Niemczewski B., *Influence of concentration of substances used in ultrasonic cleaning in alkaline solutions on cavitation intensity*, Ultrasonics Sonochemistry, 16 (2009), pp. 402–407

[124]   E. Maisonhaute, C. Prado, P.C. White, R.G. Compton, *Surface acoustic cavitation understood via nanosecond electrochemistry. Part III: shear stress in ultrasonic cleaning*, Ultrasonics Sonochemistry, 9 (2002), pp. 297–303

[125]   A. Thiemann, T. Nowak, R. Mettin, F. Holsteyns, A. Lippert, *Characterization of an acoustic cavitation bubble structure at 230 kHz*, Ultrasonics Sonochemistry, 18 (2011), pp. 595–600

[126]   Jueschke M., Koch C., *Model processes and cavitation indicators for a quantitative description of an ultrasonic cleaning vessel: Part I: Experimental results*, Ultrasonics Sonochemistry, 19 (2012), pp. 787–795

[127]   Jueschke M., Koch C., *Model processes and cavitation indicators for a quantitative description of an ultrasonic cleaning vessel: Part II – Multivariate data analysis*, Ultrasonics Sonochemistry, 19 (2012), pp. 796–802

[128]   B. Zeqiri, M. Hodnett, A.J. Carroll, *Studies of a novel sensor for assessing the spatial distribution of cavitation activity within ultrasonic cleaning vessels*, Ultrasonics, 44 (2006), pp. 73–82

[129]   K.-V. Jenderka, C. Koch, *Investigation of spatial distribution of sound field parameters in ultrasound cleaning baths under the influence of cavitation*, Ultrasonics, 44 (2006), pp. e401–e406

[130] B.A. James, C. McVeigh, S.N. Rosenbloom, E.P. Guyer, S.I. Lieberman, *Ultrasonic Cleaning-Induced Failures in Medical Devices*, Medical Device Materials Vol. 5, ASM International, 5 (2010), pp. 41–45

[131] L. Steblenko, D. Kalinichenko, A. Nadtochiy, A. Podolian, O. Korotchenkov, *Surface damage effects in ultrasonic cleaning of silicon wafers*, Physics, Chemistry and Applications of Nanostructures: Proceedings of the International Conference Nanomeeting--2011: Reviews and Short Notes: Minsk, Belarus, 26-29 May 2009, pp. 416–418

[132] International standard ISO Standard 16232:2005: *Road vehicles - Cleanliness of components of fluid circuits*

[133] M. Massarsky, D. A. Davidson, *Turbo-Abrasive machining and finishing, Metal Finishing*, 7 (1997), pp. 29–31

[134] M. Barletta, V. Tagliaferri, *Development of an abrasive jet machining system assisted by two fluidized beds for internal polishing of circular tubes*, International Journal of Machine Tools & Manufacture, 46 (2006), pp. 271–283